MODELLING, SIMULATION AND BEHAVIOUR OF SLOSHING LIQUID-TANK-SHIP COUPLED SYSTEM

LUONG VAN HAI

NATIONAL UNIVERSITY OF SINGAPORE

2008

MODELLING, SIMULATION AND BEHAVIOUR OF SLOSHING LIQUID-TANK-SHIP COUPLED SYSTEM

LUONG VAN HAI

B.Eng. (Hons.), HCM City University of Technology, Vietnam

M.Eng., University of Liege, Belgium

A THESIS SUBMITTED

FOR THE DEGREE OF DOCTOR OF PHILOSOPHY

DEPARTMENT OF CIVIL ENGINEERING

NATIONAL UNIVERSITY OF SINGAPORE

2008

To my parents,

Acknowledgements

First of all, I would like to thank my supervisors, Associate Professor Ang Kok Keng and Professor Wang Chien Ming of the Department of Civil Engineering, National University of Singapore (NUS), for their invaluable advice, guidance and encouragement as well as for introducing this wonderful research topic to me. Their scientific excitement inspired me through out my research. I feel privileged for having the opportunity to work with them.

I greatly appreciate the Centre for Ships and Ocean Structures (CeSOS) at Marine Technology Department, Norwegian University of Science and Technology (NTNU) for allowing me to adapt the ship motion program developed by Oyvind Notland Smogeli and students at NTNU 2002-2004. I am also grateful for the research scholarship provided by the National University of Singapore and the Centre for Offshore Research & Engineering (CORE) for providing all the necessary recourses to carry out my research.

Finally, and most importantly, I would like to acknowledge my parents, who sacrificed their youth during the Vietnam War and despite their difficulties and sufferings gave their very best in the upbringing of their children. They also taught me the value of hard work and act as role models through their own examples. I would also like to thank my elder sister and her husband for being there for me too. All of them have given me strong support during the entire period of my research.

Table of Contents

Summary

Liquid sloshing in tanks has been a subject of keen research for many decades due to the fact that this phenomenon is predominant in many diverse areas and more importantly the huge concerns over the potential detrimental effects that sloshing can induce. It is common knowledge that sloshing may cause large internal forces and deformation in the tank walls, particularly when the external forcing frequencies are close to the natural sloshing frequencies. Tank walls may therefore be damaged arising from high fluid dynamic pressures as a result of resonance. An example of area where the effect of sloshing is of concern is in the transportation of various types of liquid in tanks through ships. This thesis is concerned with the modeling and study of sloshing of liquid in tank due to the motion of ships across the sea. In particular, a suitable numerical model to address the complicated coupled liquid-tank-ship interaction problem will be developed and used to study the effects of liquid sloshing on the structural response of the tank walls and the stability of the ship. The mitigation of liquid sloshing so as to reduce the detrimental effects will also be examined, in particular, the effectiveness of ring-baffled devices will be investigated in detail. The entire study is investigated using the Finite Element Method.

In typical finite element modeling of tank walls, the classical theories of thin shell theories have frequently been adopted. These theories ignore the effect of transverse shear deformation, which are well-known to be inadequate when used for the modeling of thick shells and composite laminated shells. In this thesis, an axisymmetric solid-shell element based on the relative displacement (RD) concept was proposed to model the liquid-filled containers. The proposed RD-shell element accurately simulates all types of structures from thin to thick shells in only one common formulation. The

liquid inside the containers is discretized with compatible quadrilateral fluid elements. The displacements of the RD-shell and pressures of the contained liquid, which is assumed to be inviscid and incompressible, are expressed in terms of harmonic functions which are required to satisfy the prescribed boundary conditions. Based on the RD concept, a coupling force matrix was introduced to account for the liquid-structure interaction between the shell and neighboring liquid elements.

The motion of ship across the sea is modeled allowing for various environmental effects due to wind, wave and current. At each instant of time, the ship motion induces stresses and deformations in the tank walls as well as sloshing of the liquid in the tank and in return, the tank induces forces on the ship at the connection between the base of the tank and its supporting platform on the ship. The complicated interaction problem between liquid sloshing, tank and moving ship was investigated in this thesis by using the proposed RD-finite element method. Many influencing factors on the dynamic response of the coupled system were explored, including the levels of liquid-filling, number and location of tanks on the ship, ship-thruster modeling as well as environmental setting parameters such as the significant wave height, current velocity and directions of wind and wave.

List of Tables

List of Figures

List of Symbols

Abbreviations

ART	Anti-rolling tank
c(·)	cos(·)
C_n	cos($n\theta$)
CFD	Computational fluid dynamics
COG	Centre of gravity
FEM	Finite element method
LF	Low frequency
LNG	Liquefied natural gas
RD	Relative displacement
s(·)	sin(·)
S_n	sin($n\theta$)
t(·)	tan(·)
WF	Wave frequency

Scalar quantities

a, b	Dimensions of liquid element
E	Young's modulus
S_f	Free surface of liquid
S_i	Liquid-structure interface
D	Flexural rigidity

G	Shear modulus
h	Thickness of tank wall
h_b	Thickness of baffle
H	Height of container
H_b	Location of baffle from the base
H_f	Height of liquid
I	Lagrangian functional
n	Circumferential wave number
n_b	Number of baffles in the container
R	Radius of cylindrical container/Outer radius of baffle
R_b	Inner radius of baffle
s	Meridional distance along shell element
P	Total liquid pressure
P_s, P_d	Static and dynamic liquid pressures, respectively
u, v, w	Middle-surface displacement components of shell element in meridional, circumferential and normal directions, respectively
u_n, v_n, w_n	Middle-surface displacement amplitudes of shell element in meridional, circumferential and normal directions, respectively
u_s, v_s, w_s	Displacement components of shell element in the local n, θ and s directions, respectively
u_z, u_r	Velocity components of fluid element
Δu_n, Δv_n	Relative displacements of shell element along meridional and circumferential directions, respectively
V_f	Volume of liquid element

x_0	Distance from center of liquid element to geometric axis of container
XYZ	Body-fixed reference frame
$X_E Y_E Z_E$	Earth-fixed reference frame
$\beta = H_f / H$	Liquid-to-container height ratio
λ, ψ, ζ	Frequency parameters
γ_r	Current direction relative to the vessel
θ	Circumferential angle
ν	Poisson's ratio
ρ_s, ρ_f	Mass densities of shell and liquid, respectively
κ	Shear modification factor
∇^2	Laplacian operator in cylindrical coordinates
ϕ	Angle between the r and s axes
Φ	Liquid velocity potential
$\eta(r,\theta,z,t)$	Displacement of the free surface of liquid about the horizontal plane
σ_z	Normal stresses transverse to the middle surface
ω_n	Natural sloshing frequency

Vector quantities & matrices

$\mathbf{B}_b$	Bending strain matrix of shell element
$\mathbf{B}_m$	Membrane strain matrix of shell element
$\mathbf{B}_s$	Transverse shear strain matrix of shell element

$\mathbf{C}_{RB}(\mathbf{v})$	Skew-symmetric Coriolis matrix of the rigid-body
$\mathbf{C}_{A}(\mathbf{v}_r)$	Centripetal matrix of the rigid-body
$\mathbf{D}_b$	Flexural rigidity matrix of shell element
$\mathbf{D}_m$	Membrane rigidity matrix of shell element
$\mathbf{D}_s$	Shear rigidity matrix of shell element
$\mathbf{D}_L$	Strictly positive linear damping matrix
$\mathbf{D}_p(\omega)$	Wave radiation damping matrix
$\mathbf{D}_{NL}(\upsilon_r, \gamma_r)$	Nonlinear damping vector
$\mathbf{E}(\boldsymbol{\eta})$	Inverse matrix of $\mathbf{J}(\boldsymbol{\eta})$
$\mathbf{f}$	Generalized force vector
$\mathbf{G}(\boldsymbol{\eta})$	Matrix of linear generalized gravitation and buoyancy force coefficients
$\mathbf{I}$	The unit matrix
$\mathbf{J}(\boldsymbol{\eta})$	The transformation matrix
$\mathbf{K}_s$, $\mathbf{K}_f$	Stiffness matrices of shell and liquid, respectively
$\hat{\mathbf{K}}$, $\hat{\mathbf{M}}$	Symmetric stiffness and mass matrices of the coupled system, respectively
$\mathbf{M}_{eff}$	Effective mass matrix
$\mathbf{M}_s$, $\mathbf{M}_f$	Mass matrices of shell and liquid, respectively
$\mathbf{N}_f$, $\mathbf{N}_f^s$, $\mathbf{N}_f^i$	Shape function matrices of liquid element
$\mathbf{N}_s$, $\mathbf{N}_s^w$	Shape function matrices of shell element
$\mathbf{P}$	Density matrix of the material

$\mathbf{p}$	Liquid nodal pressure vector
$\mathbf{q}$	Generalized nodal displacement vector of shell
$\ddot{\mathbf{q}}$	Generalized nodal acceleration vector of shell
$\mathbf{S}$, $\mathbf{S}_b$, $\mathbf{S}_{bf}$, $\mathbf{S}_s$	Liquid-structure coupling force matrices
$\boldsymbol{\varepsilon}_\mathbf{m}$	Membrane strain matrix of shell element
$\boldsymbol{\varepsilon}_\mathbf{b}$	Bending strain matrix of shell element
$\boldsymbol{\varepsilon}_\mathbf{s}$	Transverse shear strain matrix of shell element
$\boldsymbol{\eta}$	Position and orientation vector of ship motion
$\boldsymbol{\eta}_{Rw}$	WF motion vector in the Earth-fixed frame
$\boldsymbol{\upsilon}$	Linear and angular velocity vector of ship motion
$\boldsymbol{\upsilon}_r$	Relative velocity vector with respect to water current
$\boldsymbol{\tau}_{con1}$, $\boldsymbol{\tau}_{con2}$	Vectors consisting of forces and moments produced at the base of containers for WF and LF, respectively
$\boldsymbol{\tau}_{env2}$	Slowly-varying environmental load vector
$\boldsymbol{\tau}_{moor}$	Vector of generalized mooring forces
$\boldsymbol{\tau}_{thr}$	Control vector consisting of forces and moments produced by the thruster system
$\boldsymbol{\tau}_{wind}$	Mean wind load vector
$\boldsymbol{\tau}_{wave1}$	First order wave excitation vector
$\boldsymbol{\tau}_{wave2}$	Second order wave drift load vector

CHAPTER 1 INTRODUCTION

1.1 Background

When a fluid moves and interacts with its container, the dynamic pressures of such an interaction may cause large deformation in the container wall as well as the supporting structure. The motion of liquid arises due to the dynamic motion of the container which can occur under various circumstances. This phenomenon of liquid in containers is known as liquid sloshing, which can also be described as the motion of a fluid as it attempts to attain a state of equilibrium arising from the effective instantaneous acceleration felt by the liquid.

The problem of liquid sloshing has been investigated by many researchers from a wide range of disciplines. In seismology, the effects of liquid sloshing have been studied on water tanks and large dams under earthquake excitation (e.g. Westergaard, 1933). In the aerospace industry, the influence of liquid propellant sloshing on the stability of jet vehicles has been a major concern to engineers and researchers since the early 1960s (e.g. McCarty and Stephens, 1960; Stofan and Pauli, 1962). This is because sloshing is a potential critical disturbance to the vehicle stability due to the interacting forces and the shift in the center of gravity of the vehicle. In the building industry, liquid tanks on roofs are employed as passive dampers to mitigate the movement of the structure due to wind loading or ground motions (e.g. Nukulchai and Tam, 1999). The first building in the world that employed tuned sloshing water dampers is the One Wall Centre in Vancouver, British Columbia. This 48-story building has two specially shaped tanks, each containing about 50,000 gal (189,250 L)

of water, in the tower's mechanical penthouse. In the offshore industry, ships carrying liquid cargo are probably one of the most common types of vessels plying across the many shipping routes of the world. Marine vessels play a large part in transporting fuel and gas from their source to far away consumers. Containers holding fuel and liquefied natural gas (LNG) have to be designed against not only the static pressure but also the dynamic pressure arising from the sloshing of the fuel and LNG as the ship moves across the ocean. Owing to the effects of environmental influences on the moving ship, wave-induced ship motions can cause significant fluid oscillations or sloshing. This may lead to large local structural stresses and deformations induced in the containers. Significant sloshing may also affect the motion and stability of the ship. The aforementioned effects of liquid sloshing are expected to be large when the external forcing frequencies of the ship are close to the natural sloshing frequencies. Accurate prediction of the response of the coupled liquid-tank-ship system is important towards the safe design of containers and ships.

1.2 Literature review

There are three basic areas of literature relevant to this research work. The first covers the background research on liquid sloshing in containers. The fluid-structure interaction problems in liquid-filled storage containers based on various assumptions and using different methods will be reviewed. The second deals with liquid sloshing in containers due to external forces arising from earthquakes, ship motions and moving vehicles. Studies on the coupled interaction between the liquid sloshing and moving ship will be presented. The third focuses on the various methods investigated for mitigating the effects of liquid sloshing.

1.2.1 Sloshing of liquid-filled containers

Since the early 1900s, extensive research efforts have been made to understand the problem of liquid sloshing in many kinds of structures. For example, Westergaard (1933) investigated the problem of fluid sloshing on vertical rigid dams. Subsequently, Hoskins and Jacobsen (1934) conducted an analytical and experimental study of rigid rectangular and cylindrical containers under a simulated horizontal earthquake motion. Jacobsen (1949) presented a closed-form solution of the Laplace's equation for rigid cylindrical containers. Based on the assumption of rigid tank wall, the radial velocity of liquid elements at the liquid-structure interface is taken to be the same as that of neighbouring shell elements of the tank wall, which equals to that of the ground motion.

So far, many of these early studies on liquid sloshing of storage tanks were carried out with the assumption that the tank walls are rigid and that the tanks have the same motion as the ground support. The coupling effect between the liquid motion and the dynamic response of the tank structure is totally ignored. Perhaps, the most notable of these methods is that proposed by Housner (1967), which has been widely adopted for the design of structures containing fluids such as water tanks and fuel containers. In Housner's approach, the pressure is assumed to be caused by the liquid that accelerates with the tank and also by the liquid that sloshes within the tank. Based on this assumption, simplified expressions for approximating the pressure of fluid inside the containers were developed. In particular, the motion of the liquid content is separated into the "impulsive mode", which represents the liquid motion in unison with the container wall, and the "convective mode", which represents the vertical oscillating liquid motion, and is usually referred to "sloshing". The impulsive pressure acting on the container wall is obtained by applying Newton's law on the finite volume of liquid.

The liquid pressure caused by the convective liquid motion is analyzed by Hamilton's principle. Based on the suggestion by Housner (1967), containers are categorized into two types, namely broad tanks with liquid height-to-radius ratios $H_f / R \le 1.5$ and tall tanks with $H_f / R > 1.5$. Housner recommended that for tall tanks, only the portion of liquid from the free surface to a depth of $1.5R$ should be used to estimate the effect of the impulsive mode and the rest of liquid should be treated as a rigid mass moving in unison with the container wall. By adapting Housner's work, Epstein (1976) presented design curves for estimating the maximum bending and overturning moments for cylindrical containers as well as for rectangular rigid containers.

These aforementioned methods however are based on the assumption that the container walls are rigid and the effects of fluid-structure interactions are omitted. In reality, tank walls do deform significantly under external forces and the dynamic behaviour experienced by the liquid-tank system is much more complex than that based on rigid tank walls. By ignoring the effects of fluid-structure interaction, one may end up with an unsafe structure, especially if resonance occurs.

Vibration analyses of fluid-structure interaction problems have gained much attention with various approaches proposed for solution. For example, solutions for the dynamic pressure and the impulsive mass under the assumption of certain deformation patterns of the tank wall were presented by Veletsos and Yang (1974, 1976 and 1977). A comprehensive overview of the hydrodynamic forces on fluid-filled tanks subjected to lateral excitation under assumed wall deformation patterns was conducted by Yang (1976). The modified boundary conditions of the liquid motion, which were developed by Jacobsen (1949), considering the coupling effect between the hydrodynamic load and the dynamic response of the tank wall was presented by Veletsos (1974). In the study, the radial velocity of the liquid is the same as that of the tank wall at the liquid-

tank wall interface. By considering the coupling effect, the motion of tank wall is affected by the ground excitation, and the hydrodynamic load is no longer the same as that of the ground support. Subsequently, a comprehensive analysis of dynamic response of liquid-filled cylindrical containers under a rocking base motion was conducted by Veletsos and Tang (1987). The mechanical models for both rigid and flexible tanks were generalized to allow for the effect of base rocking.

Balendra and Nash (1978, 1980) solved the fluid-structure interaction problems by developing an axisymmetric two-noded thin shell element. Each node has four degrees of freedom, namely the axial, circumferential, radial displacements and the slope of the radial displacement with respect to the axial coordinate. The liquid domain is discretized using annular ring elements of rectangular cross section with the hydrodynamic pressures as the nodal degrees of freedom. However, the effect of liquid sloshing was neglected due to serious numerical difficulties in solving the coupled equations of liquid and shell motion. As a result of this over simplification, an "added mass" was introduced to model the effects of the contained liquid. Ang (1980) extended Balendra and Nash's work to incorporate the effects of liquid sloshing by using a coupling matrix for the shell and fluid elements. Liquid sloshing in flexible cylindrical tanks subjected to horizontal base excitation was studied by Haroun and Housner (1981a, 1981b, 1982) using the boundary element and finite element methods. The sloshing displacements and hydrodynamic pressures in partially liquid-filled containers under earthquake ground motions were calculated by Aslam (1981) using the Galerkin finite element method. Ma et al. (1982) carried out a study of the seismic response of elastic tanks based on an alternative approach which considered both acoustic and sloshing interaction of the fluid and structure. The seismic response of shell structures containing fluid was generally evaluated with the aid of the added-

mass concept and the post-earthquake sloshing behavior was also examined in the study. Rammerstorfer et al. (1988) obtained the vibration mode shape of the container shell wall by using an iterative procedure which starts by adopting an initial guess of the mode shape. The refined mode shape was addressed by considering the hydrodynamic pressure as “added mass”. Following this line of investigation, To and Wang (1991) and Subhash and Bhattacharyya (1996) employed the finite element method that made use of two-node thin elastic shell and eight-node fluid elements for the coupled vibration analysis of the liquid-filled cylindrical containers. Khai (1993) developed a numerical model for the seismic analysis of tanks with single and double curvatures using a combined finite element and boundary element numerical procedure. The coupled seismic liquid-shell interaction problem was solved by using finite shell elements for the tank structure while the boundary element method was used to model the fluid part. The study considered the free surface sloshing of liquid and the tank wall flexibility. Later, Kim and Yun (1997) performed fluid-structure interaction analysis of liquid storage structures under earthquake loadings by modeling the contained liquid using displacement-based fluid elements. They proposed a combined usage of rotational penalty and mass projection to remove spurious modes in the free vibration analysis of rectangular liquid storage structures. Recently, Amabili (2000) employed the Rayleigh-Ritz method to study the vibration of simply supported, circular cylindrical shells partially-filled with an incompressible sloshing liquid. In particular, the Rayleigh quotient is transformed into a simpler expression where the potential energies of the compressible fluid and free surface waves do not appear. Cho et al. (2002a) carried out analytical and numerical studies on the free vibration of fluid-structure interaction problems considering the fluid compressibility. In their study, the Novozhilov thin shell theory was used to split the structure region into wet and dry

parts. Shrimali and Jangid (2002) obtained the seismic response of the liquid storage tanks that are isolated by lead-rubber bearings under bi-directional earthquake excitation. The biaxial force-deformation behaviour of the bearings was considered as bi-linear models by using coupled non-linear differential equations. The seismic response of an isolated tank is found to be insensitive to the interaction effect of the bearing forces. In addition, there exists an optimum value of isolation damping for which the base shear in the tank attains the minimum value. Frandsen (2004) explored the behavior of liquid motions in a forced tank prescribed to move simultaneously in both horizontal and vertical directions.

In the meantime, many analytical studies have been conducted to obtain the exact solution for the problem of liquid sloshing in partially-filled containers. For example, Tedesco et al. (1989) presented an analytical method for the seismic analysis of ground supported, circular cylindrical liquid storage tanks subject to a horizontal component of earthquake ground motion. The free vibration of either a partially liquid-filled or a partially liquid-surrounded circular cylindrical shell with various classical boundary conditions was studied by Kyeong and Seong (1995). In their study, the liquid-shell coupled system was divided into two regions. One region is the empty shell part in which Sanders' shell equations are formulated without the liquid effect. The other is the wetted shell region in which the shell equations are formulated with consideration of the liquid dynamic effect. The same authors (Kyeong and Seong, 1998) later extended the study to the hydroelastic vibration of partially liquid-filled cylindrical containers with arbitrary boundary conditions. It was found that the variation of the natural frequencies depends on the axial mode number and circumferential wave number. Vamsi and Ganesan (2006) presented a semi-analytical finite element approach to discretise the shell structure in cylindrical containers filled with fluid. The

fluid velocity potential was approximated by polynomial functions instead of Bessel functions. The study was carried out for both elastic and viscoelastic shells. The natural frequencies of the system obtained by the polynomial approach compared very well with other results using numerical methods. They concluded that the polynomial approach would be more elegant and general than the Bessel function approach since in the later approach, Bessel function values have to be evaluated depending on shell dimensions.

The aforementioned numerical and analytical studies considered only thin cylindrical shells. When the shell is thick, the effect of transverse shear deformation has to be allowed for as the effect is no longer insignificant. Ma et al. (2005, 2006) proposed a new RD-solid element that is formulated based on the concept of relative displacement (RD). Stiffness and mass matrices were derived using the isoparametric concept. A major advantage of this element is its ability to handle laminated composite problems because the element not only considers the shear flexibility but also models layer-wise in-plane displacement of the laminated composite structures. Another advantage is that the RD-solid element can be applied to handle both thin and thick shell structures.

1.2.2 Interaction between sloshing in liquid-filled containers and moving ship

The idea of using liquid sloshing as absorber systems for the stabilization of ship motions has been addressed for a long time. Froude (1874) may be the first one who used anti-roll water tanks to mitigate the ship motion. The mechanism in which a roll damping moment is created by the wave action of the liquid in rectangular tanks placed on a ship was introduced by Watts (1883, 1885). Since the early 1960s, the stabilizing effects of liquid tanks on the roll motion of ships were introduced and investigated by many researchers (Vasta et al., 1961 and Dalzell et al., 1964). Reed

(1961) showed that the maximum roll motion of the ship can be reduced significantly from 15^0 to 5^0 by using properly designed anti-rolling tanks. In addition, the roll stabilization is only effective if the roll frequency of moving ship is equal to or larger than the natural frequency of the water oscillation. By considering sea wave effects on ships, it is realistic that wave-induced ship motions can cause resonant fluid oscillations. One can have extremely high impact pressures acting on the shell walls in gasoline tankers or ship cargo tanks when hydraulic jumps or traveling waves are present (Akita, 1967; Brathu et al., 1972; Bass, 1975; Faltinsen, 1978 and Arai, 1986). This can lead to large local structural loads on the tank and has an important effect on the global ship motions. In order to model the ship motion, Abdel et al. (2001) used a single degree-of-freedom model in roll. Subsequently, a six degrees-of-freedom model was introduced by Youssef et al. (2002) to capture a more accurate prediction of ship motion. In the study, passive anti-roll tanks were adopted for the stabilization of the moving ship. In addition, experimental and analytical studies were carried out by Weng (1992) and Bass (1998) with the view to understand the behaviour of anti-roll liquid containers. Numerical tank models were verified against experimental test results and then used in determining the optimum shape of the tanks.

Effects of the moving ship on sloshing of liquid in containers have been extensively investigated by various researchers. For example, Mikelis and Journee (1984) presented a two-dimensional finite difference transient solution for the prediction of liquid motions and induced pressures in partially-filled containers mounted on ships. Experiments were also conducted on scaled tanks and the measured pressures and bending moments were compared with numerical predictions. Lee and Choi (1999) presented results of experimental and numerical analysis of the sloshing problem in cargo tanks. The fluid motion was investigated using a higher order boundary element

method and the structure was modeled by using classical thin plate theory. The study found that in cases of low filling depths, hydraulic jumps were formed when the excitation frequency is close to the resonance frequency whereas in the case of high filling depths, a large impact pressure was obtained. In these studies, one assumed that the resulting sloshing of liquid in the tanks on the ship does not affect the motion of the ship. In other words, there is no interaction between the tank and the ship. This assumption is only valid for situations in which the size of the ship is large comparison with the size of the tank.

All the aforementioned studies have considered either the effects of tank sloshing on global motions of the ship (Vasta et al., 1961; Dalzell et al., 1964; Faltinsen, 1978; Arai, 1986; Abdel et al., 2001; Youssef et al., 2002) or the effects of the moving ship on the liquid sloshing in containers (Mikelis and Journee, 1984; Lee and Choi, 1999). However, the fully coupled interaction problem between liquid, tank and ship has not been considered due to inherent difficulty and complication. Some recent studies (Kim, 2002; Rognebakke and Faltinsen, 2003; Kim et al., 2006; Lee et al., 2007a & b) have shown the significance of coupled interaction between the liquid sloshing, container wall and moving ship, especially when the ratio of volume of the containers to that of the ship exceeds a critical value. Hence, it is important that both the sloshing phenomenon and associated ship motion behaviour should be studied.

So far, several investigations on coupled liquid-container-ship motion have been carried out by various researchers. For example, Journee (1997) analyzed a ship model with liquid cargo tanks and the model was tested in beam waves at zero forward speed for a wide range of filling levels. The measured roll data of the model were compared with the results obtained from the strip theory calculations. Kim (2002) employed a numerical technique to solve the coupling problem of the ship motion and sloshing

flow. The study focused on the anti-rolling tank which was found to have significant coupling effects on ship motion and sloshing. The three dimensional sloshing flow was simulated using the finite difference method, while the ship motion was obtained using a time domain panel method. Rognebakke and Faltinsen (2003) carried out two dimensional experiments on a hull section containing tanks filled with different levels of water and excited in sway by regular waves. They obtained a good agreement between test results and numerical simulated results of the coupling problem. Their study also revealed that the coupled motion is sensitive to the damping of the sloshing motion in a certain frequency range where the coupled sloshing and ship motions cause resonant ship motions. Faltinsen et al. (2005) classified the full set of three-dimensional resonant steady state waves occurring due to two types of harmonic forcing (longitudinal and diagonal) in a square-base ship tank. The study treated the evaluation of horizontal hydrodynamic forces on the ship tank due to sloshing. They concluded that even if a tank oscillates with small amplitude, forcing frequencies in the vicinity of a natural frequency for the fluid motion inside a smooth tank can lead to violent surface wave response. The obtained results were also validated by experiments both qualitatively and quantitatively. Kim et al. (2006) considered the coupling effects of ship motion and sloshing in a rectangular anti-rolling tank. The linear ship motion obtained in the time domain was solved using an impulse response function (IRF) method, while the nonlinear sloshing flow was simulated using a finite difference method. They showed that the ship motion is strongly sensitive to the wave slope due to the nonlinearity of sloshing flow. Recently, Lee et al. (2007a) carried out a series of parametric sensitivity studies on unmatched dimensionless scale parameters of the LNG tank sloshing loads by using a computational fluid dynamics (CFD) program. The CFD simulations were also validated by experimental results. They

concluded that the effects of viscosity and density ratio are insignificant, while its compressibility plays an appreciable role. Zhang and Suzuki (2007) introduced a numerical simulation of collision between a container ship and a large size double hulled crude carrier. Three different simulation methods were used to model the fluid–structure interaction in liquid-filled cargo tank, namely the arbitrary Lagrangian–Eulerian FEM, Lagrangian FEM and linear sloshing model. The results showed that the fluid-structure interaction of liquid cargo-filled tank has a significant effect on the motion and structural response of the cargo tank. Further, Lee et al. (2007b) analyzed the coupling and interactions between ship motion and inner-tank sloshing using a time-domain simulation scheme. Wind and sea current were however not accounted in the ship calculations. The study considered environmental forces that were due to the wave loading only.

1.2.3 Mitigation of liquid sloshing

As mentioned above, the fluid-structure interaction problem poses a challenging research topic in numerous practical applications. If the liquid is allowed to slosh freely, it can produce large additional forces that may lead to failure of the container. Therefore, suppression of liquid motion to reduce stresses developed in the tank wall is a major concern in fluid-structure interaction problems. Various types of slosh-suppression devices can be employed to damp the liquid motion and prevent the instability of system. They are also used to control the liquid motion inside the containers and hence to reduce the structural loads induced by the sloshing liquid.

Some experimental and analytical studies have been carried out in the past to understand the damping phenomenon in containers fitted with various types of devices for liquid suppression (Howell and Ebler, 1956; Silveira et al., 1961; Stephens and Scholl, 1967). Figures 1.1a-1.1i show some common types of baffles and anti-sloshing

devices designed for suppression of the fluid mobility, which are documented recently by Ibrahim (2005). These devices are classified as follows

1. Horizontal baffle rings, which can be movable or fixed (Figures 1.1a-1.1b)
2. Conical baffles, which are placed upright or inverted (Figures 1.1c-1.1d)
3. Radial or sectored baffles (Figures 1.1e-1.1h)
4. Annular containers (Figure 1.1i)

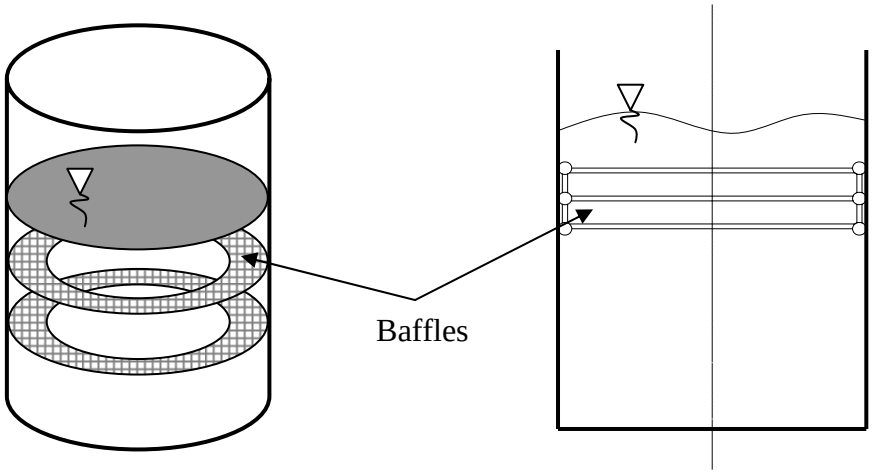

(a) Flat ring baffle system (b) Self-positioning fixed baffle system

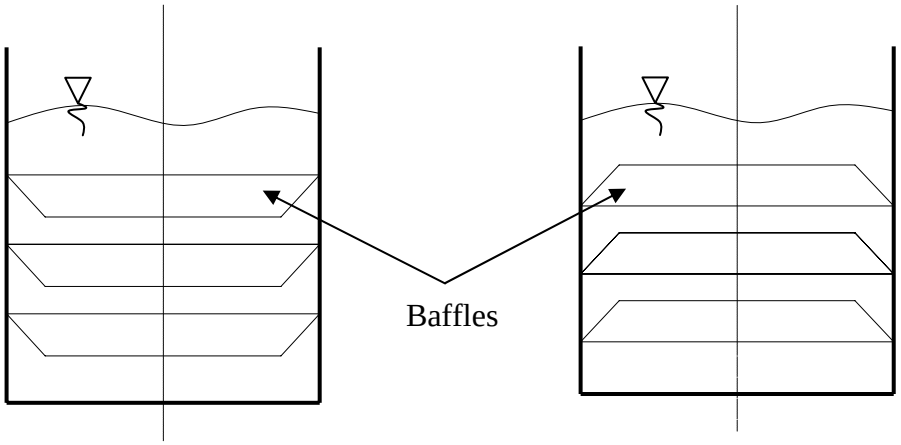

(c) Upright conic section baffle (d) Inverted conic section baffle

Figure 1.1 Sloshing suppression devices

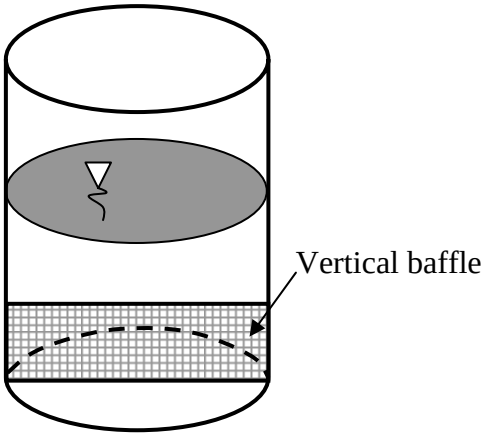

(e) 180^0-sectored container

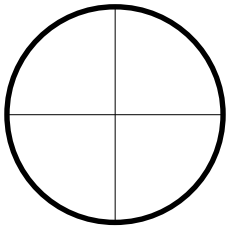

(f) 90^0-sectored container

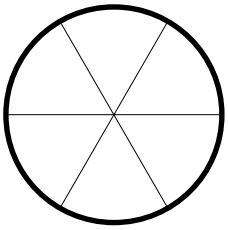

(g) 60^0-sectored container

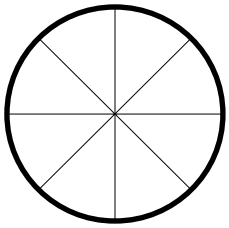

(h) 45^0-sectored container

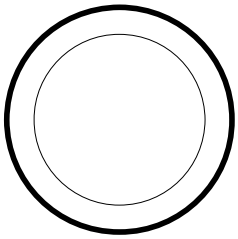

(i) Annular container

Figure 1.1 Sloshing suppression devices (cont')

A disc-type baffle with an inner hole has been widely used in liquid-storage containers because it is more practical and easy to install. Sloshing effect is suppressed in the liquid-filled containers by the baffles, which serve as passive slosh damping devices. Several works have been carried out in this direction to investigate the effects of baffles on sloshing. For example, linear sloshing in a circular cylindrical container with rigid baffles was investigated by Watson and Evans (1991) using the finite element method. Yue et al. (1996) presented an analytical method to solve the coupled oscillations problem of liquid in a cylindrical container with an elastic damping spacer. The coupled frequency equation was obtained by using double velocity potential functions corresponding respectively to the liquid above and below the damping spacer. Warnitchai and Pinkaew (1998) predicted the effects of flow damping devices on sloshing in rigid rectangular tanks using a two-dimensional model. In their formulation, the liquid was assumed to be inviscid, incompressible and irrotational. Surface tension effects were ignored. Their numerical model was used to determine the effects of vertical poles, baffles and nets on controlling liquid sloshing. Gedikli and Ergüven (1999) employed the boundary element method to study the effects of rigid baffles on the natural frequencies and seismic response of liquid in a circular cylindrical tank. Anderson et al. (2001) introduced a simple device consisting of two plates for the control of liquid sloshing in rigid cylindrical containers. By focusing on the ratio of the mass of the controller to that of the liquid to be controlled, the experimental results showed that the devices are effective in suppressing sloshing wave amplitudes. Another analytical study on the fluid-structure interaction using baffles was presented by Gavrilyuk et al. (2006), who provided accurate approximations of natural frequencies and modes of a vertical circular cylindrical tank having a thin rigid-ring horizontal baffle.

However, the aforementioned studies considered the baffles or container walls as rigid. Amabili et al. (1998) analyzed the dynamic characteristics of partially-filled cylindrical tanks with a flexible bottom and ring stiffeners. The effect of free surface waves was taken into account, and thus both bulging and sloshing modes were also studied. Cho et al. (2002b) performed a parametric investigation on free vibration characteristics of baffled cylindrical liquid-storage containers by using the coupled structural-acoustic finite element method. The natural frequency may be varied by using different combinations of the number, location of baffles and the inner-hole diameter as well as the liquid height. The flexibility of baffles in containers filled with liquid was later examined carefully by Biswal et al. (2003). In the study, the natural frequencies of liquid in a liquid-filled cylindrical tank with and without baffles were determined. Finite elements were used to discretize both the liquid and rigid/flexible baffles. Unfortunately, the interaction between liquid and container wall was omitted, i.e. the containers were assumed to be rigid. In addition, the analysis considered only the asymmetric mode of vibration of liquid and flexible baffle corresponding to the first circumferential wave number. Bermudez et al. (2003) introduced a finite element method to approximate the vibration modes of a coupled system consisting of an elastic baffle plate immersed in a fluid with a free surface subject to gravity waves. However, the effects of the fluid on the coupled system were simplified by using added mass formulations. Subsequently, Biswal et al. (2004) extended their study to allow for the flexibility of both baffles and the container wall in a partially liquid-filled cylindrical tank. The slosh amplitude of liquid was computed under a translational base acceleration and considering the liquid–baffle–tank wall interaction and all circumferential modes. Cho et al. (2005) presented the numerical analysis of the resonance characteristics of liquid sloshing in a 2-D baffled tank subjected to forced

lateral excitation. The sloshing damping ratios by the baffles were calculated by varying the number, location and opening width of the baffles. Two studies of Biswal et al. (2003, 2004) treated the sloshing problem based on linear theory where the motions of the liquid as well as the container were assumed to be small. Recently, Biswal et al. (2006) performed a nonlinear sloshing analysis of liquid in a two dimensional rigid rectangular container with rigid baffles using the finite element method. The effects of baffle parameters such as position, dimension and numbers on the system response were investigated.

Based on the literature review, one can conclude that baffles can be used effectively to mitigate the sloshing of free surface liquid. It is observed that baffles which are fitted just below the liquid free surface are effective in reducing sloshing. It is also shown in experimental studies that without increasing the weights of the baffles, flexible baffles can provide greater slosh damping than rigid baffles. However, the dynamic response of storage containers is significantly affected by the baffle parameters, such as the shape, size, number and installation position of the baffles. So, the determination of a suitable combination of such baffle parameters becomes a crucial part in the design of baffled liquid-storage containers.

This research is concerned with the prediction of sloshing effects and the proposal of various methods for mitigation sloshing of liquid contained in tanks that are mounted on ship where the sloshing is induced due to the motion of the ship as it travels across the ocean. The complicated interaction problem between nonlinear ship motion and liquid sloshing in multi-containers carrying liquid cargo will be investigated. The total effects of environmental settings (including wind, wave and current) and thruster modeling are considered in this study. To model the liquid-filled

containers, an axisymmetric solid-shell element based on the relative displacement (RD) concept will be proposed.

1.3 Objective and scope

The main objective of this thesis is to develop a computational model to carry out dynamic analysis of the aforementioned fully coupled liquid-container-ship interaction problem using the proposed axisymmetric RD-shell and fluid elements. The examination of the responses of liquid, container and ship will assist one in understanding the behaviour of such a coupled interaction system. The solution for mitigating the coupled effects of fluid sloshing on this liquid-container-ship system is also explored. More specifically, this thesis will

1. introduce the RD concept and replace the traditional rotational degree-of-freedom with this new RD degree-of-freedom. The axisymmetric RD-shell and fluid elements developed on the basis of RD concept will be presented.
2. describe the interpolation of the thickness shape of the single or multi-layer shell elements by using different shape functions. Therefore, a general RD shell element can be derived without distinguishing between the thin and thick shell cases.
3. present several examples to demonstrate the accuracy, versatility and generality of the proposed RD-elements for use in analyzing the free vibration of thin/thick cylindrical containers with and without liquid. The variations of different kinds of materials, thickness-to-radius, thickness-to-container height ratios, number of layers, fiber orientations, levels of liquid-filling and boundary conditions will be considered in these examples.

4. investigate the dynamic response of liquid-filled containers due to moving ship. The problem is modeled using the proposed RD-shell and fluid elements. Many contributing factors to the vibration response of liquid-filled containers are explored, including parameters relating to the container and environmental settings such as the significant wave height and the directions of wind and wave acting on the moving ship.
5. explore the significance of allowing for the full interaction between the liquid sloshing, multi-containers and moving ship. This coupled liquid-container-ship interaction problem is inherently complicated but a computational method will be developed to solve the coupled problem. Several parameters of interests, including the shapes of containers, levels of liquid-filling, and number and location of containers on the moving ship are investigated. Their effects on global motion will also be studied.
6. examine the effectiveness of various methods for mitigating the coupled effects of liquid sloshing in liquid-filled containers on moving ship.

1.4 Organization of thesis

This thesis comprises seven chapters:

Chapter 1 presents the background of the subject matter of concern in this thesis and a general literature review of research work, followed by a statement of the objective and scope of work carried out.

Chapter 2 presents the basic formulation of the axisymmetric fluid and shell elements using the relative displacement concept. These RD-elements will be used throughout the work carried out in this thesis. The formulation for multi-layer shell element will also be developed in this chapter.

Chapter 3 discusses the use of the proposed RD-elements to determine the natural frequencies of empty/liquid-filled cylindrical containers. Examples are presented to assess the performance of the proposed RD-shell and fluid elements.

Chapter 4 shows the effect of the moving ship on the sloshing of liquid in cylindrical containers. The governing equations of coupled fluid-shell vibrations using relative displacement concept are presented. Many factors that affect the vibration response of cylindrical storage containers due to moving ship are investigated. These factors include container parameters, environmental settings such as the significant wave height and the directions of wind and wave acting on the ship.

Chapter 5 deals with the problem of complicated interaction between sloshing liquid, multi-containers and moving ship. Owing to the ship motion, stresses and deformations as well as sloshing of liquid in the containers are induced which in turn produce external stress resultants that affect the ship motion. The governing equations for this complicated liquid-container-ship interaction problem are developed. Several parameters of interests that affect the vibration response of the coupled system are investigated. These include the container parameters, levels of liquid, number and location of containers on the moving ship, environmental settings and thrusters modeling.

Chapter 6 addresses the issue of sloshing reduction and examines the effectiveness of some methods for mitigating sloshing and its effects on ship-storage containers.

Chapter 7 presents a summary of the key research findings and recommendations for future studies.

CHAPTER 2 LIQUID-TANK COUPLED SYSTEM

2.1 Introduction

The free vibration characteristics of liquid-filled containers are important when designing these structures against induced excitation caused by earthquakes in the case of ground supported containers, and by ship motions and moving vehicles in the case of containers used for the transportation of fluid through such vessels. Since the early 1950s, the sloshing analysis of liquid storage tanks was carried out by methods that assumed the tank is a rigid body. Perhaps, the most notable of these methods is that proposed by Housner (1967), which has been widely adopted for the design of structures containing fluids such as water tanks and fuel containers. In his approach, simplified expressions for approximating the pressure caused by the portion of the liquid that accelerates with the tank and the pressure caused by the portion of the liquid that sloshes within the tank were developed. By adapting Housner's work, Epstein (1976) presented design curves for estimating the maximum bending and overturning moments for cylindrical containers as well as for rectangular rigid containers. However, these foregoing methods omitted the interaction between the fluid and structure. This may end up with an unsafe structure, especially if resonance occurs.

Vibration analyses of fluid-structure interaction problems have received much attention from researchers and engineers. Various approaches have been proposed to solve the problem. For example, Balendra and Nash (1978, 1980) tackled the fluid sloshing-container interaction problem by developing an axisymmetric thin shell element with two nodes. Each node has four degrees of freedom. However, the effect

of liquid sloshing was neglected due to serious numerical difficulties in solving the coupled equations of liquid and shell motion. As a result of this over simplification, an "added mass" was introduced to model the effects of the contained liquid. Ang (1980) extended Balendra and Nash's work to incorporate the effects of liquid sloshing by using a coupling matrix for the shell and fluid elements. Following this line of investigation, To and Wang (1991) and Subhash and Bhattacharyya (1996) employed the finite element method (FEM) that made use of two-node thin elastic shell and eight-node fluid elements for the coupled vibration analysis of the liquid-filled cylindrical containers. Analytical solutions for the free vibration of cylindrical containers based on Sanders' shell theory were obtained by Kyeong and Seong (1998). Loy and Lam (1999) analyzed thick circular cylindrical containers on the basis of three-dimensional theory of elasticity. In the study, the structure was divided into a number of thin cylindrical layers in the thickness direction, which is similar in concept to the finite strip method. Recently, Amabili (2000) employed the Rayleigh-Ritz method to study the vibration of simply supported, circular cylindrical shells that are partially-filled with an incompressible sloshing liquid. In particular, the Rayleigh quotient is transformed into a simpler expression where the potential energies of the compressible fluid and free surface waves do not appear. Cho et al. (2002a) carried out analytical and numerical studies on the free vibration of fluid-structure interaction problems considering the fluid compressibility. In their study, the Novozhilov thin shell theory was used to split the structure region into wet and dry parts. Frandsen (2004) explored the behavior of liquid motions in a forced tank prescribed to move simultaneously in both horizontal and vertical directions.

The aforementioned numerical and analytical studies however treated only thin cylindrical shells. When the shell is thick, the effect of transverse shear deformation has to be allowed for since the effect becomes significant and causes the shell to deform more. Ma et al. (2005, 2006) formulated a new RD-solid element that is based on the concept of relative displacement. A major advantage of this element lies in its ability to handle laminated composite structures because the element does not only consider shear flexibility but also models layer-wise in-plane displacement of the laminated composite structure. Furthermore, the RD-solid element can be applied to handle both thin and thick shell structures using a single formulation.

2.2 Problem definition

Consider a liquid-filled cylindrical container of height H, radius R, thickness of tank wall h and supported on a rigid base slab as shown in Figure 2.1. The tank wall has a mass density ρ_s and the container contains a liquid of height H_f. The liquid in the container is assumed to be incompressible, inviscid and irrotational with mass density ρ_f.

The problem at hand is to focus on the modelling and analysis of the coupled interaction problem between the fluid and container wall in the liquid-filled cylindrical containers. The axisymmetric shell and fluid elements are developed on the basis of the proposed relative displacement concept, which will be discussed in detail in the following section.

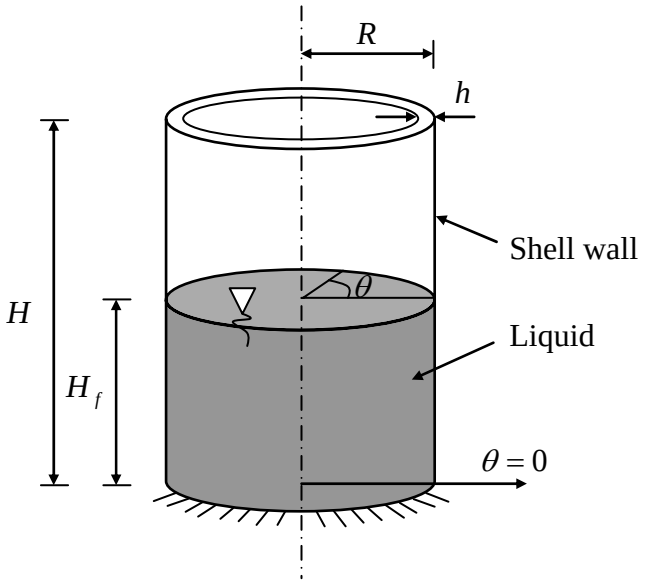

Figure 2.1 The liquid-filled cylindrical container

2.3 Finite element formulation and modelling of tank wall

The solid shell element proposed by Ma et al. (2005, 2006) will be extended to model the shell-fluid structure. This solid element is developed on the basis of the relative displacement (RD) concept. The proposed axisymmetric RD-shell element as shown in Figure 2.2 comprises three nodes per element with each node having five degrees of freedom (three absolute displacements u, v, w and two relative displacements Δu, Δv). The reference surface used in the formulation of the proposed axisymmetric RD-shell is taken to be at the middle surface of the shell.

In Figure 2.3, the black nodes denote the absolute mid-surface displacement components u, v, w in the meridional, circumferential and normal directions, respectively. The white nodes denote the displacement components at the inner/outer surface of the shell relative to the corresponding displacements at the mid-surface. These are termed the relative displacement components Δu, Δv. The absence of Δw is due to the kinematics assumption that there is no normal strain. Further, the relative

displacements Δu, Δv of the inner/outer surface are considered to be equal in magnitude but opposite in directions.

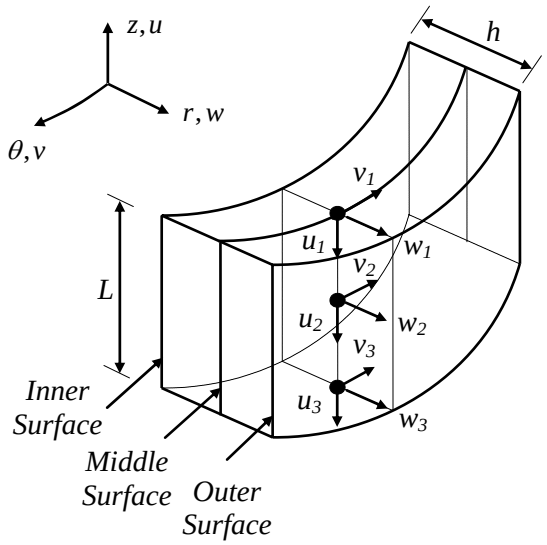

Figure 2.2 Proposed axisymmetric RD-shell element

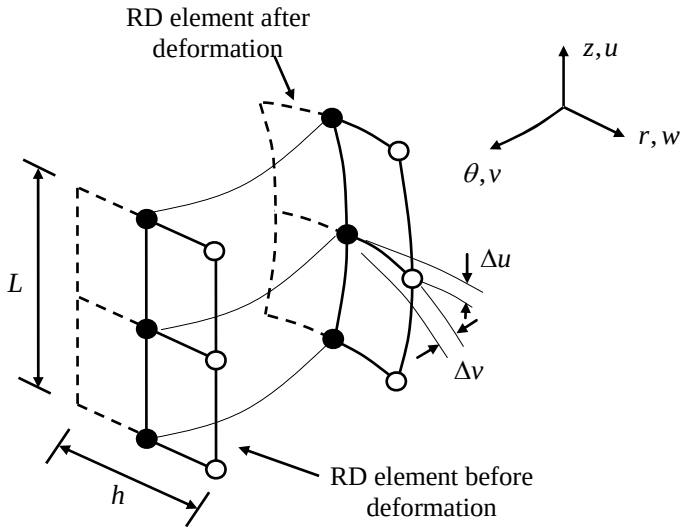

Black nodes: absolute displacements DOFs u, v, w
White nodes: relative displacements DOFs Δu, Δv

Figure 2.3 Deformation of RD-shell element

2.3.1 Basic assumptions of RD-shell concept

The Mindlin shell theory, which allows for the effect of transverse shear deformation, offers an attractive alternative to the classical thin shell theory of Kirchhoff-Love (Love, 1944). The assumptions made in this Mindlin shell theory are as follows

- Displacements are small compared with the shell thickness.
- Plane sections through a shell, normal to the middle surface, will remain plane but not necessarily normal to the deformed middle surface.
- The normal stresses σ_z transverse to the middle surface are small and can be neglected.

2.3.2 Axisymmetric single-layer RD-shell

The axisymmetric shell domain contains only one homogeneous isotropic material, whose properties are symmetrical with respect to the reference surface. The displacement functions adopted for the proposed RD-shell element are extended from the formulations used by Ernest et al. (2003). They are given by

$$u(r,\theta,z)=\sum_{n=0}^{\infty}\left[u_n(z)+\Delta u_n(r)\right]\cos(n\theta) \tag{2.1}$$

$$v(r,\theta,z)=\sum_{n=0}^{\infty}\left[v_n(z)+\Delta v_n(r)\right]\sin(n\theta) \tag{2.2}$$

$$w(z,\theta)=\sum_{n=0}^{\infty}\left[w_n(z)\right]\cos(n\theta) \tag{2.3}$$

where

$$u_n(z)=\sum_{i=1}^{3}N_i u_{in}(z),\qquad v_n(z)=\sum_{i=1}^{3}N_i v_{in}(z),\qquad w_n(z)=\sum_{i=1}^{3}N_i w_{in}(z) \tag{2.4}$$

$$\Delta u_n(r) = \sum_{i=1}^{3} \frac{2h_i}{h} N_i \Delta u_{in}(r), \quad \Delta v_n(r) = \sum_{i=1}^{3} \frac{2h_i}{h} N_i \Delta v_{in}(r), \quad h_i = \left[-\frac{h}{2}, \frac{h}{2} \right] \tag{2.5}$$

and n is the circumferential wave number; N_i and h_i the shape function and thickness at node i, respectively; Δu_{in} and Δv_{in} the relative displacements along the meridional and circumferential directions, respectively; and u_{in}, v_{in}, w_{in} the absolute mid-surface displacements along the meridional, circumferential and normal directions, respectively.

2.3.3 Axisymmetric multi-layer RD-shell

Consider a shell wall that is composed of N different isotropic layers as shown in Figure 2.4.

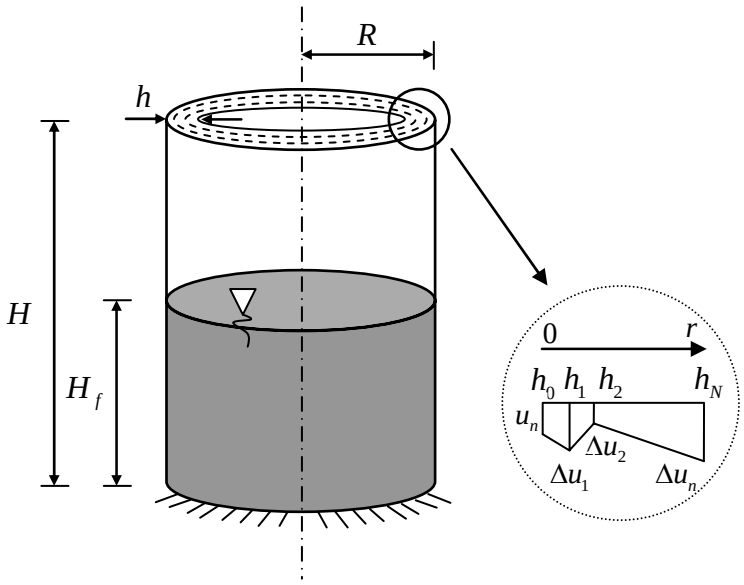

Figure 2.4 Axisymmetric multi-layer RD shell

The displacement functions in the k^{th} layer of the axisymmetric multi-layer RD-shell element can be written as

$$u(r,\theta,z)=\sum_{n=0}^{\infty}\left[u_n(z)+\frac{h_k-h(r)}{h_k-h_{k-1}}\Delta u(r)_{(k-1)}+\frac{h(r)-h_{k-1}}{h_k-h_{k-1}}\Delta u(r)_{(k)}\right]\cos(n\theta) \quad (2.6)$$

$$v(r,\theta,z)=\sum_{n=0}^{\infty}\left[v_n(z)+\frac{h_k-h(r)}{h_k-h_{k-1}}\Delta v(r)_{(k-1)}+\frac{h(r)-h_{k-1}}{h_k-h_{k-1}}\Delta v(r)_{(k)}\right]\sin(n\theta) \quad (2.7)$$

$$w(z,\theta)=\sum_{n=0}^{\infty}\left[w_n(z)\right]\cos(n\theta) \quad (2.8)$$

where $h_{k-1}\le h(r)\le h_k$ and

$$u_n(z)=\sum_{i=1}^{3}N_i u_{in}(z),\qquad v_n(z)=\sum_{i=1}^{3}N_i v_{in}(z),\qquad w_n(z)=\sum_{i=1}^{3}N_i w_{in}(z) \quad (2.9)$$

$$\Delta u(r)_{(k)}=\sum_{i=1}^{3}N_i\Delta u(r)_{i(k)},\qquad \Delta u(r)_{(k-1)}=\sum_{i=1}^{3}N_i\Delta u(r)_{i(k-1)} \quad (2.10)$$

$$\Delta v(r)_{(k)}=\sum_{i=1}^{3}N_i\Delta v(r)_{i(k)},\qquad \Delta v(r)_{(k-1)}=\sum_{i=1}^{3}N_i\Delta v(r)_{i(k-1)} \quad (2.11)$$

and n is the circumferential wave number; u, v and w the displacements along the meridional, circumferential and normal directions, respectively; u_n, v_n and w_n the displacement components at the inner (or reference) surface; $\Delta u_{(k)}$ and $\Delta v_{(k)}$ the relative displacements of the top of k^{th} layer along the meridional and circumferential directions with respect to the reference surface, respectively; and N_i the shape function at node i. It should be noted that $h(r)$ is a local coordinate in the r direction which is perpendicular to the tangent surface at any point in the shell element and h_0 is

set to zero. The subscript k denotes the layer number and $\Delta u_{(0)}$, $\Delta v_{(0)}$ are equal to zeros, which means the RD at the same location is zero, as should be the case. The formulations of the displacement functions for the two-layer cylindrical containers will next be developed in detail as a special case.

Special case: Two-layer cylindrical containers

The displacement functions for an axisymmetric RD-shell element comprising two different material layers can be expressed as

- For the first layer

$$u(r,\theta,z)=\sum_{n=0}^{\infty}\left[u_n(z)+\frac{h(r)}{h_1}\Delta u(r)_{(1)}\right]\cos(n\theta) \tag{2.12}$$

$$v(r,\theta,z)=\sum_{n=0}^{\infty}\left[v_n(z)+\frac{h(r)}{h_1}\Delta v(r)_{(1)}\right]\sin(n\theta) \tag{2.13}$$

$$w(z,\theta)=\sum_{n=0}^{\infty}\left[w_n(z)\right]\cos(n\theta) \text{ where } 0\le h(r)\le h_1 \tag{2.14}$$

- For the second layer

$$u(r,\theta,z)=\sum_{n=0}^{\infty}\left[u_n(z)+\frac{h_2-h(r)}{h_2-h_1}\Delta u(r)_{(1)}+\frac{h(r)-h_1}{h_2-h_1}\Delta u(r)_{(2)}\right]\cos(n\theta) \tag{2.15}$$

$$v(r,\theta,z)=\sum_{n=0}^{\infty}\left[v_n(z)+\frac{h_2-h(r)}{h_2-h_1}\Delta v(r)_{(1)}+\frac{h(r)-h_1}{h_2-h_1}\Delta v(r)_{(2)}\right]\sin(n\theta) \tag{2.16}$$

$$w(z,\theta)=\sum_{n=0}^{\infty}\left[w_n(z)\right]\cos(n\theta) \text{ where } h_1\le h(r)\le h_2 \tag{2.17}$$

2.3.4 Stiffness and mass matrices of axisymmetric RD-shell element

The displacement parameters associated with the RD-shell element are

$$\mathbf{q}_{in} = \left\{u_{in}, v_{in}, w_{in}, \Delta u_{in}, \Delta v_{in}\right\}^T \tag{2.18}$$

where $\mathbf{q}_{in}$ is the nodal displacement vector of the RD-shell element.

In the r and z directions of the coordinate systems as shown in Figure 2.5, the displacement components u_s and w_s may be expressed in terms of the global displacements u, Δu and w as

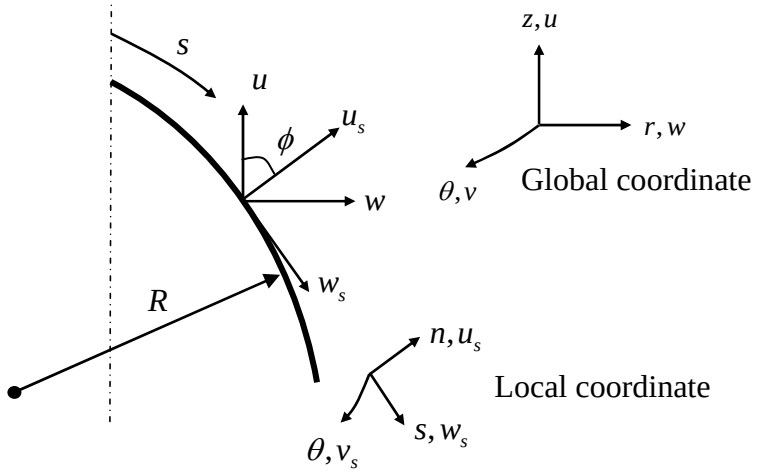

Figure 2.5 The coordinate systems

$$u_s = \left(u + \Delta u\right)\cos\phi - w\sin\phi \tag{2.19}$$

and

$$w_s = \left(u + \Delta u\right)\sin\phi + w\cos\phi \tag{2.20}$$

where u_s, v_s and w_s are the displacement components in the local n, θ and s directions, respectively and ϕ the angle between the r and s axes.

From geometrical considerations, the angle ϕ is related to the radius of curvature R by

$$\frac{d\phi}{ds} = -\frac{1}{R} \tag{2.21}$$

In the membrane strain matrix $\boldsymbol{\varepsilon}_m = \left[\varepsilon_s, \varepsilon_\theta, \gamma_{s\theta}\right]^T$, the strain ε_s in the s direction can be written in terms of the local displacements as

$$\varepsilon_s = \frac{\partial w_s}{\partial s} + \frac{u_s}{R} \tag{2.22}$$

or in terms of global displacements as

$$\varepsilon_s = \frac{\partial w}{\partial s}\cos\phi + \frac{\partial\left(u + \Delta u\right)}{\partial s}\sin\phi \tag{2.23}$$

The circumferential strain ε_θ in the θ direction may be written as

$$\varepsilon_\theta = \left(w_s \cos\phi - u_s \sin\phi + \frac{\partial\left(v + \Delta v\right)}{\partial\theta} \right)\frac{1}{r} \tag{2.24}$$

or in terms of global displacements as

$$\varepsilon_\theta = \left(w + \frac{\partial\left(v + \Delta v\right)}{\partial\theta} \right)\frac{1}{r} \tag{2.25}$$

In a similar manner, the in-plane shear strain $\gamma_{s\theta}$ may be expressed as

$$\gamma_{s\theta} = \left(\frac{\partial w_s}{\partial \theta} - (v + \Delta v)\cos\phi \right) \frac{1}{r} + \frac{\partial (v + \Delta v)}{\partial s} \tag{2.26}$$

or

$$\gamma_{s\theta} = \left(\frac{\partial w}{\partial \theta}\cos\phi + \frac{\partial (u + \Delta u)}{\partial \theta}\sin\phi - (v + \Delta v)\cos\phi \right) \frac{1}{r} + \frac{\partial (v + \Delta v)}{\partial s} \tag{2.27}$$

In the bending strain matrix $\boldsymbol{\varepsilon}_b = \left[\kappa_s, \kappa_\theta, \kappa_{s\theta} \right]^T$, the curvature κ_s in the s direction can be written in terms of the local displacements as

$$\kappa_s = -\frac{2}{h}\frac{\partial \Delta u}{\partial s} \tag{2.28}$$

The circumferential curvature κ_θ in the θ direction may be expressed as

$$\kappa_\theta = -\frac{2}{h}\left(\frac{\partial \Delta v}{\partial \theta} + \Delta u \cos\phi \right) \frac{1}{r} \tag{2.29}$$

The twisting curvature $\kappa_{s\theta}$ is given by

$$\kappa_{s\theta} = \left(-\frac{2}{h}\frac{\partial \Delta u}{\partial \theta} + \frac{2}{h}\Delta v \cos\phi + \frac{\partial (v + \Delta v)}{\partial s}\sin\phi \right) \frac{1}{r} - \frac{2}{h}\frac{\partial \Delta v}{\partial s} + \frac{\partial w_s}{\partial \theta}\frac{1}{rR} \tag{2.30}$$

or

$$\begin{aligned} \kappa_{s\theta} = & \left(-\frac{2}{h}\frac{\partial \Delta u}{\partial \theta} + \frac{2}{h}\Delta v \cos\phi + \frac{\partial (v + \Delta v)}{\partial s}\sin\phi \right) \frac{1}{r} \\ & - \frac{2}{h}\frac{\partial \Delta v}{\partial s} - \frac{d\phi}{ds}\left(\frac{\partial w}{\partial \theta}\cos\phi + \frac{\partial (u + \Delta u)}{\partial \theta}\sin\phi \right) \frac{1}{r} \end{aligned} \tag{2.31}$$

In the transverse shear strain matrix $\boldsymbol{\varepsilon}_s = \left[\gamma_{s\theta}, \gamma_{\theta\theta}\right]^T$, the transverse shear strain $\gamma_{s\theta}$ in the s-θ plane can be written in term of local displacements as

$$\gamma_{s\theta} = \frac{\partial u_s}{\partial s} - \frac{2}{h}\Delta u - \frac{w_s}{R} \tag{2.32}$$

or

$$\gamma_{s\theta} = -\frac{\partial w}{\partial s}\sin\phi + \frac{\partial\left(u + \Delta u\right)}{\partial s}\cos\phi - \frac{2}{h}\Delta u \tag{2.33}$$

The longitudinal transverse shear strain $\gamma_{\theta\theta}$ in the θ-θ plane is

$$\gamma_{\theta\theta} = \left(\frac{\partial u_s}{\partial \theta} + \left(v + \Delta v\right)\sin\phi\right)\frac{1}{r} - \frac{2}{h}\Delta v \tag{2.34}$$

or

$$\gamma_{\theta\theta} = \left(-\frac{\partial w}{\partial \theta}\sin\phi + \frac{\partial\left(u + \Delta u\right)}{\partial \theta}\cos\phi + \left(v + \Delta v\right)\sin\phi\right)\frac{1}{r} - \frac{2}{h}\Delta v \tag{2.35}$$

Therefore, the membrane strain matrix has the form

$$\mathbf{B}_{mi}^{n} = \left[\begin{array}{c|c|c|c|c} \frac{dN_i}{ds}C_n\cos\phi & 0 & \frac{dN_i}{ds}C_n\sin\phi & \frac{dN_i}{ds}C_n\cos\phi & 0 \\ \hline \frac{N_i}{r}C_n & n\frac{N_i}{r}C_n & 0 & \frac{N_i}{r}C_n & n\frac{N_i}{r}C_n \\ \hline -n\frac{N_i}{r}S_n\cos\phi & \left(\frac{dN_i}{ds} - \frac{N_i}{r}\cos\phi\right)S_n & -n\frac{N_i}{r}S_n\sin\phi & -n\frac{N_i}{r}S_n\cos\phi & \left(\frac{dN_i}{ds} - \frac{N_i}{r}\cos\phi\right)S_n \end{array}\right]_{3\times 5} \tag{2.36}$$

The bending strain matrix can be written as

$$\mathbf{B}_{bi}^{n}=\left[\begin{array}{c|c|c|c|c} 0 & 0 & 0 & -\frac{2}{h}\frac{dN_i}{ds}C_n & 0 \\ \hline 0 & 0 & 0 & -\frac{2}{h}\frac{N_i}{r}C_n\cos\phi & -n\frac{2}{h}\frac{N_i}{r}C_n \\ \hline -n\frac{N_i}{r}\frac{S_n}{R}\cos\phi & \frac{dN_i}{ds}\frac{1}{r}S_n\sin\phi & -n\frac{N_i}{r}\frac{S_n}{R}\sin\phi & n\frac{2}{h}\frac{N_i}{r}S_n-n\frac{N_i}{r}\frac{S_n}{R}\cos\phi & \frac{2}{h}\left(\frac{N_i}{r}\cos\phi-\frac{dN_i}{ds}\right)S_n+\frac{dN_i}{ds}\frac{1}{r}S_n\sin\phi \end{array}\right]_{3\times5} \tag{2.37}$$

The transverse shear strain matrix can be expressed as

$$\mathbf{B}_{si}^{n}=\left[\begin{array}{c|c|c|c|c} -\frac{dN_i}{ds}C_n\sin\phi & 0 & \frac{dN_i}{ds}C_n\cos\phi & -\frac{2}{h}N_iC_n-\frac{dN_i}{ds}C_n\sin\phi & 0 \\ \hline n\frac{N_i}{r}S_n\sin\phi & \frac{N_i}{r}S_n\sin\phi & -n\frac{N_i}{r}S_n\cos\phi & n\frac{N_i}{r}S_n\sin\phi & -\frac{2}{h}N_iS_n+\frac{N_i}{r}S_n\sin\phi \end{array}\right]_{3\times5} \tag{2.38}$$

in which $C_n=\cos(n\theta)$ and $S_n=\sin(n\theta)$.

By making use of the orthogonal property of trigonometric functions, one obtains the following shell element mass $\mathbf{M}_s^e$ and stiffness $\mathbf{K}_s^e$ matrices

$$\mathbf{M}_s^e=\int_V \mathbf{N}_s^T\mathbf{P}\mathbf{N}_s dV \tag{2.39}$$

$$\mathbf{K}_s^e=\int_V \left(\mathbf{B}_m^T\mathbf{D}_m\mathbf{B}_m+\mathbf{B}_b^T\mathbf{D}_b\mathbf{B}_b+\mathbf{B}_s^T\mathbf{D}_s\mathbf{B}_s\right)dV \tag{2.40}$$

where $\mathbf{N}_s$ is the shape function matrix of shell element; $\mathbf{P}$ the density matrix of the material; $\mathbf{B}_m$, $\mathbf{B}_b$, $\mathbf{B}_s$ the membrane, bending and transverse shear strain matrices, respectively; and $\mathbf{D}_m$, $\mathbf{D}_b$, $\mathbf{D}_s$ the matrices of membrane, flexural and shear rigidities, respectively. The detail formulations of these matrices for RD-shell element can be found in Appendix A.

The equation of motion of the shell can be written as

$$\mathbf{M}_s\ddot{\mathbf{q}} + \mathbf{K}_s\mathbf{q} = \mathbf{f} \tag{2.41}$$

where $\ddot{\mathbf{q}}$ and $\mathbf{q}$ are the generalized nodal accelerations and displacements of shell, respectively; and $\mathbf{f}$ the generalized force vector.

By solving the eigenvalue problem of Eq. (2.41) with the force vector set to 0, one obtains the natural frequencies of an empty shell container.

2.4 Finite element formulation and modelling of liquid

2.4.1 Basic equations

The following assumptions on the liquid motion are made in the formulation of the axisymmetric fluid element: (1) the liquid is inviscid and incompressible, (2) the flow is irrotational and has no source or sink, (3) the sloshing is of only small amplitude. In view of these assumptions, the potential flow theory can be used to derive the governing equation of liquid motion inside the tank which satisfies the Laplace equation as follows

$$\nabla^2 P\left(r,\theta,z\right) = 0 \tag{2.42}$$

where ∇^2 is the Laplacian operator in cylindrical coordinates and $P = P_s + P_d$ the total pressure, in which P_s and P_d are the static pressure and dynamic pressure due to motion of liquid inside the tank, respectively.

The Bernoulli equation is of the form

$$-\frac{\partial\Phi}{\partial t} + \frac{1}{2}\left(u_z^2 + u_r^2\right) + \frac{P}{\rho_f} + gz = 0 \tag{2.43}$$

where Φ is the liquid velocity potential; z the axial coordinate of any point in the liquid with the origin at the free surface; u_z and u_r the velocity components of the fluid element and are given by

$$u_z = -\frac{\partial \Phi}{\partial z}, \qquad u_r = -\frac{\partial \Phi}{\partial r} \tag{2.44}$$

For small amplitude liquid motion, the velocity components are small in comparison with the other terms and thus they may be neglected (Dean and Dalrymple, 1991). Eq. (2.43) may then be simplified to

$$-\frac{\partial \Phi}{\partial t} + \frac{P}{\rho_f} = 0 \tag{2.45}$$

2.4.2 Boundary conditions

2.4.2.1 Kinematics free surface boundary condition

At the liquid free surface, the vertical velocity component of liquid can be expressed as

$$u_z(r,\theta,z) = \frac{d\eta(r,\theta,z,t)}{dt} \text{ at } z = 0 \tag{2.46}$$

in which $\eta(r,\theta,z,t)$ is the displacement of the free surface measured with respect to the horizontal plane $z = 0$ and is given by

$$\eta = \frac{1}{g}\frac{\partial \Phi}{\partial t}\bigg|_{z=0} \tag{2.47}$$

From Eq. (2.44), the vertical velocity component can be expressed as

$$u_z(r,\theta,z) = -\frac{\partial \Phi}{\partial z} \text{ at } z = 0 \tag{2.48}$$

By substituting Eq. (2.47) into Eqs. (2.46) and (2.48), one obtains

$$\frac{1}{g}\frac{\partial^2\Phi}{\partial t^2}+\left.\frac{\partial\Phi}{\partial z}\right|_{z=0}=0 \tag{2.49}$$

In view of Eq. (2.45), Eq. (2.49) may be expressed in terms of the pressure P by

$$\frac{1}{g}\frac{\partial^2 P}{\partial t^2}+\left.\frac{\partial P}{\partial z}\right|_{z=0}=0 \tag{2.50}$$

2.4.2.2 Boundary condition at the tank bottom

At the bottom of the tank, the velocity component of liquid normal to the rigid base is zero, i.e.

$$u_z=-\left.\frac{\partial\Phi}{\partial z}\right|_{z=-H_f}=0 \tag{2.51}$$

Eq. (2.51) may be expressed in terms of P as

$$\left.\frac{\partial P}{\partial z}\right|_{z=-H_f}=0 \tag{2.52}$$

2.4.2.3 Interface between liquid and shell

At the liquid-tank wall interface, the velocity of liquid and shell elements in the normal direction must be the same, i.e.

$$u_r=-\left.\frac{\partial\Phi}{\partial r}\right|_{r=R}=\left.\frac{\partial w}{\partial t}\right|_{r=R} \tag{2.53}$$

where w is the middle-surface displacement along the normal direction of shell elements.

By substituting Eq. (2.53) into Eq. (2.45), one obtains

$$\frac{\partial^2 w}{\partial t^2} + \frac{1}{\rho_f}\frac{\partial P}{\partial r}\bigg|_{r=R} = 0 \tag{2.54}$$

2.4.3 Stiffness, mass and liquid-shell coupling force matrices

The finite element matrix equation for the liquid can be derived by applying Hamilton's principle (Zienkiewicz, 1971 and Bathe, 1996). The Lagrangian functional I can be defined as

$$I = \int_{t_1}^{t_2} \left(T - \Pi - W_p\right) dt \tag{2.55}$$

in which T and Π are the kinetic and potential energies of the liquid, respectively, and W_p the potential of the external forces. These terms are given by Hsiung and Weingarten (1973) as

$$T = \frac{1}{2}\rho_f \int_{V_f} \nabla\Phi\nabla\Phi dV \tag{2.56}$$

$$\Pi = \frac{1}{2}\int_{S_f} \eta\left(\rho_f g\eta\right) dS \tag{2.57}$$

$$W_p = \int_{S_i} \rho_f \left(\frac{\partial w}{\partial t}\right)\Phi dS \tag{2.58}$$

where V_f is the volume of liquid; S_f the free surface of liquid; S_i the liquid-tank interface and ρ_f the density of liquid.

In view of the governing equation given by Eq. (2.42) and the boundary conditions expressed in Eqs. (2.50), (2.52) and (2.54), the Lagrangian functional I in Eq. (2.55) can be expressed as (Hsiung and Weingarten, 1973)

$$I = \int_{t_1}^{t_2} \left[\frac{1}{2} \int_{V_f} \nabla P \bullet \nabla P dV - \frac{1}{2g} \int_{S_f} \left(\frac{\partial P}{\partial t} \right)^2 ds - \rho_f \int_{S_i} P \frac{\partial^2 w}{\partial t^2} ds \right] dt \tag{2.59}$$

The liquid in the cylindrical tank is discretized into annular elements of rectangular cross-sections (Balendra et al., 1982a). These elements may be considered to be formed from the intersection of concentric annular cylindrical surfaces with a set of horizontal planes. The pressures of the inviscid, incompressible liquid are expressed in terms of harmonic functions which are required to satisfy the boundary conditions. In particular, the liquid dynamic pressure P is expanded by Fourier series in the circumferential angle θ as

$$P(r,\theta,z) = \sum_n \bar{P}_n(r,\theta,z) \cos(n\theta) \tag{2.60}$$

where $\bar{P}_n(r,\theta,z)$ is the amplitude of the dynamic pressure corresponding to the n^{th} circumferential harmonic number.

By using the plane with $\theta = 0$, the 3-D problem has been reduced to a 2-D one. Therefore, the subscript $\theta = 0$ will be omitted for brevity in the formulations of dynamic pressure. Figure 2.6 shows a typical incompressible, inviscid and irrotational liquid element with dimensions $2a$ and $2b$ in the radial and axial directions, respectively. The center of the liquid element is located at a distance x_0 from the geometric axis of the tank.

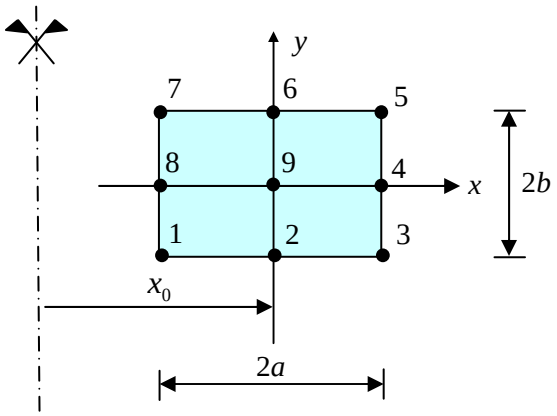

Figure 2.6 Liquid element with nine nodes

The liquid pressure at any point in the xy plane, which is described in terms of surrounding nodal pressures, is given by

$$\bar{P}(x,y) = \mathbf{N}_f \mathbf{p}_e \tag{2.61}$$

where $\mathbf{N}_f$ is the liquid element shape function and $\mathbf{p}_e$ the element nodal pressure vector.

The shape function matrix for the nine-node liquid element can be written as

$$\mathbf{N}_f = \begin{bmatrix} N_1 \\ N_2 \\ N_3 \\ N_4 \\ N_5 \\ N_6 \\ N_7 \\ N_8 \\ N_9 \end{bmatrix}^T = \begin{bmatrix} \frac{1}{4}(1-\xi)(1-\eta)-\frac{1}{4}(1-\xi)(1-\eta^2)-\frac{1}{4}(1-\xi^2)(1-\eta)+\frac{1}{4}(1-\xi^2)(1-\eta^2) \\ \frac{1}{2}(1-\xi^2)(1-\eta)-\frac{1}{2}(1-\xi^2)(1-\eta^2) \\ \frac{1}{4}(1+\xi)(1-\eta)-\frac{1}{4}(1-\xi^2)(1-\eta)-\frac{1}{4}(1+\xi)(1-\eta^2)+\frac{1}{4}(1-\xi^2)(1-\eta^2) \\ \frac{1}{2}(1+\xi)(1-\eta^2)-\frac{1}{2}(1-\xi^2)(1-\eta^2) \\ \frac{1}{4}(1+\xi)(1+\eta)-\frac{1}{4}(1-\xi^2)(1+\eta)-\frac{1}{2}(1+\xi)(1-\eta^2)+\frac{1}{4}(1-\xi^2)(1-\eta^2) \\ \frac{1}{2}(1-\xi^2)(1+\eta)-\frac{1}{2}(1-\xi^2)(1-\eta^2) \\ \frac{1}{4}(1-\xi)(1+\eta)-\frac{1}{4}(1-\xi^2)(1+\eta)-\frac{1}{4}(1-\xi)(1-\eta^2)+\frac{1}{4}(1-\xi^2)(1-\eta^2) \\ \frac{1}{2}(1-\xi)(1-\eta^2)-\frac{1}{2}(1-\xi^2)(1-\eta^2) \\ (1-\xi^2)(1-\eta^2) \end{bmatrix}^T_{9\times 1} \tag{2.62}$$

where $\xi = x/a$ and $\eta = y/b$.

From the previous section, the radial displacement amplitude of shell element can be written in terms of the nodal displacement as

$$w = \mathbf{N}_s^w \mathbf{q}_e \tag{2.63}$$

where $\mathbf{N}_s^w$ is shape function corresponding to radial displacement of the shell, details of which are given in Appendix A. The shape function may be expressed as

$$\mathbf{N}_s^w = \begin{bmatrix} 0 & 0 & N_{1w} & N_{1\Delta u} & 0 & 0 & 0 & N_{2w} & N_{2\Delta u} & 0 & 0 & 0 & N_{3w} & N_{3\Delta u} & 0 \end{bmatrix}_{1\times 15} \tag{2.64}$$

By substituting Eqs. (2.60), (2.61) and (2.63) into the integral defined in Eq. (2.59), one obtains the Lagrangian functional as

$$I = \int_{t_1}^{t_2} \left[\rho_f \left(\frac{1}{2} \mathbf{p}^T \mathbf{K}_f \mathbf{p} - \frac{1}{2} \dot{\mathbf{p}}^T \mathbf{M}_f \dot{\mathbf{p}} + \mathbf{p}^T \mathbf{S} \ddot{\mathbf{q}} \right) \right] dt \tag{2.65}$$

where the fluid element stiffness matrix $\mathbf{K}_f^e$ and mass matrix $\mathbf{M}_f^e$ can be obtained from the integration over the liquid volume V_f and the liquid free surface S_f, respectively (Balendra et al., 1980 and 1982a). The liquid-shell coupling force matrix $\mathbf{S}_e$ accounting for the fluid-structure interaction can be found by integrating over the liquid-shell interface S_i. Details of the derivation of these matrices can be found in Appendix A.

The fluid element stiffness matrix $\mathbf{K}_f^e$ can be expressed as

$$\mathbf{K}_f^e = \frac{\pi}{\rho_f} \int_{-a}^{a} \int_{-b}^{b} \left(\left[\frac{\partial \mathbf{N}_f}{\partial x} \right]^T \frac{\partial \mathbf{N}_f}{\partial x} + \left[\frac{\partial \mathbf{N}_f}{\partial y} \right]^T \frac{\partial \mathbf{N}_f}{\partial y} + \frac{n^2}{\left(x_0 + x \right)^2} \left[\mathbf{N}_f \right]^T \mathbf{N}_f \right) \left(x_0 + x \right) dxdy \tag{2.66}$$

The fluid element mass matrix $\mathbf{M}_f^e$ can be written as

$$\mathbf{M}_f^e = \frac{\pi}{\rho_f g}\int_{S_f}\left[\mathbf{N}_f\right]^T \mathbf{N}_f dS = \frac{\pi}{\rho_f g}\int_{-a}^{a}\left[\mathbf{N}_f^s\right]^T \mathbf{N}_f^s\left(x_0+x\right)dx \tag{2.67}$$

where $\mathbf{N}_f^s$ is the shape function of liquid element at the free surface ($\eta = 1$ or $y = b$) and is given by

$$\mathbf{N}_f^s = \left[\begin{array}{ccccccccc} 0 & 0 & 0 & 0 & \dfrac{\xi(1+\xi)}{2} & \left(1-\xi^2\right) & \dfrac{\xi(\xi-1)}{2} & 0 & 0 \end{array}\right]_{1\times 9} \tag{2.68}$$

Based on the RD concept, a coupling matrix is introduced to model the interaction between the shell and neighboring fluid elements. A typical liquid element in contact with a neighboring RD-shell element is shown in Figure 2.7. Three nodes of the fluid element, namely nodes 3, 4 and 5, are coupled to the three nodes, namely nodes i, j and k, of the shell element.

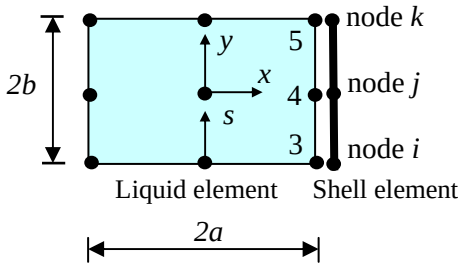

Figure 2.7 Liquid-shell coupling element

The element liquid-shell coupling matrix $\mathbf{S}^e$ based on RD concept is given by

$$\mathbf{S}^e = \pi R\int_{-b}^{b}\left[\mathbf{N}_f^i\right]^T \mathbf{N}_s^w dy \tag{2.69}$$

where $\mathbf{N}_f^i$ is the shape function for the liquid dynamic pressure at the liquid-shell interface ($\xi = 1$ or $x = a$) and can be written as

$$\mathbf{N}_f^i = \begin{bmatrix} 0 & 0 & \dfrac{\eta(\eta-1)}{2} & (1-\eta^2) & \dfrac{\eta(1+\eta)}{2} & 0 & 0 & 0 & 0 \end{bmatrix} \tag{2.70}$$

After integrating over the liquid-shell interface S_i, one obtains the element shell-liquid coupling force matrix based on the RD concept as

$$\mathbf{S}^e = \pi R b \left[\begin{array}{c|c|c|c|c|c} \dfrac{19}{70} & \dfrac{b}{35} & \dfrac{8}{105} & -\dfrac{8b}{105} & -\dfrac{1}{70} & 0 \\ \hline \dfrac{22}{105} & \dfrac{4b}{105} & \dfrac{32}{35} & 0 & \dfrac{22}{105} & -\dfrac{4b}{105} \\ \hline -\dfrac{1}{70} & 0 & \dfrac{8}{105} & \dfrac{8b}{105} & \dfrac{19}{70} & -\dfrac{b}{35} \end{array}\right]_{3\times 6} \begin{array}{l} \text{node}\,3 \\ \text{node}\,4 \\ \text{node}\,5 \end{array} \tag{2.71}$$

The equation of free vibration motion of liquid inside the container can be written as

$$\mathbf{M}_f \ddot{\mathbf{p}} + \mathbf{K}_f \mathbf{p} + \mathbf{S}\ddot{\mathbf{q}} = \mathbf{0} \tag{2.72}$$

2.5 Governing equation of liquid-tank coupled system

From Eq. (2.41), the equation of motion of the shell can be written as

$$\mathbf{M}_s \ddot{\mathbf{q}} + \mathbf{K}_s \mathbf{q} = \mathbf{f} \tag{2.73}$$

where $\mathbf{f}$ is the generalized force vector due to the dynamic pressure acting on the inner surface of container wall and can be expressed as

$$\mathbf{f} = \pi R \int_{S_i} \left[\mathbf{N}_f^s\right]^T \mathbf{N}_s^w \mathbf{p}\, dS = \mathbf{S}^T \mathbf{p} \tag{2.74}$$

By substituting Eq. (2.74) into Eq. (2.73), one obtains the following equation of motion of the shell with allowance for the interaction between the fluid and structure

$$\mathbf{M}_s\ddot{\mathbf{q}} + \mathbf{K}_s\mathbf{q} - \mathbf{S}^T\mathbf{p} = \mathbf{0} \tag{2.75}$$

By combining the equations of motion of the liquid (2.72) and the shell (2.75), the equation of motion of the coupled shell-liquid system may be written as

$$\begin{bmatrix} \mathbf{M}_s & \mathbf{0} \\ \mathbf{S} & \mathbf{M}_f \end{bmatrix} \begin{Bmatrix} \ddot{\mathbf{q}} \\ \ddot{\mathbf{p}} \end{Bmatrix} + \begin{bmatrix} \mathbf{K}_s & -\mathbf{S}^T \\ \mathbf{0} & \mathbf{K}_f \end{bmatrix} \begin{Bmatrix} \mathbf{q} \\ \mathbf{p} \end{Bmatrix} = \begin{Bmatrix} \mathbf{0} \\ \mathbf{0} \end{Bmatrix} \tag{2.76}$$

The natural frequencies and mode shapes of vibration of the coupled liquid-structure system can be obtained by solving Eq. (2.76).

If the sloshing effect of liquid is neglected, then the liquid mass matrix $\mathbf{M}_f$ corresponding to the free surface potential energy vanishes. In this case, the second row of Eq. (2.76) becomes

$$\mathbf{S}\ddot{\mathbf{q}} + \mathbf{K}_f\mathbf{p} = \mathbf{0} \tag{2.77}$$

or

$$\mathbf{p} = -\left[\mathbf{K}_f\right]^{-1}\mathbf{S}\ddot{\mathbf{q}} \tag{2.78}$$

By substituting Eq. (2.78) into the first row of Eq. (2.76), one obtains the following equation

$$\left(\mathbf{M}_s + \mathbf{S}^T\left[\mathbf{K}_f\right]^{-1}\mathbf{S}\right)\ddot{\mathbf{q}} + \mathbf{K}_s\mathbf{q} = \mathbf{0} \tag{2.79}$$

Equation (2.79) is the free vibration equation of liquid-filled containers and the mass matrix is now augmented by an "added mass matrix $\mathbf{S}^T\left[\mathbf{K}_f\right]^{-1}\mathbf{S}$" which represents the effect of the liquid inside the container.

2.6 Concluding remarks

A new three-node shell element and nine-node liquid element formulated on the basis of relative displacement concept have been presented in this chapter. The shell-liquid coupling matrix was also introduced to capture the interaction between the shell element and the neighbouring fluid element. The present method has the following important features: (1) the capability to model various forms of shell and liquid of liquid-filled axisymmetric containers with arbitrary support conditions and material parameters; (2) the formulation of the proposed RD-shell element employs only one set of equations for both thin and thick shells. Furthermore, the RD-shell element developed on the basis of relative displacement concept can be easily extended to multi-layered composite shells. The convergence, efficiency and accuracy of the proposed method using RD concept will be investigated in Chapter 3.

CHAPTER 3 FREE VIBRATION OF STORAGE CONTAINERS

3.1 Introduction

The dynamic interaction between the liquid and its shell container has been a subject of intense study, more so in recent years, due to the transportation of liquefied natural gas (LNG) in specially designed LNG vessels as well as the storage of LNG in floating terminals. Many studies on coupled liquid-container interaction have been carried out. However, most of the studies (that were reviewed in Chapter 2) adopted the classical thin shell theory for modeling the container, in which the effect of transverse shear deformation is ignored. Reddy (1984) showed that the application of the classical thin shell theory to multi-layer shells may result in 30% error when estimating the natural frequencies. His study concluded that the classical thin shell theory is highly inadequate in modeling thick shells and composite laminated shells. So far, vibration analyses of multi-layer shells have been carried out using different approaches. For example, Jing and Tzeng (1993) proposed a refined shear deformation theory for laminated shells by using an independently assumed transverse shear force field. A layer-wise modelling for free vibration of thick composite cylindrical shells was presented by Huang and Dasgupta (1995), who approximated the displacement field by finite element interpolation shape functions along the thickness direction. Chang and Chiou (1995) obtained the natural frequencies of clamped-clamped laminated cylindrical shells conveying fluid by using Hamilton's principle. Lam and Wu (1999) analyzed thick, rotating, cross-ply laminated composite cylindrical shells using the first

order shear deformation shell theory. The analytical solution considered the initial curvature in the stress-strain relationship. George and Pawel (2004) presented a refined theory for thick spherical shells. The results given in their approach incorporated the effects of transverse shear deformation, initial curvature and radial stress.

This chapter examines the efficiency and accuracy of the proposed RD concept, which was developed in Chapter 2, for the free vibration analysis of liquid-filled cylindrical containers. Numerous cases are considered to show the versatility and accuracy of the method in handling different kinds of materials, thickness-to-radius, container height-to-thickness ratios, number of layers, fiber orientations, levels of liquid-filling and boundary conditions of the containers such as clamped-free (C-F), simply supported-simply supported (S-S) and clamped-clamped (C-C). The free vibration behaviour of axisymmetric single and multi-layer cylindrical containers filled with and without liquid will be investigated. Results of natural frequencies are presented in the form of tables and figures for comparison purposes.

3.2 Axisymmetric single-layer RD shell

In this section, the free vibration analysis of single-layer cylindrical containers filled with and without liquid is carried out. The natural frequency obtained using the proposed RD concept is compared with available results in the literature. Both thin and thick shells are considered so as to illustrate the advantage of the RD concept in the finite element modelling of shells of any thickness in one single formulation.

3.2.1 Cylindrical containers without liquid

A comparison of natural frequencies of empty cylindrical containers obtained by the present method using the RD concept with those of other experimental and analytical methods is carried out for different boundary conditions, such as C-F, S-S and C-C.

The material properties and geometrical parameters for the C-F empty cylindrical containers are the same as those used by Naeem and Sharma (2000), which are shown in Table 3.1. The material properties and geometrical parameters for the S-S and C-C empty cylindrical containers are the same as those of the C-F containers, except for the height of container which is $H = 0.6096m$.

Table 3.1 Material and geometrical parameters of C-F empty cylindrical containers

H	Height of container	$0.6255\,m$
R	Radius of container	$0.2423\,m$
h	Thickness of container	$0.648\,mm$
ν	Poisson's ratio	0.315
E	Young's modulus	$68.95\,GPa$
ρ_s	Mass density of shell	$2714.5\,kg/m^3$

To calculate the natural frequencies of empty cylindrical containers, the number of axisymmetric shell elements N for modelling the container wall is varied from $N = 2$ to $N = 20$ as shown in Figure 3.1. The container wall is modeled with 1-D axisymmetric solid shell elements which were discussed in Chapter 2.

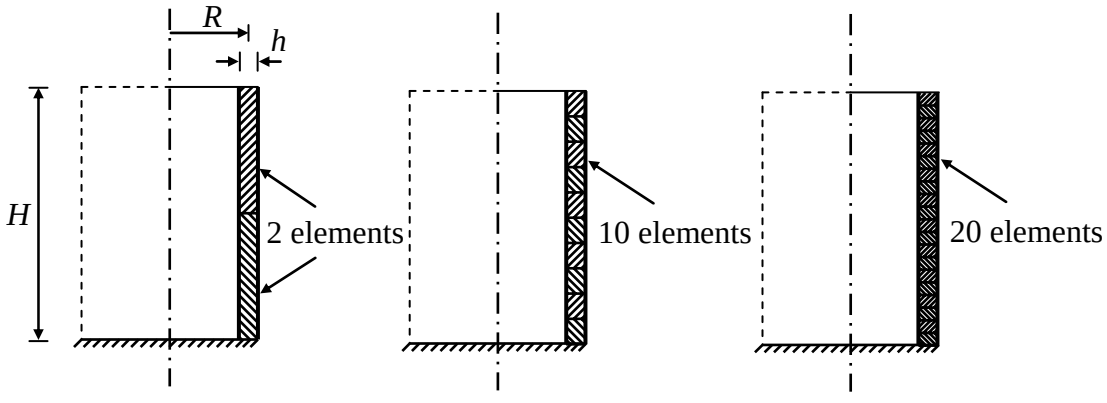

Figure 3.1 Number of 1-D axisymmetric shell elements of C-F empty cylindrical containers

Tables 3.2, 3.3 and 3.4 show the convergence characteristics of the RD-shell element for the vibration analysis of empty cylindrical containers with C-F, S-S and C-C boundary conditions, respectively. The results presented are the lowest frequency values for a given circumferential wave number n (from 2 to 15) and for different numbers of shell element $N = 2$, 5, 10, 20. One can observe that the convergence of natural frequencies is obtained rapidly as the number of axisymmetric shell elements increases. It can be seen that $N = 10$ will suffice for converged results of these containers. In addition, the fundamental frequency obtained depends on the type of the boundary condition and the circumferential wave number n. In particular, the fundamental frequency for the C-F cylindrical container is associated with $n = 5$. On the other hand, the fundamental frequencies are obtained with $n = 7$ and $n = 8$ for the S-S and C-C cylindrical containers, respectively.

Tables 3.2, 3.3 and 3.4 also present a comparison of the lowest natural frequencies of these containers obtained by the present RD-shell element with the numerical results obtained by Naeem and Sharma (2000) using the Ritz method and the experimental results obtained by Sewall and Naumann (1968). The excellent agreement of natural frequency results of the present study with those obtained experimentally and analytically for the empty containers with different boundary conditions is shown in these tables. Thereby, this study validated the proposed RD-shell elements in predicting the vibration behaviours of empty containers. It should be noted that the maximum error between the RD-shell element results and Ritz results is within 1% for the three cases of containers considered.

Table 3.2 Convergence and comparison of the lowest natural frequency of C-F empty cylindrical containers for a given circumferential wave number

Circumferential wave number n	Present study				Ritz results by Naeem and Sharma (2000)	Experimental results by Sewall and Naumann (1968)
	$N=2$	$N=5$	$N=10$	$N=20$		
2	321.58	317.80	317.26	317.18	318.71	-
3	171.40	168.61	168.26	168.21	169.12	157
4	110.19	108.19	107.96	107.92	108.47	107
5	**93.71**	**92.41**	**92.26**	**92.24**	**92.55**	**91**
6	105.72	104.94	104.82	104.81	105.05	102
7	133.99	133.44	133.32	133.31	133.60	130
8	171.73	171.25	171.11	171.10	171.45	166
9	216.37	215.88	215.71	215.70	216.09	208
10	266.99	266.44	266.24	266.23	266.69	260
11	323.26	322.63	322.39	322.38	322.92	317
12	385.03	384.31	384.02	384.01	384.62	374

Table 3.3 Convergence and comparison of the lowest natural frequency of S-S empty cylindrical containers for a given circumferential wave number

Circumferential wave number n	Present study				Ritz results by Naeem and Sharma (2000)	Experimental results by Sewall and Naumann (1968)
	$N=2$	$N=5$	$N=10$	$N=20$		
4	293.09	287.75	287.59	287.58	287.59	287
5	206.51	201.98	201.84	201.84	201.85	203
6	170.20	166.68	166.57	166.57	166.59	175
7	**168.68**	**166.29**	**166.21**	**166.20**	**166.22**	**169**
8	190.81	189.32	189.27	189.27	189.29	188
9	227.82	226.91	226.87	226.87	226.88	224
10	274.68	274.10	274.08	274.08	274.09	268
11	329.01	328.64	328.62	328.62	328.64	326
12	389.75	389.50	389.49	389.49	389.49	385
13	456.40	456.22	456.21	456.21	456.21	440
14	528.71	528.57	528.56	528.56	528.57	-
15	606.56	606.45	606.44	606.44	606.45	590

Table 3.4 Convergence and comparison of the lowest natural frequency of C-C empty cylindrical containers for a given circumferential wave number

Circumferential wave number n	Present study				Ritz results by Naeem and Sharma (2000)	Experimental results by Sewall and Naumann (1968)
	$N=2$	$N=5$	$N=10$	$N=20$		
4	528.27	476.69	474.11	473.85	476.75	-
5	411.80	352.92	350.32	350.06	352.48	325
6	341.79	279.36	276.92	276.66	278.50	263
7	304.42	243.14	241.01	240.78	242.06	233
8	**292.81**	**237.50**	**235.82**	**235.63**	**236.44**	**227**
9	302.43	255.93	254.69	254.55	255.03	244
10	329.17	291.70	290.79	290.69	290.99	281
11	369.43	339.66	338.99	338.91	339.09	-
12	420.42	396.71	396.20	396.14	396.27	386
13	480.26	461.17	460.76	460.71	460.80	453
14	547.74	532.14	531.79	531.74	531.82	515
15	622.08	609.14	608.83	608.78	608.84	-

3.2.2 Cylindrical containers filled with liquid

Examples presented in the previous section demonstrated the ability of the RD-shell element in analyzing accurately the free vibration of empty cylindrical containers with different boundary conditions. The aforementioned analytical method (Naeem and Sharma, 2000) focused on the study of empty cylindrical containers and did not cover cylindrical containers that are filled with liquid. In this section, the RD-concept will now be extended to model the liquid-shell interaction in the free vibration problem of fluid-filled cylindrical containers. The effects of boundary conditions, container parameters on the natural frequencies of liquid-filled cylindrical containers are analyzed. The minimum frequency parameters can be obtained by plotting the frequency envelopes. The next few examples also test the convergence, validity as well as the accuracy of the proposed method for fluid-filled cylindrical containers.

Figure 3.2 shows the mesh discretization ($i \times j \times k$) of the liquid-filled cylindrical container, where i is the number of fluid elements in the radial direction and R/i is the width of each fluid element; j is the number of shell elements in the lower part of container that is in contact with liquid and H_f / j is the height of each lower shell element; k is the number of shell elements in the upper part of container that is not in contact with liquid and $\left(H - H_f\right)/k$ is the height of each upper shell element.

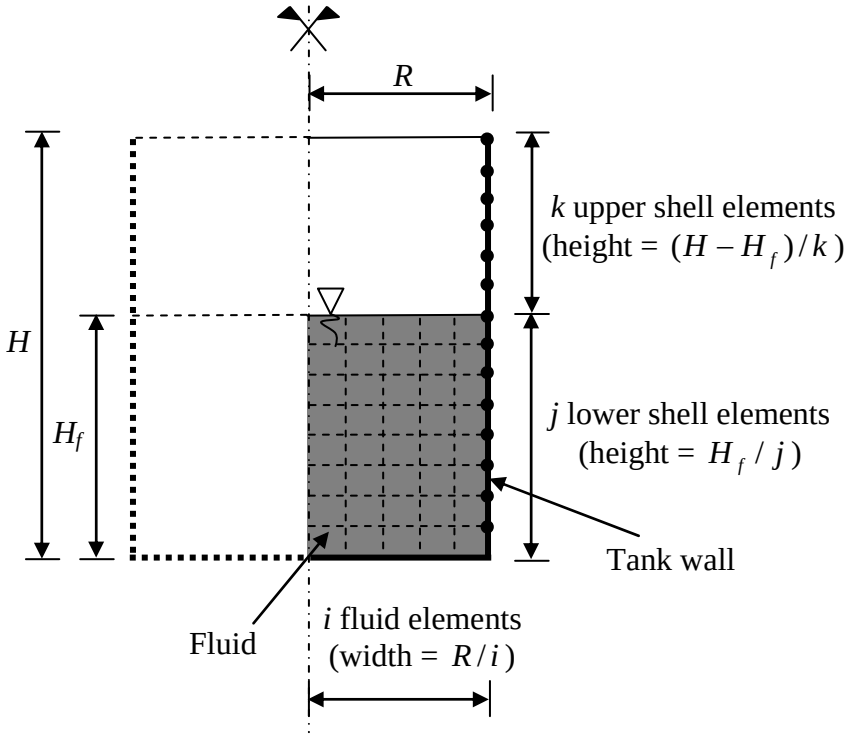

Figure 3.2 Finite element mesh of liquid-filled cylindrical container

To test the convergence of the RD-shell element method, the natural frequencies of C-F liquid-filled cylindrical containers are calculated for different number of liquid and shell elements. The dimensions and properties used for the C-F liquid-filled cylindrical containers are the same as those used by Kyeong and Seong (1998), which are shown in Table 3.5.

Table 3.5 Material and geometrical parameters of C-F liquid-filled cylindrical containers

H	Height of container	$0.365\,m$
H_f	Height of liquid	$0.1825\,m$
R	Radius of container	$0.115\,m$
h	Thickness of container	$3\,mm$
ν	Poisson's ratio	0.3
E	Young's modulus	$69\,GPa$
ρ_s	Mass density of shell	$2700\,kg/m^3$
ρ_f	Mass density of liquid	$1000\,kg/m^3$

An asymptotic convergence of the lowest natural frequencies for different circumferential wave numbers is obtained in Table 3.6 with respect to the increasing number of elements discretization from $2\times2\times2$ to $15\times15\times15$. It can be seen that the results converge rapidly as the number of liquid and shell elements is increased. The natural frequencies are noted to have converged (within 0.1% tolerance) when the number of elements of containers is only $10\times10\times10$.

In Table 3.6, the lowest natural frequencies of partially liquid-filled cylindrical containers obtained by the RD concept are also compared with those presented by Kyeong and Seong (1998) to verify the accuracy of the present method for the modelling of fluid-structure interaction problem. It can be seen that the results are in rather good agreement between the proposed RD-finite element method and the analytical study by Kyeong and Seong (1998) for different circumferential wave numbers n. The maximum discrepancy between the results is less than 3% for high harmonic n values. Therefore, this study demonstrated the efficiency and validity of the present method using the RD concept for the free vibration analysis of liquid-filled cylindrical containers.

Table 3.6 Convergence and comparison of the lowest natural frequency of C-F liquid-filled cylindrical containers for a given circumferential wave number

Circumferential wave number n	Present study				Kyeong and Seong (1998)
	$2\times2\times2$	$5\times5\times5$	$10\times10\times10$	$15\times15\times15$	
1	908.65	898.20	896.86	896.61	895.1
2	**446.84**	**443.28**	**442.90**	**442.83**	**443.2**
3	448.17	444.15	443.69	443.61	434.7
4	672.29	660.27	659.18	659.01	645.1
5	912.97	895.01	893.71	893.53	872.9
6	1259.75	1235.00	1233.50	1233.31	1200.4

3.2.3 Effect of boundary conditions

In this section, the effect of boundary conditions on the frequency parameters of liquid-filled cylindrical containers with different circumferential wave numbers and liquid-to-container height ratios is investigated. The following three boundary conditions are employed, namely the C-F, S-S and C-C liquid-filled cylindrical containers. From this point, the frequency parameter for liquid-filled cylindrical containers $\lambda = \omega R\sqrt{\frac{\rho_s\left(1-\nu^2\right)}{E}}$ is used for comparison between the results. It should be noted that the fluid and shell elements used to model the containers are $10\times10\times10$.

Figure 3.3 shows the variation of the frequency parameter λ with respect to the circumferential wave number n for the various types of boundary conditions of the fluid-filled cylindrical container. The parameters for this liquid-filled cylindrical container are the same as those used by Kyeong and Seong (1998), except that the level of liquid is equal to the container height $H_f = H = 0.365m$, i.e. the container is fully-filled with liquid. As can be seen from Figure 3.3, the frequency parameters of the three sets of boundary conditions first decrease and then increase gradually with the circumferential wave number. When the circumferential wave number exceeds

beyond a certain value $(n \geq 5)$, the corresponding frequency parameters of the three sets of boundary conditions converge to each other. One can conclude that the influence of boundary conditions becomes negligible for higher values of the circumferential wave number. For small values of the circumferential wave number $(n \leq 4)$, the frequency parameters of the S-S cylindrical container are larger than that of the C-F cylindrical container and smaller than the corresponding frequency parameters of the C-C cylindrical container.

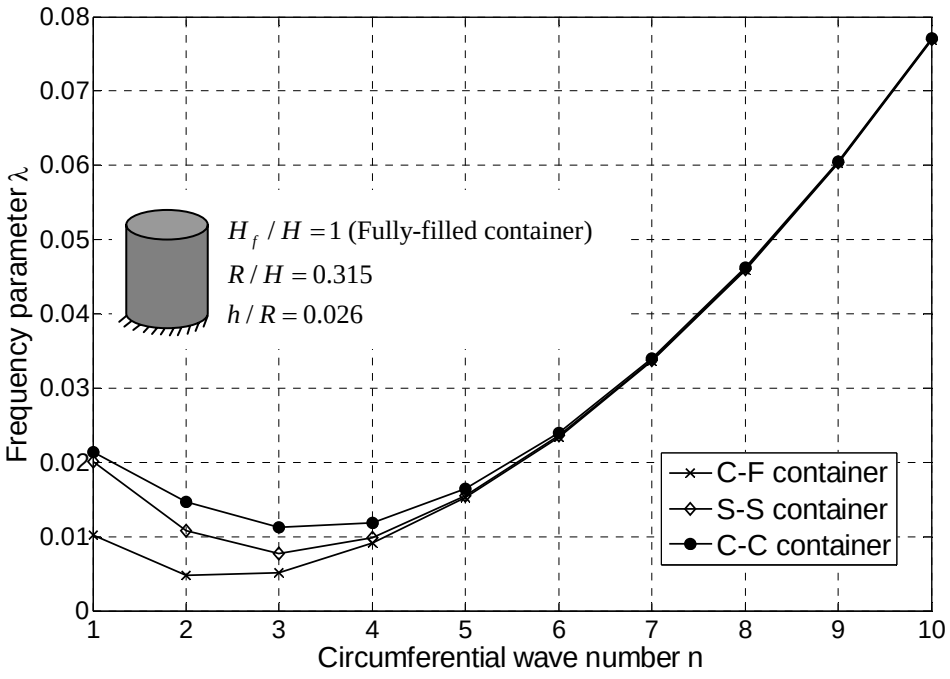

Figure 3.3 Effect of boundary condition on frequency parameters of fully-filled cylindrical containers

Figures 3.4, 3.5 and 3.6 present the variation of the frequency parameter λ with respect to the ratio of liquid-to-container height $\beta = H_f / H$ for the three types of boundary conditions of fluid-filled cylindrical containers. Figure 3.4 corresponds to the circumferential wave number $n = 1$, Figure 3.5 corresponds to $n = 2$ and Figure 3.6 corresponds to $n = 3$. The liquid-to-container height ratio β is varied from $\beta = 0$ (i.e.

empty container) to $\beta = 1$ (i.e. completely liquid-filled container). It is observed that the frequency parameter decreases as the level of liquid H_f increases. This is due to the fact that the fluid increases the total mass, thereby resulting in the decrease of the frequency parameter. It is evident from these figures that the difference in results between the C-F, S-S and C-C liquid-filled cylindrical containers would decrease when the ratio of liquid-to-container height β increases from 0 to 1. For a certain level of liquid, the frequency parameter of the C-C cylindrical container is the largest, followed by the S-S cylindrical container and then the C-F cylindrical container in this order. This finding is the same with the foregoing example with varying the circumferential wave number.

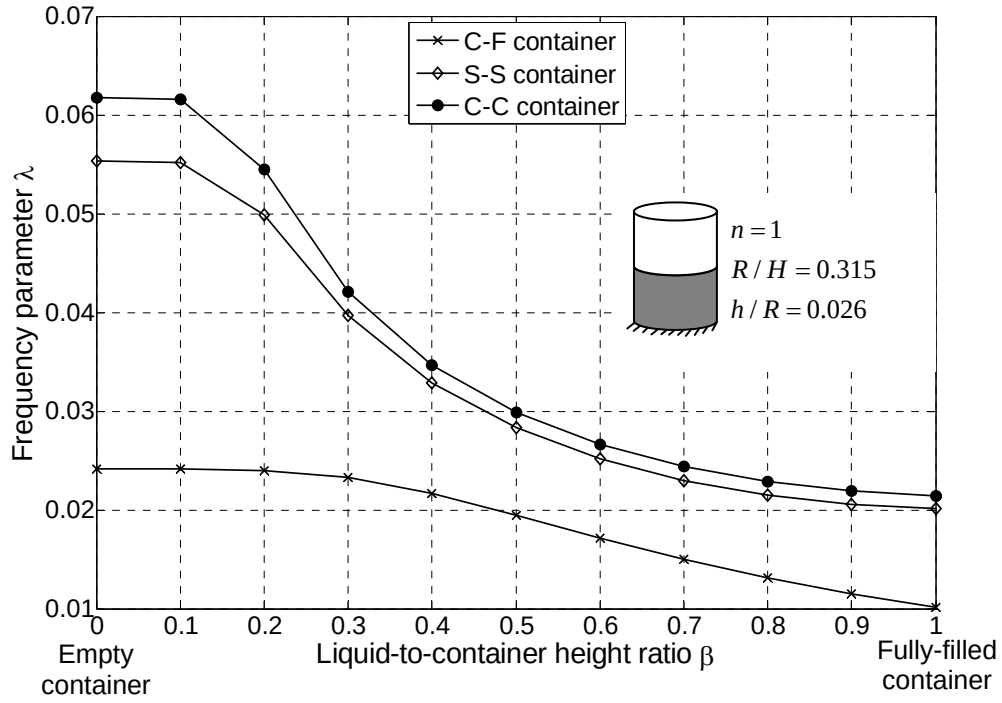

Figure 3.4 Effect of boundary condition and liquid level on frequency parameters of liquid-filled cylindrical containers for circumferential wave number $n = 1$

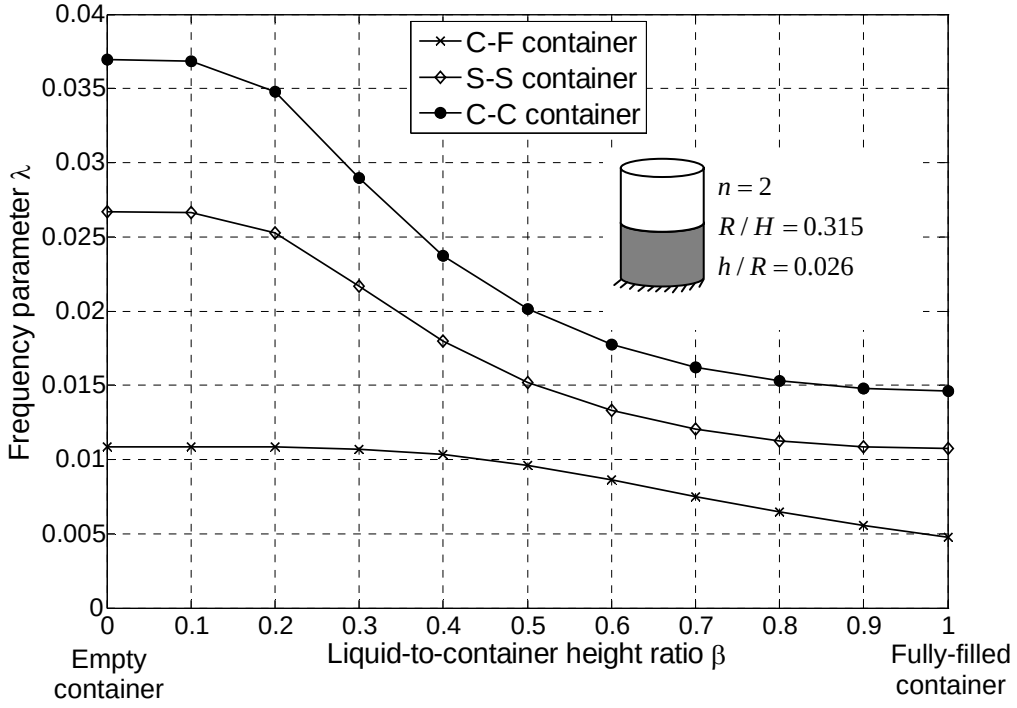

Figure 3.5 Effect of boundary condition and liquid level on frequency parameters of liquid-filled cylindrical containers for circumferential wave number $n = 2$

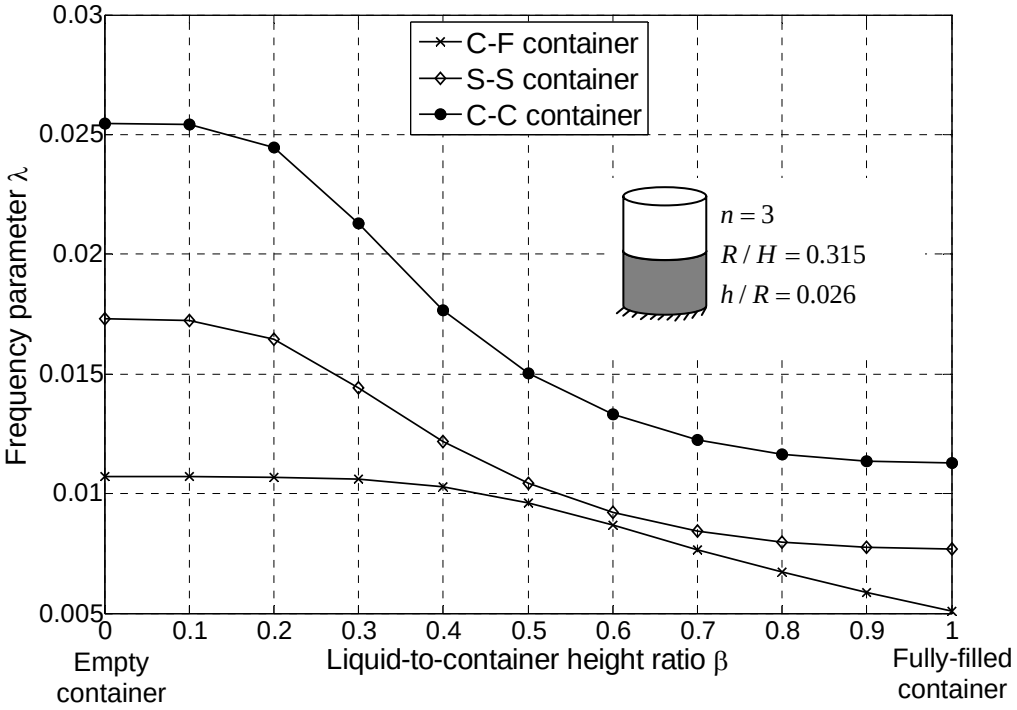

Figure 3.6 Effect of boundary condition and liquid level on frequency parameters of liquid-filled cylindrical containers for circumferential wave number $n = 3$

3.2.4 Frequency envelopes

The frequency envelopes of liquid-filled cylindrical containers are determined using the RD concept and presented in this section. These envelopes are useful towards avoiding resonance which occurs when the external forcing frequencies of the liquid-filled cylindrical containers are close to the natural sloshing frequencies. The range of frequency parameters can be obtained by drawing the envelopes of the frequency curves for a given circumferential wave number, liquid-to-container height, radius-to-thickness and container height-to-radius ratios. In the next following studies, the circumferential wave number is varied from 1 to 10. The study is confined to the case in which the boundary condition of the containers is C-F.

The effect of liquid level on the sloshing frequency parameters of containers is first investigated. Figure 3.7 shows the variation of frequency envelopes with respect to the liquid-to-container height ratio $\beta = H_f / H$ (from 0 to 1) and the circumferential wave number n. The other parameters of the container are the same as those used by Kyeong and Seong (1998). It can be seen from Figure 3.7 that the minimum frequency parameter varies depending on the liquid level and expectedly increases for higher circumferential wave number n. For a certain value of n, the frequency parameter decreases as the liquid level increases. The spectra of minimum frequency parameters correspond to the circumferential wave numbers $n = 2, 3$ for the entire range of liquid-filling level considered. One can observe that the frequency parameter is significantly reduced for the cases of empty containers and liquid-filled containers. This means that the liquid has an important role in shifting the sloshing frequencies of the containers. Thus, the liquid inside containers can be used effectively in avoiding the resonance. The frequency parameter is noted to converge upon reaching a certain liquid level ($\beta \geq 0.6$).

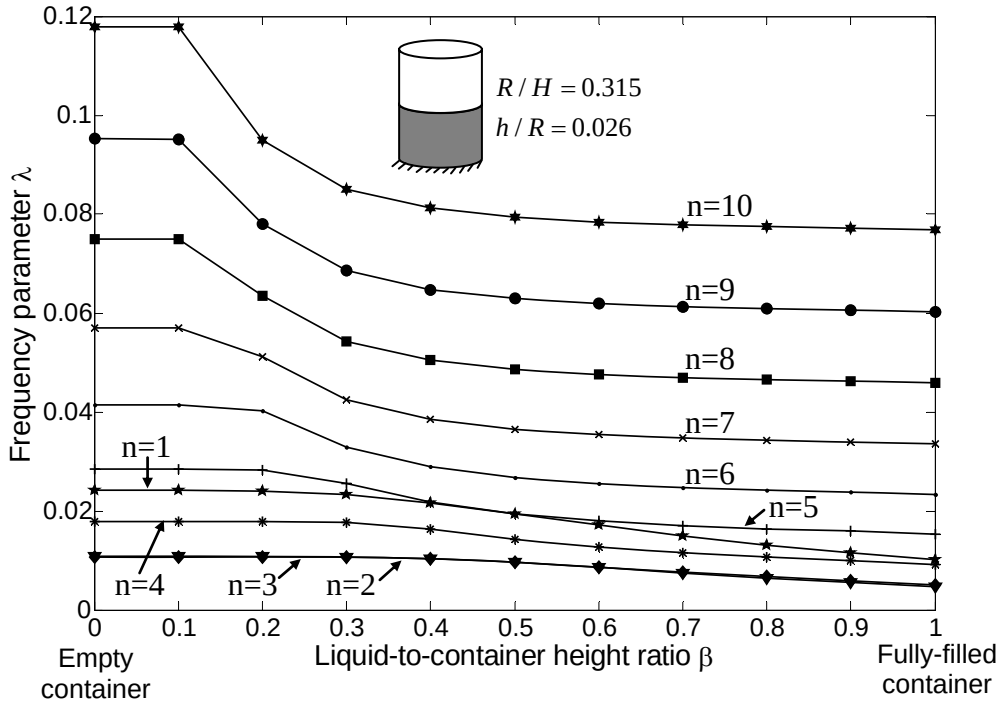

Figure 3.7 Frequency envelopes of liquid-filled containers with varying liquid level

In the next study, the effect of container height-to-radius ratio on the sloshing frequency parameters of containers is investigated. The container parameters are: thickness $h = 3mm$, Poisson's ratio $\nu = 0.3$, Young's modulus $E = 69 \times 10^9 N/m^2$, mass density of shell $\rho_s = 2700 kg/m^3$ and mass density of liquid $\rho_f = 1000 kg/m^3$. In this example, the containers are assumed to be fully-filled with liquid. The thickness is kept constant while the radius and container height are varied. The frequencies envelopes in Figures 3.8, 3.9 and 3.10 are determined for radius-to-thickness ratios $R/h = 20$, 100 and 500, respectively. The volume of containers is varied by changing the container height H. The ratio of container height-to-radius is varied from very short ($H/R = 0.2$) to very tall ($H/R = 100$) liquid-filled cylindrical containers.

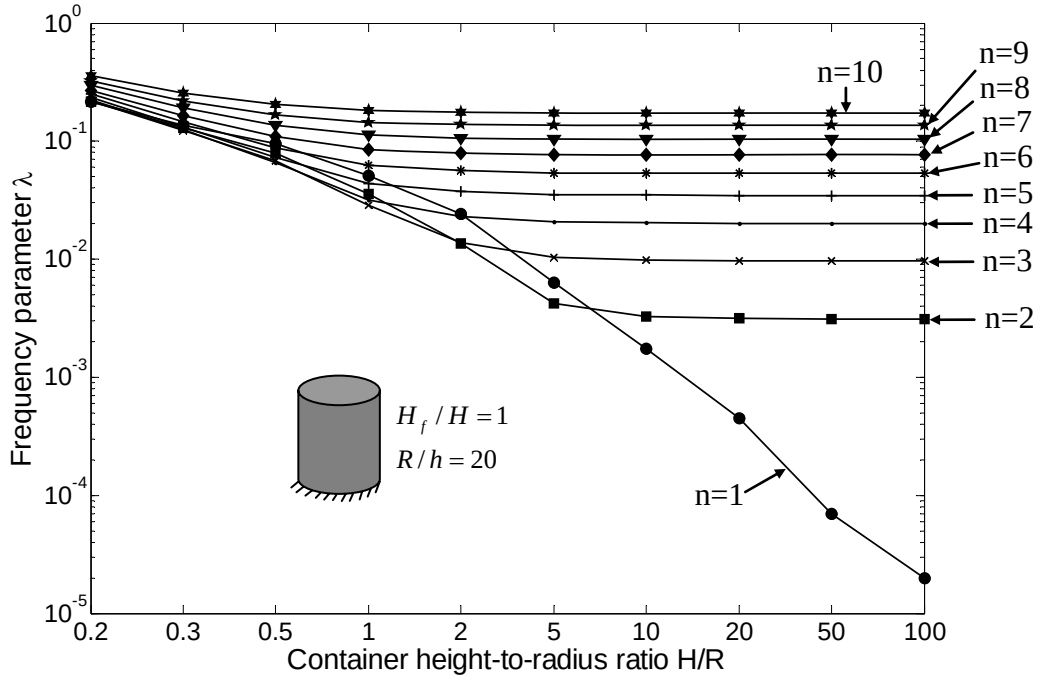

Figure 3.8 Frequency envelopes of fully-filled containers with varying container height and $R/h = 20$

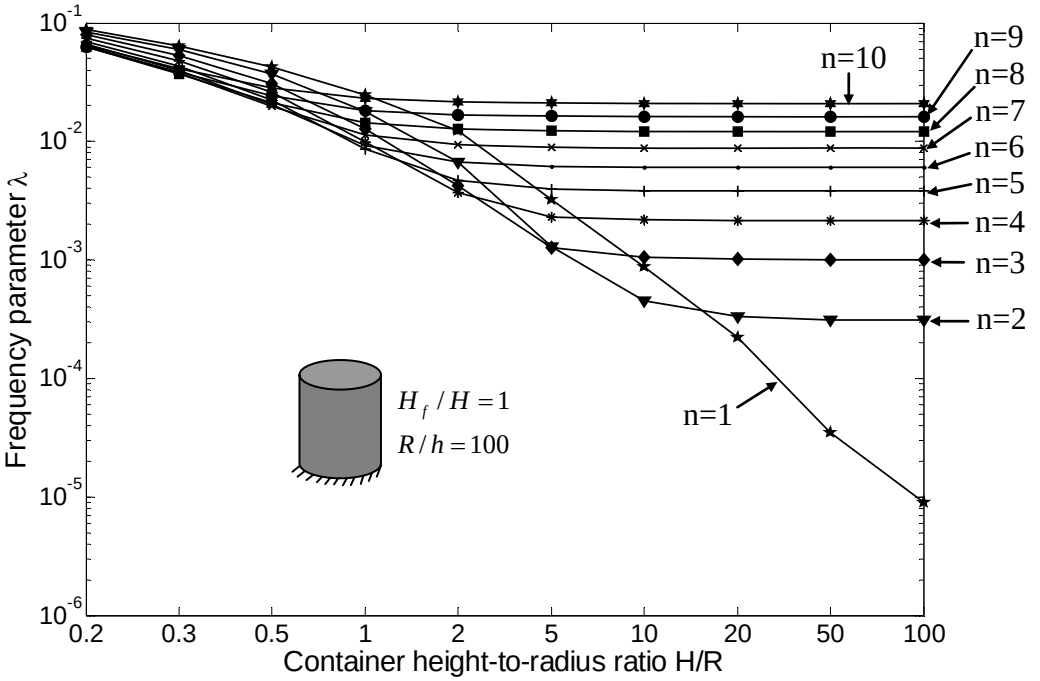

Figure 3.9 Frequency envelopes of fully-filled containers with varying container height and $R/h = 100$

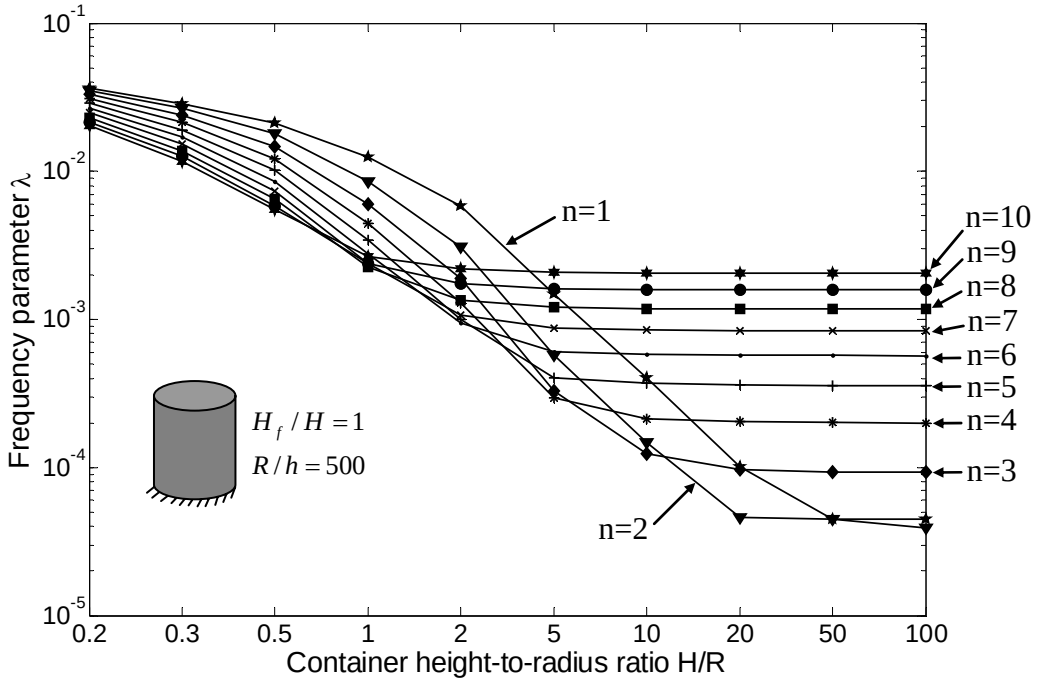

Figure 3.10 Frequency envelopes of fully-filled containers with varying container height and $R/h = 500$

Figures 3.8, 3.9 and 3.10 depict the variation of frequency envelopes with respect to the container height-to-radius ratio H/R and the circumferential wave number n. It can be seen from these figures that the frequency parameter decreases as the container height-to-radius ratio H/R increases. This can be attributed to the fact that as H/R increases, the volume of liquid in the fully-filled containers increases resulting in an increase in the mass of the liquid-container system. Consequently, the frequency parameter of the liquid-container system decreases. The frequency parameter is also noted to converge to each other for small values of container height-to-radius ratio, i.e. for very short and stocky liquid-filled cylindrical containers, the frequency parameter is not affected by the circumferential wave number. For a container height-to-radius ratio H/R of 0.2, the frequency parameter is nearly the same for different values of the circumferential wave number n. The minimum frequency is obtained when the circumferential wave number $n = 2$. The spectra of minimum frequencies are

associated with the circumferential wave numbers $n = 2$, 3 and 4 as increasing value of H/R in the interval $0.2 \le H/R \le 1.0$. For $H/R \ge 10$, i.e. reasonably tall liquid-filled cylindrical containers, the minimum frequency is associated with the circumferential wave number $n = 1$.

Next, the effect of radius-to-thickness ratio on the sloshing frequency parameter of liquid-filled cylindrical containers is studied. The container parameters are: thickness $h = 3mm$, Poisson's ratio $\nu = 0.3$, Young's modulus $E = 69 \times 10^9 N/m^2$, mass density of shell $\rho_s = 2700 kg/m^3$ and mass density of liquid $\rho_f = 1000 kg/m^3$. The containers are also assumed to be fully-filled with liquid for all cases. The thickness is kept constant while the radius and container height are varied. The frequency envelopes shown in Figures 3.11, 3.12 and 3.13 correspond to the container height-to-thickness ratios $H/h = 100$, 300 and 500, respectively. The volume of containers is varied by changing the radius of the container R and the radius-to-thickness ratio R/h is varied from very thick ($R/h = 10$) to very thin ($R/h = 500$) liquid-filled cylindrical containers.

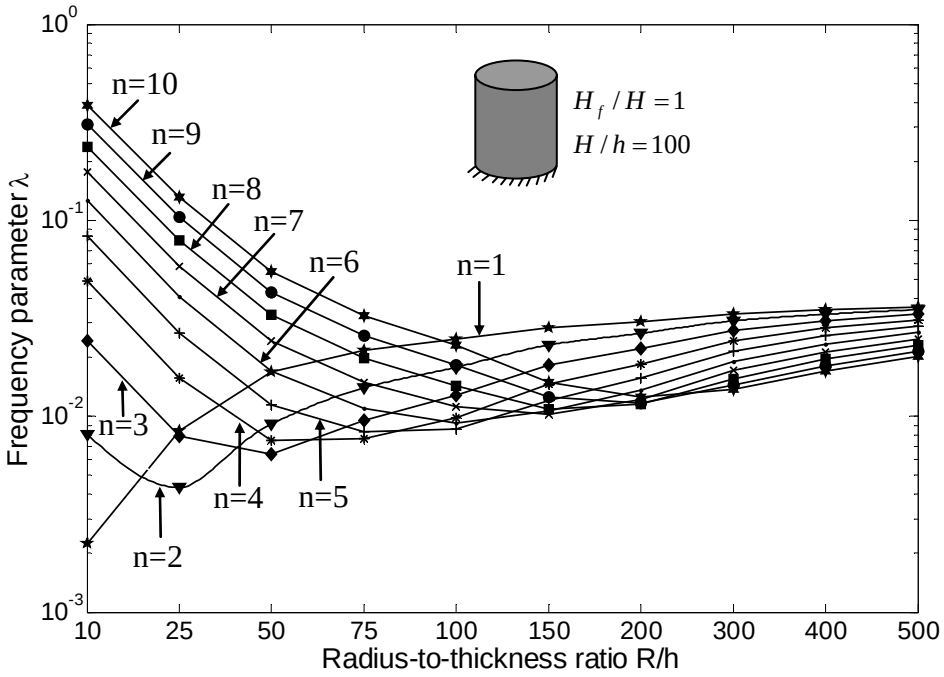

Figure 3.11 Frequency envelopes of fully-filled containers with varying container radius and $H / h = 100$

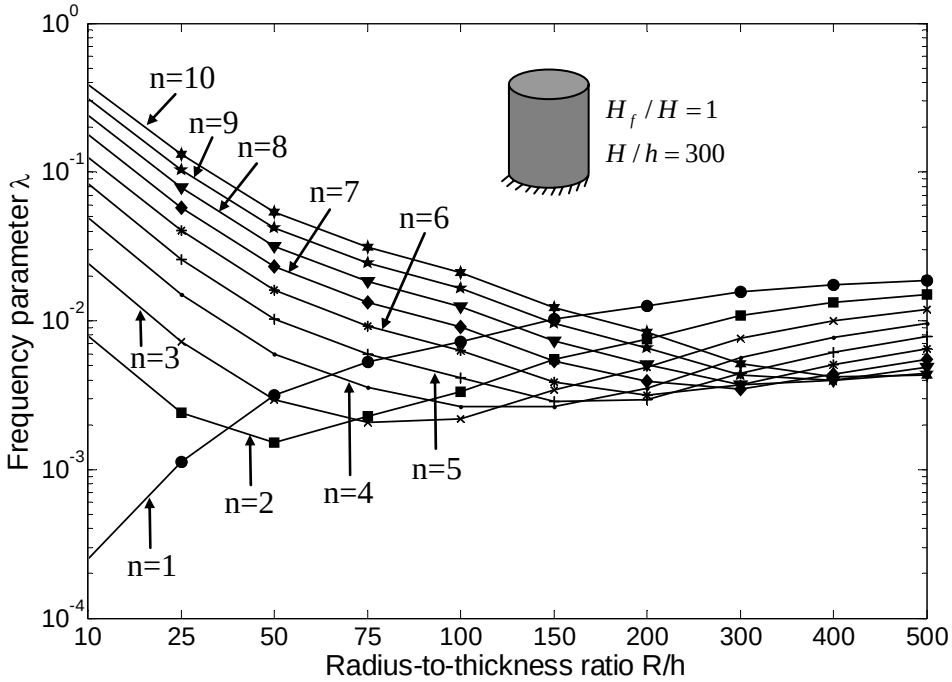

Figure 3.12 Frequency envelopes of fully-filled containers with varying container radius and $H / h = 300$

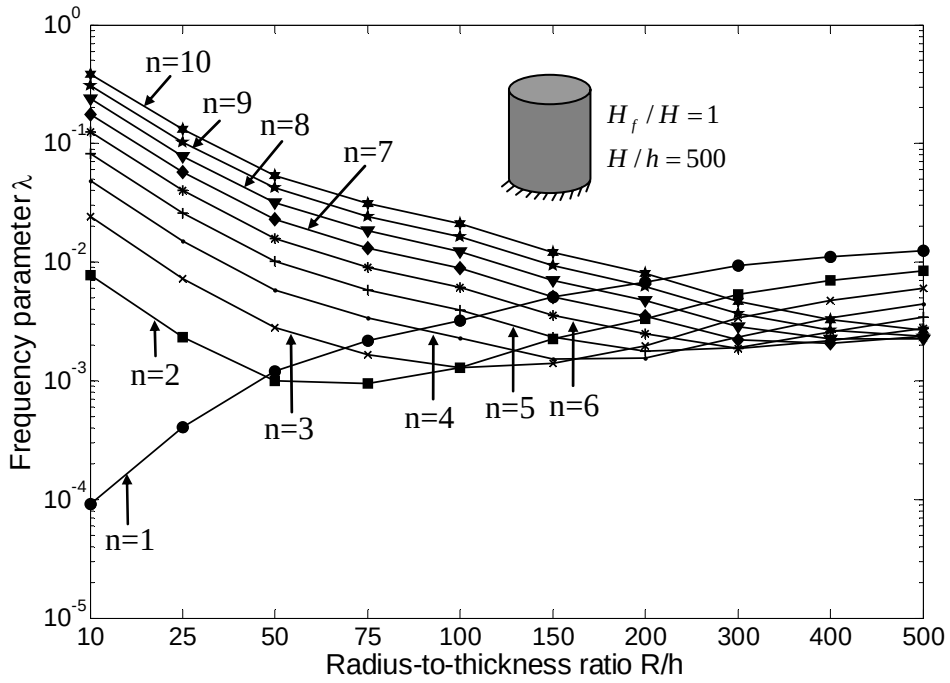

Figure 3.13 Frequency envelopes of fully-filled containers with varying container radius and $H / h = 500$

Figures 3.11, 3.12 and 3.13 show the frequency envelopes for different values of the circumferential wave number n. From these figures, it is noted that the frequency parameter associated with $n = 1$ increases as the radius-to-thickness ratio R / h increases. On the other hand, for higher values of n, the frequency parameter first decreases rapidly and then increases slowly as the radius-to-thickness ratio increases. The frequency parameter also tends to converge to each other for large values of radius-to-thickness ratios. In other words, for very thin cylindrical containers, the frequency parameter is not affected by the circumferential wave number. For very thick cylindrical containers, i.e. small radius-to-thickness ratios, the minimum frequency parameter is obtained when the circumferential wave number $n = 1$. On the other hand, for very thin cylindrical containers, i.e. large values of radius-to-thickness ratio, the minimum frequency parameter is noted to occur at higher values of the circumferential wave number.

3.3 Axisymmetric multi-layer RD shell

Examples presented in the previous section 3.2 demonstrated the application of the RD-shell elements in determining the coupled natural frequencies of single-layer cylindrical containers filled with and without liquid. In this section, the RD-concept will be extended to model the coupled interaction in the case of multi-layer cylindrical containers. The vibration behaviours of multi-layer containers will be presented for different kinds of materials, geometrical parameters, number of layers, fiber orientations and boundary conditions.

3.3.1 Two-layer cylindrical containers without liquid

Consider first an empty, two-layer cylindrical container as shown in Figure 3.14. The non-dimensional properties of this container are the same as those used by Kumar and Rao (1988) with fiber orientation of $\left(0^0, 90^0\right)$, thickness of shell $h = 1.0$, container height-to-radius ratio $H/R = 2$, Poisson's ratio $\nu_{12} = \nu_{13} = \nu_{23} = 0.25$, Young's and shear moduli $E_2 = 0.025E_1$, $G_{12} = G_{13} = 0.5E_2$, $G_{23} = 0.416E_2$. The natural frequencies of C-F two-layer cylindrical container obtained by the present study using the RD concept will be compared with those obtained by Kumar and Rao (1988), who employed the conventional FEM.

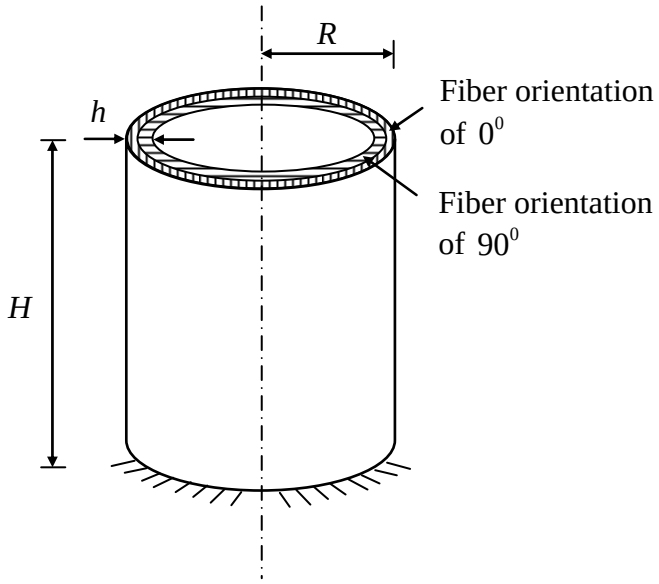

Figure 3.14 Two-layer, empty cylindrical container

A comparison of the frequency parameter $\zeta = \dfrac{\omega H^2}{\pi^2}\sqrt{\dfrac{24\rho_s\left(1-\nu_{12}\nu_{13}\right)}{\left(1+E_2/E_1\right)E_1h^3}}$ between the present RD element results and Kumar and Rao's results is shown in Table 3.7. It can be seen that the frequencies are in good agreement particularly for the circumferential wave number $n=1$ for different radius-to-thickness ratios R/h considered. For $n=2$, the difference in the frequency parameter obtained by the two methods is noted to be larger but is still within 5% of each other. Thus, this example illustrates the validity of the present RD concept for the analysis of the multi-layer, empty cylindrical containers.

Table 3.7 Frequency parameter ζ of two-layer, empty cylindrical container

R/h	n	Kumar and Rao (1988)	Present study	Error %
5	1	1.133	1.131	0.18
	2	2.578	2.476	4.12
20	1	4.606	4.571	0.77
	2	7.456	7.689	3.03
50	1	11.643	11.440	1.77
	2	17.484	18.319	4.56

3.3.2 Multi-layer cylindrical containers filled with liquid

The proposed RD-finite element method will now be used to determine the natural vibration frequencies of multi-layer, liquid-filled cylindrical containers with different thicknesses, radii, liquid heights, fiber orientations and boundary conditions. The frequency parameter for multi-layer, liquid-filled cylindrical container $\lambda = \omega R\sqrt{\frac{\rho_s\left(1-\nu_{12}^2\right)}{E_1}}$ is used to present the results.

3.3.3 Effect of boundary conditions

The effect of boundary conditions (C-F, S-S and C-C) on the frequency parameter of two-layer, liquid-filled cylindrical containers with different liquid-to-container height ratios is first investigated. The laminated material properties and geometrical parameters used for this two-layer graphite-epoxy cylindrical container are: container height-to-thickness ratio of $H/h = 150$, container height-to-mean radius ratio of $H/R = 3$, Poisson's ratio $\nu_{12} = \nu_{13} = 0.24$, $\nu_{23} = 0.49$, Young's and shear moduli $E_1 = 132.4GPa$, $E_2 = E_3 = 10.76GPa$, $G_{12} = G_{13} = 5.654GPa$, $G_{23} = 3.606GPa$, mass density of shell $\rho_s = 1779kg/m^3$, mass density of liquid $\rho_f = 1000kg/m^3$. The cross-ply configuration considered is $\left(0^0, 90^0\right)$. The circumferential wave number $n = 1$ is considered. The thickness is equal for each layer. The liquid-to-container height ratio $\beta = H_f/H$ is varied from $\beta = 0$ (i.e. empty container) to $\beta = 1$ (i.e. fully liquid-filled container).

Figure 3.15 depicts the variation of the frequency parameter λ with respect to the ratio of liquid-to-container height β for the considered three cases of boundary conditions (C-F, S-S and C-C) of two-layer, fluid-filled cylindrical containers. It is

observed that the frequency parameter decreases monotically as the liquid level increases. This is easily attributed to the fact that the liquid increases the total mass, which therefore leads to a decrease in the frequency parameter. It is also evident from Figure 3.15 that the difference in the frequency parameter between the C-F, S-S and C-C liquid-filled cylindrical containers reduces as the ratio of liquid-to-container height β increases from 0 to 1. For any given level of liquid, the frequency parameter of the C-C cylindrical container is the largest, followed by the S-S cylindrical container and then the C-F cylindrical container in this order. These findings are the same as the case of single layer RD-shell.

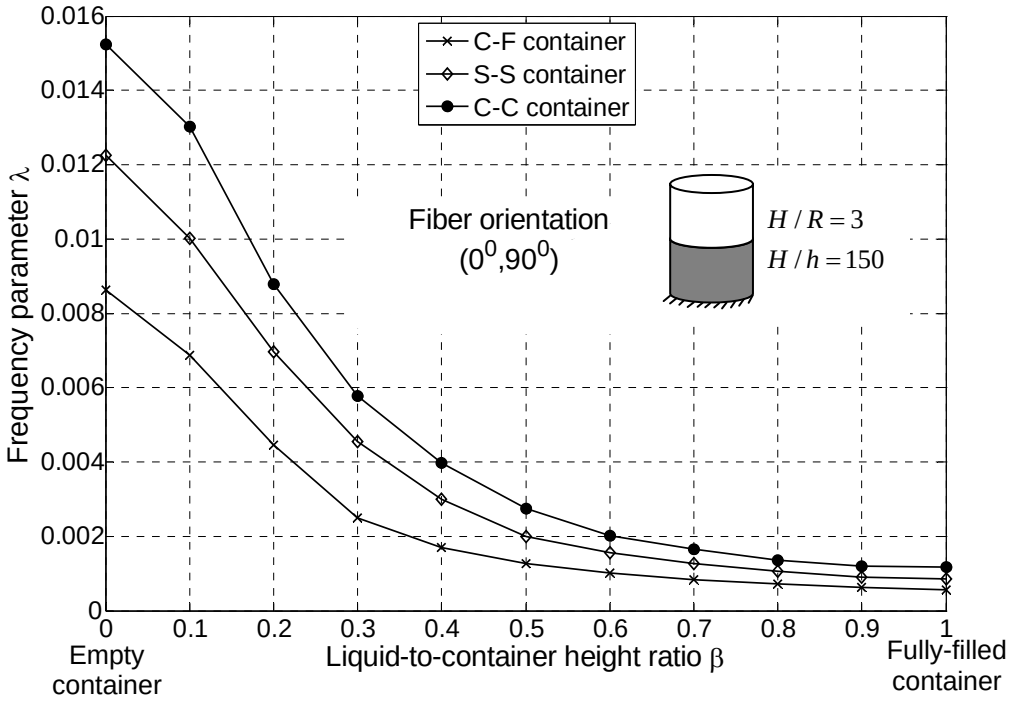

Figure 3.15 Effect of boundary condition and liquid level on frequency parameters of two-layer, liquid-filled containers

3.3.4 Frequency envelopes

The frequency envelopes of three-layer cylindrical containers filled with liquid are also determined using the RD finite element concept. The range of frequency parameters can be obtained by plotting the envelopes of the frequency curves for constant value of the circumferential wave number, mean radius-to-thickness and container height-to-mean radius ratios. In the following study, the circumferential wave number considered ranges from 1 to 10. The boundary condition of the containers is C-F for all cases. The laminated material properties and geometrical parameters used for the three-layer, fully-filled cylindrical containers are: Poisson's ratio $\nu_{12} = \nu_{13} = 0.28$, $\nu_{23} = 0.33$, Young's and shear moduli $E_1 = 181.0GPa$, $E_2 = E_3 = 10.3GPa$, $G_{12} = G_{13} = 7.17GPa$, $G_{23} = 3.87GPa$, mass density of shell $\rho_s = 1580kg/m^3$, mass density of liquid $\rho_f = 1000kg/m^3$. The fiber orientation considered is $\left(45^0, 90^0, 45^0\right)$. The effect of container height-to-mean radius ratio H/R on the sloshing frequency parameters of containers is investigated. The containers are assumed to be fully-filled with liquid for all cases. The thickness is kept constant while the mean radius and container height are varied. The frequencies envelopes in Figures 3.16 and 3.17 are presented for mean radius-to-thickness ratios R/h of 40 and 150, respectively. The ratio of container height-to-mean radius H/R is varied from very short ($H/R = 0.2$) to very tall ($H/R = 100$) cylindrical containers.

Figures 3.16 and 3.17 show the variation of the frequency envelopes with respect to H/R and the circumferential wave number n. It can be seen from these figures that the frequency parameter decreases as H/R increases. The frequency parameter is also noted to converge to each other for small values of container height-to-mean radius ratios. Thus, for very short liquid-filled cylindrical containers, the frequency

parameters are not affected by the circumferential wave number. In particular, for a container height-to-mean radius ratio $H/R = 0.2$, the frequency parameters are virtually the same for different circumferential wave numbers n. For $0.2 \le H/R \le 0.3$, the spectra of minimum frequency parameters are associated with the circumferential wave number $n = 4$ and for $H/R \ge 0.5$, the minimum frequency parameters correspond to the circumferential wave number $n = 1$.

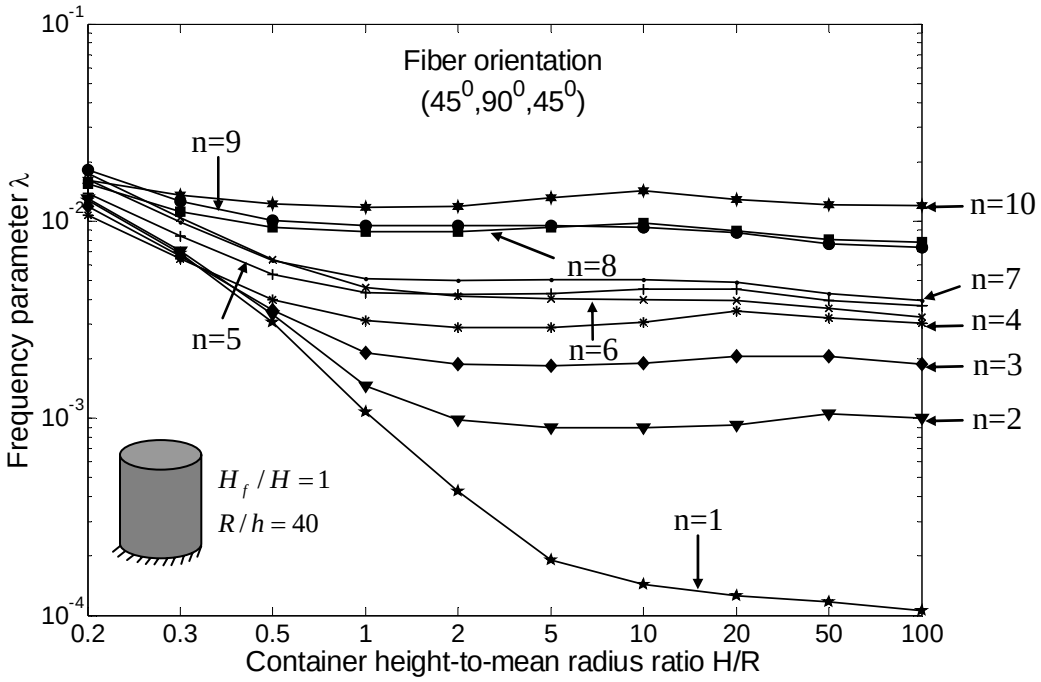

Figure 3.16 Frequency envelopes of three-layer, fully-filled containers with varying container height and $R/h = 40$

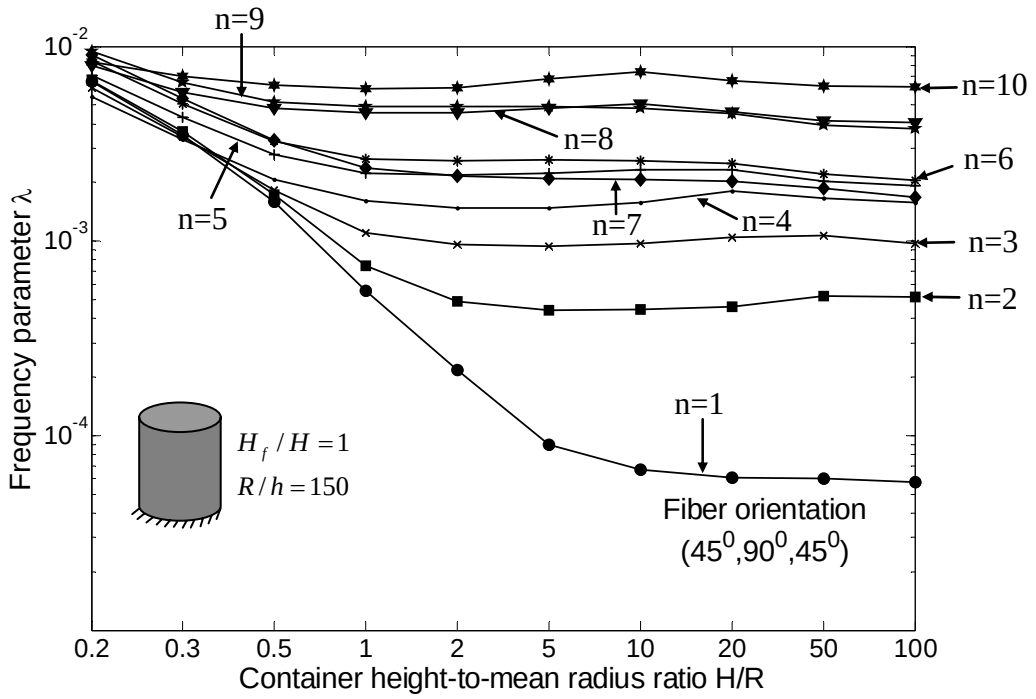

Figure 3.17 Frequency envelopes of three-layer, fully-filled containers with varying container height and $R/h = 150$

In the next study, the effect of mean radius-to-thickness ratio on the sloshing frequency parameters of liquid-filled cylindrical containers is conducted. The container parameters are the same as in the foregoing example, except that the fiber orientation is $\left(30^0, 0^0, 60^0\right)$. The frequency envelopes in Figures 3.18 and 3.19 are shown for $H/h = 100$ and $H/h = 300$, respectively. The volume of containers is varied by changing the mean radius R and the mean radius-to-thickness ratio R/h is varied from very thick ($R/h = 10$) to very thin ($R/h = 500$) cylindrical containers.

Figures 3.18 and 3.19 show the variation of frequency envelopes with respect to the mean radius-to-thickness ratio R/h and circumferential wave number n. It can be seen from these figures that the minimum frequency parameters are associated with the circumferential wave number $n = 1$ for different R/h values. It is also evident that the frequency parameters converge to each other for larger values of mean radius-to-

thickness ratios, i.e. for very thin liquid-filled cylindrical containers, the frequency parameters are basically the same for various values of the circumferential wave number.

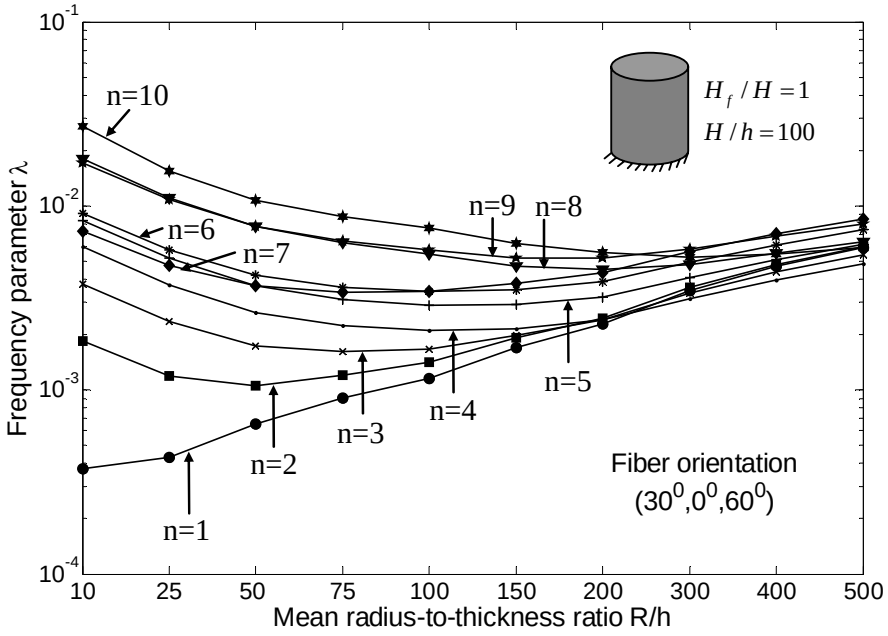

Figure 3.18 Frequency envelopes of three-layer, fully-filled containers with varying container radius and $H / h = 100$

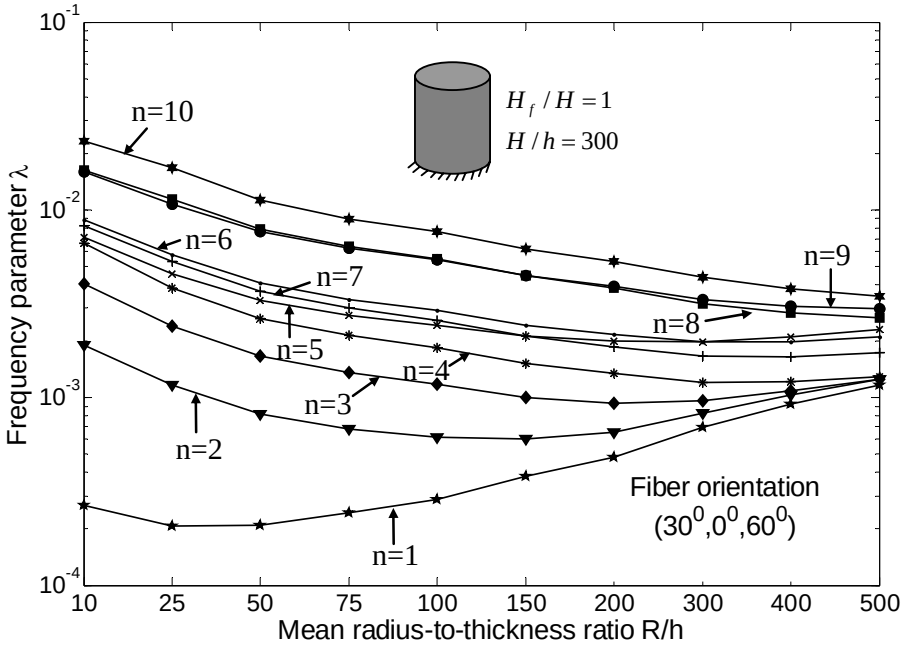

Figure 3.19 Frequency envelopes of three-layer, fully-filled containers with varying container radius and $H / h = 300$

3.4 Concluding remarks

In this chapter, an axisymmetric RD-shell element developed in Chapter 2 is used to determine the coupled natural frequencies of cylindrical containers filled with an inviscid and incompressible liquid. The liquid-shell interaction problem is accounted for with the use of a coupling matrix between the shell element and the neighbouring fluid element.

The example problems considered herein demonstrated that the proposed RD-finite element method furnishes vibration results that are in good agreement with those obtained by previous researchers who have employed other methods. Through several examples, the convergence, efficiency and accuracy of the proposed method using the RD-shell element were investigated. Many influencing factors to the vibration behaviour of liquid-filled cylindrical containers were also studied. These factors include boundary conditions, container parameters such as the liquid level, the container height-to-radius, radius-to-thickness, container height-to-thickness ratios, number of layers and the fiber orientation. It may be remarked that the present method can easily be extended to study the influence of arbitrary support conditions, arbitrary geometrical and material parameters of containers on the natural frequency characteristics.

CHAPTER 4 LIQUID SLOSHING IN CONTAINERS DUE TO SHIP MOTION

4.1 Introduction

Sea transportation plays an important role in the modern world economy today. Moan (2003) pointed out that over 70% of world trade and 95% of international transportation takes place through ships and that all countries are dependent on such transportation modes for the movement of fuels, raw materials, food and manufactured goods.

Ships carrying liquid cargo are probably one of the most common vessels plying across the many shipping routes of the world. As the ship moves across the ocean, the motion of the ship causes the liquid in the containers to slosh. Liquid sloshing may cause large internal stresses and deformation in the walls of containers, particularly when the external forcing frequencies of ship are close to the natural sloshing frequencies. Thus, many naval architects and marine engineers have conducted research studies on the sloshing problem in cargo containers. For example, Mikelis and Journee (1984) presented a two-dimensional, finite difference, transient solution for the prediction of liquid motions and induced pressures in partially filled containers on ships. Experiments were also conducted on scaled tanks and the measured pressures and bending moments were compared with numerical predictions. Journee (1997) analyzed a ship model with liquid cargo tanks and the model was tested in beam waves at zero forward speed for a wide range of filling levels. The measured roll data of the model were compared with the results obtained from strip theory calculations. Lee and

Choi (1999) conducted experiments and numerical analysis on the sloshing problem in cargo tanks. The fluid motion was predicted using a high order boundary element method and the structure was modeled based on the classical thin plate theory. In cases of low filling depths, hydraulic jumps were formed when the excitation frequency is close to the resonance frequency whereas in the case of high filling depths, a large impact pressure was obtained. Kim (2002) employed a numerical technique to solve the coupling problem of the ship motion and sloshing flow. The study was focused on the anti-rolling tank, which has the most significant coupling effects of ship motion and sloshing flow problem. The three dimensional sloshing flow was simulated using the finite difference method, while the ship motion was obtained using a time domain panel method. Rognebakke and Faltinsen (2003) investigated two dimensional experiments of a hull section containing tanks filled with different levels of water excited in sway by regular waves. They obtained a good agreement between test results and numerical simulated results of the coupling problem. The study also revealed that the coupled motion is sensitive to the damping of the sloshing motion in a certain frequency range where the coupled sloshing and ship motions cause resonant ship motions.

Recently, Lee et al. (2007a) carried out a study on rectangular LNG tanks subjected to external loadings by using a computational fluid dynamics (CFD) program. The CFD simulations were verified against experimental results. They concluded that the effects of viscosity and density of fluid on impact pressures are insignificant, while the compressibility of fluid plays an appreciable role. Zhang and Suzuki (2007) carried out numerical simulations of collisions between a container ship and a double-hull crude carrier. Three different simulation methods were used to model the fluid-structure interaction in liquid-filled cargo tank. They are the arbitrary Lagrangian-Eulerian

FEM, Lagrangian FEM and linear sloshing model. The results showed that the fluid-structure interaction of liquid cargo-filled tank has a significant effect on the motion and structural response of the cargo tank. Further, Lee et al. (2007b) analyzed the coupling and interaction between ship motion and inner-tank sloshing using a time-domain simulation scheme. Wind and current were however not accounted in the ship calculations. The study considered environmental forces that were due to the wave loading only. In general, all the aforementioned studies considered the coupling interaction between the liquid and thin shell structures. The effects of transverse shear deformation and rotary inertia, which are neglected in the thin shell theory, have to be taken into consideration when dealing with thick shells. In addition, these past studies treated the ship motion using simple linear models, which do not account for the real environmental effects, such as the combination of wind, wave and current loads.

In this chapter, the dynamic behaviour of the coupled interaction problem between the fluid and cylindrical tank wall in liquid-filled container subject to ship motion is investigated. The proposed RD-shell elements in Chapter 2, which account for the effects of both transverse shear deformation and rotary inertia, are used to model the tank wall. In addition, the realistic environmental factors including the combination of wind, wave and current effects will be considered in the ship motion program using nonlinear models. In order to demonstrate the effectiveness of the present method, some results of the coupled dynamic system such as displacement time history, maximum deformation and stress resultants in the shell walls will be presented and compared with other available numerical results.

4.2 Modeling of marine vessels

The typical moving ship at sea is subjected to six oscillating motions, i.e. surge, sway, heave, roll, pitch and yaw as shown in Figure 4.1. These motions are produced by wave action and evidently depend on the heading and size of the ship with respect to the waves.

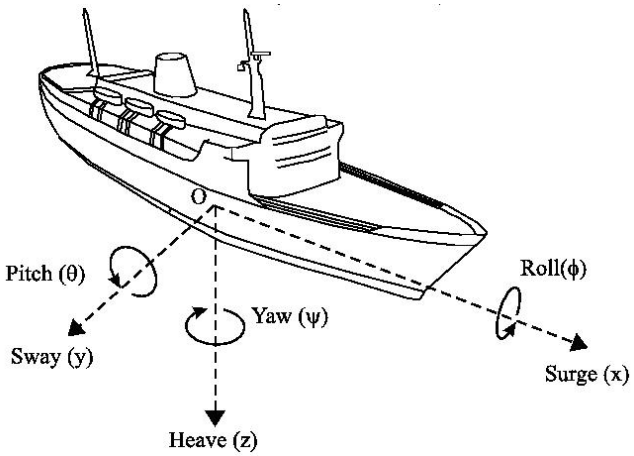

Figure 4.1 Motion variables of marine vessels

4.2.1 Coordinate systems and transformation equations

In order to describe the positions of marine vessels, two coordinate systems are commonly used. They are the earth-fixed and body-fixed reference frames as shown in Figure 4.2. The earth-fixed reference $X_E Y_E Z_E$-frame is fixed to a point on the surface of the earth which serves as an inertial frame. The body-fixed reference *XYZ*-frame is fixed to the ship. According to Fossen (2002), the transformation between these two reference frames is accomplished by kinematic equations which treat only geometrical aspects of motion.

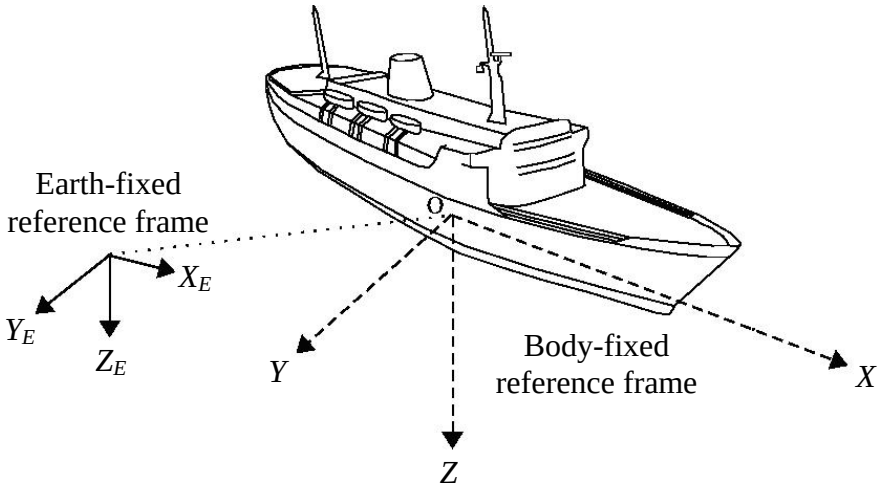

Figure 4.2 Coordinate systems of marine vessels

The general motion of marine vessels is described by the Society of Naval Architects & Marine Engineers (SNAME, 1950) as shown in Table 4.1. The position and orientation vector $\boldsymbol{\eta}$ of the moving ship is measured in the earth-fixed $X_E Y_E Z_E$ coordinate system, where the variables x, y and z represent the motions in surge, sway and heave, respectively; and ϕ, θ and ψ are the rotations about the X_E, Y_E and Z_E axes (roll, pitch and yaw), respectively. The linear and angular velocity vector $\boldsymbol{\upsilon}$ of the ship motion is measured in the body-fixed XYZ coordinate system, where the variables u, v and w are the surge, sway and heave linear velocities, respectively; and p, q and r are the roll, pitch and yaw angular velocities, respectively.

Table 4.1 Notations for position and velocity of marine vessels

Position and orientation in earth-fixed frame	$\boldsymbol{\eta} = [\underbrace{x \quad y \quad z}_{\text{position}} \quad \underbrace{\phi \quad \theta \quad \psi}_{\text{orientation}}]^T$
Velocity in body-fixed frame	$\boldsymbol{\upsilon} = [\underbrace{u \quad v \quad w}_{\text{linear velocity}} \quad \underbrace{p \quad q \quad r}_{\text{angular velocity}}]^T$

The relation between the two velocity vectors $\boldsymbol{\eta}$ and $\boldsymbol{\upsilon}$ can be expressed as

$$\dot{\boldsymbol{\eta}} = \mathbf{J}(\boldsymbol{\eta})\boldsymbol{\upsilon}, \quad \boldsymbol{\upsilon} = \mathbf{E}(\boldsymbol{\eta})\dot{\boldsymbol{\eta}} \tag{4.1}$$

where $\mathbf{J}(\boldsymbol{\eta})$ is the transformation matrix between the earth-fixed coordinate system and the body-fixed coordinate system and $\mathbf{E}(\boldsymbol{\eta})$ is its inverse. The matrices $\mathbf{J}(\boldsymbol{\eta})$ and $\mathbf{E}(\boldsymbol{\eta})$ are given by

$$\mathbf{J}(\boldsymbol{\eta}) = \begin{bmatrix} \mathrm{c}\psi\,\mathrm{c}\theta & -\mathrm{s}\psi\,\mathrm{c}\theta + \mathrm{c}\psi\,\mathrm{s}\theta\,\mathrm{s}\phi & \mathrm{s}\psi\,\mathrm{s}\phi + \mathrm{c}\psi\,\mathrm{c}\phi\,\mathrm{s}\theta & 0 & 0 & 0 \\ \mathrm{s}\psi\,\mathrm{c}\theta & \mathrm{c}\psi\,\mathrm{c}\phi + \mathrm{s}\phi\,\mathrm{s}\theta\,\mathrm{s}\psi & -\mathrm{c}\psi\,\mathrm{s}\phi + \mathrm{s}\theta\,\mathrm{s}\psi\,\mathrm{c}\phi & 0 & 0 & 0 \\ -\mathrm{s}\theta & \mathrm{c}\theta\,\mathrm{s}\phi & \mathrm{c}\theta\,\mathrm{c}\phi & 0 & 0 & 0 \\ 0 & 0 & 0 & 1 & \mathrm{s}\phi\,\mathrm{t}\theta & \mathrm{c}\phi\,\mathrm{t}\theta \\ 0 & 0 & 0 & 0 & \mathrm{c}\phi & -\mathrm{s}\theta \\ 0 & 0 & 0 & 0 & \mathrm{s}\phi/\mathrm{c}\theta & \mathrm{c}\phi/\mathrm{c}\theta \end{bmatrix}_{6\times 6}$$

(4.2)

$$\mathbf{E}(\boldsymbol{\eta}) = \begin{bmatrix} \mathrm{c}\psi\,\mathrm{c}\theta & \mathrm{s}\psi\,\mathrm{c}\theta & -\mathrm{s}\theta & 0 & 0 & 0 \\ -\mathrm{s}\psi\,\mathrm{c}\phi + \mathrm{c}\psi\,\mathrm{s}\theta\,\mathrm{s}\phi & \mathrm{c}\psi\,\mathrm{c}\phi + \mathrm{s}\psi\,\mathrm{s}\theta\,\mathrm{s}\phi & \mathrm{c}\theta\,\mathrm{s}\phi & 0 & 0 & 0 \\ \mathrm{s}\psi\,\mathrm{s}\phi + \mathrm{c}\psi\,\mathrm{s}\theta\,\mathrm{c}\phi & -\mathrm{c}\psi\,\mathrm{s}\phi + \mathrm{s}\psi\,\mathrm{s}\theta\,\mathrm{c}\phi & \mathrm{c}\theta\,\mathrm{c}\phi & 0 & 0 & 0 \\ 0 & 0 & 0 & 1 & 0 & -\mathrm{s}\theta \\ 0 & 0 & 0 & 0 & \mathrm{c}\phi & \mathrm{c}\theta\,\mathrm{s}\phi \\ 0 & 0 & 0 & 0 & -\mathrm{s}\phi & \mathrm{c}\theta\,\mathrm{c}\phi \end{bmatrix}_{6\times 6}$$

(4.3)

in which c(·) = cos(·), s(·) = sin(·) and t(·) = tan(·).

If only surge, sway and yaw (3-DOF) are considered, the transformation in Eq. (4.1) is simplified to:

$$\begin{bmatrix} \dot{x} \\ \dot{y} \\ \dot{\psi} \end{bmatrix} = \left[\begin{array}{c|c|c} \mathrm{c}\psi & -\mathrm{s}\psi & 0 \\ \hline \mathrm{s}\psi & \mathrm{c}\psi & 0 \\ \hline 0 & 0 & 1 \end{array}\right] \begin{bmatrix} u \\ v \\ r \end{bmatrix} \tag{4.4}$$

4.2.2 Vessel model

The ship is considered to be a single rigid body with six degrees of freedom as mentioned above. In the traditional modeling of the marine vessel dynamics, it is common to consider using two models: the low frequency (LF) model and the wave frequency (WF) model (Balchen et al., 1980; Fossen, 2002 and Sørensen, 2004). In particular, the WF model accounts primarily for motions due to first-order wave loads whereas the LF model accounts predominantly for motions due to second-order varying wave loads, sea currents and wind loads. The total motion of marine vessels is the sum of the corresponding LF and the WF components.

The coupled equations of linear WF in the body-fixed *XYZ*-frame and nonlinear LF models of a moving vessel proposed by Sørensen (2004) are expressed, respectively, as follows

$$\mathbf{M}(\omega)\dot{\mathbf{v}}_w + \mathbf{D}_p(\omega)\mathbf{v}_w + \mathbf{G}\boldsymbol{\eta}_{Rw} = \boldsymbol{\tau}_{wave1} \tag{4.5}$$

$$\mathbf{M}\dot{\boldsymbol{\upsilon}} + \mathbf{C}_{RB}(\boldsymbol{\upsilon})\boldsymbol{\upsilon} + \mathbf{C}_A(\boldsymbol{\upsilon}_r)\boldsymbol{\upsilon}_r + \mathbf{D}_L\boldsymbol{\upsilon} + \mathbf{D}_{NL}(\boldsymbol{\upsilon}_r, \gamma_r) + \mathbf{G}(\boldsymbol{\eta}) = \boldsymbol{\tau}_{env2} + \boldsymbol{\tau}_{thr} \tag{4.6}$$

where $\boldsymbol{\eta}_{Rw}$ is the WF motion vector in the earth-fixed frame; $\mathbf{G}$ the matrix of linear generalized gravitation and buoyancy force coefficients; $\boldsymbol{\upsilon}_r$ the relative velocity vector with respect to water current; γ_r the current direction relative to the vessel; $\mathbf{D}_p(\omega)$ the

wave radiation damping matrix; $\mathbf{D}_L$ the strictly positive linear damping matrix caused by the linear wave drift damping and the laminar skin friction; $\mathbf{D}_{NL}(\boldsymbol{\upsilon}_r, \gamma_r)$ the nonlinear damping vector; $\mathbf{M}$ the system inertia mass including the added mass and is defined as

$$\mathbf{M} = \begin{bmatrix} m - X_{\dot{u}} & 0 & -X_{\dot{w}} & 0 & mz_G - X_{\dot{q}} & 0 \\ 0 & m - Y_{\dot{v}} & 0 & -mz_G - Y_{\dot{p}} & 0 & mx_G - Y_{\dot{r}} \\ -Z_{\dot{u}} & 0 & m - Z_{\dot{w}} & 0 & -mx_G - Z_{\dot{q}} & 0 \\ 0 & -mz_G - K_{\dot{v}} & 0 & I_{xx} - K_{\dot{p}} & 0 & -I_{xz} - K_{\dot{r}} \\ mz_G - M_{\dot{u}} & 0 & -mx_G - M_{\dot{w}} & 0 & I_{yy} - M_{\dot{q}} & 0 \\ 0 & mx_G - N_{\dot{v}} & 0 & -I_{zx} - N_{\dot{p}} & 0 & I_{zz} - N_{\dot{r}} \end{bmatrix}_{6\times 6} \tag{4.7}$$

in which m is the vessel mass; I_{xx}, I_{yy} and I_{zz} the moments of inertial about the x, y and z axes, respectively; and $I_{xz} = I_{zx}$ the products of inertia about the x, z axes. The zero-frequency added mass coefficients $X_{\dot{u}}$, $X_{\dot{w}}$, $X_{\dot{q}}$, $Y_{\dot{v}}$, $Y_{\dot{p}}$, $Y_{\dot{r}}$, $Z_{\dot{u}}$, $Z_{\dot{w}}$, $Z_{\dot{q}}$, $K_{\dot{v}}$, $K_{\dot{p}}$, $K_{\dot{r}}$, $M_{\dot{u}}$, $M_{\dot{w}}$, $M_{\dot{q}}$, $N_{\dot{v}}$, $N_{\dot{p}}$ and $N_{\dot{r}}$ at low speed in surge, sway, heave, roll, pitch and yaw due to accelerations along the corresponding and the coupled axes are defined in Faltinsen (1990). In addition, it should be noted that this inertia matrix $\mathbf{M}$ is symmetrical and positive definite.

$\mathbf{C}_{RB}(\boldsymbol{\upsilon})$ and $\mathbf{C}_A(\boldsymbol{\upsilon}_r)$ in Eq. (4.6) are the skew-symmetric Coriolis matrix and centripetal matrix of the rigid-body and potential induced added mass part of the current load, respectively. The skew-symmetric Coriolis and centripetal matrix $\mathbf{C}_{RB}(\boldsymbol{\upsilon})$ is proposed by Fossen (2002) as follows

$$\mathbf{C}_{RB}(\boldsymbol{\upsilon}) = \begin{bmatrix} 0 & 0 & 0 & c_{41} & -c_{51} & -c_{61} \\ 0 & 0 & 0 & -c_{42} & -c_{52} & -c_{62} \\ 0 & 0 & 0 & -c_{43} & -c_{53} & -c_{63} \\ -c_{41} & c_{42} & c_{43} & 0 & -c_{54} & -c_{64} \\ c_{51} & -c_{52} & c_{53} & c_{54} & 0 & -c_{65} \\ c_{61} & c_{62} & -c_{63} & c_{64} & c_{65} & 0 \end{bmatrix}_{6\times 6} \tag{4.8}$$

where

$$\begin{aligned} &c_{41} = mz_G r, && c_{42} = mw, && c_{43} = m(z_G p - v), && \\ &c_{51} = m(x_G q - w), && c_{52} = m(z_G r + x_G p), && c_{53} = m(z_G q + u), && c_{54} = I_{xz} p - I_z r, \\ &c_{61} = m(v + x_G r), && c_{62} = -mu, && c_{63} = mx_G p, && c_{64} = I_y q, \\ &c_{65} = I_x p + I_{xz} r && && && \end{aligned} \tag{4.9}$$

The potential induced added mass matrix $\mathbf{C}_A(\boldsymbol{\upsilon}_r)$ of the current load is given by (Sørensen et al., 1996)

$$\mathbf{C}_A(\boldsymbol{\upsilon}_r) = \begin{bmatrix} 0 & 0 & 0 & 0 & -c_{a51} & -c_{a61} \\ 0 & 0 & 0 & -c_{a42} & 0 & -c_{a62} \\ 0 & 0 & 0 & -c_{a43} & -c_{a53} & 0 \\ 0 & c_{a42} & c_{a43} & 0 & -c_{a54} & -c_{a64} \\ c_{a51} & 0 & c_{a53} & c_{a54} & 0 & -c_{a65} \\ c_{a61} & c_{a62} & 0 & c_{a64} & c_{a65} & 0 \end{bmatrix}_{6\times 6} \tag{4.10}$$

where

$$\begin{aligned} &c_{a42} = -Z_{\dot{w}} w - Z_{\dot{w}} u_r - Z_{\dot{q}} q, && c_{a43} = Y_{\dot{p}} p + Y_{\dot{v}} v_r + Y_{\dot{r}} r, && \\ &c_{a51} = Z_{\dot{q}} q + Z_{\dot{w}} w + X_{\dot{w}} u_r, && c_{a53} = -X_{\dot{q}} q - X_{\dot{u}} u_r - X_{\dot{w}} w, && c_{a54} = Y_{\dot{r}} v_r + K_{\dot{r}} p + N_{\dot{r}} r, \\ &c_{a61} = -Y_{\dot{v}} v_r - Y_{\dot{p}} p - Y_{\dot{r}} r, && c_{a62} = X_{\dot{u}} u_r + X_{\dot{w}} w + X_{\dot{q}} q, && c_{a64} = X_{\dot{q}} u_r + Z_{\dot{q}} w + M_{\dot{q}} q, \\ &c_{a65} = Y_{\dot{v}} v_r + K_{\dot{v}} p + K_{\dot{r}} r && && \end{aligned} \tag{4.11}$$

In Eq. (4.5), $\boldsymbol{\tau}_{wave1}$ is the first order wave excitation vector, which will be modified for varying vessel headings relative to the incident wave direction. In Eq. (4.6), $\boldsymbol{\tau}_{thr}$ is the control vector consisting of forces and moments produced by the thruster system and $\boldsymbol{\tau}_{env2}$ is the slowly-varying environmental loads and consists of mean wind load and second-order wave drift load vector and is given by Fossen (2002) as

$$\boldsymbol{\tau}_{env2} = \boldsymbol{\tau}_{wind} + \boldsymbol{\tau}_{wave2} \tag{4.12}$$

where more detail of the mean wind load $\boldsymbol{\tau}_{wind}$ and second-order wave drift load vector $\boldsymbol{\tau}_{wave2}$ can be found in Appendix B.

4.3 Governing equation of liquid sloshing-container system due to ship motion

The present study assumes that the resulting sloshing of liquid in the containers on the ship does not affect the motion of the ship. In other words, there is no interaction between the container and the ship. This assumption is valid for situations in which the size of the ship is large when compared to the size of the container. Thus, the problem is confined to only the effect of ship motion on the sloshing of the contained liquid. Only cylindrical containers will be considered. The containers mounted on the ship are modeled with axisymmetric RD-shell and fluid elements that were developed in Chapter 2 on the basis of the proposed relative displacement concept.

From Chapter 2, the free vibration equation of motion of the shell-liquid system may be written as

$$\begin{bmatrix} \mathbf{M}_s & \mathbf{0} \\ \mathbf{S} & \mathbf{M}_f \end{bmatrix} \begin{Bmatrix} \ddot{\mathbf{q}} \\ \ddot{\mathbf{p}} \end{Bmatrix} + \begin{bmatrix} \mathbf{K}_s & -\mathbf{S}^T \\ \mathbf{0} & \mathbf{K}_f \end{bmatrix} \begin{Bmatrix} \mathbf{q} \\ \mathbf{p} \end{Bmatrix} = \begin{Bmatrix} \mathbf{0} \\ \mathbf{0} \end{Bmatrix} \tag{4.13}$$

where $\mathbf{M}_s$ and $\mathbf{K}_s$ are the mass and stiffness matrices of the shell, respectively; $\mathbf{M}_f$ and $\mathbf{K}_f$ the mass and stiffness matrices of the liquid, respectively; $\mathbf{S}$ the liquid-shell coupling force matrix which accounts for the fluid-structure interaction; $\mathbf{q}$ and $\ddot{\mathbf{q}}$ the generalized shell nodal displacements and accelerations, respectively; $\mathbf{p}$ and $\ddot{\mathbf{p}}$ the liquid nodal pressure and its second derivative, respectively.

Based on Eq. (4.13), the governing equations of motion of the coupled liquid-tank due to external forces may be expressed in a single matrix equation as follows (Ang, 1980 and Balendra et al., 1982b)

$$\begin{bmatrix} \mathbf{M}_{bb} & \mathbf{M}_b^T & \mathbf{0} \\ \mathbf{M}_b & \mathbf{M} & \mathbf{0} \\ \mathbf{S}_b & \mathbf{S} & \mathbf{M}_f \end{bmatrix} \begin{Bmatrix} \ddot{\mathbf{q}}_b \\ \ddot{\mathbf{q}} \\ \ddot{\mathbf{p}} \end{Bmatrix} + \begin{bmatrix} \mathbf{K}_{bb} & \mathbf{K}_b^T & -\mathbf{S}_b^T \\ \mathbf{K}_b & \mathbf{K} & -\mathbf{S}^T \\ \mathbf{0} & \mathbf{0} & \mathbf{K}_f \end{bmatrix} \begin{Bmatrix} \mathbf{q}_b \\ \mathbf{q} \\ \mathbf{p} \end{Bmatrix} = \begin{Bmatrix} \mathbf{F}_b \\ \mathbf{0} \\ \mathbf{0} \end{Bmatrix} \tag{4.14}$$

The resulting motions of the ship obtained from the mathematical model of the ship described earlier in section 4.2.2, such as displacement, velocity and acceleration, are applied to the containers in the form of support motions. The matrices in Eq. (4.14) associated with the shell and the coupling force matrix have therefore been partitioned in order to separate the base and off-base nodal parameters. Thus, $\mathbf{q}_b$ and $\ddot{\mathbf{q}}_b$ are the applied base nodal displacements and accelerations of the shell, respectively, due to the motion of the ship; and $\mathbf{q}$, $\mathbf{p}$ the unknown total off-base nodal displacements of the shell and liquid nodal pressures, respectively. The symbols $\mathbf{M}$, $\mathbf{K}$ and $\mathbf{S}$ are being redefined to represent the shell mass, stiffness and liquid-shell coupling matrices associated with off-base nodes, respectively. The vector $\mathbf{F}_b$ denotes the base reactions corresponding to the five degrees of freedom of the base nodes, namely the three absolute displacements u_n, v_n, w_n and the two relative displacements Δu_n, Δv_n.

At any time t, the total off-base nodal displacements $\mathbf{q}$ of the shell can be considered as the sum of two parts

$$\mathbf{q} = \mathbf{q}_s + \mathbf{q}_d \tag{4.15}$$

in which $\mathbf{q}_s$ is the static term and also a function of the displacement of the ship, while $\mathbf{q}_d$ the dynamic term which depends on the acceleration history of ship motions.

While the stiffness and mass matrices of the shell and liquid are symmetric, it can be seen from Eq. (4.14) that the generalized governing stiffness and mass matrices of the coupled liquid-tank system are, however, not symmetric. This makes the extraction of eigenvalues and the corresponding eigenvectors of the homogeneous system of equations rather difficult, especially when dealing with very large matrices. Through some matrix operations given in following steps, Balendra et al. (1982b) was able to derive an equivalent form of the governing equations involving only symmetric system matrices. These operations are explained below.

From the second row of Eq. (4.14), one obtains

$$\ddot{\mathbf{q}} = -\mathbf{M}^{-1}\left(\mathbf{K}_b\mathbf{q}_b + \mathbf{K}\mathbf{q} - \mathbf{S}^T\mathbf{p} + \mathbf{M}_b\ddot{\mathbf{q}}_b\right) \tag{4.16}$$

The substitution of Eq. (4.16) into the third row of Eq. (4.14) leads to

$$\left(\mathbf{S}_b - \mathbf{S}\mathbf{M}^{-1}\mathbf{M}_b\right)\ddot{\mathbf{q}}_b + \mathbf{M}_f\ddot{\mathbf{p}} - \left(\mathbf{S}\mathbf{M}^{-1}\mathbf{K}_b\right)\mathbf{q}_b - \left(\mathbf{S}\mathbf{M}^{-1}\mathbf{K}\right)\mathbf{q} + \left(\mathbf{K}_f + \mathbf{S}\mathbf{M}^{-1}\mathbf{S}^T\right)\mathbf{p} = \mathbf{0} \tag{4.17}$$

and after pre-multiplying the second row of Eq. (4.14) by $\mathbf{K}\mathbf{M}^{-1}$, one obtains

$$\left(\mathbf{K}\mathbf{M}^{-1}\mathbf{M}_b\right)\ddot{\mathbf{q}}_b + \mathbf{K}\ddot{\mathbf{q}} + \left(\mathbf{K}\mathbf{M}^{-1}\mathbf{K}_b\right)\mathbf{q}_b + \left(\mathbf{K}\mathbf{M}^{-1}\mathbf{K}\right)\mathbf{q} - \left(\mathbf{K}\mathbf{M}^{-1}\mathbf{S}^T\right)\mathbf{p} = \mathbf{0} \tag{4.18}$$

By combining the first row of Eq. (4.14) with Eqs. (4.17) and (4.18), one obtains the following equivalent matrix equation of motion of coupled system

$$\left[\begin{array}{c|c|c} \mathbf{M}_{bb} & \mathbf{M}_b^T & \mathbf{0} \\ \hline \mathbf{K}\mathbf{M}^{-1}\mathbf{M}_b & \mathbf{K} & \mathbf{0} \\ \hline \mathbf{S}_b - \mathbf{S}\mathbf{M}^{-1}\mathbf{M}_b & \mathbf{0} & \mathbf{M}_f \end{array}\right] \left\{\begin{array}{c} \ddot{\mathbf{q}}_b \\ \ddot{\mathbf{q}}_s + \ddot{\mathbf{q}}_d \\ \ddot{\mathbf{p}} \end{array}\right\} + \left[\begin{array}{c|c|c} \mathbf{K}_{bb} & \mathbf{K}_b^T & -\mathbf{S}_b^T \\ \hline \mathbf{K}\mathbf{M}^{-1}\mathbf{K}_b & \mathbf{K}\mathbf{M}^{-1}\mathbf{K} & -\mathbf{K}\mathbf{M}^{-1}\mathbf{S}^T \\ \hline -\mathbf{S}\mathbf{M}^{-1}\mathbf{K}_b & -\mathbf{S}\mathbf{M}^{-1}\mathbf{K} & \mathbf{K}_f + \mathbf{S}\mathbf{M}^{-1}\mathbf{S}^T \end{array}\right] \left\{\begin{array}{c} \mathbf{q}_b \\ \mathbf{q}_s + \mathbf{q}_d \\ \mathbf{p} \end{array}\right\} = \left\{\begin{array}{c} \mathbf{F}_b \\ \mathbf{0} \\ \mathbf{0} \end{array}\right\} \tag{4.19}$$

The static nodal displacements $\mathbf{q}_s$ may be computed readily from the static relationships (Clough, 1969)

$$\mathbf{K}_b\mathbf{q}_b + \mathbf{K}\mathbf{q}_s = \mathbf{0} \tag{4.20}$$

in which the only loading is the specified support displacement vector $\mathbf{q}_b$.

Solving Eq. (4.20) for the nodal displacements gives

$$\mathbf{q}_s = -\mathbf{K}^{-1}\mathbf{K}_b\mathbf{q}_b \tag{4.21}$$

The vector $\mathbf{q}_s$ in Eq. (4.21) can be expressed numerically as a series of $\mathbf{q}_b$ and it is developed through rigid body displacements consistent with $\mathbf{q}_b$ as follows

$$\mathbf{q}_s = \left\{\begin{array}{c} \mathbf{q}_{s1} \\ \mathbf{q}_{s2} \\ \mathbf{q}_{s3} \\ \cdots \\ \cdots \\ \mathbf{q}_{sN} \end{array}\right\} = \left[\begin{array}{c} \mathbf{I} \\ \mathbf{I} \\ \mathbf{I} \\ \cdots \\ \cdots \\ \mathbf{I} \end{array}\right] \mathbf{q}_b \tag{4.22}$$

where $\mathbf{q}_b$ is the (5×1) vector comprising the meridional, circumferential and radial displacements as well as the relative displacements along the meridional and circumferential directions of the generator about the base; $\mathbf{q}_{si}$ the displacement vector of node i; N the total number of shell elements and $\mathbf{I}$ a (5×5) unit matrix.

By substituting Eqs. (4.21) and (4.22) into the second row and the third row of Eq. (4.19), one obtains

$$\hat{\mathbf{M}}\ddot{\mathbf{U}} + \hat{\mathbf{K}}\mathbf{U} = \mathbf{M}_{eff}\ddot{\mathbf{q}}_b \tag{4.23}$$

where $\mathbf{M}_{eff}$ is the effective mass matrix given by

$$\mathbf{M}_{eff} = -\begin{bmatrix} \mathbf{K}\mathbf{M}^{-1}\mathbf{M}_b + \mathbf{K}\begin{bmatrix}\mathbf{I}\\ \mathbf{I}\\ \mathbf{I}\\ \cdots\\ \cdots\\ \mathbf{I}\end{bmatrix} \\ \cdots\cdots\cdots\cdots\cdots \\ -\mathbf{S}\mathbf{M}^{-1}\mathbf{M}_b + \mathbf{S}_b \end{bmatrix} \tag{4.24}$$

and $\mathbf{U} = \begin{Bmatrix}\mathbf{q}_d\\ \mathbf{p}\end{Bmatrix}$ the generalized system displacement vector, comprises $\mathbf{q}_d$ the dynamic displacements of the container walls and $\mathbf{p}$ the pressures in the liquid. The generalized symmetric matrices $\hat{\mathbf{K}}$ and $\hat{\mathbf{M}}$ of the coupled system are now symmetric and are defined from Eq. (4.19) upon setting the external forces to be zero as follows

$$\hat{\mathbf{K}} = \left[\begin{array}{c|c} \mathbf{K}\mathbf{M}^{-1}\mathbf{K} & -\mathbf{K}\mathbf{M}^{-1}\mathbf{S}^T \\ \hline -\mathbf{S}\mathbf{M}^{-1}\mathbf{K} & \mathbf{K}_f + \mathbf{S}\mathbf{M}^{-1}\mathbf{S}^T \end{array}\right] \tag{4.25}$$

$$\hat{\mathbf{M}} = \begin{bmatrix} \mathbf{K} & \mathbf{0} \\ \mathbf{0} & \mathbf{M}_f \end{bmatrix} \tag{4.26}$$

The dynamic response of the coupled liquid-tank system due to the motion of the ship transporting the liquid-filled containers can be obtained by solving Eq. (4.23). In order to solve this differential equation of dynamic motion, one may use any of the standard numerical methods such as the Euler, improved Euler, Taylor series, Runge-Kutta, Central difference, Houbolt, Wilson and Newmark methods (Rao, 1990; Geradin and Rixen, 1994; Chopra, 1995; and Joseph, 1999). The Wilson-θ method with $\theta = 1.4$ is employed to solve the dynamic equation.

4.4 Verification of computer code

The following examples are considered in order to verify the foregoing procedures and computer code. This example concerns the dynamic analysis of a partially liquid-filled cylindrical container subjected to a sinusoidal ground acceleration. The amplitude of the ground acceleration is $0.25\,g$ and its frequency is $2\,cps$. The effect of the liquid sloshing on the flexibility of the container wall is studied by using the RD-finite element program developed. The boundary condition of this liquid-filled container is clamped-free. The material properties and geometrical parameters used for the liquid-filled container are the same as those used by Subhash and Bhattacharyya (1996), which are shown in Table 4.2.

Table 4.2 Material and geometrical parameters of liquid-filled containers subjected to sinusoidal ground acceleration

H	Height of container	$2.1\,m$
H_f	Height of liquid	$1.8\,m$
R	Radius of container	$0.7\,m$
h	Thickness of container	$25.4\,mm$
ν	Poisson's ratio	0.3
E	Young's modulus	$20.67 \times 10^7\,kPa$
ρ_s	Mass density of shell	$7840\,kg/m^3$
ρ_f	Mass density of liquid	$1000\,kg/m^3$

The Wilson-θ method has been used for the time integration. The sinusoidal ground acceleration and the comparison of radial displacement w at the free end of the container wall are shown in Figures 4.3 and 4.4, respectively.

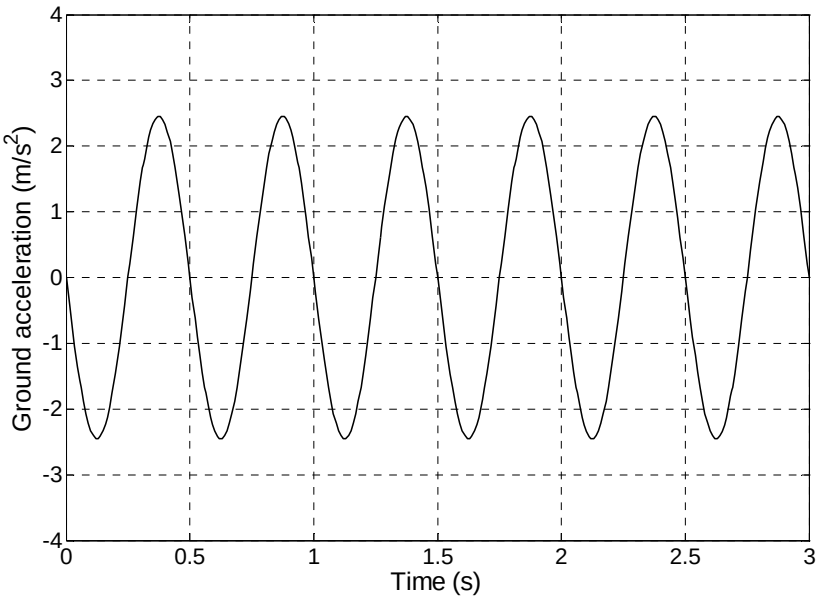

Figure 4.3 Sinusoidal ground acceleration

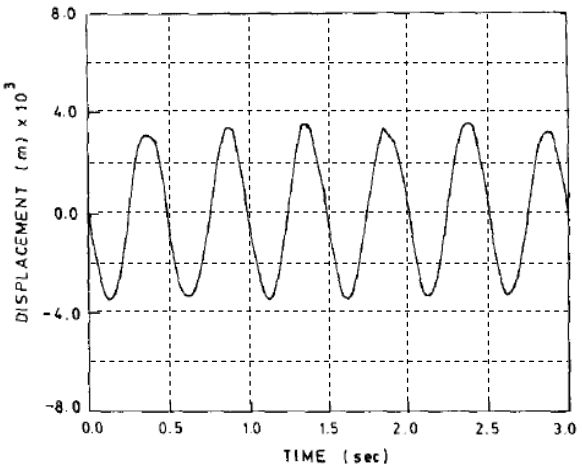

Reproduction from paper of Subhash and Bhattacharyya (1996)

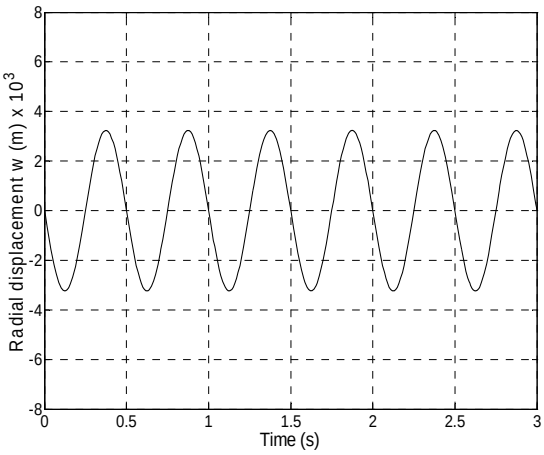

Present study using RD concept

Figure 4.4 Radial displacement at free end of the container wall

It can be seen from Figure 4.4 that the radial displacements obtained using thin shell elements (Subhash and Bhattacharyya, 1996) and those obtained in this study using the relative displacement concept are in excellent agreement. This provides evidence that the proposed methodology and developed computer codes may be used to analyse the response of liquid sloshing-container system due to ship motion which will be dealt with in the next section.

4.5 Dynamic analysis of liquid-filled cylindrical containers due to ship motion

The motion of the ship is governed by the sea state, which is defined by several parameters. These parameters and their values adopted are (1) the calculated peak wave frequency $0.72 rad/s$, (2) the mean wind velocity at a height of 10 meters, $u_{10} = 7.65 m/s$ and (3) the mean wind direction 60^0. These values are based on the NORSOK wind gust and JONSWAP wave spectrums that use 30 harmonic wave components. The spectral density function is written as:

$$S(\omega) = 155 \frac{H_s^2}{T_1^4} \omega^{-5} \exp\left(-\frac{944}{T_1^4} \omega^{-4} \right) \gamma^Y \tag{4.27}$$

where the significant wave height $H_s = 0.5m$, gamma parameter $\gamma = 3.3$ and

$$Y = \exp\left[-\left(\frac{0.191\omega T_1 - 1}{\sqrt{2}\sigma}\right)^2\right] \tag{4.28}$$

where T_1 the average wave period, ω the frequency of the spectrum and

$$\sigma = \begin{cases} 0.07 & for \ \ \omega \le 5.24 / T_1 \\ 0.09 & for \ \ \omega > 5.24 / T_1 \end{cases} \tag{4.29}$$

The supply ship design main parameters and the JONSWAP wave spectrum are given in Table 4.3 and Figure 4.5, respectively.

Table 4.3 Supply ship design parameters

V_{dis}	Displacement volume	$6000\,m^3$
m	Mass	$2433\,Ton$
L_{oa}	Overall length	$120\,m$
B	Breadth	$17.4\,m$
T	Design draught	$5.6\,m$
r_{cg}	Vector from COH (center of hydrodynamic) to center of gravity	$[-2.3\ 0\ -5.2]\,m$
r_{cb}	Vector from COH to center of buoyancy	$[-2.3\ 0\ -3.0]\,m$
r_{ca}	Vector from COH to center of added mass	$[0\ 0\ 0]\,m$
r_{cd}	Vector from COH to center of damping	$[-2.3\ 0\ -5.2]\,m$
$r_{current}$	Coordinates in which current data are specified	$[-2.3\ 0\ -5.6]\,m$
r_{wind}	Coordinates in which wind data are specified	$[-2.3\ 0\ -5.6]\,m$
$r_{wavedrift}$	Coordinates in which wavedrift data are specified	$[-2.3\ 0\ -5.6]\,m$
$\left(\tau_{surge}\right)_{\max}$	Maximum thrust force in surge	$0.3\times10^6\,N$
$\left(\tau_{sway}\right)_{\max}$	Maximum thrust force in sway	$0.12\times10^6\,N$
$\left(\tau_{yaw}\right)_{\max}$	Maximum thrust force in yaw	$9.7\times10^6\,N$
$\left(A_{wind}\right)_{surge}$	Projected wind force area, surge	$330\,m^2$
$\left(A_{wind}\right)_{sway}$	Projected wind force area, sway	$720\,m^2$
$\left(A_{current}\right)_{surge}$	Projected current force area, surge	$100\,m^2$
$\left(A_{current}\right)_{sway}$	Projected current force area, sway	$430\,m^2$

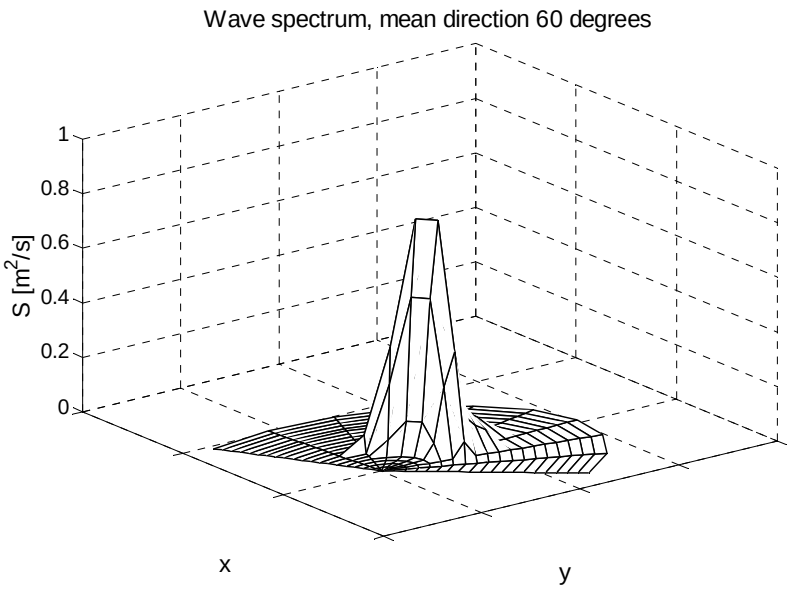

Figure 4.5 JONSWAP wave spectrum

The following numerical examples illustrate the capability of the current model in capturing the liquid sloshing in the cylindrical containers that are placed on a moving ship. For all other problems considered, the containers are assumed to be fixed at the base and free at the top end. It should be noted that the center of the base of container coincides with the COG of the ship. The effect of liquid sloshing on the flexibility of cylindrical container walls is also considered. A parametric study is carried out to investigate the effects of various parameters of the containers and environmental settings such as the directions of wave and wind acting on the moving ship.

4.5.1 Parametric study of sloshing in containers

Various values of liquid-filled cylindrical container parameters including thickness-to-radius h/R, liquid-to-container height $\beta = H_f / H$ and radius-to-container height R/H ratios are considered. In this study, the variation of maximum radial displacement $w_{\max}$ of the container walls with respect to liquid height and thickness-

to-radius ratio is determined. The parameters used for the cylindrical container are shown in Table 4.4.

Table 4.4 Material and geometrical parameters of liquid-filled containers on the moving ship

H	Height of container	$8\,m$
R	Radius of container	$4\,m$
ν	Poisson's ratio	0.3
E	Young's modulus	$200\times10^{9}\,N/m^{2}$
ρ_s	Mass density of shell	$7800\,kg/m^{3}$
ρ_f	Mass density of oil	$820\,kg/m^{3}$

Figure 4.6 shows the variation of the maximum radial displacement $w_{\max}$ with respect to different values of liquid-to-container height ratio $\beta = H_f / H$ and the thickness-to-radius ratio h/R. In particular, the liquid-to-container height ratio is varied from $\beta = 0$ (i.e. empty cylindrical container) to $\beta = 1$ (i.e. completely liquid-filled cylindrical container) and the thickness-to-radius ratio h/R is also varied from 0.01 to 0.05. Referring to this figure, it is found that the maximum radial displacement expectedly decreases when the tank wall increases in stiffness with increasing thickness-to-radius ratio h/R. For any value of h/R ratio, the maximum radial displacement $w_{\max}$ increases when the tank is filled with more liquid with increasing liquid-to-container height ratio β. In particular, the maximum radial displacement is noted to be minimum and at the same value for all thickness-to-radius h/R ratios when the liquid height ratio β is smaller than 0.4. Therefore, one can conclude that the effect of liquid sloshing on the vibration response of the tank wall is negligible for low liquid level (the container is less than 40% of its capacity), but its influence tends to increase appreciably for containers filled beyond this critical level.

For liquid level ratios $\beta > 0.4$, it is found that the sloshing effect is reduced significantly with increasing the thickness-to-radius ratio h/R from 0.01 to 0.05. For example, it is noted that the maximum radial displacement for the case of fully-filled containers ($\beta = 1$) decreases appreciably by 46% when the thickness-to-radius ratio h/R doubles from 0.01 to 0.02. The reduction is smaller at 28% when the thickness-to-radius ratio h/R increases from 0.02 to 0.03. As can be seen from Figure 4.6, the reduction continues to decrease as the tank thickness keeps on increasing. Thus, it may be conducted that increasing the thickness of the tank wall beyond a certain critical value may not be cost-effective in limiting the maximum deformation in the tank wall.

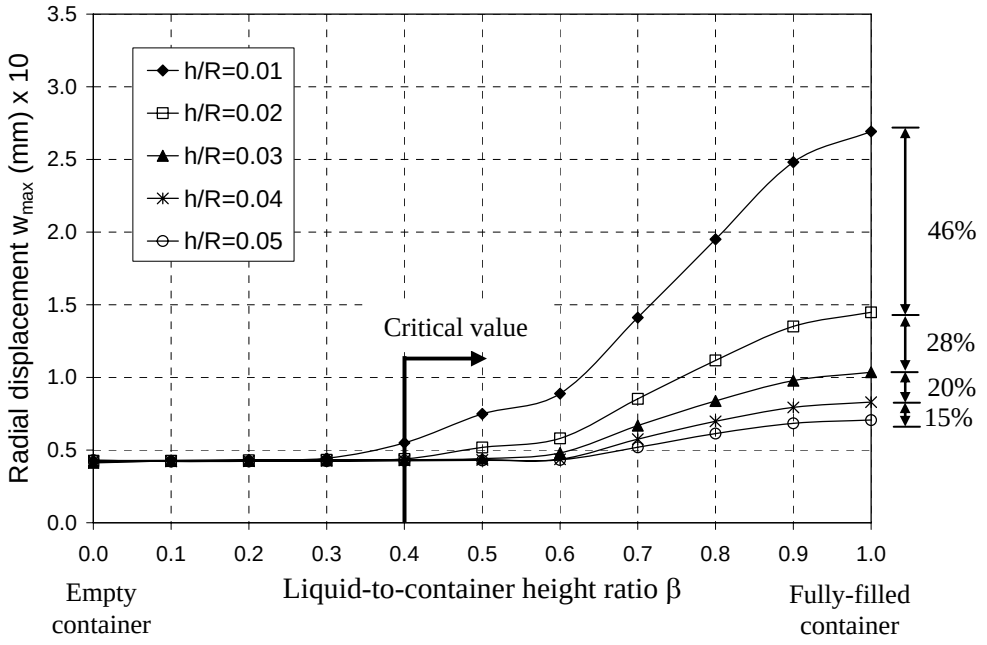

Figure 4.6 Effect of liquid height and thickness-to-radius ratio

Figure 4.7 displays the variation of maximum radial displacement $w_{\max}$ of the container walls with respect to thickness-to-radius ratio h/R and radius-to-container height ratio R/H. The container is assumed to be fully-filled with liquid. The material and geometrical parameters used for the clamped-free container are given in Table 4.5.

Table 4.5 Material and geometrical parameters of fully-filled containers on the moving ship

H	Height of container	$8\,m$
H_f	Height of liquid	$8\,m$
ν	Poisson's ratio	0.3
E	Young's modulus	$200\times10^9\,N/m^2$
ρ_s	Mass density of shell	$7800\,kg/m^3$
ρ_f	Mass density of oil	$820\,kg/m^3$

The radius-to-container height ratio R/H is varied from 0.4 (i.e. reasonably tall and slender liquid-filled cylindrical container) to 1.0 (i.e. short and stocky liquid-filled cylindrical container) and the thickness-to-radius ratio h/R is also varied from 0.01 to 0.05. As can be seen from Figure 4.7 that the maximum radial displacement $w_{\max}$ decreases when the radius-to-container height ratio R/H increases, i.e. the container becomes more stocky in shape. As expected, the maximum radial displacement increases when the thickness-to-radius ratio h/R decreases. From this figure, it can be concluded that for containers with R/H smaller than the critical value of 0.8, the sloshing effect becomes significant. In particular, when containers are relatively slender (i.e. the radius-to-container height ratio R/H is less than 0.8), there is a significant increase in the maximum radial displacement $w_{\max}$ as the thickness-to-radius ratio h/R is reduced by half from 0.02 to 0.01.

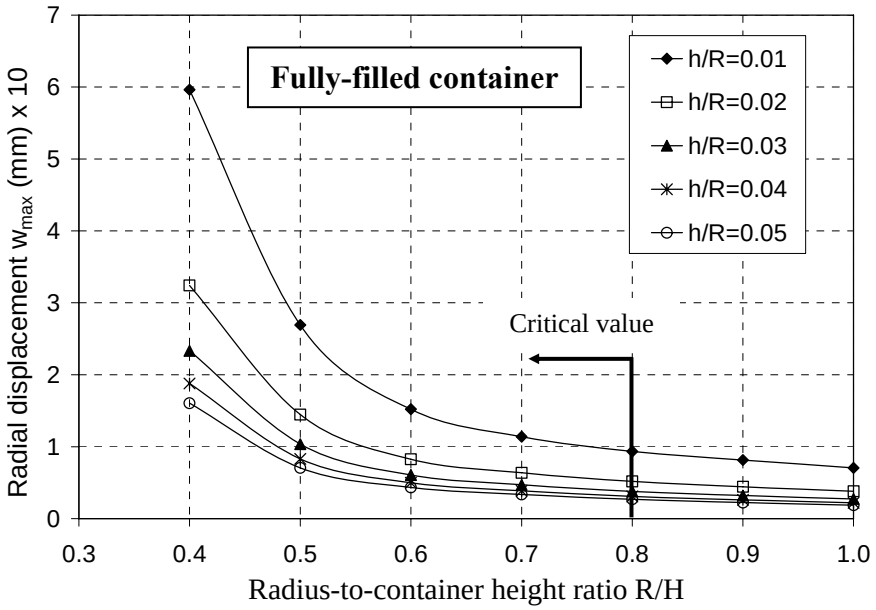

Figure 4.7 Effect of radius-to-container height and thickness-to-radius ratios

From the two foregoing case studies, one can conclude that by increasing slightly the thickness, the maximum radial displacement w_{max} in the tank wall can be decreased significantly. However, there is lesser and lesser decrease in maximum displacement when the tank wall set relatively thick. This prediction of the container wall displacements due to liquid sloshing is useful in the design of liquid-filled containers.

4.5.2 Effect of mean wave and wind directions

Among several factors that can affect a moving ship, the environmental settings that the ship is subjected to are the most significant. Environmental settings such as the directions of wave and wind acting on the moving ship are investigated next. The material and geometrical parameters of the fully liquid-filled cylindrical containers used in this part of the study are presented in Table 4.6.

Table 4.6 Material and geometrical parameters of liquid-filled containers on the moving ship

H	Height of container	$8\,m$
H_f	Height of liquid	$8\,m$
R	Radius of container	$4\,m$
ν	Poisson's ratio	0.3
E	Young's modulus	$200\times10^9\,N/m^2$
ρ_s	Mass density of shell	$7800\,kg/m^3$
ρ_f	Mass density of oil	$820\,kg/m^3$

In the definition of sea state codes (Price and Bishop, 1974) as shown in Table 4.7, one can observe that the sea state considered in this study may be regarded as a mild sea since the significant wave height $H_s = 0.5m$.

Table 4.7 Definition of Sea State codes

Sea state code	Sea states	Wave height $H_s(m)$
0	Calm (glassy)	0
1	Calm (ripples)	0-0.1
2	Smooth (wavelets)	0.1-0.5
3	Slight	0.5-1.25
4	Moderate	1.25-2.5
5	Rough	2.5-4.0
6	Very Rough	4.0-6.0
7	High	6.0-9.0
8	Very high	9.0-14.0
9	Phenomenal (Extreme)	Over 14.0

Figures 4.8 and 4.9 show the variation of the maximum radial displacement $w_{\max}$ of container walls with respect to mean wave and wind directions, respectively. It should be noted that the mean directions of wave and wind are varied from 0^0 to 180^0 (0^0 is aft and 180^0 is stern direction) at 30^0 intervals. The thickness-to-radius ratio h/R is varied from 0.01 to 0.05, which is the same as foregoing studies. From Figures 4.8 and 4.9, it can be seen that $w_{\max}$ is largest when the wave or wind acts in the sway

direction. This critical direction of 90^0 is an important finding which needs to be considered in the design of the ships for use under different sea states.

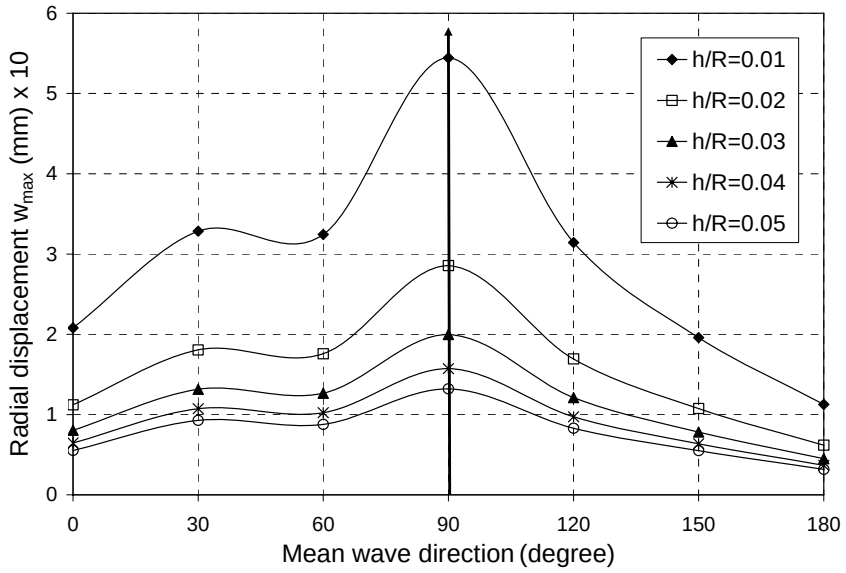

Figure 4.8 Effect of mean wave direction

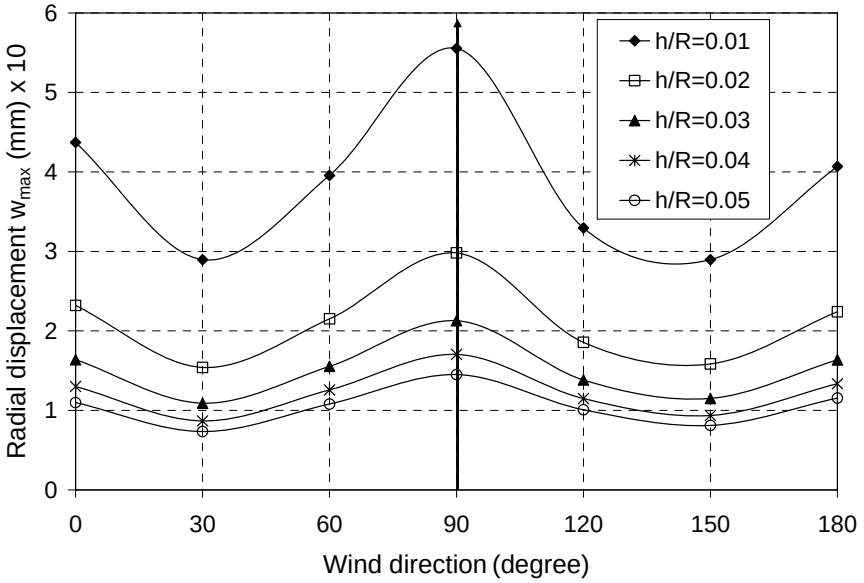

Figure 4.9 Effect of wind direction

4.5.3 Stress resultants of containers

Next, the stress response of fully liquid-filled cylindrical containers due to ship motion is investigated. The parameters of the containers are the same as those used in the foregoing examples (see Table 4.6) and the thickness-to-radius ratio h/R adopted is 0.01.

Figure 4.10 presents the time history plot of the acceleration of ship motion in the surge direction. The acceleration of the ship is entered as input data into the sloshing analysis program which is used to compute the equivalent external forces acting at the container base. The radial displacement w time history response at the top of container wall is shown in Figure 4.11. As can be seen from Figures 4.10 and 4.11, the maximum acceleration of the ship in surge is $1.49\,m/s^2$ and the resulting maximum radial displacement $w_{\max}$ at the free end of the container wall is found to be $0.78\,mm$.

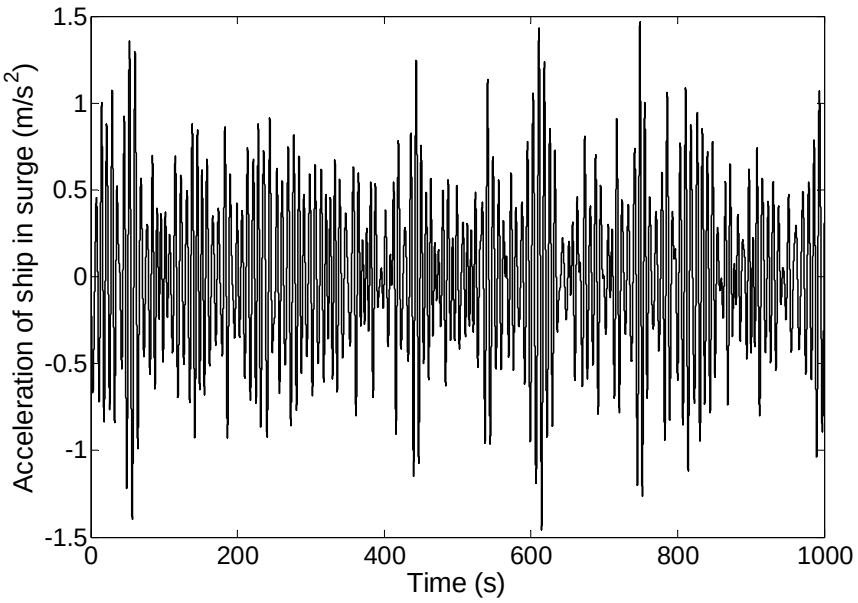

Figure 4.10 Acceleration time history of ship motion in surge

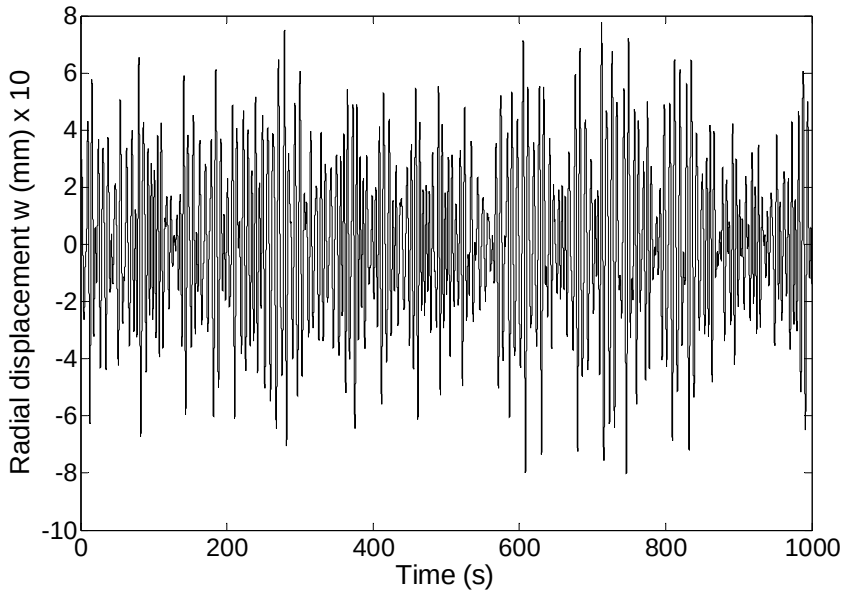

Figure 4.11 Radial displacement time history response at free end of container wall

The moments M_s, M_θ, $M_{s\theta}$, $M_{\theta s}$ and stress resultants σ_s, σ_θ, $\sigma_{s\theta}$, $\sigma_{\theta s}$ on a typical cylindrical shell element are shown in Figure 4.12.

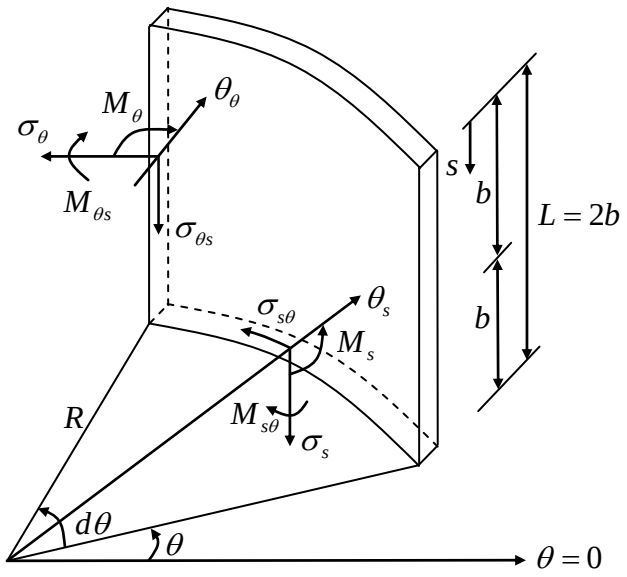

Figure 4.12 Stress resultants of typical cylindrical shell element

Figure 4.13 displays the typical distribution of maximum stress resultants in the shell wall along the height of the liquid-filled cylindrical containers. It should be pointed out that the maximum stress resultants may not occur at the same section of the container. In particular, the axial stress σ_s and the membrane shear stress $\sigma_{s\theta}$ are noted to be maximum at the base whereas the maximum hoop stress σ_θ is found to occur either at the base or at a section above the base depending on the liquid height.

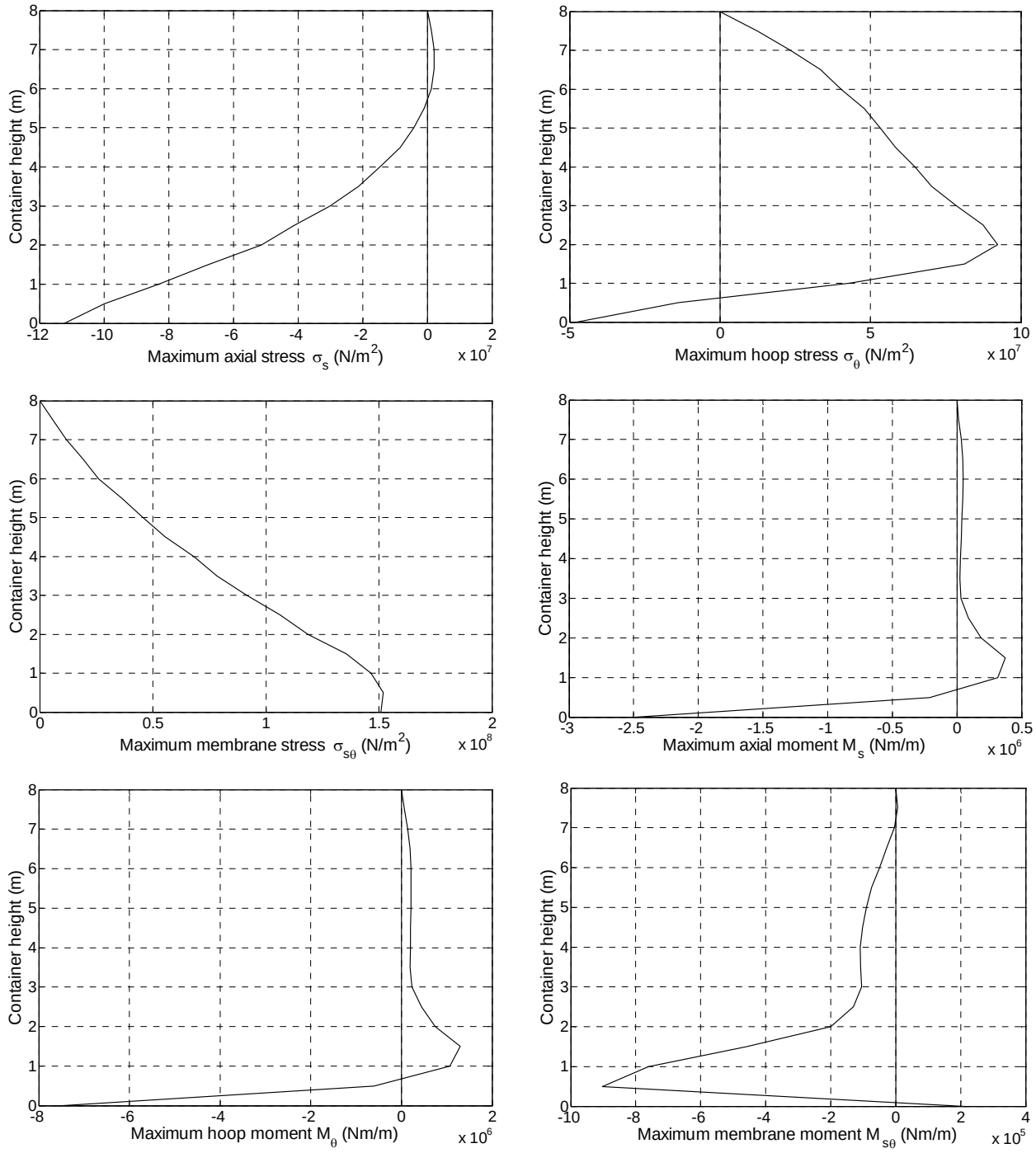

Figure 4.13 Stress resultants in the shell wall of liquid-filled cylindrical containers

4.6 Concluding remarks

A finite element method based on the relative displacement concept was developed to predict the dynamic behavior of liquid-filled cylindrical containers that are fixed at the base to a moving ship. Through several examples, the validity of the proposed method was verified. Many factors influencing the dynamic response of liquid-filled containers due to ship motion were investigated. These factors include container parameters and environmental settings such as the directions of wave and wind acting on the moving ship. Some interesting findings include:

- Sloshing is significant when (1) the liquid-to-container height ratio H_f / H is greater than 0.4, (2) containers are slender with radius-to-container height ratios R / H that are smaller than 0.8, (3) the wave and wind act in the sway direction.
- Significant increase in sloshing effect is noted when thickness-to-radius ratio h / R decreases below 0.02, i.e. for thin cylindrical containers.
- For clamped-free containers, the results show that the stress resultants σ_s, $\sigma_{s\theta}$ are maximum at the base of containers, σ_θ is maximum at the base or the section above the base depending on the liquid level.

In general, the proposed RD-finite element method can be used as an effective tool for the dynamic analysis of liquid-filled cylindrical containers due to any base motions such as those arising from earthquakes, ship motions and moving vehicles.

CHAPTER 5 FULLY COUPLED INTERACTION BETWEEN LIQUID SLOSHING, CONTAINERS AND MOVING SHIP

5.1 Introduction

In order to power the large economies of USA, Japan, China and many other developed nations, vast amounts of fuel and gas have to be transported rapidly and cheaply from the oil and gas fields. Marine vessels play a large role in the transportation of fuel and gas from their sources to far away consumers. Containers holding fuel and liquefied natural gas (LNG) have to be designed against not only the static pressure but also the dynamic pressure due to the sloshing of the fuel and LNG as the ship moves across the ocean. The knowledge of realistic impact problem between fluid sloshing and container wall will govern the design of these containers. Another problem that should be considered is the seakeeping of the moving ship. This is because fluid motions inside the containers can significantly change the ship response in waves. So far, in conventional ship motion analyses, the effects of tank sloshing on the global motions of ship were assumed to be negligible and hence ignored (Mikelis and Journee, 1984; Lee and Choi, 1999). These studies are only valid when the ship size is very much larger than the size of the containers. Otherwise, the interactive effects between them become significant as the ratio of volume of the containers to that of the ship exceeds a critical value. Hence, both the sloshing phenomenon and associated ship motion behaviour should be treated in a general case.

Several investigations on coupled liquid-container-ship motion have been reported. For example, the linear potential theory in the frequency domain was adopted in the coupling analysis between the sloshing liquid and ship motion (Molin et al., 2002; Malenica et al., 2003). A numerical study on sloshing flows coupled with ship motions was conducted by Kim (2002). In the study, the use of Anti-Rolling Tank (ART) revealed the significant coupling effect between ship motion and sloshing flow. Park et al. (2005) carried out a numerical analysis of the sloshing impact pressure of the LNG carriers in rough sea. The three-dimensional numerical model using SOLA-VOF (Solution Algorithm-Volume of Fluid) scheme was adopted to predict the violent free surface movements in the LNG tank. Kim et al. (2005) presented a numerical approach to evaluate the sloshing-ship motion coupling effect on the sloshing impact load of the LNG containment system. The motion of liquid cargo inside a LNG tank was solved by using the FEM under the assumption of potential theory in the time domain. Recently, Lee et al. (2007a) carried out a study on rectangular LNG tanks subjected to external loadings by using a computational fluid dynamics (CFD) program. The CFD simulations were verified against experimental results. Kim et al. (2007) investigated the coupling effects between ship motion and sloshing liquid in a rectangular anti-rolling tank. The results were verified by comparing the motion Response Amplitude Operators (RAOs) between the frequency domain solution and the solution obtained by the impulse response function (IRF) method. It was found that the nonlinearity of sloshing flow is very important in coupling analysis and the ship motion is strongly sensitive to the wave slope. In addition, Lee et al. (2007b) analyzed the coupling and interaction between ship motion and tank sloshing using a time-domain simulation scheme. However, wind and current were not considered in the ship calculations. The study treated environmental forces that were due to wave loading only.

So far, very few studies have been carried out to understand the real fully coupled interaction between the sloshing phenomenon and associated ship motion. In general, all the aforementioned studies were confined to the coupling interaction problem between the moving ship and only one or two liquid-filled containers. In reality, a vessel carries several containers. Moreover, linear ship motion using simple models was adopted in the earlier studies. The total effects of environmental settings (wind, wave and current) and thruster modeling were not considered.

In this chapter, the complicated interaction problem between nonlinear ship motion and liquid sloshing in multi-containers carrying liquid cargo (see Figure 5.1) will be investigated. The axisymmetric RD-elements formulated on the basis of the relative displacement concept proposed in the current work will be employed to model the multi-container walls. Several parameters of interests, including the container parameters, levels of liquid, number and location of containers, environmental settings and thruster modeling will be investigated. Their effects on global liquid-container-moving ship system will be studied in detail. Presented herein are some results of the coupled liquid-container-ship motion system such as displacement and acceleration time histories of the moving ship, deformation and stresses in the shell walls for different number of containers and levels of liquid-filling. In order to show the significance of coupled interaction effects, the present study will compare the results of two cases, namely (1) case one assumes that the resulting liquid-container interaction does not affect the motion of the ship and (2) case two considers the full complicated interaction between the liquid sloshing, multi-containers and the moving ship.

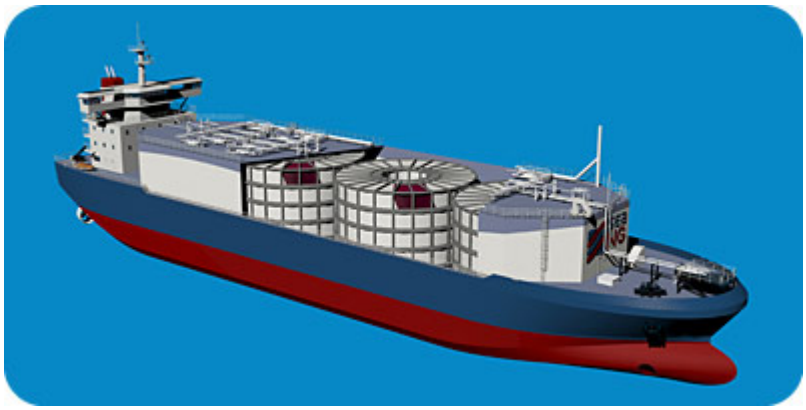

Figure 5.1 Ship carrying multi-tanks containing liquid fuel

Source: www.coselle.com

5.2 Governing equation of marine vessels

A moving ship is modeled as a single rigid body with six degrees-of-freedom. The components of nonlinear ship motion such as displacement, velocity and acceleration were presented in Chapter 4 for low frequency and wave frequency modes. The complicated interaction problem between the liquid sloshing, multi-containers and the moving ship is considered in this chapter. At each time step, the ship motion induces stresses and deformations as well as sloshing of fluid in the liquid-filled containers and in return, these containers produce reaction forces that affect the ship motion. The resulting motions of liquid sloshing inside each container are applied to the moving ship in the form of external forces $\boldsymbol{\tau}_{con1}$ and $\boldsymbol{\tau}_{con2}$, which will shortly be defined later, for WF and LF models, respectively. Based on suggestions by Sørensen (2004) presented in Chapter 4, the coupled equations of linear WF in the body-fixed *XYZ*-frame and nonlinear LF models that allow for the coupled interaction between multi-containers and the moving ship are extended, respectively, as

$$\mathbf{M}(\omega)\dot{\mathbf{v}}_w + \mathbf{D}_p(\omega)\mathbf{v}_w + \mathbf{G}\boldsymbol{\eta}_{Rw} = \boldsymbol{\tau}_{wave1} + \boldsymbol{\tau}_{con1} \tag{5.1}$$

$$\begin{aligned}\mathbf{M}\dot{\mathbf{v}} + \mathbf{C}_{RB}(\mathbf{v})\mathbf{v} + \mathbf{C}_A(\mathbf{v}_r)\mathbf{v}_r + \mathbf{D}_L\boldsymbol{\upsilon} \\ + \mathbf{D}_{NL}(\boldsymbol{\upsilon}_r, \gamma_r) + \mathbf{G}(\boldsymbol{\eta}) = \boldsymbol{\tau}_{env2} + \boldsymbol{\tau}_{thr} + \boldsymbol{\tau}_{con2}\end{aligned} \tag{5.2}$$

where $\mathbf{M}$ is the inertia mass matrix of system; $\boldsymbol{\eta}_{Rw}$ the WF motion vector in the earth-fixed frame; $\mathbf{G}$ the matrix of linear generalized gravitation and buoyancy force coefficients; $\boldsymbol{\upsilon}_r$ the relative velocity vector with respect to water current; γ_r the current direction relative to the vessel; $\mathbf{C}_{RB}(\mathbf{v})$ and $\mathbf{C}_A(\mathbf{v}_r)$ the skew-symmetric Coriolis matrix and centripetal matrix of the rigid-body and potential induced added mass part of the current load, respectively; $\mathbf{D}_p(\omega)$ the wave radiation damping matrix; $\mathbf{D}_L$ the strictly positive linear damping matrix caused by the linear wave drift damping and the laminar skin friction; $\mathbf{D}_{NL}(\boldsymbol{\upsilon}_r, \gamma_r)$ the nonlinear damping vector; $\boldsymbol{\tau}_{wave1}$ the first order wave excitation vector, which will be modified for varying vessel headings relative to the incident wave direction; $\boldsymbol{\tau}_{thr}$ the control vector consisting of forces and moments produced by the thruster system; $\boldsymbol{\tau}_{con1}$ and $\boldsymbol{\tau}_{con2}$ the vectors consisting of forces and moments produced at the bases of multi-containers for WF and LF models, respectively; $\boldsymbol{\tau}_{env2}$ the slowly-varying environmental loads.

5.3 Governing equation of liquid sloshing-container system

At each time step, the resulting motion of the moving ship obtained from previous mathematical LF and WF models such as displacement, velocity and acceleration is applied to each container in the form of support motions. Transformation vectors are adopted to transfer these motions from the centre of gravity (COG) of the ship to the base of each container. The absolute velocity and acceleration of point B at the base of each container can be determined from the following equations (Hibbeler, 2006)

$$\mathbf{v}_B = \mathbf{v}_A + \boldsymbol{\omega} \times \mathbf{r}_{B/A} \tag{5.3}$$

$$\mathbf{a}_B = \mathbf{a}_A + \boldsymbol{\alpha} \times \mathbf{r}_{B/A} + \boldsymbol{\omega} \times \left(\boldsymbol{\omega} \times \mathbf{r}_{B/A} \right) \tag{5.4}$$

where $\mathbf{v}_A$, $\mathbf{a}_A$ are the absolute velocity and acceleration of point A at COG of the moving ship, respectively; $\boldsymbol{\omega}$, $\boldsymbol{\alpha}$ are the angular velocity and acceleration of the moving ship, respectively; $\mathbf{r}_{B/A}$ the relative position of point B with respect to point A.

The governing equation of motion of the coupled liquid-tank due to the moving ship can be written in a single matrix equation as follows (Ang, 1980 and Balendra et al., 1982b)

$$\hat{\mathbf{M}}\ddot{\mathbf{U}} + \hat{\mathbf{K}}\mathbf{U} = \mathbf{M}_{eff}\ddot{\mathbf{q}}_b \tag{5.5}$$

where $\ddot{\mathbf{q}}_b$ is the applied base nodal accelerations due to the motion of ship; $\mathbf{M}_{eff}$ the effective mass matrix derived in Chapter 4 and is expressed as

$$\mathbf{M}_{eff} = -\begin{bmatrix} \mathbf{K}\mathbf{M}^{-1}\mathbf{M}_b + \mathbf{K}\begin{bmatrix} \mathbf{I} \\ \mathbf{I} \\ \mathbf{I} \\ \cdots \\ \cdots \\ \mathbf{I} \end{bmatrix} \\ \cdots\cdots\cdots\cdots\cdots \\ -\mathbf{S}\mathbf{M}^{-1}\mathbf{M}_b + \mathbf{S}_b \end{bmatrix} \tag{5.6}$$

where $\mathbf{I}$ is a (5×5) unit matrix; and $\mathbf{U} = \begin{Bmatrix} \mathbf{q}_d \\ \mathbf{p} \end{Bmatrix}$ the generalized system displacement vector comprising $\mathbf{q}_d$ the unknown off-base dynamic displacements of container walls, which depend on the acceleration history of the moving ship, and $\mathbf{p}$ the

pressures in liquid. The generalized symmetric matrices $\hat{\mathbf{K}}$ and $\hat{\mathbf{M}}$ derived earlier in Chapter 4 are expressed as

$$\hat{\mathbf{K}} = \left[\begin{array}{c|c} \mathbf{K}\mathbf{M}^{-1}\mathbf{K} & -\mathbf{K}\mathbf{M}^{-1}\mathbf{S}^{T} \\ \hline -\mathbf{S}\mathbf{M}^{-1}\mathbf{K} & \mathbf{K}_{f} + \mathbf{S}\mathbf{M}^{-1}\mathbf{S}^{T} \end{array}\right] \tag{5.7}$$

$$\hat{\mathbf{M}} = \begin{bmatrix} \mathbf{K} & \mathbf{0} \\ \mathbf{0} & \mathbf{M}_{f} \end{bmatrix} \tag{5.8}$$

where $\mathbf{M}$ and $\mathbf{K}$ have been redefined to represent the mass and stiffness shell matrices associated with off-base nodes, respectively.

By solving Eq. (5.5), the dynamic response of the coupled liquid-tank system due to the moving ship can be obtained at each time step. In return, the combined stress resultants at the base of each container due to liquid sloshing are applied to the moving ship as external forces $\boldsymbol{\tau}_{con1}$ and $\boldsymbol{\tau}_{con2}$ for both WF and LF models, which were described earlier in Eqs. (5.1) and (5.2), respectively.

5.4 Algorithm of fully coupled liquid-container-ship program

The flow chart in Figure 5.2 summarizes the algorithm involved in analyzing the coupled liquid-container-ship motion. Ship parameters including the dimension of the ship and thruster data are keyed into the program. Next, the parameters of each container including geometry, location on the ship and material data are also read in. These parameters are keyed in for the initialization of container and ship calculation. At each time step, the environmental settings that include the wind, wave and current data are keyed into the program as the external loads acting on the moving ship. It should be noted that the program is initiated with the external forces of the moving ship at zero for the first time step.

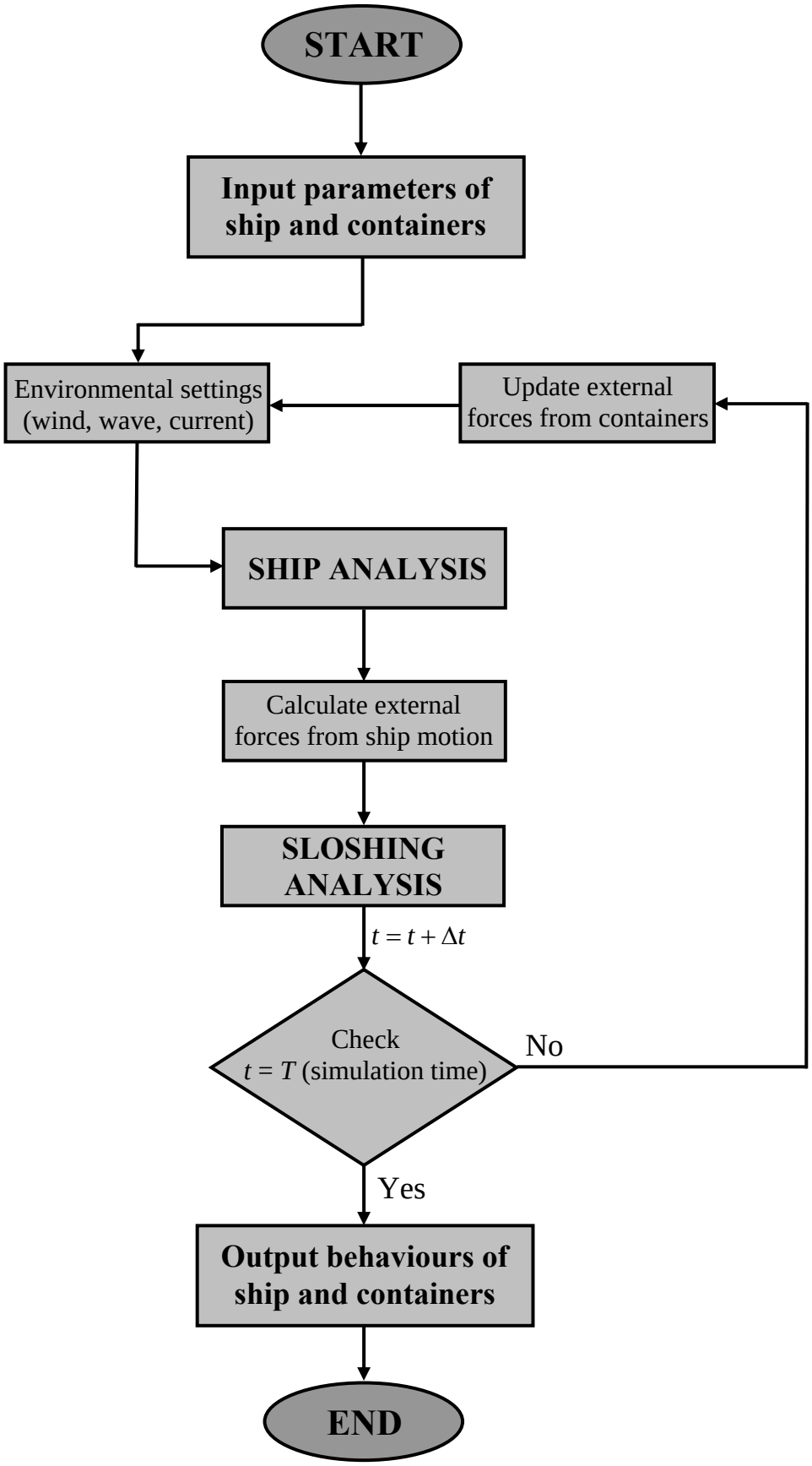

Figure 5.2 Flow chart of fully coupled liquid-container-ship program

The output from the ship program for each time step consists of the forces of the ship acting on the containers due to the external excitations caused by the wind, wave, current and thruster. These forces will induce stresses and deformations as well as sloshing flow in the liquid-filled containers and in return, the corresponding sloshing analysis of containers yields the external forces at the base of each container that affect the ship motion at the same time step. The resulting motions of liquid sloshing inside each container are applied to the moving ship in the form of the external forces $\boldsymbol{\tau}_{con1}$ and $\boldsymbol{\tau}_{con2}$ for WF and LF models, respectively. This loop of coupled interaction will continue running for each incremental time step Δt until the desired total time duration T is obtained.

5.5 Numerical examples

Several example problems will be solved using the RD-finite element method to study the effects of liquid cargo containers (such as different liquid heights, number and location of containers) and thruster on the global ship motions. The flexibility of the cylindrical container walls is considered so as to capture more realistically the effect of liquid-container interaction on the ship. The containers are assumed to be fixed at the base and free at the top end. The supply ship design main parameters, environmental settings including wind, wave, current and so on were earlier given in Chapter 4.

Two different cases are considered in the present study:

- Case 1 - No Ship-Container Interaction (NSCI). This case is to study the interaction of the liquid sloshing and the deformation of the container due to ship motion.

- Case 2 - Ship-Container Interaction (SCI). This case is to study the full interaction play between the liquid sloshing, container deformation and the ship motion.

5.5.1 Effect of number of containers on the moving ship

In the first example, the effect of the number of cylindrical liquid-filled containers on the moving ship is studied. All containers are assumed to be fully-filled with oil and have the same material and geometrical parameters as shown in Table 5.1. The containers are equally spaced along the length of the ship and the spacing between two consecutive containers is $0.5\,m$. The number of containers is varied from 3, 5, 7 and 9, and their detail locations on the moving ship are shown in Figures 5.3a-5.3d, respectively. In these figures, the center of the base of container 1 coincides with the COG of the ship and all containers are considered to be at the same level. It is to be noted that the container arrangement is symmetric about the y axis in the body-fixed reference XYZ-frame.

Table 5.1 Material and geometrical parameters of liquid-filled cylindrical containers on the moving ship

H	Height of container	$6\,m$
H_f	Height of liquid	$6\,m$
R	Radius of container	$6\,m$
h	Thickness of container	$10\,mm$
ν	Poisson's ratio	0.3
E	Young's modulus	$2.1\times10^{11}\,N/m^2$
ρ_s	Mass density of shell	$7800\,kg/m^3$
ρ_f	Mass density of oil	$820\,kg/m^3$

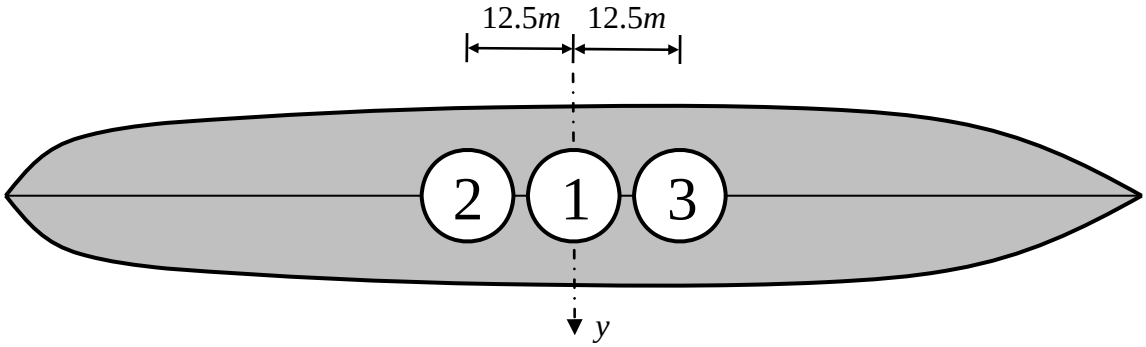

Figure 5.3a Plan view of the moving ship and location of three containers

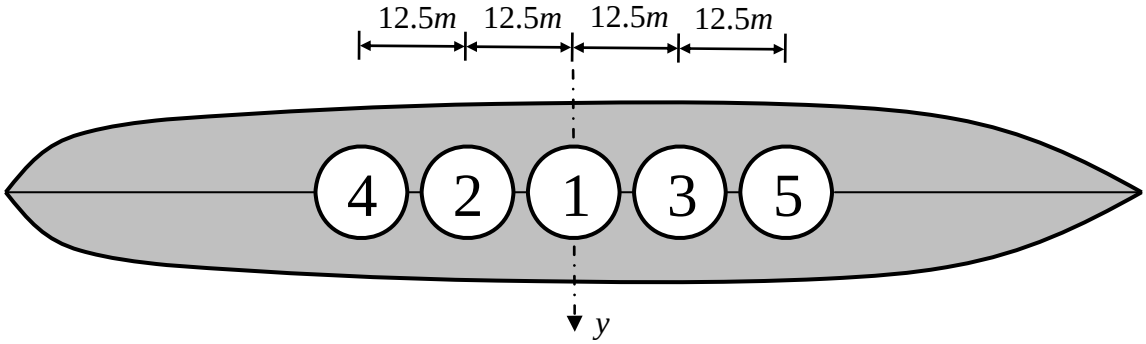

Figure 5.3b Plan view of the moving ship and location of five containers

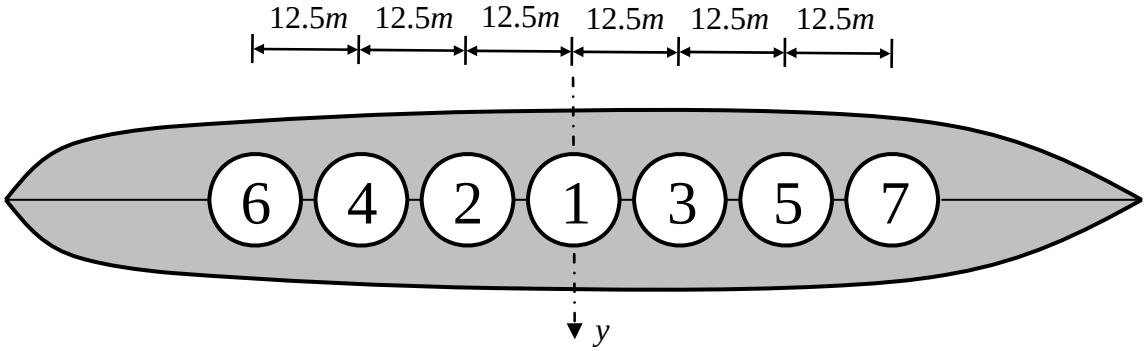

Figure 5.3c Plan view of the moving ship and location of seven containers

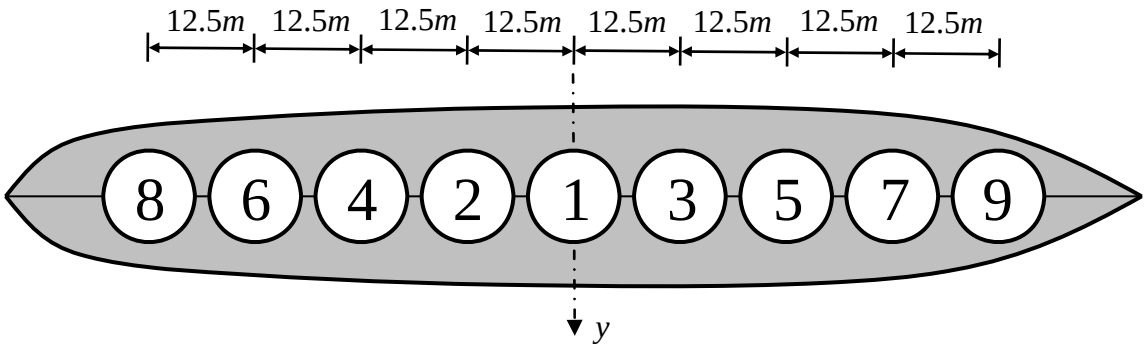

Figure 5.3d Plan view of the moving ship and location of nine containers

The roll motions of the ship are plotted with respect to the number of containers (i.e. 3, 5, 7 and 9) for the two cases NSCI and SCI in Figures 5.4a-5.4d, respectively. Although the total duration for the dynamic analysis is $1000s$, the results are presented for the first $200s$ as they suffice in providing information on the behaviour of the system. It can be seen from Figure 5.4a that the results between NSCI and SCI cases are somewhat similar when there are three containers on the ship which corresponds to the situation in which the total mass of the filled containers is relatively small as compared to the ship mass. In such a situation, the effect of these few containers on the moving ship can be ignored. The difference in the results of the two cases increases as the number of containers increases from three to nine as can be noted from Figures 5.4a-5.4d. In other words, when the volume of containers-to-volume of ship ratio V_{con}/V_{ship} exceeds a critical value, the effect of liquid sloshing inside the containers on the moving ship becomes significant and thus the interaction effect between containers and ship cannot be ignored. The behaviour of ship motion in the other degrees of freedom such as surge, sway, heave, pitch and yaw are similar to the aforementioned findings for the roll motion.

It is interesting to note that the amplitudes of motion of the moving ship for the NSCI case are larger than those of the corresponding SCI case, i.e. the motion of the ship without considering the effects of liquid sloshing on ship motion would have been more serious than those that allowing for full interaction between the liquid sloshing, multi-containers and the moving ship. This can be seen from Figure 5.4d where it is clear that there is a significant difference between NSCI and SCI results for the case of nine containers placed on the moving ship. Therefore, the fully coupled liquid-container-moving ship should be analysed when dealing with this kind of problem.

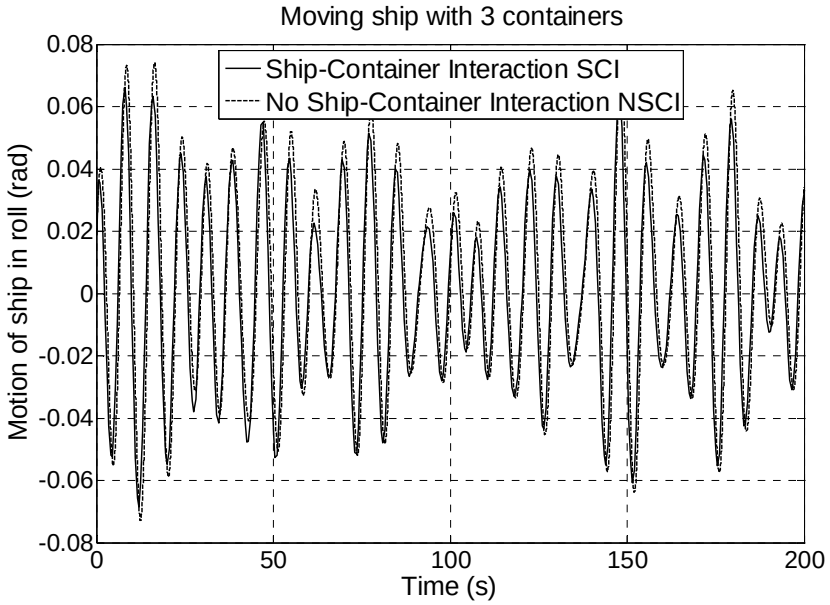

Figure 5.4a Effect of three containers on ship motion in roll

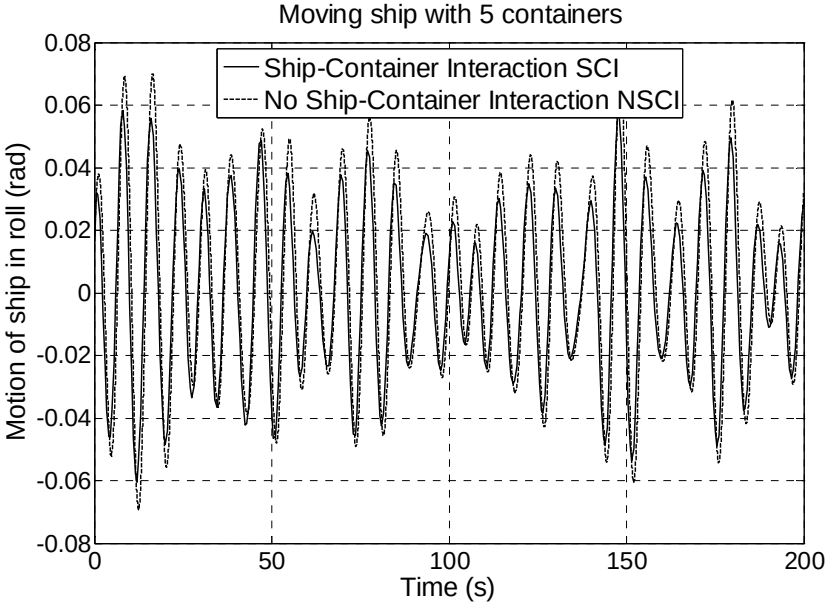

Figure 5.4b Effect of five containers on ship motion in roll

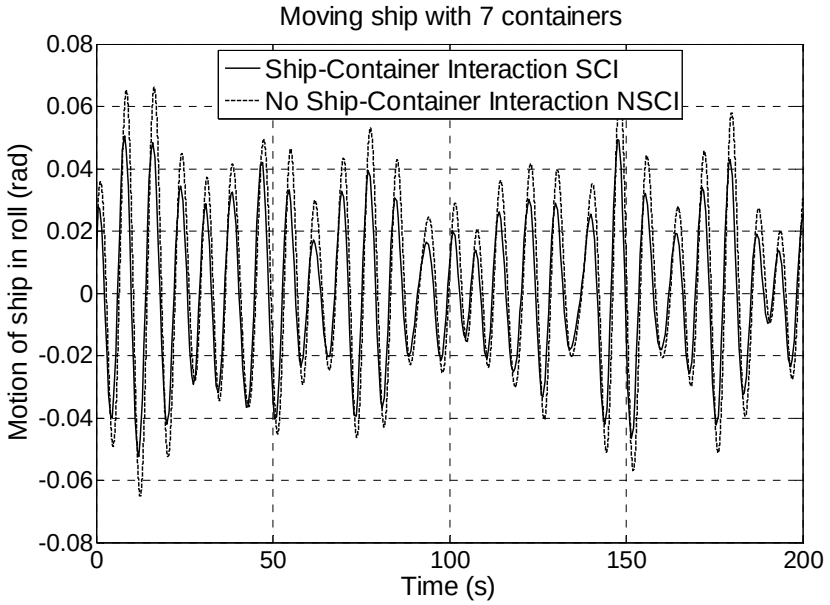

Figure 5.4c Effect of seven containers on motion of ship in roll

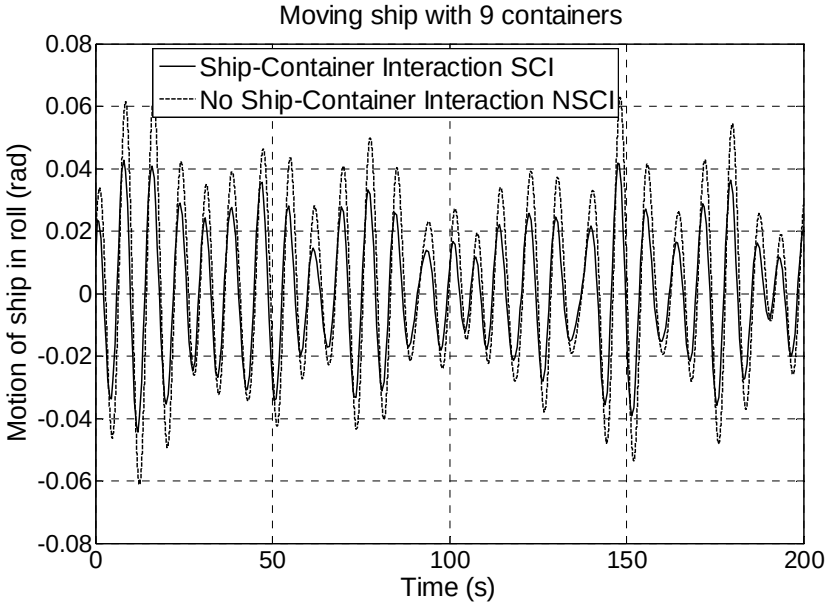

Figure 5.4d Effect of nine containers on motion of ship in roll

5.5.2 Effect of coupled interaction on responses of containers

The deformation of container wall for the NSCI and SCI cases is studied in this section. The nine-container case is considered since this has been found earlier to be the most critical. The material, geometrical properties and locations of these containers are the same as those used in the previous section. Figures 5.5 and 5.6 show the radial displacement w time histories at the free end of the container 1 for NSCI and SCI cases, respectively. The maximum radial displacement $w_{\max}$ at the free end is found to occur at time $t \approx 250s$. Therefore, a comparison of displacement results of container walls between these two cases is conducted for the time interval from 0 to $300s$, which means that the displacement components would have reached their respective maximum values.

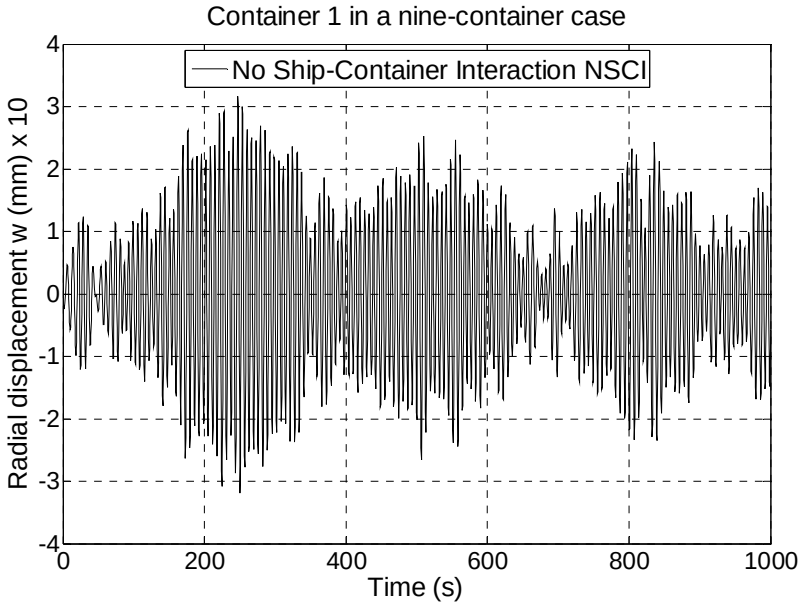

Figure 5.5 Radial displacement time history of container 1 for NSCI

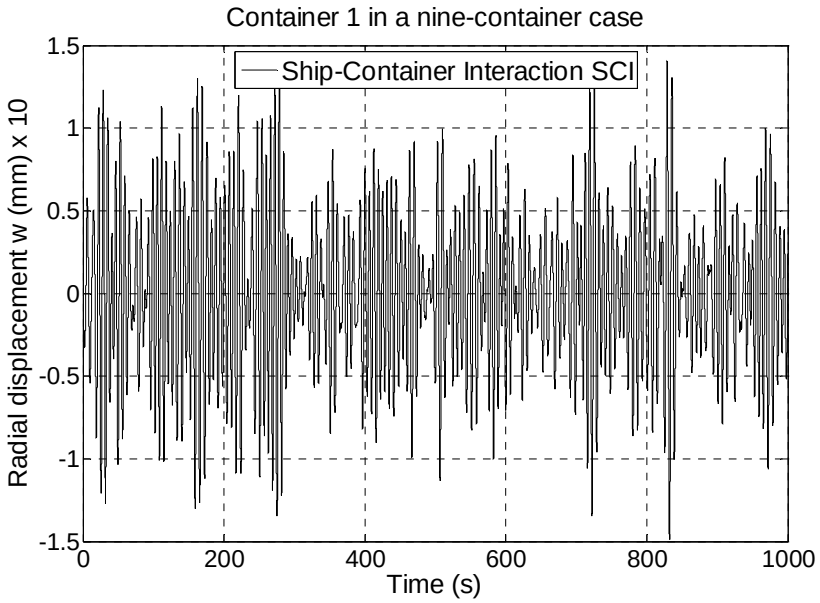

Figure 5.6 Radial displacement time history of container 1 for SCI

The meridional u, circumferential v and radial w displacement time histories at the free end of container 1 are shown in Figures 5.7, 5.8 and 5.9 for NSCI and SCI cases. It can be seen that at an early stage (less than $50s$), the displacement components of the container wall for the two cases are nearly the same due to the transient state in which the structure is subjected to a sudden excitation. After the transient state, the difference in results is significant. In particular, the displacement components of container wall reduce appreciably for SCI. This example shows the importance of the coupled liquid-container-ship interaction on the behaviour of containers. Therefore, one can conclude that the effect of SCI should be taken into consideration when designing containers.

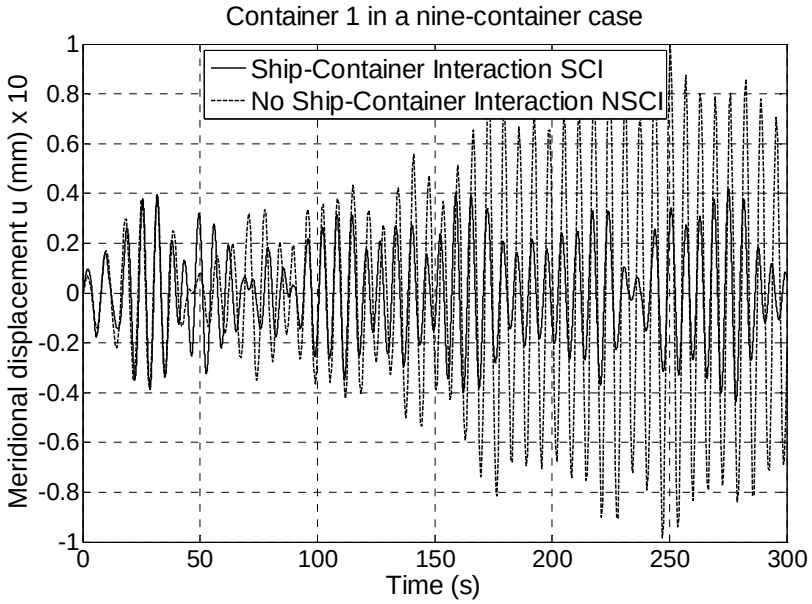

Figure 5.7 Meridional displacement time history of container 1

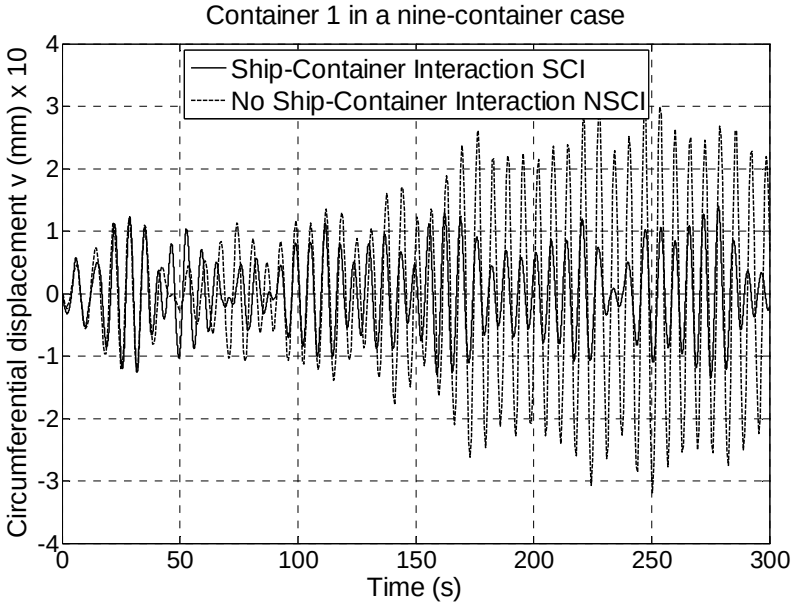

Figure 5.8 Circumferential displacement time history of container 1

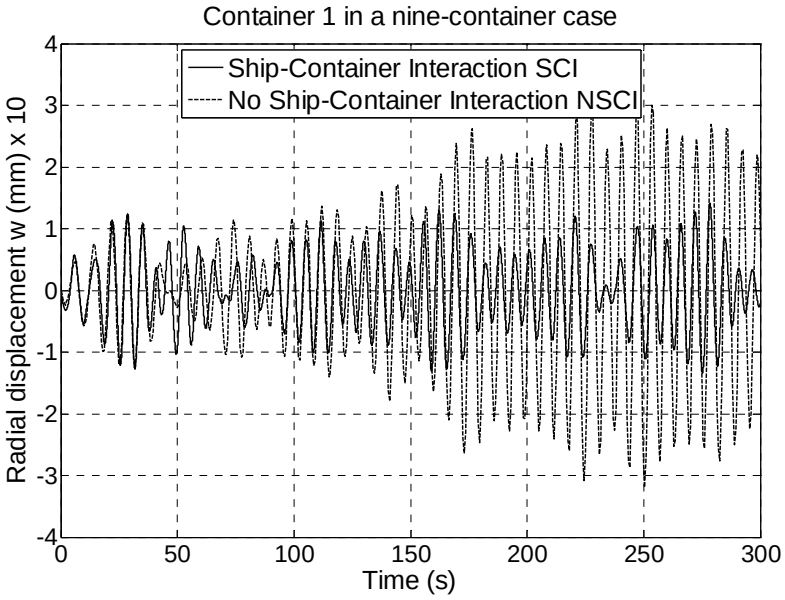

Figure 5.9 Radial displacement time history of container 1

Figures 5.10, 5.11 and 5.12 show the comparison of typical maximum axial stress σ_s, hoop stress σ_θ and membrane shear stress $\sigma_{s\theta}$, respectively, in container 9 between the NSCI and SCI results. The significant difference of maximum stress between two cases is visibly obvious. It can be seen that the maximum value of stress at the container base is signficantly reduced for the SCI case. In particular, the maximum difference is about 30% between two considered cases for the axial stress σ_s at the base of container 9. Therefore, one can observe that the NSCI case over estimates the response of the liquid-filled cylindrical containers placed on the moving ship. Design of tank dimensions based on NSCI would therefore be over conservative. A more accurate design should be carried out using the SCI approach, i.e. allowing for interaction between liquid sloshing, containers and ship.

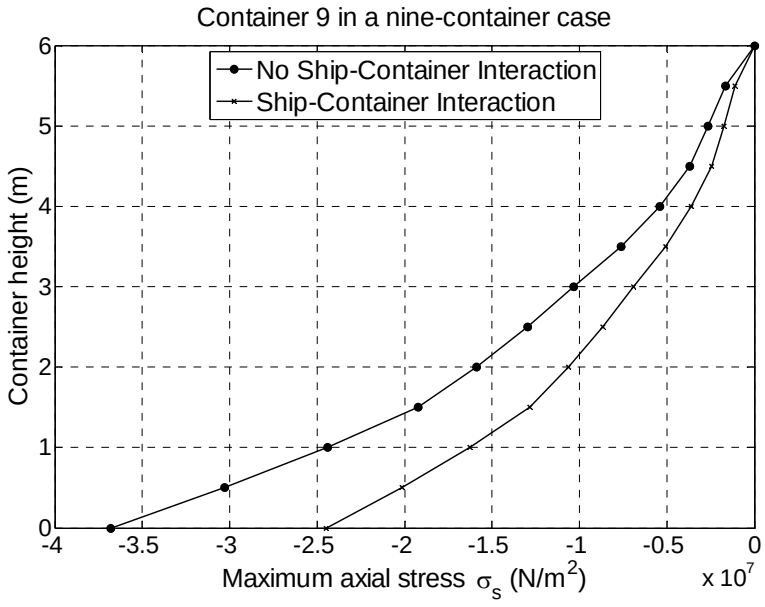

Figure 5.10 Maximum axial stress of container 9

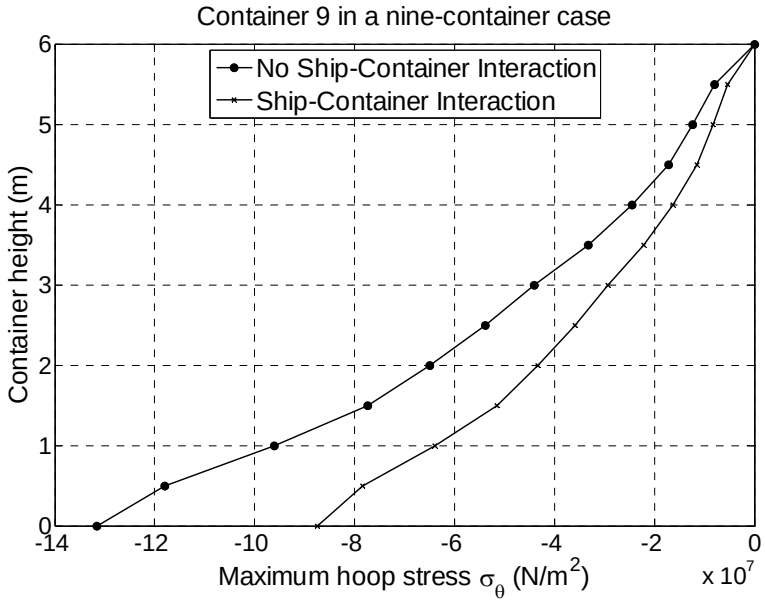

Figure 5.11 Maximum hoop stress of container 9

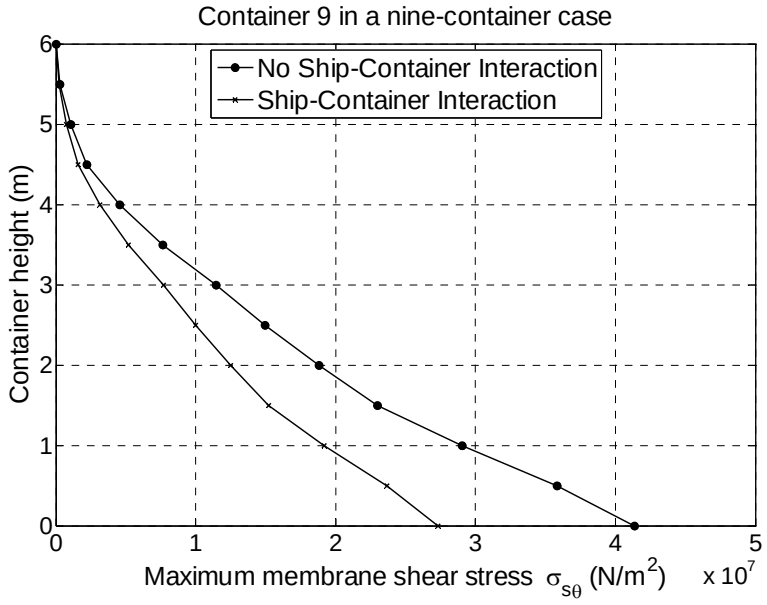

Figure 5.12 Maximum membrane stress of container 9

5.5.3 Effect of location of containers

The deformation, stresses and moments induced in the containers at various locations on the moving ship will be investigated next. Figures 5.13, 5.14 and 5.15 show the comparison of the radial displacement w at the free end, the axial stress σ_s and the membrane moment $M_{s\theta}$ induced in containers 1, 3, 5, 7 and 9, respectively. These containers are placed at the bow of the ship. A full interaction between liquid-container-moving ship SCI is considered in this study. It can be seen from these figures that the amplitudes of the displacement, stress and moment in containers 1, 3, 5, 7 and 9 are significantly affected by the location of containers. In particular, those amplitudes of container 9 are noted to be the largest, followed by those of containers 7, 5, 3 and 1 in that order. Thus, containers which are located further away from the COG of the ship would experience higher stresses. It should be also noted that the axial

stress is maximum at the container base and the membrane moment is maximum at a section just above the container base.

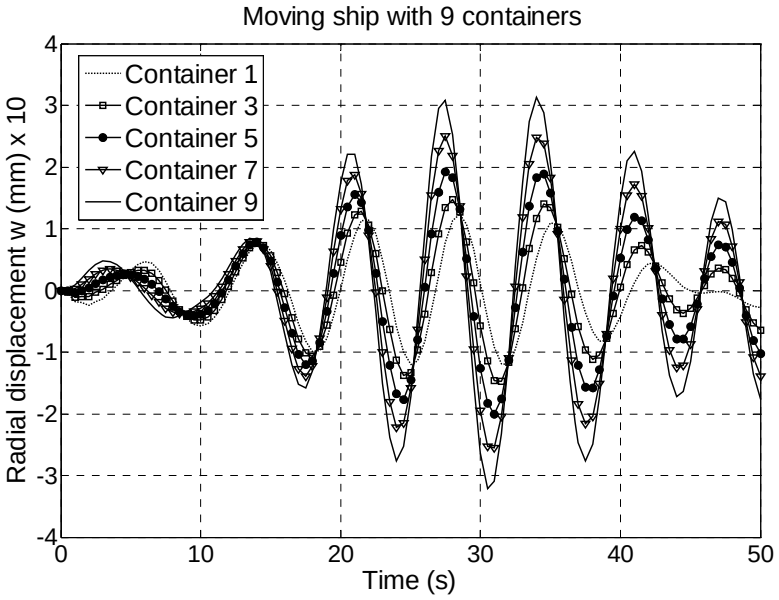

Figure 5.13 Radial displacement at the free end of containers

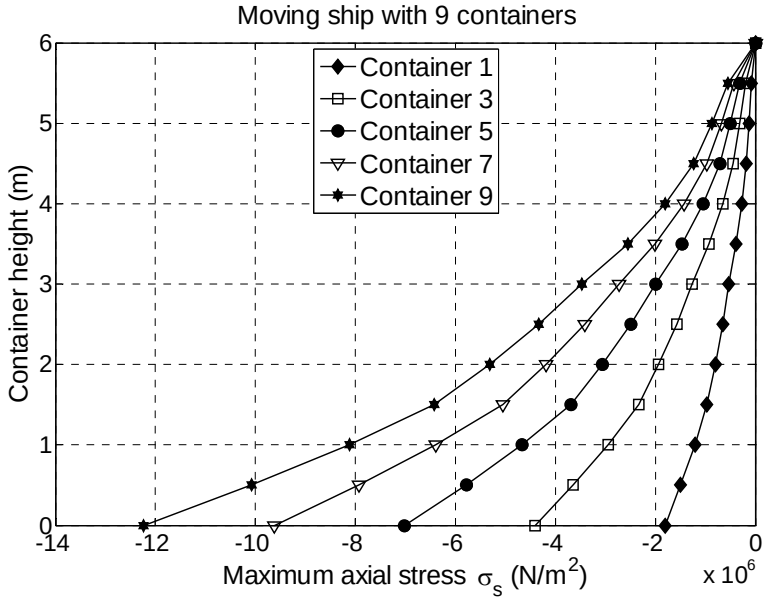

Figure 5.14 Maximum axial stress of containers

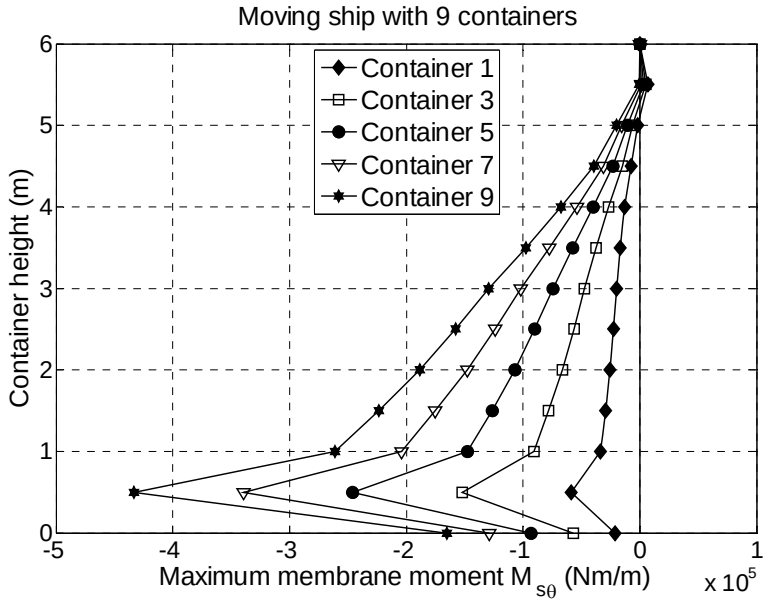

Figure 5.15 Maximum membrane moment of containers

Figures 5.16a-5.16d and Figures 5.17a-5.17d depict the variation of radial displacement time history w at the free end of containers placed at the bow and stern of the ship, respectively. It can be seen from these figures that the degree of influence from the interaction between sloshing liquid, containers and the ship in the radial displacement of container walls depends on the location of each container. For containers located far away from the COG of the moving ship, the difference in the container wall displacements between NSCI and SCI cases becomes relatively large. In other words, the difference in displacements between NSCI and SCI cases for container 9 is the largest, followed by that of containers 7, 5, 3 and 1 at the bow, in that order. These findings are also applicable for containers 8, 6, 4 and 2 at the stern of the ship.

Figures 5.18a-5.18h show the typical instantaneous variation of the radial displacement from the tank base to the top free end of containers mounted at the stern and bow of the ship. The graphs are plotted at the time step $t = 1000s$ and are presented to highlight the difference in results between the NSCI and SCI cases. It can

be seen from these figures that the group of containers (numbers 3, 5, 7 and 9) at the bow of the ship experiences larger difference in displacements between the NSCI and SCI cases than their counterparts (containers 2, 4, 6 and 8) at the stern of the ship. It should be noted that the difference in maximum radial displacements of container wall between NSCI and SCI cases for container 9 at the bow of the ship is the largest (40%), followed by the displacement of container 1 at the middle of the ship (35%) and then container 8 at the stern of the ship (32%). Therefore, this study shows that the deformation induced in the container wall is largely affected by its location on the ship. These results indicate that containers mounted at the bow should be designed stiffer than those mounted at the stern of the moving ship since they undergo greater deformations.

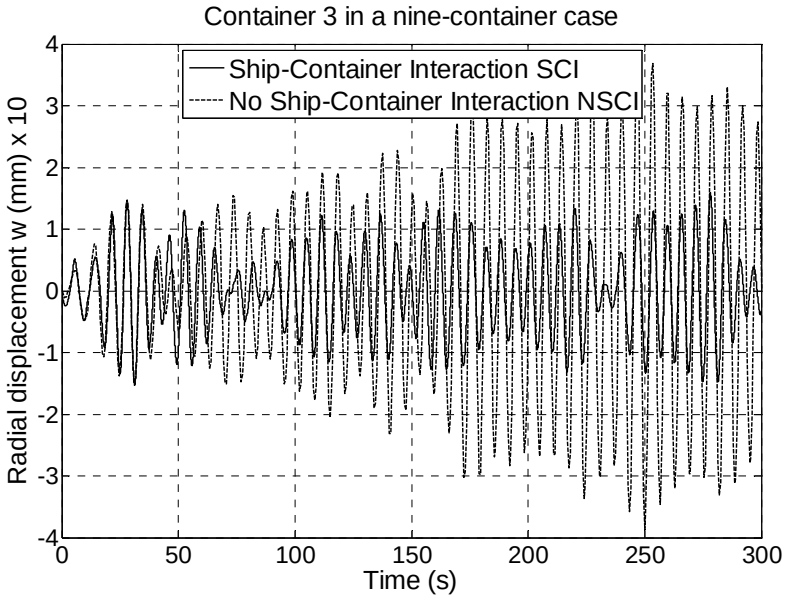

Figure 5.16a Radial displacement of container 3 placed at the ship's bow

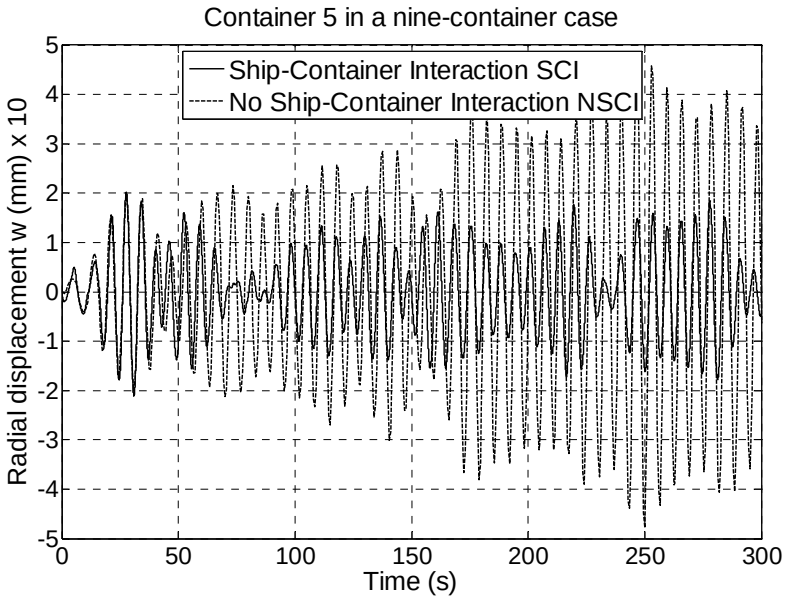

Figure 5.16b Radial displacement of container 5 placed at the ship's bow

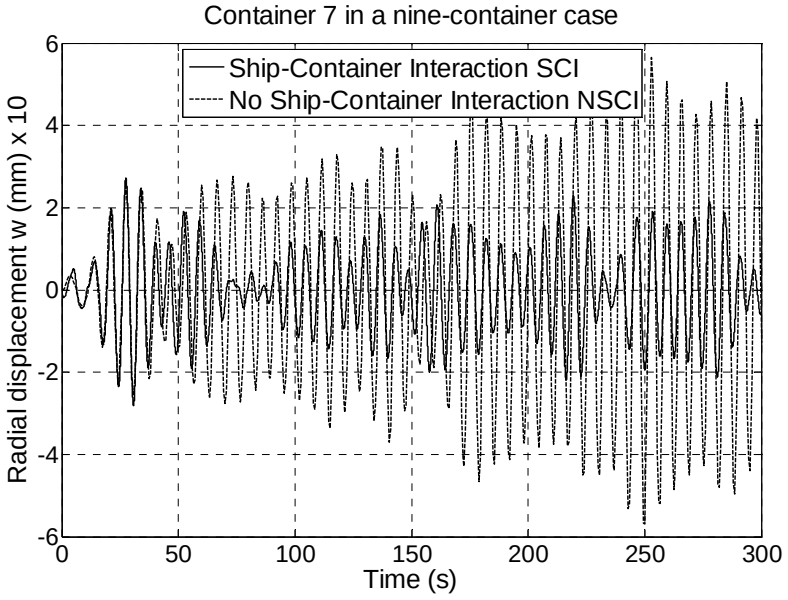

Figure 5.16c Radial displacement of container 7 placed at the ship's bow

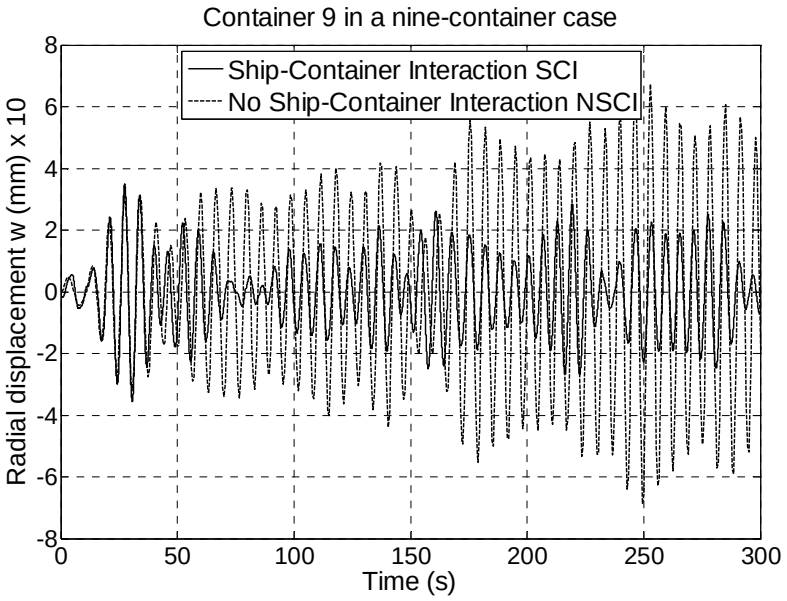

Figure 5.16d Radial displacement of container 9 placed at the ship's bow

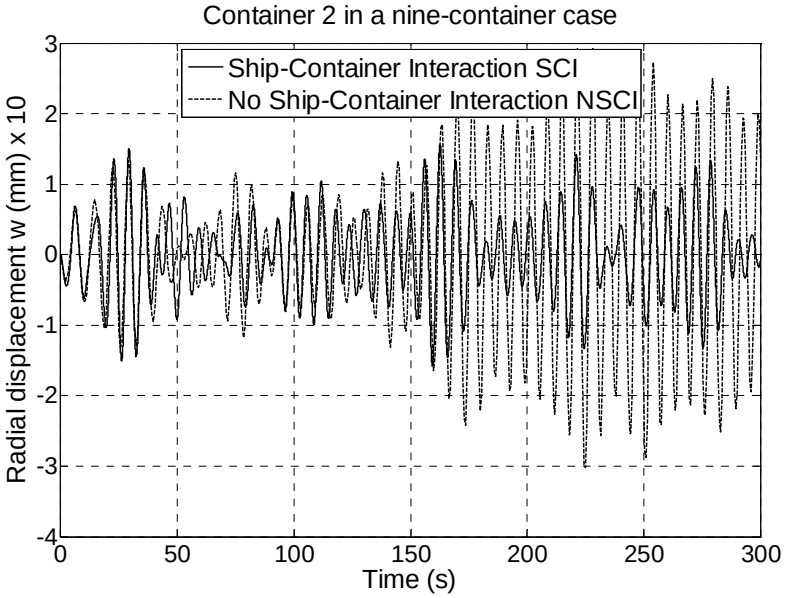

Figure 5.17a Radial displacement of container 2 placed at the ship's stern

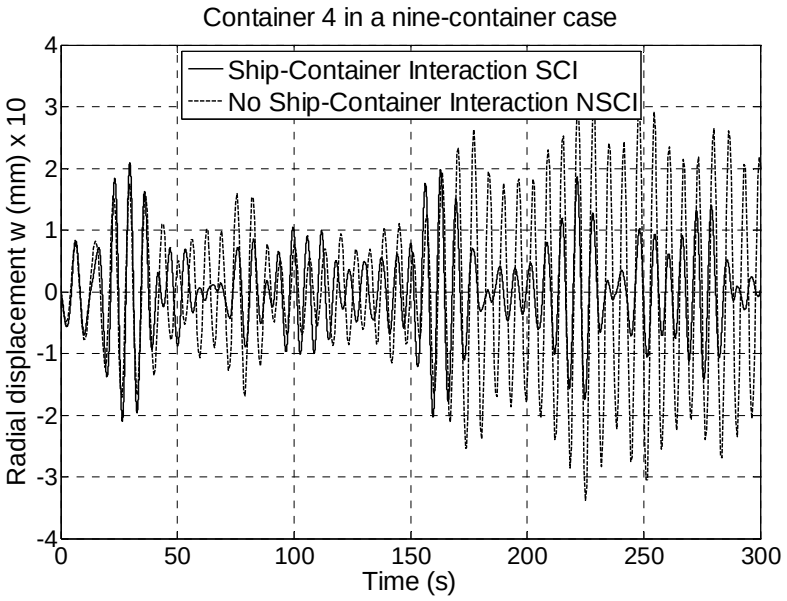

Figure 5.17b Radial displacement of container 4 placed at the ship's stern

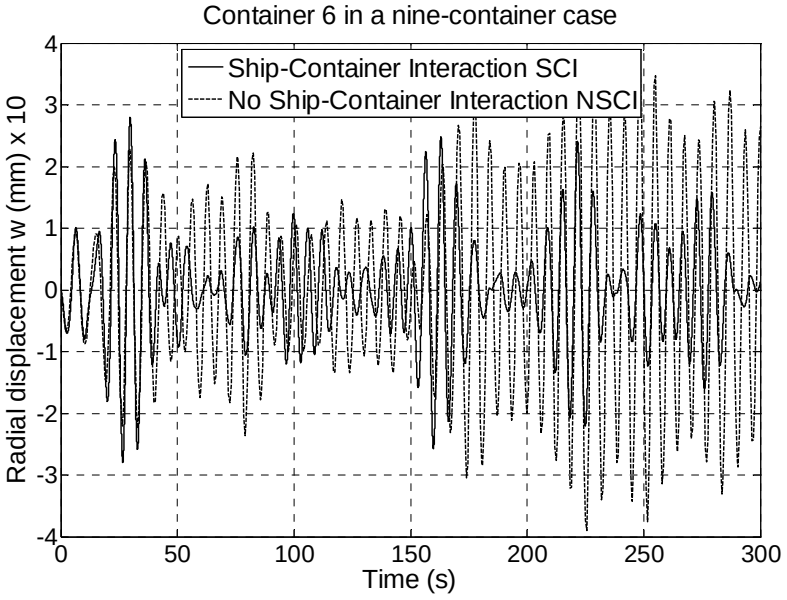

Figure 5.17c Radial displacement of container 6 placed at the ship's stern

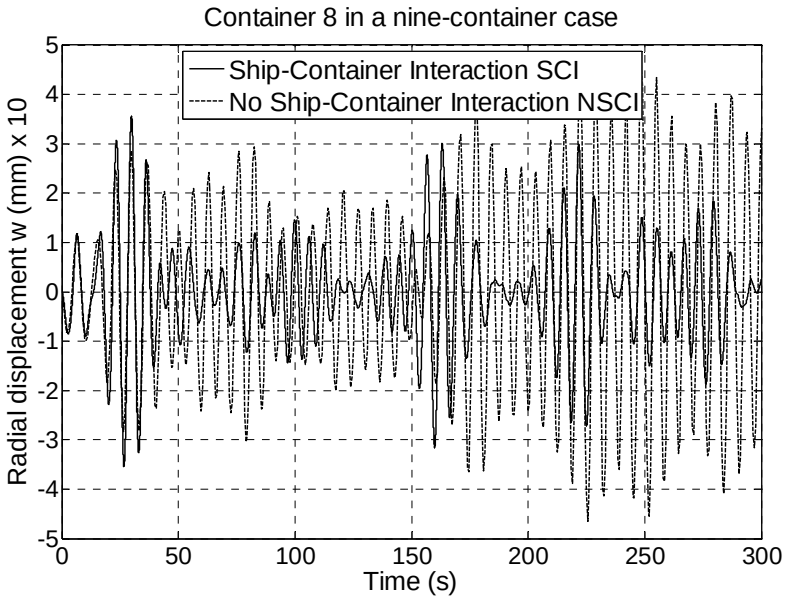

Figure 5.17d Radial displacement of container 8 placed at the ship's stern

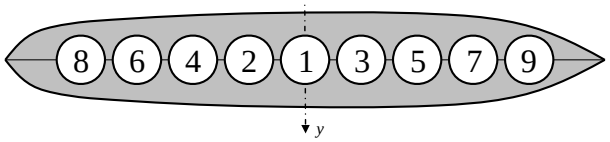

Stern of ship **Bow of ship**

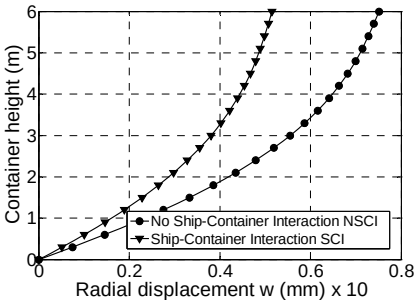

(a) Container 2

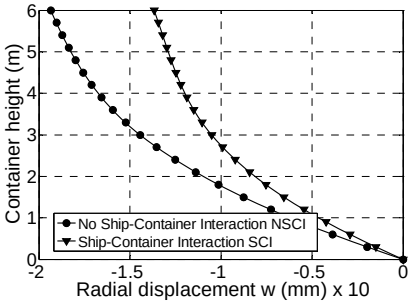

(b) Container 3

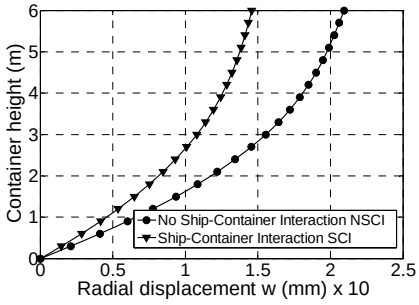

(c) Container 4

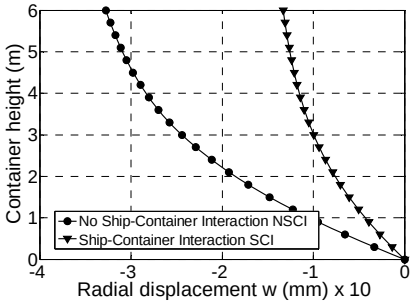

(d) Container 5

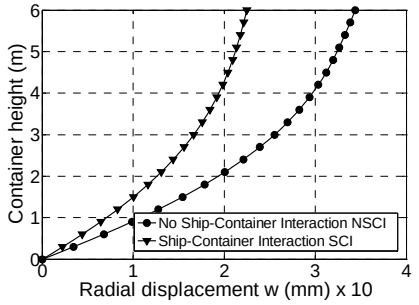

(e) Container 6

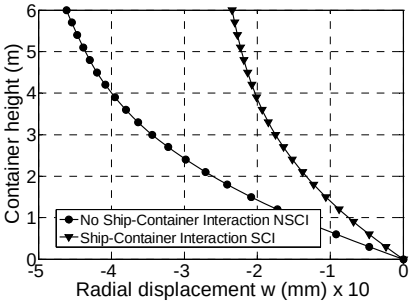

(f) Container 7

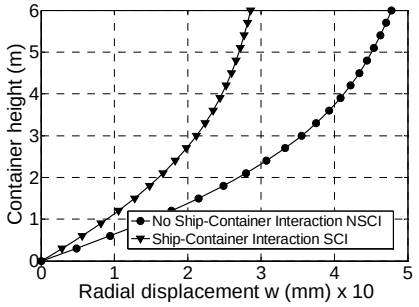

(g) Container 8

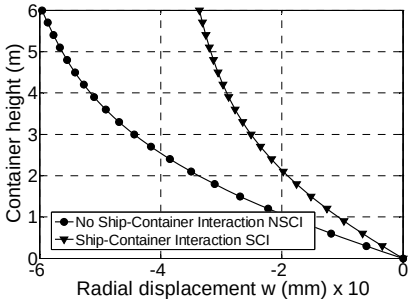

(h) Container 9

Figure 5.18 Plan view of ship and radial displacement of tank wall at $t = 1000s$

5.5.4 Effect of liquid level in containers

The effect of liquid-to-container height ratio $\beta = H_f / H$ on the maximum meridional, circumferential and radial displacements as well as maximum stresses produced in the container wall is next investigated. The material, geometrical properties and locations of the nine containers are the same as those used in section 5.5.2. The level of liquid H_f for all containers ranges from 0 to H. In other words, the liquid-to-container height ratio β is varied from 0 (empty container) to 1 (fully liquid-filled container). The other geometrical properties are kept constant and the total time for calculation is taken as $1000s$. Figure 5.19 shows the variation of the maximum meridional, circumferential and radial displacements of container walls with respect to the liquid level. It can be seen from this figure that these maximum displacement components increase with increasing liquid level in the containers. As the liquid level increases, the total mass of the system increases. This increase in mass produces greater sloshing loads on the container walls and thereby resulting in an increase in the displacement components. It is also found that the effect of sloshing on the maximum displacements of container walls may not be significant when the liquid-to-container height ratio β is smaller than 0.4. This means that containers that are less than 40% filled do not experience appreciable deformation due to liquid sloshing. Conversely, when the containers are filled beyond 40% of their capacities, liquid sloshing effect on the container wall deformation becomes appreciable.

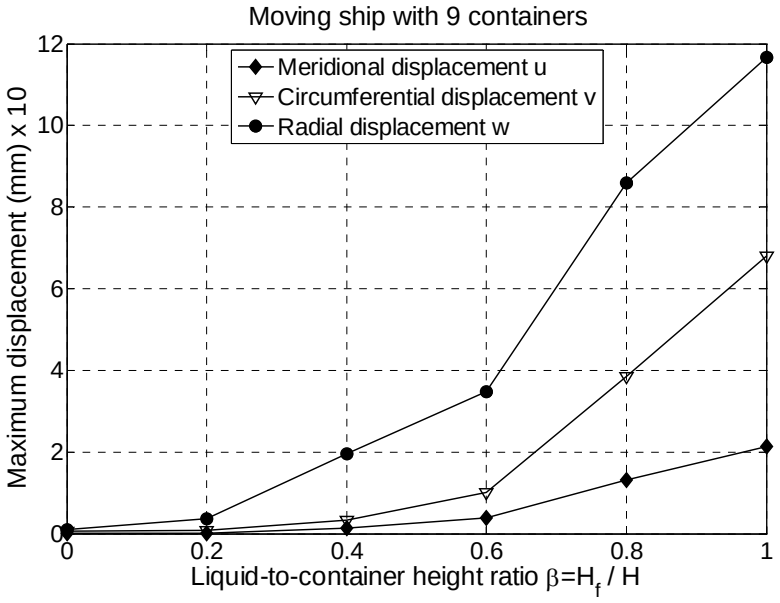

Figure 5.19 Effect of liquid-to-container height ratio on maximum displacements of container walls

Figures 5.20, 5.21 and 5.22 show the effect of liquid-to-container height ratio β on the maximum axial σ_s, hoop σ_θ and membrane shear stresses $\sigma_{s\theta}$ of container 1, respectively. It is evident from these figures that the amplitudes of these stresses for fully liquid-filled containers ($\beta = 1$) are the largest, followed by that of the half liquid-filled containers ($\beta = 0.5$) and then the empty cylindrical containers ($\beta = 0$) in this order. This trend is the same as that obtained for the displacement behaviour of containers.

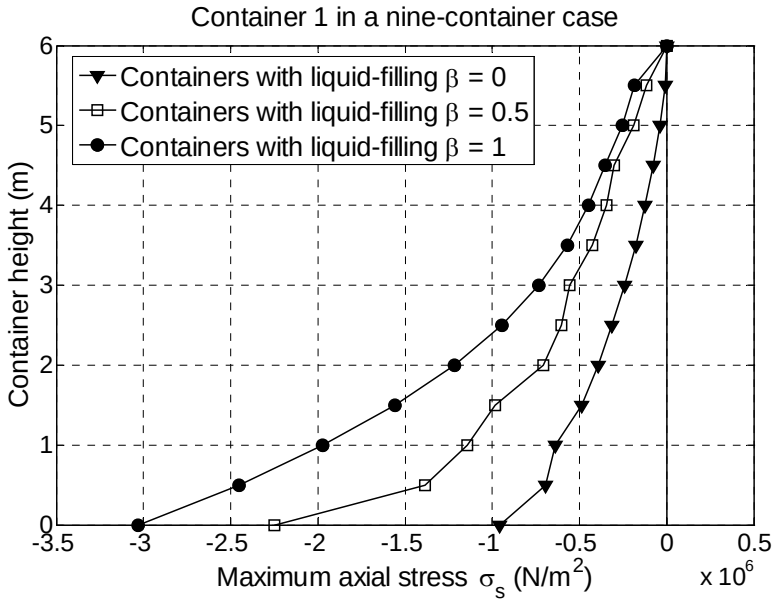

Figure 5.20 Effect of liquid-to-container height ratio on maximum axial stress of container walls

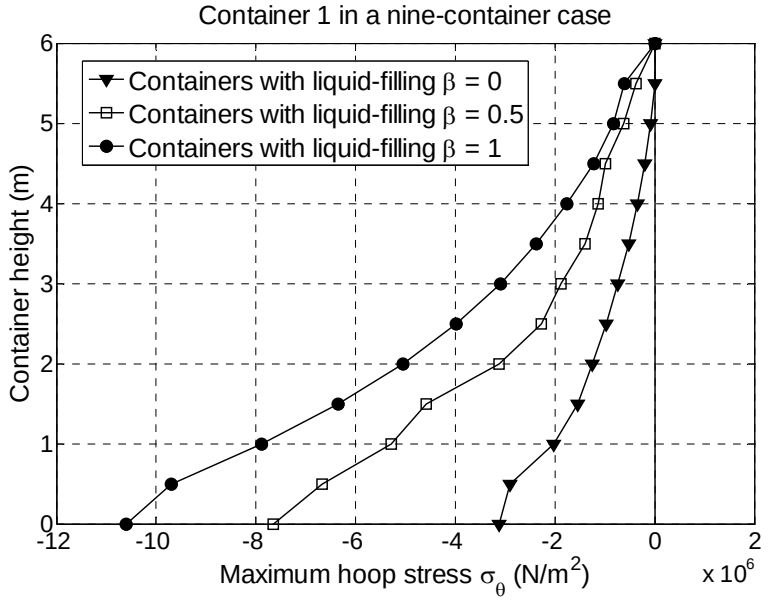

Figure 5.21 Effect of liquid-to-container height ratio on maximum hoop stress of container walls

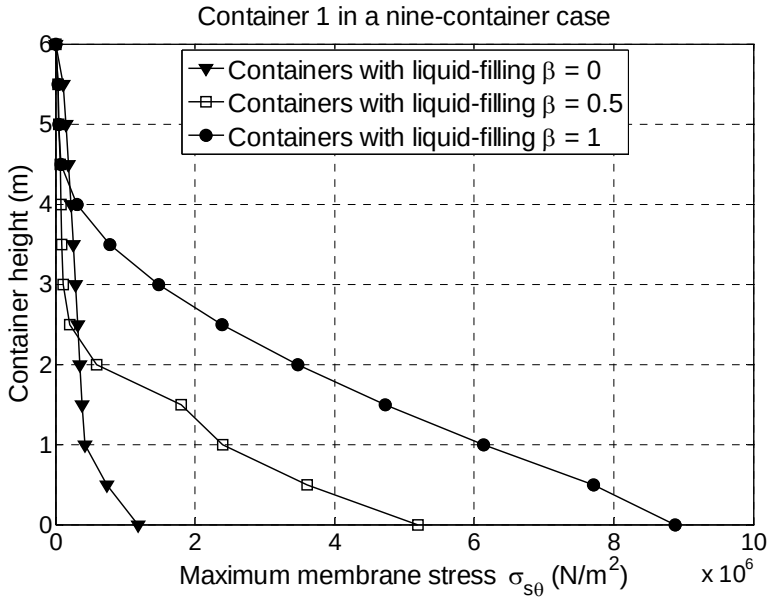

Figure 5.22 Effect of liquid-to-container height ratio on maximum membrane shear stress of container walls

Figures 5.23 and 5.24 illustrate the effect of liquid-to-container height ratio β on the roll motion and roll acceleration of the ship, respectively. It is clear from these figures that there is less coupling interaction on the ship motion when there is more liquid in the containers. In fact, the amplitudes of roll motion and acceleration in the ship with empty containers are largest, followed by those containers with 50% and 100% of their capacities filled with liquid. One can conclude that in some cases, the liquid cargo can be a useful vibration absorber for ship motion if the external forcing frequencies of the ship are away from the natural sloshing frequencies. This phenomenon is similar to the use of liquid tanks on the roofs of tall buildings in mitigating the building movement due to seismic shocks by dissipating the energy through liquid sloshing.

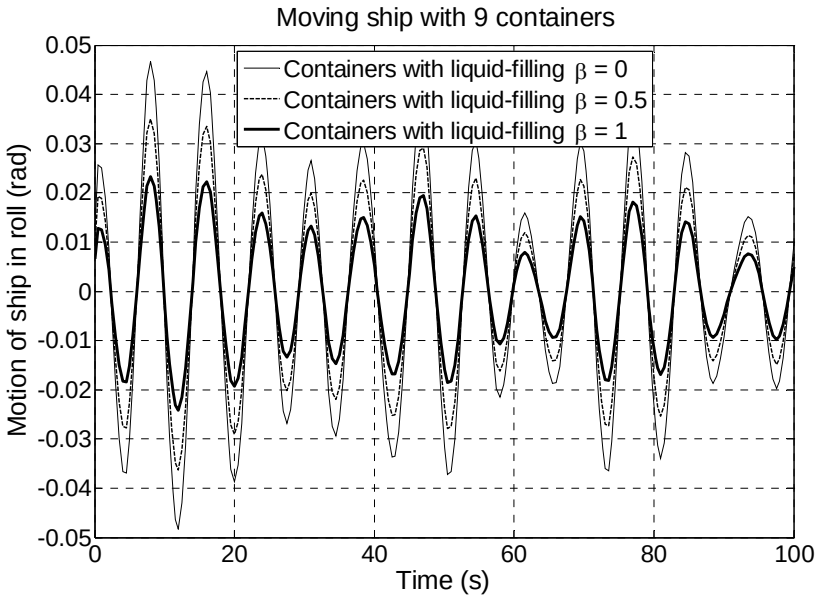

Figure 5.23 Effect of liquid-to-container height ratio on ship motion in roll

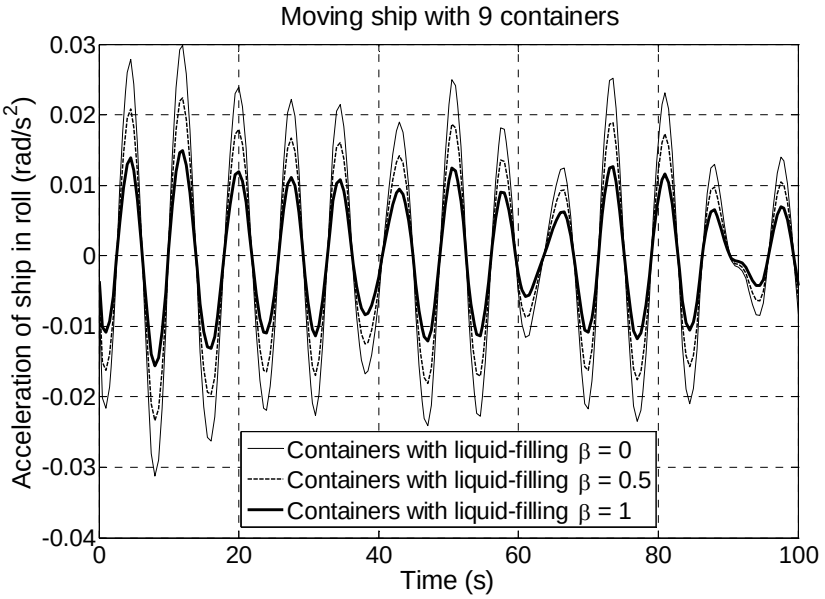

Figure 5.24 Effect of liquid-to-container height ratio on ship acceleration in roll

5.5.5 Effect of thruster modelling

A thruster refers to a configuration of ship propellers placed in pods that can be rotated in any horizontal direction so as to provide the ship with better maneuverability and stability. The primary advantages of thrusters are electrical efficiency, better use of ship space, and lower maintenance costs. Ships with thrusters do not need tugs to dock, though they still require tugs to maneuver in difficult places. As shown in Table 4.3 of Chapter 4, the maximum thrust forces in surge, sway and yaw are $\left(\tau_{surge}\right)_{\max} = 0.3\times10^{6}N$, $\left(\tau_{sway}\right)_{\max} = 0.12\times10^{6}N$ and $\left(\tau_{yaw}\right)_{\max} = 9.7\times10^{6}N$, respectively. In this section, the effect of having thruster on the ship motion and the sloshing fluid-containers will be investigated next. A complete interaction between liquid-container-ship (SCI) is considered. For the analysis, the parameters and number of containers placed on the moving ship are the same as those used in section 5.5.2. In order to study the effect of the thruster on global ship motions, the analysis is conducted over a $1000s$ time interval but results will only be presented for the first $200s$ since the typical behaviour can be observed by then. The displacement and acceleration of the ship in the roll direction are shown in Figures 5.25 and 5.26, respectively. In each of these plots, the two curves presented correspond to the case when thruster is considered and when thruster is not considered. All containers are assumed to be completely filled with liquid, i.e. $\beta = 1$. It can be seen from these figures that there is a significant difference in the responses of ship motion between the cases for which thruster is absent and for which thruster is present. The presence of thruster reduces the amplitudes of motion and acceleration of the ship, thereby making the ship more stable. Therefore, thrusters are recommended for marine vessels carrying liquid cargo in tanks on board.

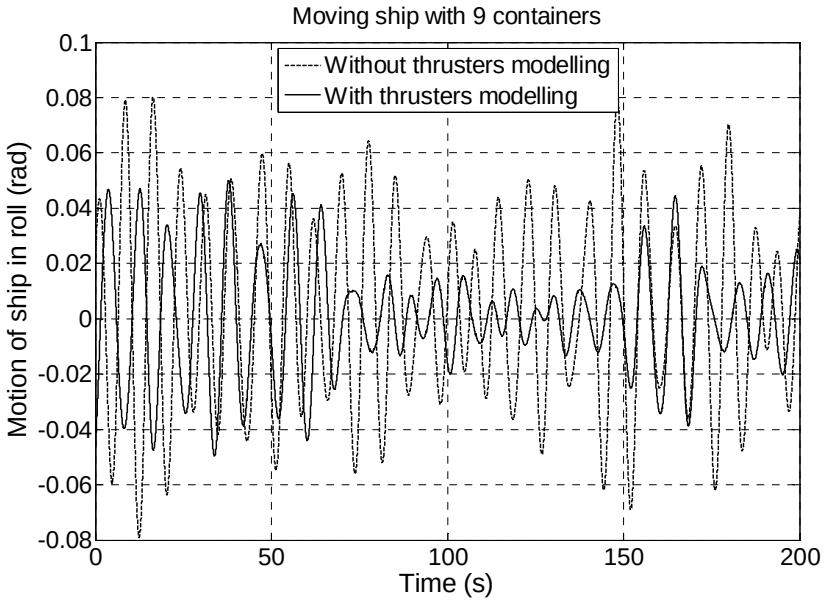

Figure 5.25 Effect of thruster on ship motion in roll

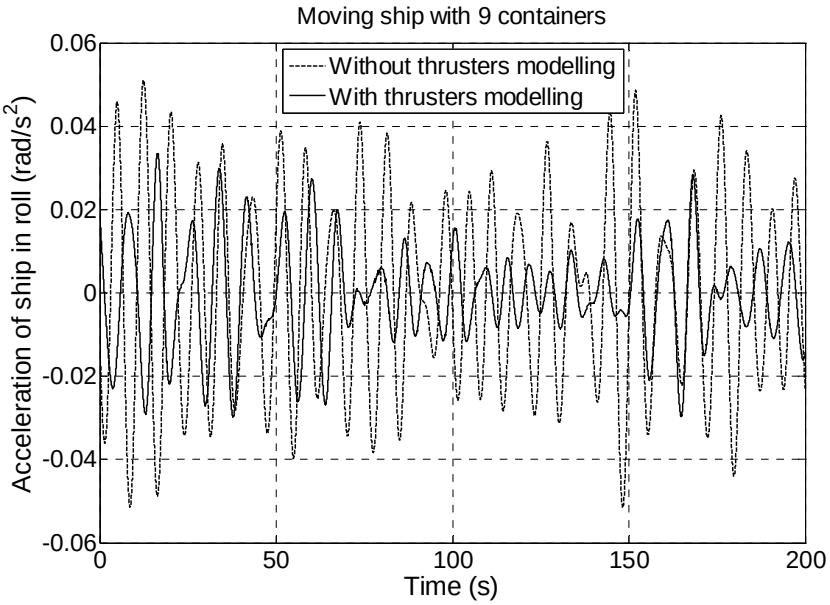

Figure 5.26 Effect of thruster on ship acceleration in roll

The meridional, circumferential and radial displacements at the free end of container 9 are shown in Figures 5.27, 5.28 and 5.29, respectively, for the cases with and without thruster modeled. From these figures, it can be seen that the displacement components of container have been significantly reduced with the use of thruster. In particular, the maximum radial displacements $w_{\max}$ with and without considering thruster are $0.57mm$ and $0.68mm$, respectively. Thus, the radial displacement decreases significantly by 16% when using thrusters. Therefore, thruster modeling can be used in analyzing the coupled liquid-container-ship interaction problem in order to obtain better stability of the ship and to reduce the effect of liquid sloshing on the container walls.

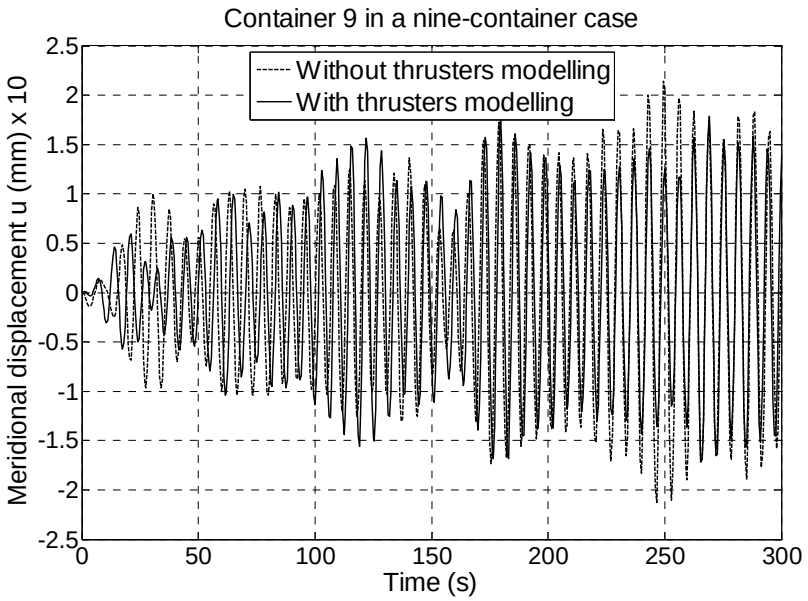

Figure 5.27 Effect of thruster on meridional displacement of container wall

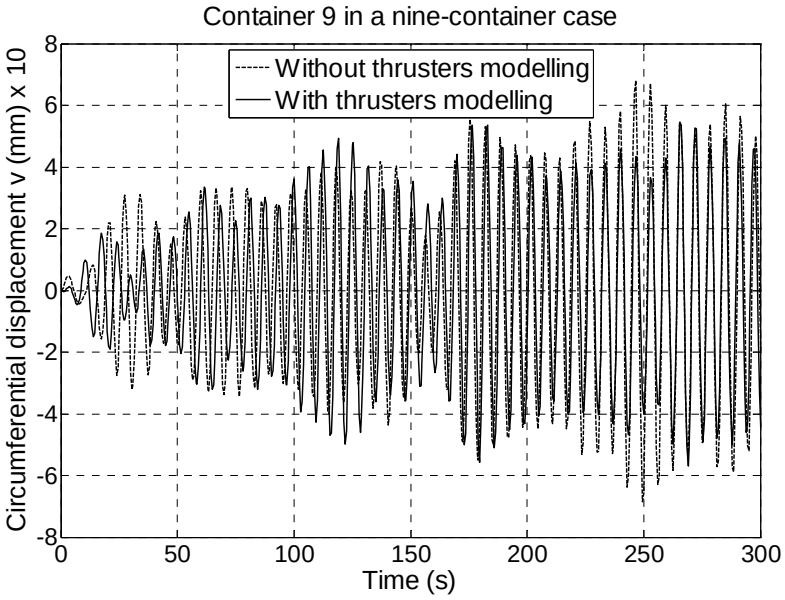

Figure 5.28 Effect of thruster on circumferential displacement of container wall

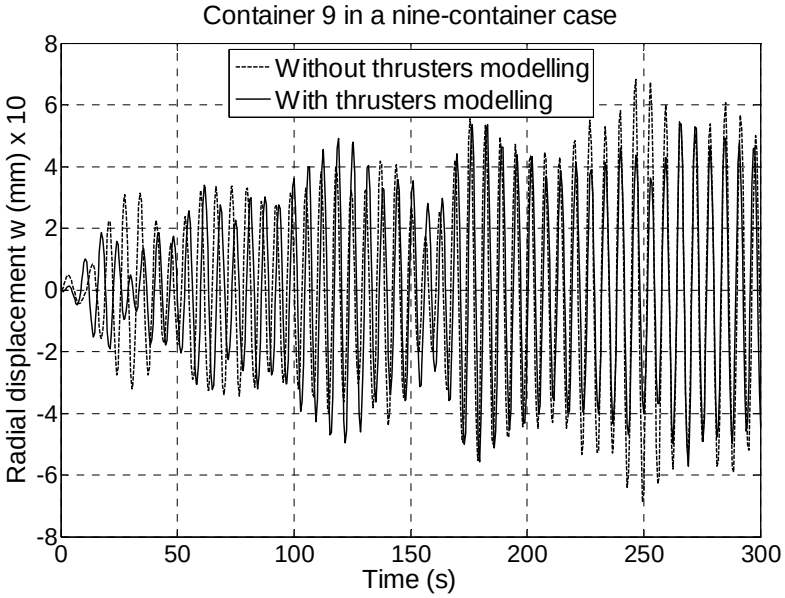

Figure 5.29 Effect of thruster on radial displacement of container wall

5.5.6 Effect of shape of containers

In this section, the shape of containers is investigated to determine its effectiveness in holding liquid. In particular, cylindrical and hemispherical containers will be compared. The number of containers on the moving ship is taken to be nine. The geometrical and material parameters for these containers are given in Table 5.2.

Table 5.2 Material and geometrical parameters of liquid-filled cylindrical and hemispherical containers on the moving ship

	Parameters	Cylindrical container	Hemispherical container
α	Roll down angle	N/A	90^0
H	Height of container	$6\,m$	N/A
H_f	Height of liquid	$2.75\,m$	$3\,m$
R	Radius of container	$6\,m$	$6\,m$
h	Thickness of container	$0.01\,m$	$0.01\,m$
ν	Poisson's ratio	0.3	0.3
E	Young's modulus	$2.1\times10^{11}\,N/m^2$	$2.1\times10^{11}\,N/m^2$
ρ_s	Mass density of shell	$7800\,kg/m^3$	$7800\,kg/m^3$
ρ_f	Mass density of oil	$820\,kg/m^3$	$820\,kg/m^3$

In order to consider which shape is better for containers, the volume of liquid and the area at the base of each cylindrical and hemispherical containers are chosen to be the same, i.e. $V_f^{cyl} = V_f^{sph}$ and $A_{base}^{cyl} = A_{base}^{sph}$, as shown in Figure 5.30.

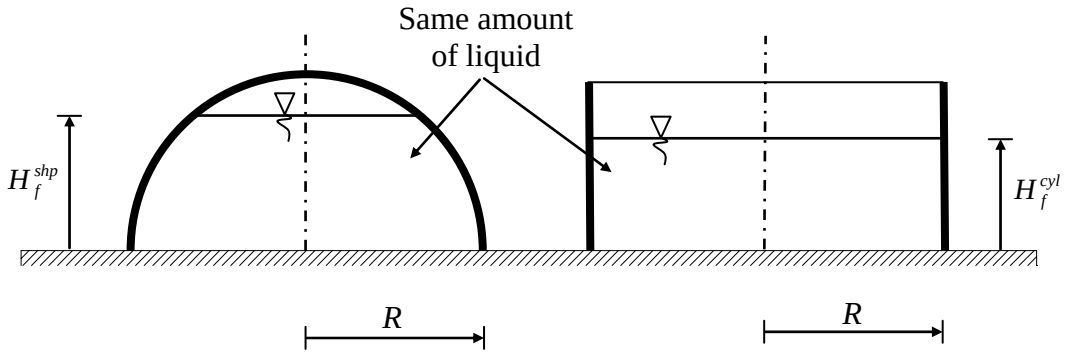

Figure 5.30 Hemispherical and cylindrical containers on the moving ship

Figure 5.31 presents the effect of hemispherical and cylindrical containers on the motion of ship in roll. One can notice that there is not much significant difference in motion of ship in roll between the hemispherical and cylindrical containers. The reason is that the ship motion could be mostly controlled by the total weight of carrying bulks and cargos. As the volume of these containers is the same in this study, it is thus to be expected that the same behaviour in ship motion is obtained for both shapes of containers. Comparing with the aforementioned study in section 5.5.4 where the volume of container was varied, one can conclude that the volume of liquid is one of the most important factors that may have major influence on the ship motion.

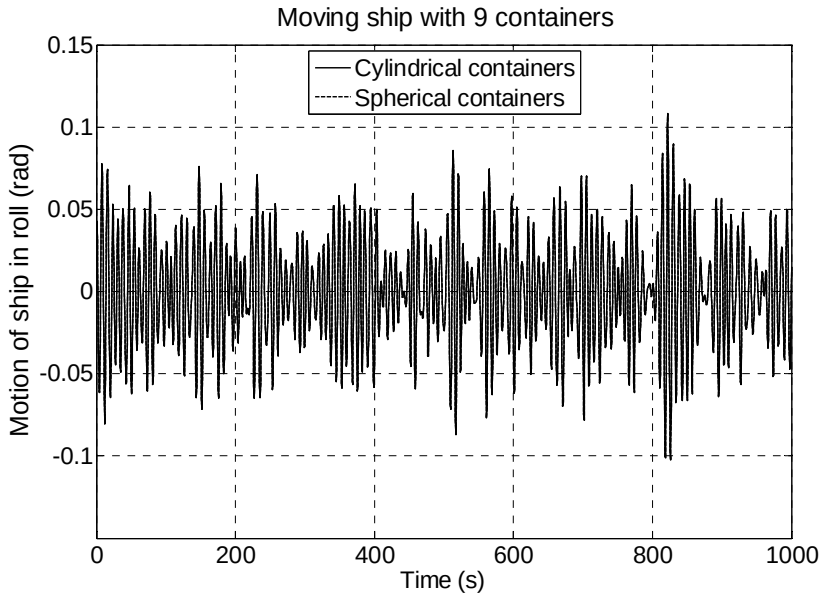

Figure 5.31 Effect of shape of containers on ship motion in roll

The comparison of maximum meridional, circumferential and radial displacements between the hemispherical and cylindrical container 1 is shown in Figures 5.32, 5.33 and 5.34, respectively. From Figure 5.32, it can be seen that the difference in results of the meridional displacement between two kinds of containers is small. On the other hand, these results are significantly different between the hemispherical and cylindrical

containers for the circumferential and radial displacements. In particular, the displacements of cylindrical container are noticeable smaller as compared with those of hemispherical container. The reason is that as both shapes of containers have the same amount of liquid and the same tank base radius and thickness as well as material properties of liquid and tank wall. The length of shell wall which has interaction with liquid would be longer for the hemispherical container than that of the cylindrical container. This therefore led to more deformation being induced in the tank wall for hemispherical container as compared with cylindrical container. In view of this, it is therefore recommended that cylindrical shape containers be employed rather than hemispherical shape containers in the transportation of the same amount of liquid in ship across the ocean to reduce the effect of liquid sloshing on the deformation of container walls.

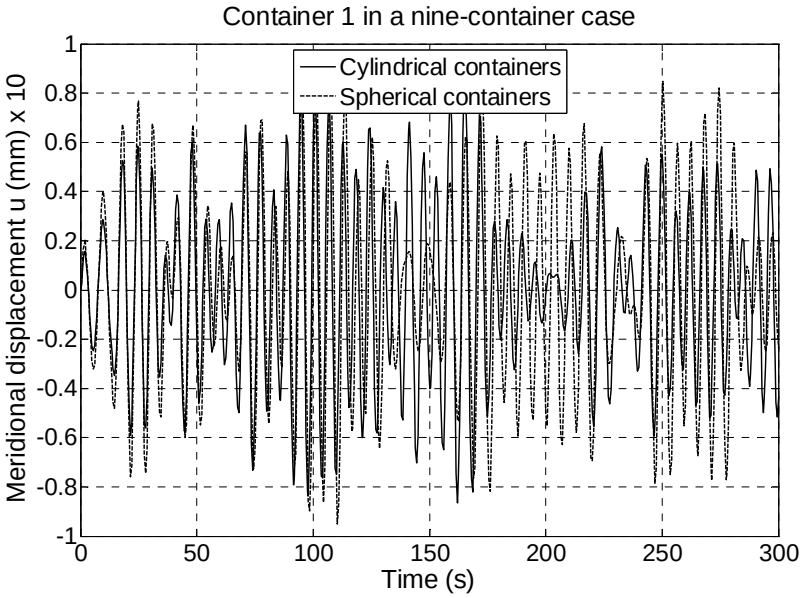

Figure 5.32 Meridional displacement of hemispherical and cylindrical containers

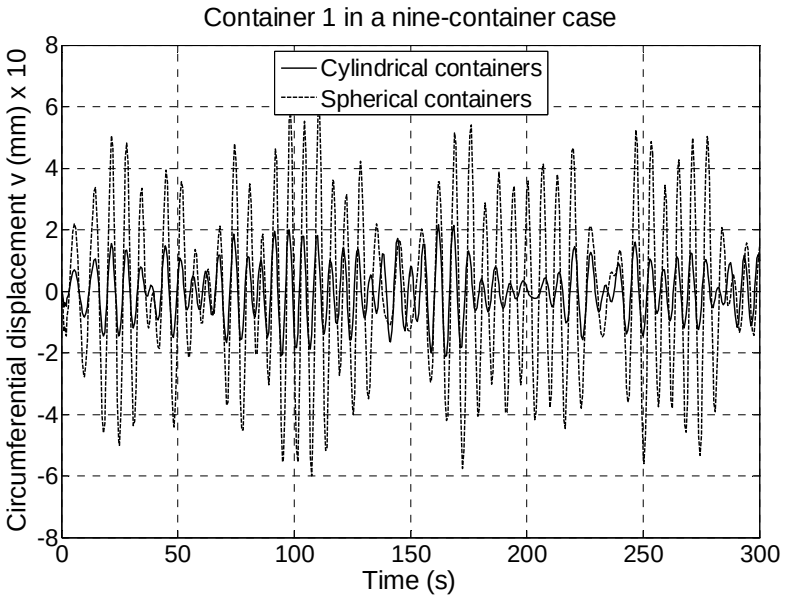

Figure 5.33 Circumferential displacement of hemispherical and cylindrical containers

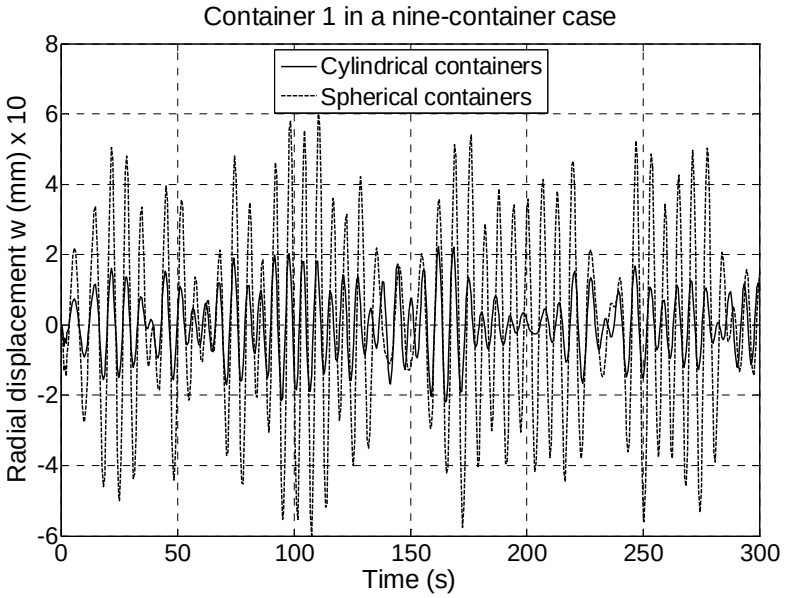

Figure 5.34 Radial displacement of hemispherical and cylindrical containers

5.6 Concluding remarks

The complicated fully interaction problem between liquid sloshing, multi-containers and ship moving across the ocean was considered in this chapter. Through several examples, the behaviour of the ship and the deformation as well as the stresses and bending moments of container walls were presented. Results obtained demonstrated the significant influence of liquid-container-ship interaction and the effect of level of liquid-filling, the number and location of containers and thruster modelling in global system motions. Some interesting findings include:

- The effects of liquid sloshing on the ship are significant when (1) the volume of container-to-volume of ship ratio V_{con}/V_{ship} increases beyond a critical value and (2) the ship's thruster is not used to control the ship motion.
- The effects of liquid sloshing on the containers tend to increase appreciably as the liquid-to-container height ratio $\beta = H_f / H$ is greater than the critical value of 0.4.
- The further the containers are from the COG of the ship, the more effects they will have on the global ship motion.
- A fully interacting liquid-container-ship should be employed in the modelling of the system in order to obtain a more accurate analysis.

In summary, the proposed RD-finite element program developed should be a useful tool for the dynamic analysis of coupled liquid-container-ship system. Some interesting further studies including the way to mitigate sloshing due to coupled ship motion will be explored in the next Chapter.

CHAPTER 6 MITIGATION OF LIQUID SLOSHING

6.1 Introduction

Sloshing of liquid in containers due to induced motion as a result of transportation can lead to additional liquid forces that can affect the stability of the tank-vessel system as well as cause structural failure of the container. Therefore, suppression of liquid motion to reduce stresses developed in the tank wall is a major concern in fluid-structure interaction problems. Various types of slosh-suppression devices, such as baffles and U-tubes, can be employed to mitigate the liquid motion and prevent the instability of the system. They are also useful in reducing the structural loads on the container.

Some experimental and analytical studies have been carried out in the past to understand the damping phenomenon in containers fitted with various types of devices (Howell and Ebler, 1956; Silveira et al., 1961; Stephens and Scholl, 1967). An annular disc-type baffle has been widely used in practice because it is more practical and easy to install in storage containers. This system consists of a series of annular ring baffles arranged in the inner wall of the tank. These ring-baffles run continuously around the periphery of the inside of the tank and are spaced vertically apart by a given distance. These baffles not only suppress the sloshing effect but they also stiffen the container wall.

Recently, several works have been carried out to observe the effects of baffles used in a coupled liquid-container system. A review of the studies on the use of baffles will be presented in three groups: Group 1 – Effect of baffles on liquid sloshing, Group 2 – Effect of baffles on the coupled natural frequency of the liquid-filled container, and Group 3 – Effect of baffles on structural responses of the container wall.

6.1.1 Effect of baffles on liquid sloshing

The sloshing of the liquid can be suppressed effectively with the proper use of baffles. For example, the vortex damping of sloshing in tanks with plate baffles was investigated by Buzhinskii (1990, 1998). His experimental studies showed that the effectiveness of the baffle-damping decreases when the acceleration of the system is increased. Later, Watson and Evans (1991) used the FEM to investigate the effect of rigid baffles on the linear sloshing in a circular cylindrical container. Anderson et al. (2001) introduced a simple device consisting of two plates for the control of liquid sloshing in rigid cylindrical containers. By focusing on the ratio of the mass of the controller to that of the liquid to be controlled, the experimental results showed that the devices are effective in suppressing sloshing wave amplitudes. Cho et al. (2005) presented the numerical analysis of the resonance characteristics of liquid sloshing in a 2-D baffled tank subjected to a forced lateral excitation. The sloshing damping ratios by the baffles were calculated by varying the number, location and opening width of the baffle. An analytical estimation of hydrodynamic damping ratio of liquid sloshing in baffled tanks under horizontal excitation was developed by Maleki and Ziyaeifar (2007). The theoretical results were also checked against experimental test results in order to validate the proposed models.

6.1.2 Effect of baffles on coupled natural frequency of liquid-filled containers

The effect of baffles on the coupled natural frequency of liquid-filled container has been investigated by various researchers. For example, Yue et al. (1996) presented an analytical method to solve the coupled oscillations problem of liquid in a cylindrical container with elastic damping spacers. The coupled frequency equation was obtained by using double velocity potential functions corresponding to the liquid above and below the damping spacers. Gedikli and Ergüven (1999) employed the boundary element method to study the effects of rigid baffles on the natural frequencies and seismic response of liquid in a circular cylindrical tank. Cho et al. (2002) performed a parametric investigation on free vibration characteristics of baffled cylindrical liquid-storage containers by using the coupled structural-acoustic finite element method. The variations of natural frequency were determined through various combinations of the number, location of baffles and the inner-hole diameter as well as the liquid height. The flexibility of baffles in containers filled with liquid was later examined by Biswal et al. (2003). In the study, the natural frequencies of liquid in a liquid-filled cylindrical tank with and without baffles were determined. Finite elements were used to discretize both the liquid and rigid/flexible baffles. Unfortunately, the interaction between liquid and container wall was omitted, i.e. the containers were assumed to be rigid. In addition, the analysis considered only the asymmetric mode of vibration of liquid and flexible baffle corresponding to the first circumferential wave number. Subsequently, Biswal et al. (2004) extended their study by considering the flexibility of both baffles and the container wall in a partially liquid-filled cylindrical tank. The sloshing amplitude of liquid was computed under translational base acceleration by taking into consideration the liquid–baffle–tank wall interaction and all circumferential modes. Shin et al. (2006) presented an analytical method to estimate the sloshing natural

periods for a prismatic liquid cargo tank with baffles on the bottom. This approach is also applicable for cases of variable baffle size and distribution. An analytical study on the fluid-structure interaction having baffles was presented by Gavrilyuk et al. (2006), who provided accurate approximations of natural frequencies and modes of a vertical circular cylindrical tank having a thin rigid-ring horizontal baffle.

6.1.3 Effect of baffles on structural responses of container wall

The use of baffles to mitigate the sloshing of liquid inside the container has the additional role of stiffening also the container. The deformation and the stress resultants in the tank wall are expected to be significantly reduced by the baffles. Many researchers have investigated the effect of baffles on the structural behaviours. For example, Amabili et al. (1998) analyzed the dynamic characteristics of partially-filled cylindrical tanks with a flexible bottom and ring stiffeners. The effect of free surface waves was taken into account, and thus both bulging and sloshing modes were also studied in their work. Two studies by Biswal et al. (2003, 2004) treated the sloshing problem based on the linear theory where the deformation of tank wall and the motion of liquid were assumed to be small. Recently, Biswal et al. (2006) developed the nonlinear sloshing analysis of liquid in a two dimensional, rigid, rectangular container with rigid baffles by using the finite element method. The effects of baffle parameters such as position, dimension and numbers on the structural response were investigated. Maleki and Ziyaeifar (2008) considered using baffles in cylindrical storage tanks for reducing earthquake responses. In their research, the liquid velocity contours in a cylindrical tank were analyzed to determine the optimal shape of baffles. They found that ring baffles are more effective than blade baffles in damping the sloshing mode.

In view of the above mentioned studies, very few researches have been conducted on the fully coupled interaction between the sloshing phenomenon inside the containers with baffles and the associated ship motion. In this chapter, the coupled interaction between the liquid sloshing, baffle-stiffened, container wall and the moving ship is analyzed by extending the RD-finite element method presented in Chapter 2. The formulation of the present problem allows for the flexibilities of both baffles and the container wall. In order to show the effectiveness of baffles, some results of the coupled dynamic system such as the maximum deformation and stress resultants in the tank walls will be presented and compared with corresponding results of cylindrical containers without baffles.

6.2 Extension of RD-finite element method for presence of baffles in containers

6.2.1 Problem definition

Figure 6.1 shows a typical cylindrical tank-baffle system with a fixed base. The container has a height H, radius R, wall thickness h and contains a liquid of height H_f. There are a number of ring baffles, each baffle has a thickness h_b and a width of $R - R_b$, where R_b and R are the inner and outer radii of the baffle, respectively. A typical j^{th} baffle is located at the distance $H_b^{(j)}$ from the fixed base of container. Note that the baffles need not necessarily be arranged at equal spacing from one another. In other words, $H_b^{(j)} - H_b^{(j+1)} \neq H_b^{(j-1)} - H_b^{(j)}$ where $H_b^{(j+1)} < H_b^{(j)} < H_b^{(j-1)}$. If the baffles are of equal spacing then the distance between two consecutive baffles is $H/(n_b+1)$, where n_b is the number of installed baffles.

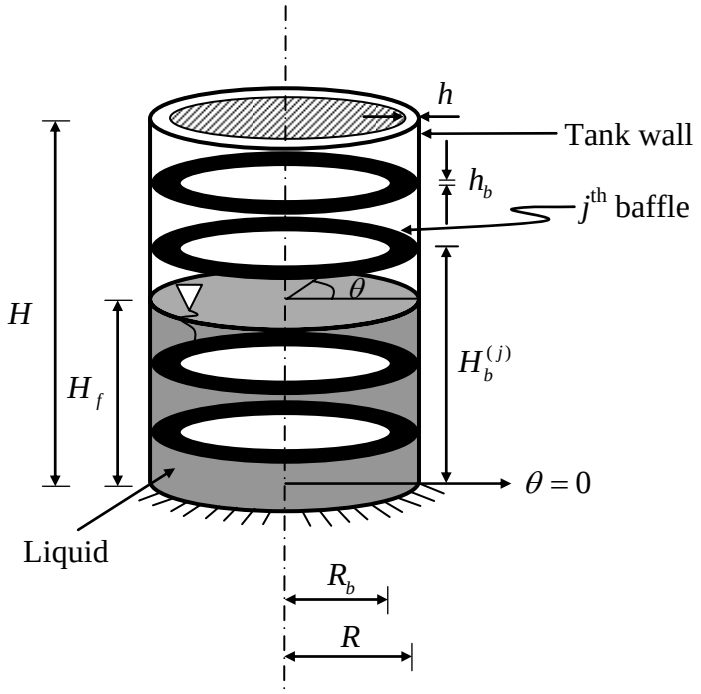

Figure 6.1 A liquid-filled cylindrical container with baffles

The problem at hand is to consider the effect of baffle location H_b, inner radius R_b, baffle thickness h_b and number baffles n_b on the coupled interaction between the liquid, baffle-container and ship. Some useful recommendations on the baffle design for the effective mitigation of liquid sloshing effect in containers will be presented.

6.2.2 Finite element formulation of coupled liquid-baffle-container system

The liquid in the container is considered as incompressible, inviscid and irrotational. The governing equation of motion of liquid inside the tank may be modeled by the potential flow theory which requires the satisfaction of the Laplace's equation,

$$\nabla^2 P(r,\theta,z,t) = 0 \tag{6.1}$$

in which $P = P_s + P_d$ is the total pressure where P_s, P_d are the static and dynamic pressures of liquid inside the tank, respectively. ∇^2 is the Laplacian operator in cylindrical coordinates given by

$$\nabla^2 = \frac{\partial^2}{\partial r^2} + \frac{1}{r}\frac{\partial}{\partial r} + \frac{1}{r^2}\frac{\partial^2}{\partial \theta^2} + \frac{\partial^2}{\partial z^2} \tag{6.2}$$

The boundary conditions for liquid-filled containers with baffles can be expressed as follows:

Kinematics free surface boundary condition

The linearized free-surface condition from Eq. (2.50) in Chapter 2 can be written as

$$\frac{1}{g}\frac{\partial^2 P}{\partial t^2} + \left.\frac{\partial P}{\partial z}\right|_{z=0} = 0 \tag{6.3}$$

However, if the free surface wave of the liquid is ignored then the pressure $P = 0$.

Boundary condition at the tank bottom

At the bottom of the tank, the velocity component of liquid normal to the rigid base is zero, which is the same as in Eq. (2.52) in Chapter 2, i.e.

$$\left.\frac{\partial P}{\partial z}\right|_{z=-H_f} = 0 \tag{6.4}$$

The interaction boundary condition between liquid and structure

At the liquid-tank wall and liquid-baffle interface, the velocity of liquid and structure in the normal direction must be equal, i.e.

$$\frac{\partial P}{\partial n} = -\rho_f \ddot{q}_n \tag{6.5}$$

where ρ_f is the density of the liquid, q_n the displacement of the structure in the normal direction and n is the outwardly drawn normal to the structure surface.

6.2.3 Modelling of baffles

The baffle is modeled as a thin annular plate. The assumed displacement functions of the baffle element can be expressed in the polar coordinate system as (Biswal et al., 2004)

$$u_b = (\alpha_1 + \alpha_2 r)\cos(n\theta) \tag{6.6}$$

$$v_b = (\alpha_3 + \alpha_4 r)\sin(n\theta) \tag{6.7}$$

$$w_b = (\alpha_5 + \alpha_6 r + \alpha_7 r^2 + \alpha_8 r^3)\cos(n\theta) \tag{6.8}$$

where u_b, v_b and w_b are the radial, circumferential and axial displacement components of the baffle element, respectively; α_i the coefficient of the displacement functions; and n the circumferential wave number.

The baffle element stiffness matrix $\mathbf{K}_{bf}^{e}$ is given by

$$\mathbf{K}_{bf}^{e} = \int_0^{2\pi}\int_{R_b}^{R} \mathbf{B}^T\mathbf{D}\mathbf{B}\, r\, dr\, d\theta \tag{6.9}$$

where $\mathbf{B}$ is the flexural strain-displacement matrix and $\mathbf{D}$ the flexural rigidity matrix.

The baffle element mass matrix $\mathbf{M}_{bf}^{e}$ can be expressed as

$$\mathbf{M}_{bf}^{e} = \pi\rho h_b \int_{R_b}^{R} \mathbf{N}_b^T\mathbf{N}_b\, r\, dr \tag{6.10}$$

where $\mathbf{N}_b$ is the baffle shape function matrix.

The tank wall coordinate system is taken as the global coordinate for the baffle-tank domain. The element stiffness matrix $\mathbf{K}_{bf}^{e}$ and mass matrix $\mathbf{M}_{bf}^{e}$ of baffles are transformed according to the global coordinate system. By assembling the stiffness and mass matrices of the tank wall and baffles, one can obtain the global stiffness matrix $\mathbf{K}_s$ and mass matrix $\mathbf{M}_s$ of the tank-baffle system.

6.2.4 Liquid-structure coupling matrix

Figure 6.2a shows the mesh discretization of the liquid-filled cylindrical container with baffles. Figure 6.2b shows the connectivity between the liquid element and baffle element, where nodes 1, 2 and 3 of the liquid element are connected to nodes i, j and k of the baffle element at the interface $y = -b$. The inner and outer radii of the baffle element are R_1 and R_2, respectively.

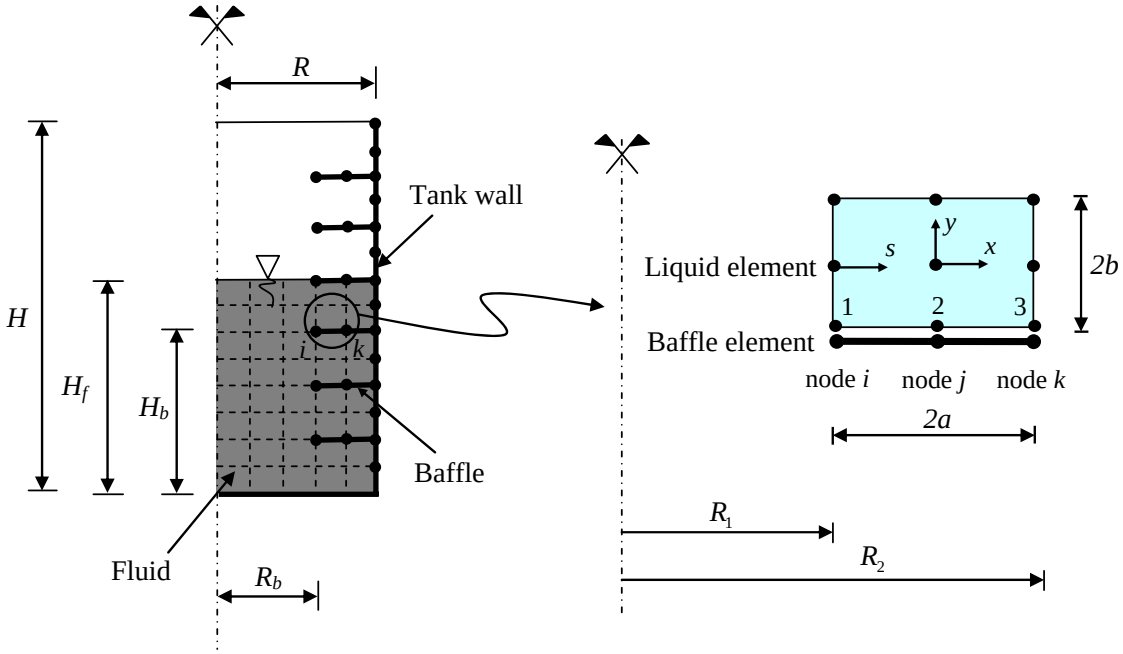

Figure 6.2a Finite element mesh of container with baffles

Figure 6.2b Liquid-baffle coupling element ($y = -b$)

The element liquid-baffle coupling matrix $\mathbf{S}_{bf}^{e}$ can be written as

$$\mathbf{S}_{bf}^{e} = \int_{baffle} \left[\mathbf{N}_{f}^{i}\right]^{T} \mathbf{N}_{b} dS \tag{6.11}$$

where $\mathbf{N}_{f}^{i}$ is the shape function of liquid element at the liquid-baffle interface, which was described in Eq. (2.62) of Chapter 2, and $\mathbf{N}_{b}$ the shape function of the baffle element.

Equation (6.11) can be expressed as

$$\mathbf{S}_{bf}^{e} = \int_{baffle} \left[\mathbf{N}_{f}^{i}\right]^{T} \mathbf{N}_{b} r dr d\theta \tag{6.12}$$

where the radius r is

$$r = \frac{R_2 - R_1}{2a} x + \frac{R_2 + R_1}{2} \tag{6.13}$$

in which $x = [-a, a]$.

By substituting Eq. (6.13) into Eq. (6.12), the element liquid-baffle coupling matrix $\mathbf{S}_{bf}^{e}$ at $y = -b$ can be expressed as

$$\mathbf{S}_{bf}^{e} = \pi \frac{R_2 - R_1}{2a} \int_{-a}^{a} \left[\mathbf{N}_{f}^{i}\right]^{T} \mathbf{N}_{b} \left[\frac{R_2 - R_1}{2a} x + \frac{R_2 + R_1}{2} \right]_{y=-b} dx \tag{6.14}$$

After integrating over the liquid-baffle interface, the element liquid-baffle coupling matrix $\mathbf{S}_{bf}^{e}$ can be written as

$$\mathbf{S}_{bf}^{e} = \frac{\pi\left(R_2 - R_1\right)}{2}\left[\begin{array}{c|c|c|c} \frac{1}{210}\left(52R_1+5R_2\right) & \frac{1}{315}\left(8R_1+R_2\right)a & \frac{8}{105}R_1 & \ldots \\ \hline \frac{2}{105}\left(8R_1+3R_2\right) & \frac{4}{315}\left(2R_1+R_2\right)a & \frac{16}{35}\left(R_1+R_2\right) & \ldots \\ \hline -\frac{1}{210}\left(5R_1-2R_2\right) & -\frac{1}{315}\left(R_1-R_2\right)a & \frac{8}{105}R_2 & \ldots \end{array}\right.$$

$$\left.\begin{array}{c|c|c|l} -\frac{8}{315}\left(2R_1+R_2\right)a & \frac{1}{210}\left(2R_1-5R_2\right) & -\frac{1}{315}\left(R_1-R_2\right)a & \text{node}\,1 \\ \hline -\frac{16}{315}\left(R_1-R_2\right)a & \frac{2}{105}\left(3R_1+8R_2\right) & \frac{4}{315}\left(R_1+2R_2\right)a & \text{node}\,2 \\ \hline \frac{8}{315}\left(R_1+2R_2\right)a & \frac{1}{210}\left(5R_1+52R_2\right) & \frac{1}{315}\left(R_1+8R_2\right)a & \text{node}\,3 \end{array}\right]_{3\times 6} \tag{6.15}$$

Following the same procedure, the element coupling matrix $\mathbf{S}_{bf}^{e}$ for the interaction between the liquid element (i.e. at nodes 5, 6 and 7) and the baffle element at location $y = b$ as shown in Figure 6.3 can be expressed as

$$\mathbf{S}_{bf}^{e} = \pi\frac{R_2 - R_1}{2a}\int_{-a}^{a}\left[\mathbf{N}_f^i\right]^T \mathbf{N}_b\left[\frac{R_2 - R_1}{2a}x + \frac{R_2 + R_1}{2}\right]_{y=b} dx \tag{6.16}$$

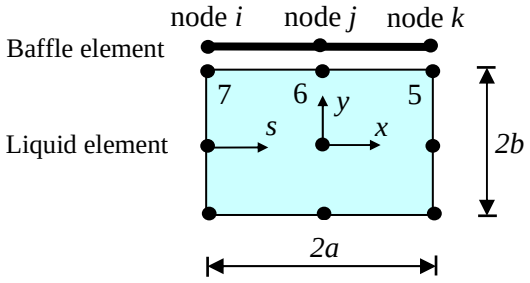

Figure 6.3 Liquid-baffle coupling element ($y = b$)

Upon integrating Eq. (6.16), one obtains the element liquid-baffle coupling matrix $\mathbf{S}_{bf}^{e}$ at location $y = b$

$$\mathbf{S}_{bf}^{e}=\frac{\pi\left(R_2-R_1\right)}{2}\left[\begin{array}{ccc|ccc}
-\frac{1}{210}\left(5R_1-2R_2\right) & -\frac{1}{315}\left(R_1-R_2\right)a & \frac{8}{105}R_2 & \cdots & & \\
\frac{2}{105}\left(8R_1+3R_2\right) & \frac{4}{315}\left(2R_1+R_2\right)a & \frac{16}{35}\left(R_1+R_2\right) & \cdots & & \\
\frac{1}{210}\left(52R_1+5R_2\right) & \frac{1}{315}\left(8R_1+R_2\right)a & \frac{8}{105}R_1 & \cdots & & \\
\hline
\frac{8}{315}\left(R_1+2R_2\right)a & \frac{1}{210}\left(5R_1+52R_2\right) & \frac{1}{315}\left(R_1+8R_2\right)a & \multicolumn{3}{l}{\text{node}\,5} \\
-\frac{16}{315}\left(R_1-R_2\right)a & \frac{2}{105}\left(3R_1+8R_2\right) & \frac{4}{315}\left(R_1+2R_2\right)a & \multicolumn{3}{l}{\text{node}\,6} \\
-\frac{8}{315}\left(2R_1+R_2\right)a & \frac{1}{210}\left(2R_1-5R_2\right) & -\frac{1}{315}\left(R_1-R_2\right)a & \multicolumn{3}{l}{\text{node}\,7}
\end{array}\right]_{3\times 6} \tag{6.17}$$

The element liquid-tank wall coupling matrix $\mathbf{S}_s^e$ which accounts for the interaction between nodes 3, 4 and 5 of liquid element and shell element at $x=a$, which was derived in Chapter 2, can be written as

$$\mathbf{S}_s^e=\pi R_2 b\left[\begin{array}{cccccc}
\frac{19}{70} & \frac{b}{35} & \frac{8}{105} & -\frac{8b}{105} & -\frac{1}{70} & 0 \\
\frac{22}{105} & \frac{4b}{105} & \frac{32}{35} & 0 & \frac{22}{105} & -\frac{4b}{105} \\
-\frac{1}{70} & 0 & \frac{8}{105} & \frac{8b}{105} & \frac{19}{70} & -\frac{b}{35}
\end{array}\right]_{3\times 6}\begin{array}{l}\text{node}\,3\\ \text{node}\,4\\ \text{node}\,5\end{array} \tag{6.18}$$

The liquid-baffle $\mathbf{S}_{bf}$ and liquid-tank wall $\mathbf{S}_s$ coupling matrices are assembled to obtain the global coupling matrix $\mathbf{S}$, i.e.

$$\mathbf{S}=\mathbf{S}_{bf}+\mathbf{S}_s \tag{6.19}$$

Note that the coupling matrix $\mathbf{S}$ is used to account for the fluid-structure interaction between the liquid element and the neighbouring shell and baffle elements.

6.2.5 Governing equation of coupled liquid-baffle-container system

The equation of motion of tank-baffle system when subjected to the external force $\mathbf{F}_{ex}$ and the force due to the liquid dynamic pressure $\mathbf{F}_{in}$ takes the form of

$$\mathbf{M}_s\ddot{\mathbf{q}} + \mathbf{K}_s\mathbf{q} = \mathbf{F}_{ex} + \mathbf{F}_{in} \tag{6.20}$$

where $\mathbf{M}_s$ and $\mathbf{K}_s$ are the mass and stiffness matrices of the tank wall-baffle system, respectively; $\ddot{\mathbf{q}}$ and $\mathbf{q}$ the generalized nodal accelerations and displacements of the shell (including tank wall and baffles), respectively; $\mathbf{F}_{ex}$ the external nodal force; $\mathbf{F}_{in}$ the nodal force exerted on the tank-baffle system due to the liquid dynamic pressure is given by

$$\mathbf{F}_{in} = \mathbf{S}^T\mathbf{p} \tag{6.21}$$

Equation (6.20) can be rewritten as

$$\mathbf{M}_s\ddot{\mathbf{q}} + \mathbf{K}_s\mathbf{q} = \mathbf{F}_{ex} + \mathbf{S}^T\mathbf{p} \tag{6.22}$$

In the absence of external forces, Eq. (6.22) reduces to

$$\mathbf{M}_s\ddot{\mathbf{q}} + \mathbf{K}_s\mathbf{q} - \mathbf{S}^T\mathbf{p} = \mathbf{0} \tag{6.23}$$

The equation of motion of liquid inside the container was expressed in Chapter 2 as

$$\mathbf{M}_f\ddot{\mathbf{p}} + \mathbf{K}_f\mathbf{p} + \mathbf{S}\ddot{\mathbf{q}} = \mathbf{0} \tag{6.24}$$

where $\mathbf{M}_f$ and $\mathbf{K}_f$ are the mass and stiffness matrices of the liquid, respectively; $\mathbf{p}$ and $\ddot{\mathbf{p}}$ the liquid nodal dynamic pressure and its second derivative, respectively.

By combining the equations of motion of the tank-baffle system Eq. (6.23) and the liquid Eq. (6.24), the governing equation of motion of the coupled liquid-tank-baffle system may be written as

$$\begin{bmatrix} \mathbf{M}_s & \mathbf{0} \\ \mathbf{S} & \mathbf{M}_f \end{bmatrix} \begin{Bmatrix} \ddot{\mathbf{q}} \\ \ddot{\mathbf{p}} \end{Bmatrix} + \begin{bmatrix} \mathbf{K}_s & -\mathbf{S}^T \\ \mathbf{0} & \mathbf{K}_f \end{bmatrix} \begin{Bmatrix} \mathbf{q} \\ \mathbf{p} \end{Bmatrix} = \begin{Bmatrix} \mathbf{0} \\ \mathbf{0} \end{Bmatrix} \tag{6.25}$$

The natural frequencies and mode shapes of vibration of the coupled liquid-tank-baffle system can be obtained by solving Eq. (6.25).

6.3 Verification of computer code

The coupled fluid-structure interaction problem between the liquid and partially-filled cylindrical container with a flexible baffle will now be investigated. Results obtained in the present study will be compared with available results in the literature to validate the proposed RD-finite element concept and the corresponding computer code. The baffle is assumed to have the shape of a thin annular plate, which is fitted to the inner periphery of the tank at different locations. Table 6.1 shows the material properties and geometrical parameters for the containers with a single baffle. These parameters are the same as those used by Biswal et al. (2004) so that a comparison of results can be carried out.

Table 6.1 Material and geometrical parameters of liquid-filled cylindrical containers with a single baffle

Container wall	H	Height of container	$0.5207\,m$
	R	Radius of container	$0.508\,m$
	h	Thickness of container wall	$0.001\,m$
	ν	Poisson's ratio	0.3
	E	Young's modulus	$103\,GPa$
	ρ_s	Mass density of shell	$4500\,kg/m^3$
Baffle	R_b	Inner radius of the baffle	$0.305\,m$
	h_b	Thickness of the baffle	$0.001\,m$
Liquid	H_f	Height of liquid	$0.508\,m$
	ρ_f	Mass density of liquid	$1000\,kg/m^3$

The fundamental sloshing frequencies of coupled liquid-baffle-tank system are determined for different locations of the flexible baffle from the liquid surface $H_b^{'} = H_f - H_b$. In this study, the ratio $H_b^{'} / H_f$ is varied from 0.1 to 0.8, which is the same as that used in the study by Biswal et al. (2004). Figure 6.4 shows the comparison of the fundamental sloshing frequencies of liquid. It is to be noted that the traditional finite element method was employed in the study by Biswal et al. (2004) whereas the present study employs the FEM based on the relative displacement concept. The sloshing frequency of liquid in the flexible tank without any baffle is $0.925\,Hz$ and this is shown in Figure 6.4 as a straight line. From this figure, it can be seen that the results of two studies agree very well with each other. As can be seen, the sloshing frequencies are found to increase as the ratio $H_b^{'} / H_f$ increases, i.e. as the baffle is placed closer to the liquid free surface, the greater the influence the baffle has on the sloshing frequencies. The effectiveness of the baffle is gradually reduced when it is moved towards the bottom of the container. This phenomenon can be explained easily that the liquid near the bottom behaves like a rigid mass, thus the effect of the baffle to the coupled system is not significant. In contrast, the liquid near the free surface has a greater sloshing and thus by placing the baffle nearer the liquid free surface, the greater the ability of the baffle in mitigating liquid sloshing. It can also seen that when the baffle is placed near the bottom of the container ($H_b^{'} / H_f = 0.8$), the sloshing frequencies of the liquid-filled container with and without a single baffle are nearly equal.

The sloshing frequencies of a rigid tank with a rigid baffle, i.e. the moduli of the tank wall and the baffle are very large, were also presented by Biswal et al. (2004). From Figure 6.4, it can be seen that the sloshing frequencies of the flexible tank with flexible baffle are always smaller than those of the rigid tank with rigid baffle. Thus, it

is important to note that the model that allows for the flexibility of both tank wall and baffle would lead to a more accurate analysis than that which assumed rigid tank and baffle. In view of the excellent agreement of results of the present study with those obtained numerically by Biswal et al. (2004) for the liquid-filled container for different locations of a single baffle, it can be said that the developed RD-finite element program can be used for the study of liquid-baffled-tank system.

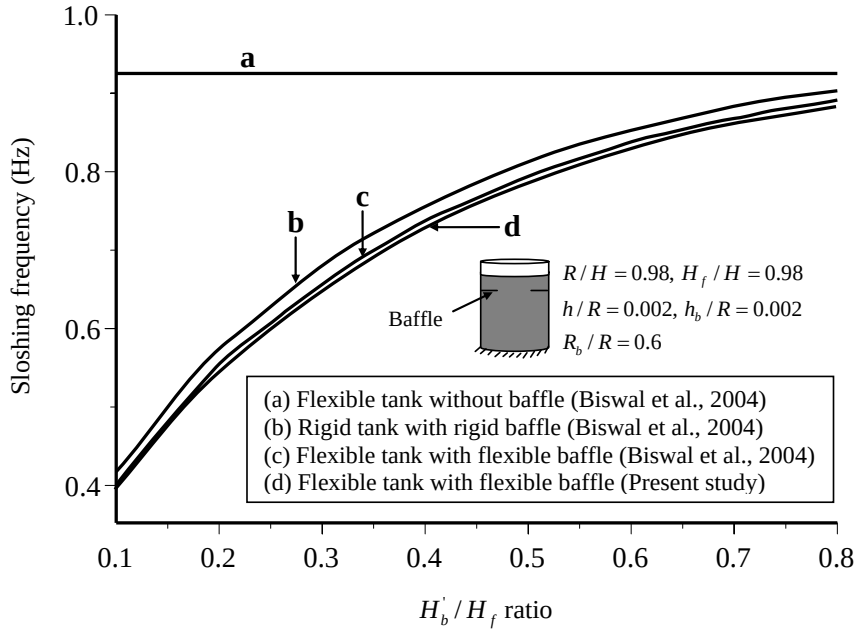

Figure 6.4 Comparison of sloshing frequency of liquid-filled cylindrical containers with/without a single baffle

6.4 Mitigation of liquid sloshing using baffles

Next, the effect of the location, size and number of the baffle on the interaction between liquid sloshing, containers and moving ship is considered. The ship is assumed to carry seven equally spaced containers along its length. All containers are assumed to be fixed at the base and free at the top end. The material and geometrical parameters of these containers are chosen such that they reflect a practical design. The

ship design parameters and environmental settings including wind, wave and current are the same as those used in Chapter 4. The fully coupled interaction between the liquid sloshing, baffle-container deformation and the ship motion is investigated and presented in the next few sub-sections.

6.4.1 Effect of location of single baffle

The effect of location of a single baffle on the coupled system is studied in this example. The height of liquid is kept constant at $H_f = 0.9H$, where the container height is $H = 5m$. The location of baffle is allowed to vary from $H_b / H = 0.1$ to 0.9 at 0.1 intervals. All containers are assumed to be partially-filled with oil and have the same material and geometrical parameters as listed in Table 6.2. The stresses and deformation of containers without and with one baffle are determined and compared for various baffle locations as described earlier.

Performance indices $\overline{q}_u$, $\overline{q}_v$ and $\overline{q}_w$ are introduced to assess the reduction in the maximum displacement components of the container with and without baffle. They are defined as

$$\overline{q}_u = \frac{(u_b)_{\max}}{u_{\max}},\ \overline{q}_v = \frac{(v_b)_{\max}}{v_{\max}} \text{ and } \overline{q}_w = \frac{(w_b)_{\max}}{w_{\max}} \tag{6.26}$$

where u, v and w are the displacement components of tank wall in meridional, circumferential and radial directions, respectively. The subscript b denotes the case of the container with baffles. For example, the w-displacement index $\overline{q}_w$ indicates the reduction of the radial displacement for the cylindrical tank with a baffle.

Table 6.2 Material and geometrical parameters of liquid-filled cylindrical containers with a single baffle

Container wall	H	Height of container	$5\,m$
	R	Radius of container	$5\,m$
	h	Thickness of container wall	$0.01\,m$
	ν	Poisson's ratio	0.3
	E	Young's modulus	$210\,GPa$
	ρ_s	Mass density of shell	$7850\,kg/m^3$
Baffle	R_b	Inner radius of baffle	$4.5\,m$
	h_b	Thickness of baffle	$0.005\,m$
Liquid	H_f	Height of liquid	$4.5\,m$
	ρ_f	Mass density of oil	$820\,kg/m^3$

Figure 6.5 shows the variation of the meridional displacement index $\overline{q}_u$, circumferential displacement index $\overline{q}_v$ and radial displacement index $\overline{q}_w$ with respect to different locations of the baffle H_b/H. The container without a baffle is represented by the case where $H_b/H=0$. As it can be seen from this figure, the displacement indices $\overline{q}$ are always less than unity since the baffle suppresses the liquid motion as well as it enhances the stiffness of the tank.

It can be seen from Figure 6.5 that the displacement components of the container wall are gradually reduced when the location of the baffle is increased from $H_b/H=0.1$ (i.e. the baffle is near the tank bottom) to $H_b/H=0.9$ (i.e. the baffle is near the liquid free surface). This means that when the baffle is fitted near the free surface of liquid, the maximum reduction in the deformation of the tank wall is achieved. On the other hand, its effect is negligible when the location of the baffle is near the tank bottom. For example, the radial displacement index for the container with the baffle placed near the tank bottom ($H_b/H=0.1$) is $\overline{q}_w=0.96$. When compared to the results of the container with the baffle placed near the liquid free surface ($H_b/H=0.9$), the radial displacement index significantly decreases to $\overline{q}_w=0.64$.

Therefore, one can conclude that a properly designed location of the baffle can significantly reduce the effect of liquid sloshing in the tanks.

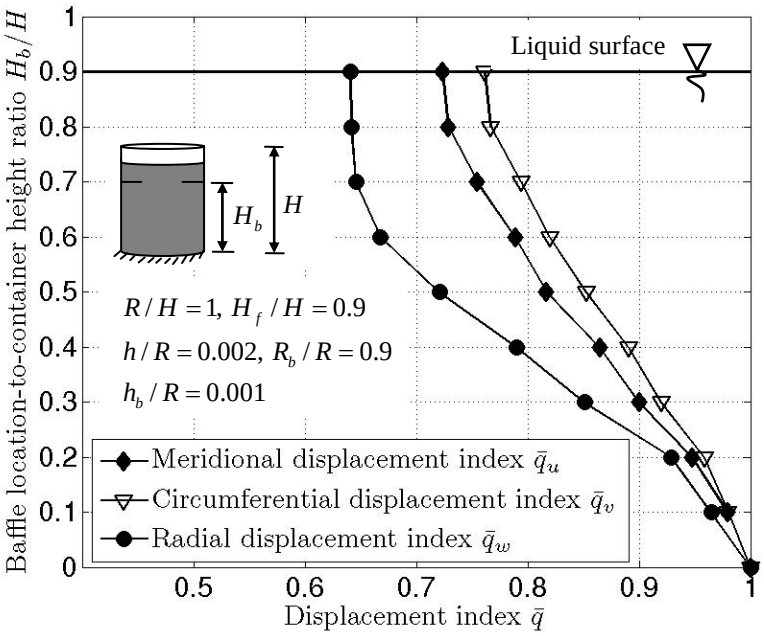

Figure 6.5 Effect of location of baffle-to-container height ratio on maximum displacement of container wall

The stress index $\bar{\sigma}$ is also introduced to facilitate the comparison between the stress components of the container with and without baffles. This ratio is defined as

$$\bar{\sigma}_s = \frac{\left(\sigma_s^b\right)_{\max}}{\left(\sigma_s\right)_{\max}},\ \bar{\sigma}_\theta = \frac{\left(\sigma_\theta^b\right)_{\max}}{\left(\sigma_\theta\right)_{\max}} \text{ and } \bar{\sigma}_{s\theta} = \frac{\left(\sigma_{s\theta}^b\right)_{\max}}{\left(\sigma_{s\theta}\right)_{\max}} \tag{6.27}$$

where σ_s, σ_θ and $\sigma_{s\theta}$ are the axial stress, hoop stress and membrane shear stress of the tank wall, respectively. The superscript b denotes the case of the container with baffles.

Figure 6.6 shows the variation of the stress indices with respect to different locations of the single baffle H_b/H. As can be seen from this figure, the stress components in the tank wall decrease gradually as the baffle location is shifted from

the tank bottom ($H_b / H = 0$) to near the liquid free surface ($H_b / H = 0.9$). This finding is similar for the deformation indices of the container wall.

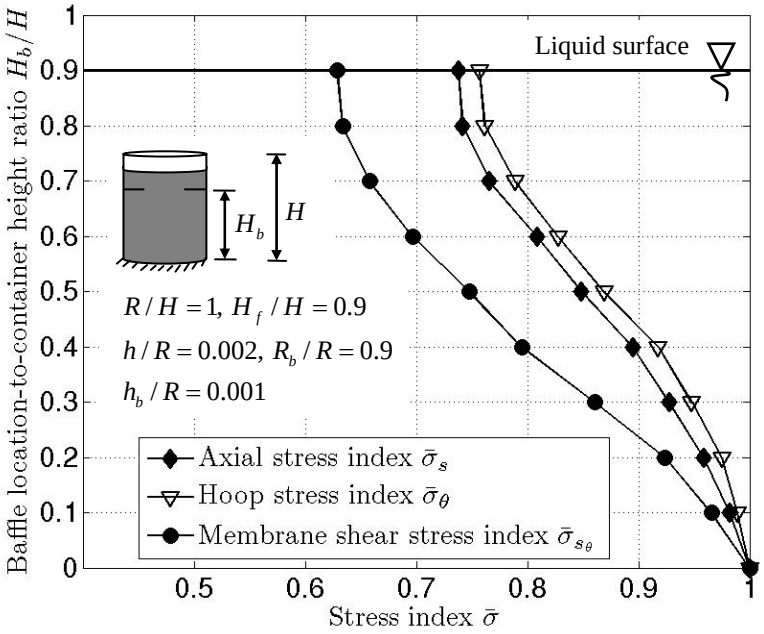

Figure 6.6 Effect of location of baffle-to-container height ratio on stress component of container wall

One can observe that there is an effective region of the H_b / H ratio from 0.2 to 0.8 where the baffle is more effective in mitigating the sloshing effect on the stress components of the tank wall. For the baffle location near the tank bottom ($H_b / H = 0 \approx 0.2$), the effect of the baffle on the deformation and stress of the container is noted to be marginal as compared to those of the container without the use of baffle. For example, the reduction of the stress index $\bar{\sigma}$ is less than 5% when the baffle is located at $H_b / H = 0.1$. For the value of $0.2 < H_b / H < 0.8$, there is a significant reduction in the stresses and deformation of tank wall through the use of a baffle. However, the reduction of these components is mostly constant when the baffle moves towards the liquid free surface, i.e. $0.8 < H_b / H < 1$. Therefore, the location of

the baffle from the tank base is recommended to be approximately $H_b / H = 0.9$ for maximum baffle effectiveness in near-filled cylindrical tanks.

6.4.2 Effect of size of single baffle

Next, the effect of baffle size on the coupled interaction between liquid sloshing, multi-containers and the moving ship is investigated. The inner radius of the baffle is varied from $R_b / R = 1/12$ to 11/12 at 1/6 intervals. The outer radius R of the baffle, which is the same as the radius of container, is taken to be $6m$ in this study. The thickness h_b and location of the baffle from the container base H_b are held constant. The geometrical and material properties of the liquid-filled, container-baffle system are shown in Table 6.3.

Table 6.3 Material and geometrical parameters of liquid-filled cylindrical containers with a single baffle

Container wall	H	Height of container	$6\,m$
	R	Radius of container	$6\,m$
	h	Thickness of container wall	$0.01\,m$
	ν	Poisson's ratio	0.3
	E	Young's modulus	$210\,GPa$
	ρ_s	Mass density of shell	$7850\,kg/m^3$
Baffle	H_b	Location of baffle from the container base	$5\,m$
	h_b	Thickness of baffle	$0.005\,m$
Liquid	H_f	Height of liquid	$5\,m$
	ρ_f	Mass density of oil	$820\,kg/m^3$

Figure 6.7 shows the variation of the displacement indices $\overline{q}_u$, $\overline{q}_v$ and $\overline{q}_w$ with respect to different ratios of the inner radius of the baffle-to-container radius R_b / R. Note that $R_b / R = 1$ corresponds to the case where no baffle is used. As shown in Figure 6.7, the deformation indices of the tank wall using a single baffle in meridional,

circumferential and radial directions are significantly reduced as compared to that of the tank without a baffle. The displacement indices of the container wall are found to decrease gradually as the size of baffle increases, i.e. when the inner radius of baffle-to-container radius R_b / R ratio decreases from 1 (i.e. container without baffle) to 1/12. The reduction of the radial displacement index $\bar{q}_w$ increases significantly when the R_b / R ratio exceeds the critical value of $R_b / R = 0.6$. On the other hand, the reduction of the meridional displacement $\bar{q}_u$ and circumferential displacement $\bar{q}_v$ indices increases sharply when the R_b / R ratio is greater than 0.7. Therefore, the deformation of the tank wall will decrease significantly when the ratio R_b / R goes beyond 0.65.

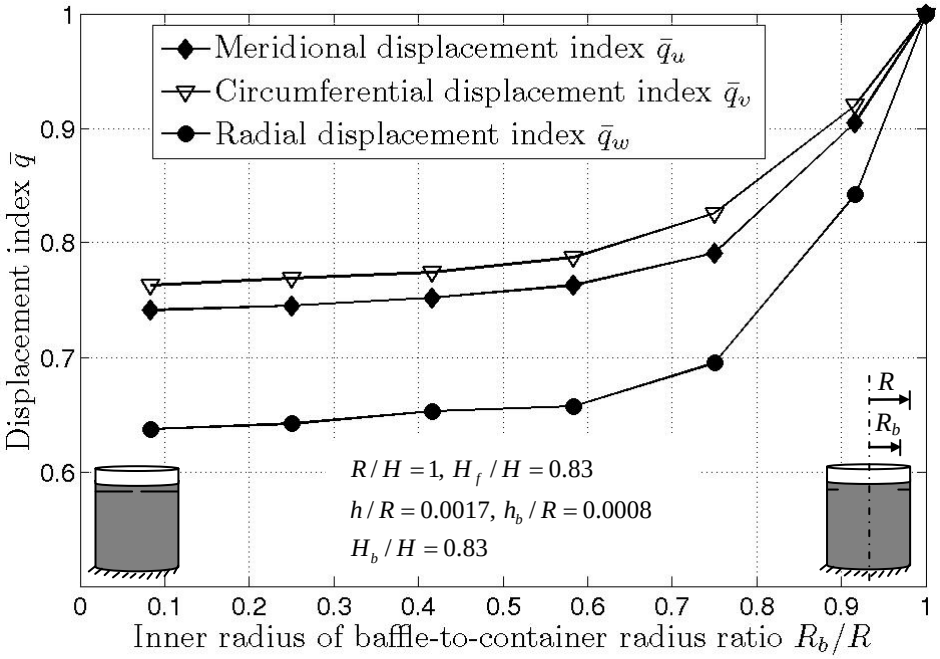

Figure 6.7 Effect of inner radius of baffle-to-container radius ratio on maximum displacement of container wall

Figure 6.8 shows the variation of the stress indices $\bar{\sigma}_s$, $\bar{\sigma}_\theta$ and $\bar{\sigma}_{s\theta}$ with respect to different ratios of R_b / R. The inner radius of the baffle-to-container radius R_b / R ratio is also varied from 1/12 to 11/12 and the container without the baffle is associated with $R_b / R = 1$. Referring to this figure, the stress indices $\bar{\sigma}_s$, $\bar{\sigma}_\theta$ and $\bar{\sigma}_{s\theta}$ are also reduced significantly when the inner radius of the baffle-to-container radius R_b / R ratio decreases from 1 (i.e. container without baffle) to 1/12 (i.e. containers using baffle). When the ratio of radius R_b / R is less than the value of 0.6, the reduction in the stresses and deformation of the tank wall is not appreciable as compared to the case when $R_b / R > 0.6$. It is therefore recommended that the inner radius R_b of the baffle should be around $R_b = 0.6R$ which appears to be more cost-effective in the mitigation of liquid sloshing effect on the stresses and deformation of the tank wall.

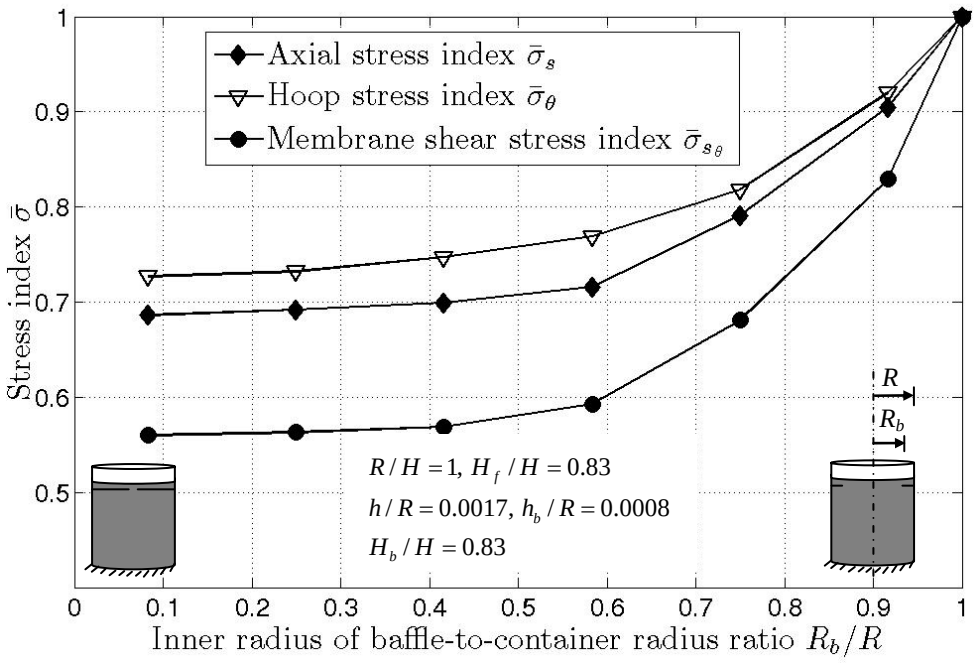

Figure 6.8 Effect of inner radius of baffle-to-container radius ratio on stress components of container wall

6.4.3 Effect of thickness of single baffle

The effect of baffle thickness h_b on the coupled interaction between liquid sloshing, baffle-container and ship is next investigated. The baffle thickness is varied from $h_b / h = 0.1$ to 3.0 at 0.5 intervals while the thickness of container wall h is fixed at $0.01\,m$. The case of container without baffle is associated with $h_b / h = 0$. The other parameters of the baffle such as inner radius R_b and the location from the container base H_b are kept constant in this study. The flexibilities of both baffle and tank wall are considered in our modelling. The geometrical and material properties of the liquid-filled, container-baffle system are given in Table 6.4.

Table 6.4 Material and geometrical parameters of liquid-filled cylindrical containers with a single baffle

Container wall	H	Height of container	$6\,m$
	R	Radius of container	$6\,m$
	h	Thickness of container wall	$0.01\,m$
	ν	Poisson's ratio	0.3
	E	Young's modulus	$210\,GPa$
	ρ_s	Mass density of shell	$7850\,kg/m^3$
Baffle	R_b	Inner radius of baffle	$5\,m$
	H_b	Location of baffle from the container base	$4.5\,m$
Liquid	H_f	Height of liquid	$5\,m$
	ρ_f	Mass density of oil	$820\,kg/m^3$

Figure 6.9 presents the variation of the displacement indices $\overline{q}_u$, $\overline{q}_v$ and $\overline{q}_w$ with respect to different ratios of baffle thickness-to-container thickness h_b / h. It can be seen from this figure that the displacement index $\overline{q}$ decreases when the ratio of the baffle thickness-to-container thickness h_b / h increases from 0 to 3 since the tank's stiffness is enhanced. This means that the effect of the baffle thickness h_b on the

deformation in container wall due to liquid sloshing is significantly reduced when the baffle thickness is increased. In addition, the reduction of the deformation in tank wall is noted to be appreciable when the ratio $h_b / h < 1$, i.e. when the baffle thickness h_b is less than or equal to the container thickness h. In particular, the displacement indices in meridional, circumferential and radial directions are $\bar{q}_u = 0.84$, $\bar{q}_v = 0.86$ and $\bar{q}_w = 0.74$, respectively, for $h_b / h = 1$. When h_b / h is greater than 1, the displacement indices in the three directions $\bar{q}_u$, $\bar{q}_v$ and $\bar{q}_w$ are noted to stay approximately constant. In other words, any further increase of the baffle thickness beyond the thickness of the container wall will not bring any additional significant effects in the mitigation of container's deformation.

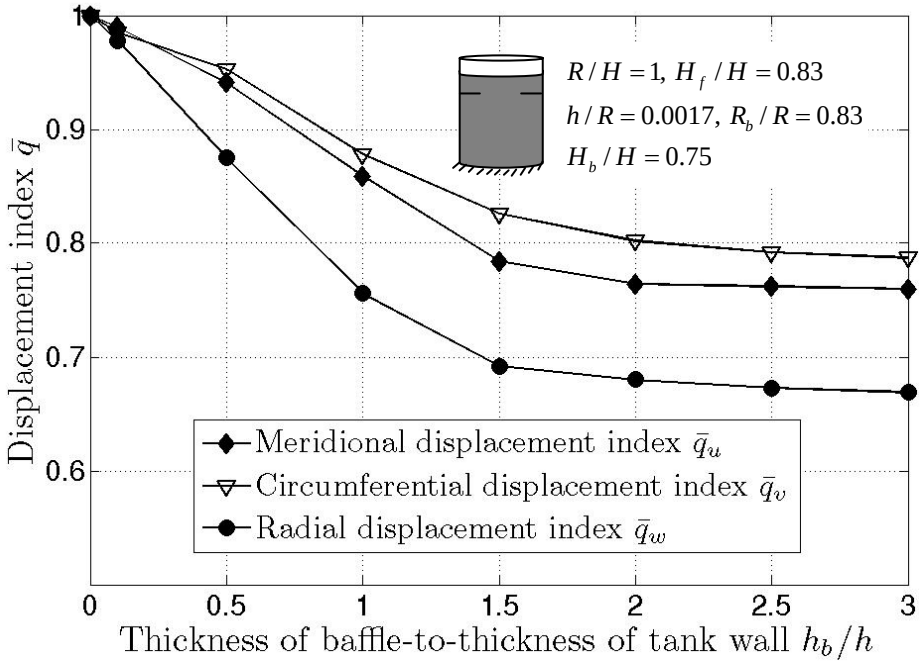

Figure 6.9 Effect of baffle thickness-to-container thickness ratio on maximum displacement of container wall

Figure 6.10 shows the variation of the axial $\bar{\sigma}_s$, hoop $\bar{\sigma}_\theta$ and membrane shear $\bar{\sigma}_{s\theta}$ stress indices with respect to different ratios of baffle thickness-to-container thickness h_b/h. The thickness ratio h_b/h is varied from 0.1 to 3 at 0.5 intervals. The case of container without any baffle is associated with the ratio $h_b/h=0$. It can be observed from Figure 6.10 that the stress index $\bar{\sigma}$ is reduced when the thickness ratio h_b/h increases from 0 to 3. In addition, the mitigation of liquid sloshing in terms of stress indices $\bar{\sigma}_s$, $\bar{\sigma}_\theta$ and $\bar{\sigma}_{s\theta}$ induced in the tank wall is observed to be more effective when the baffle thickness h_b is less than or equal to the container thickness h. When h_b/h ratio exceeds 1, the reduction in the stress of tank wall becomes insignificant and remains mostly constant, especially for the axial stress and the hoop stress components. This finding is the same as that noticed for the deformation in the tank wall. Based on this finding, it is therefore recommended that the baffle thickness should be chosen close to the container wall thickness for a more cost-effective for the mitigation of liquid sloshing effect.

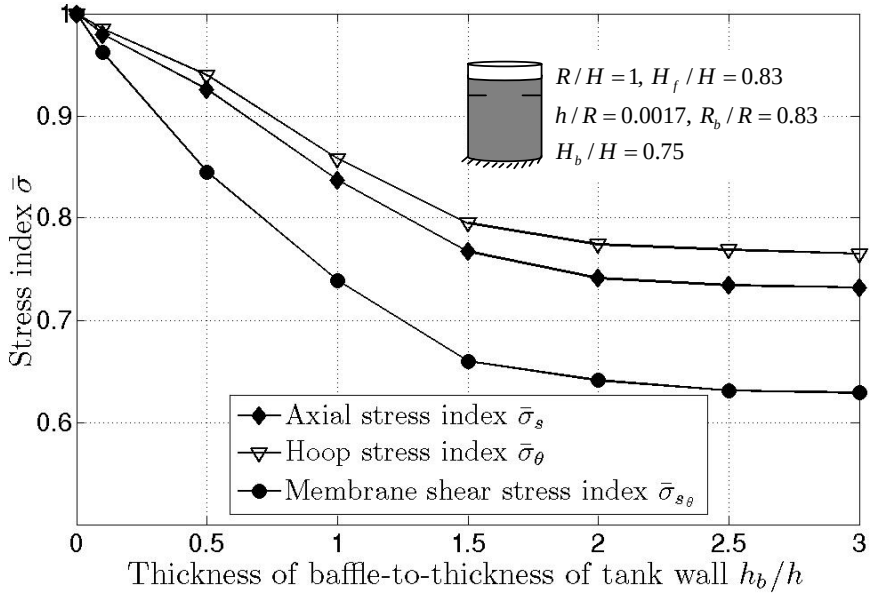

Figure 6.10 Effect of baffle thickness-to-container thickness ratio on stress components of container wall

6.4.4 Effect of number of baffles

In the foregoing study, only a single baffle was considered. When the baffle is relatively thick, the effectiveness of the baffle in reducing the deformation and stresses in the container is small as mentioned in previous section. Therefore, it might be more effective to use many thin baffles than a single thick baffle in the container. The quantitative effect of several baffles n_b on the coupled interaction between the liquid sloshing, baffle-container and the ship is next investigated. The best location of baffles that leads to minimum deformation in the tank wall will be considered. The number of baffles n_b will be varied from 1 to 5. Based on the foregoing study on the single baffle location, the first baffle will be fixed at $H_b^{(1)} = 0.9H$ from the tank base. The locations of other baffles between the tank base and the first baffle will be determined with the aim of minimizing the deformation in the tank. The geometrical and material properties of the liquid-filled, container-baffle system are shown in Table 6.5.

Table 6.5 Material and geometrical parameters of liquid-filled cylindrical containers with many thin baffles

Container wall	H	Height of container	$5\,m$
	R	Radius of container	$5\,m$
	h	Thickness of container wall	$0.01\,m$
	ν	Poisson's ratio	0.3
	E	Young's modulus	$210\,GPa$
	ρ_s	Mass density of shell	$7850\,kg/m^3$
Baffles	R_b	Inner radius of baffles	$4\,m$
	h_b	Thickness of baffles	$0.01\,m$
Liquid	H_f	Height of liquid	$4.8\,m$
	ρ_f	Mass density of oil	$820\,kg/m^3$

Cylindrical container with two baffles

The cylindrical container with two baffles is first treated. The first baffle is fixed at the location of $H_b^{(1)} = 0.9H$ from the tank base. The location of the second baffle $H_b^{(2)}$, placed below the first one, is varied from 0 (i.e. at the tank base) to near $0.9H$ as shown in Figure 6.11.

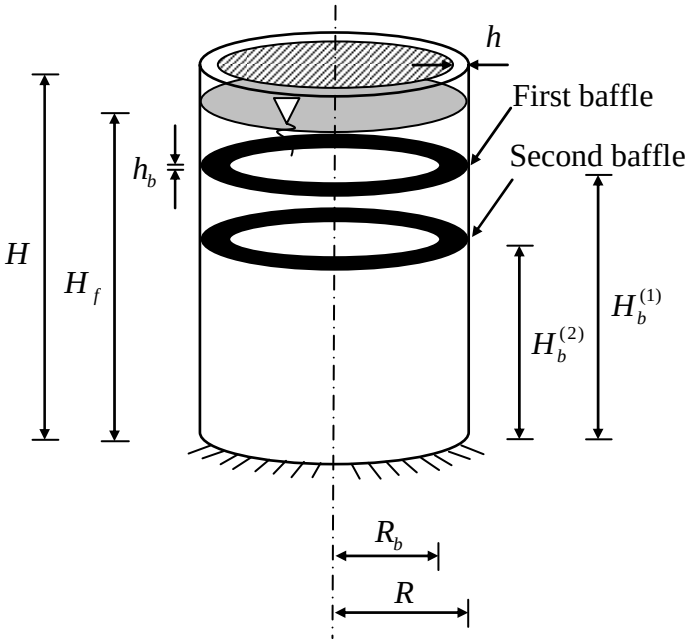

Figure 6.11 A liquid-filled cylindrical container with two baffles

The displacement index $\bar{q}$ is again introduced to facilitate the comparison between the maximum displacement components of the containers with two baffles and with only one baffle. The minimum deformation of tank wall with two baffles can be obtained by varying the location of the second baffle. Figure 6.12 shows the variation of displacement indices $\bar{q}$ with respect to the different ratios of the location of second baffle-to-container height $H_b^{(2)} / H$. It can be seen that when the location of second baffle $H_b^{(2)}$ moves from the tank base to the position of first baffle $H_b^{(1)}$, the

displacement index $\bar{q}$ first gradually decreases up to the location $H_b^{(2)} = 0.7H$ and then slightly increases beyond this critical value. In particular, the minimum displacement indices in meridional, circumferential and radial directions are $\bar{q}_u = 0.80$, $\bar{q}_v = 0.84$ and $\bar{q}_w = 0.69$, respectively, for the location of second baffle $H_b^{(2)} = 0.7H$. Therefore, one can conclude that the effective locations of the first and second baffles for the container with two baffles are $0.9H$ and $0.7H$, respectively.

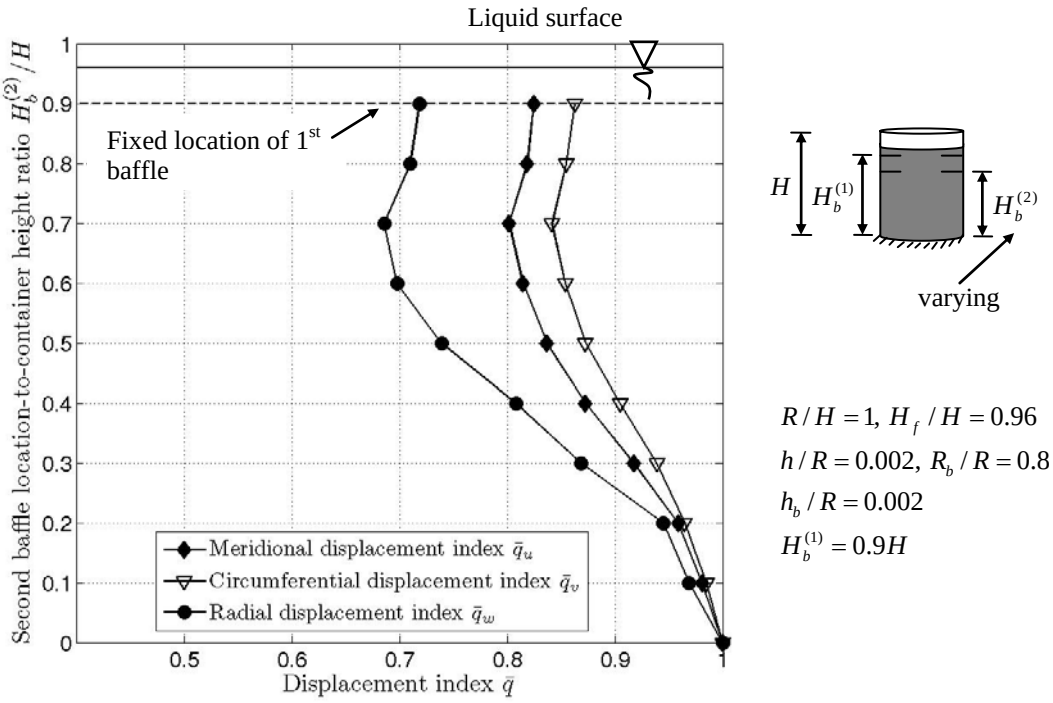

Figure 6.12 Effect of location of second baffle-to-container height ratio on maximum displacement of container wall

Cylindrical container with three baffles

Next, the container with three baffles is considered. Based on the result of foregoing study, the first and second baffles are fixed at the location of $H_b^{(1)} = 0.9H$ and $H_b^{(2)} = 0.7H$ from the tank base, respectively. The location of third baffle $H_b^{(3)}$ placed

below the second one is varied from 0 (i.e. at the tank base) to $0.7H$ as shown in Figure 6.13.

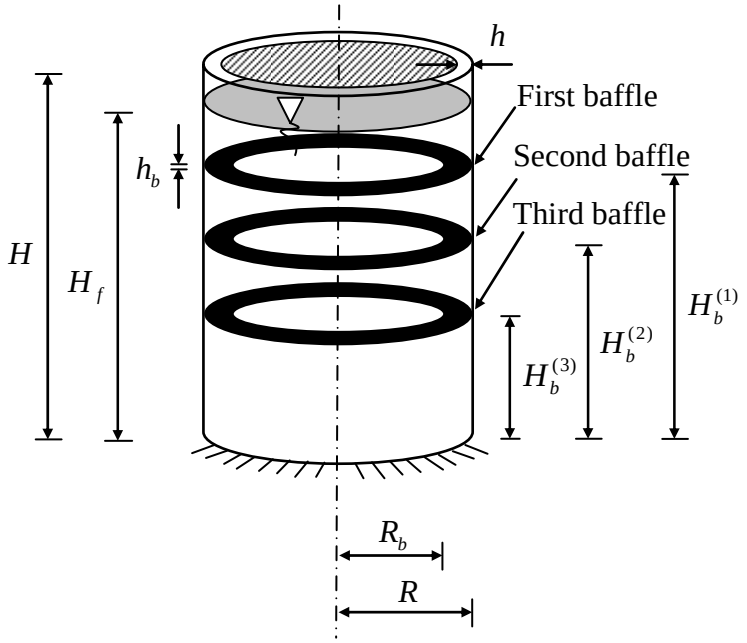

Figure 6.13 A liquid-filled cylindrical container with three baffles

The displacement index $\overline{q}$ for this case is defined to be the ratio of the maximum displacement components of the containers with three baffles and two baffles. By varying the location of the third baffle $H_b^{(3)}$, the minimum deformation of tank wall with three baffles can be determined. Figure 6.14 shows the variation of displacement index $\overline{q}$ in meridional, circumferential and radial directions with respect to the ratio $H_b^{(3)}/H$. It can be seen that when the location of the third baffle $H_b^{(3)}$ moves from the tank base to the position of second baffle $H_b^{(2)}$, the displacement index $\overline{q}$ first gradually decreases up to the location $H_b^{(3)} = 0.5H$ and then slightly increases beyond this critical value. In particular, the minimum displacement indices in meridional, circumferential and radial directions are $\overline{q}_u = 0.81$, $\overline{q}_v = 0.84$ and $\overline{q}_w = 0.73$, respectively, when third baffle is located at $H_b^{(3)} = 0.5H$. Therefore, one can conclude

that the effective locations of the first, second and third baffles for the container with three baffles are $0.9H$, $0.7H$ and $0.5H$, respectively.

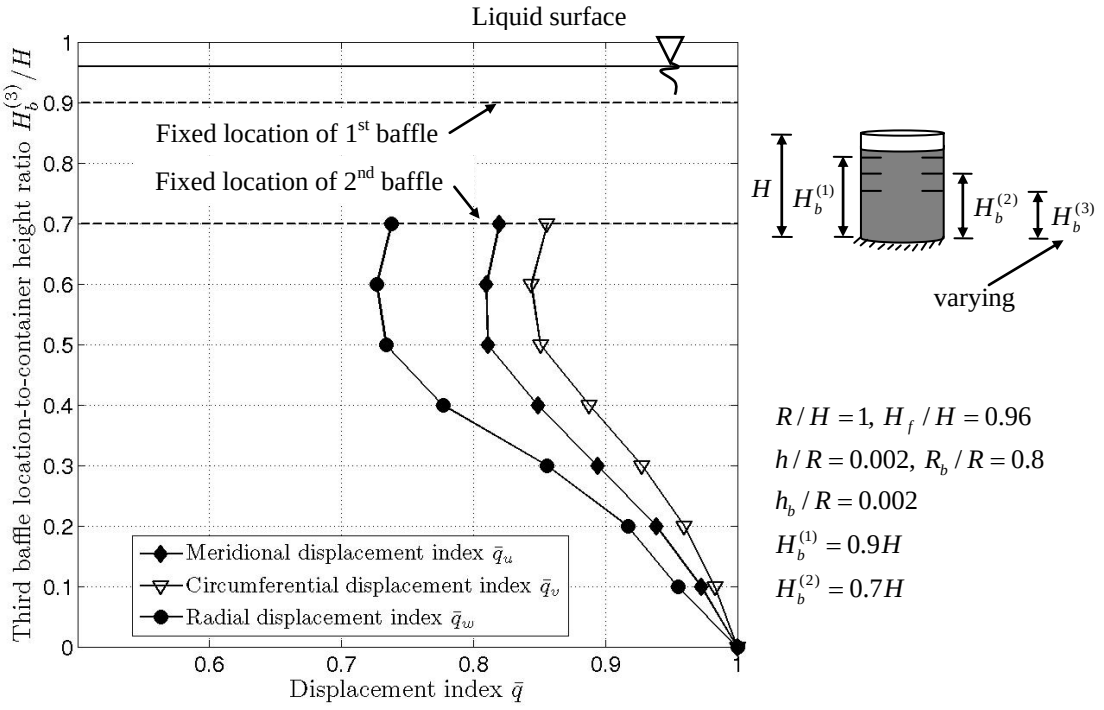

Figure 6.14 Effect of location of third baffle-to-container height ratio on maximum displacement of container wall

Cylindrical container with five baffles

To suppress effectively the sloshing effect on the structural response, the cylindrical container with five baffles is next considered. The material and geometrical parameters of this container are the same as those used in the previous study. The locations of these baffles are $H_b^{(1)}=0.9H$, $H_b^{(2)}=0.7H$, $H_b^{(3)}=0.5H$, $H_b^{(4)}=0.4H$ and $H_b^{(5)}=0.3H$. The thickness and inner radius of baffles are fixed at $h_b=0.005m$ and $R_b=4.5m$, respectively.

Figures 6.15 and 6.16 show respectively the variation of the radial displacement index $\bar{q}_w$ and the membrane shear stress index $\bar{\sigma}_{s\theta}$ with respect to different numbers of baffles n_b. The results are compared with the case in which all the baffles are located at equal spacing in the container. The number of baffle n_b is varied from 0 to 5 and the container without baffle is associated with $n_b = 0$. It can be seen from these figures that the radial displacement index $\bar{q}_w$ and stress index $\bar{\sigma}_{s\theta}$ decrease when the number of baffles n_b increases from 0 to 5. This means that the presence of more baffles will lead to a reduction in both displacements and stresses in the tank wall. Note that there is not much significant difference in the displacements and stress values for containers with uniformly and non-uniformly spaced baffles when the number of baffles increases.

The reduction of the deformation and stress resultants in tank wall is appreciable when the number of baffle n_b is larger than 1. For example, the radial displacement indices are $\bar{q}_w = 0.82$ for $n_b = 1$ and $\bar{q}_w = 0.68$ for $n_b = 5$, respectively. The difference in radial deformation of containers between two cases is significantly decreased up to 21%. Therefore, it is recommended that more baffles with thicknesses close to the tank wall thickness should be used to achieve the desired reduction in sloshing effect on the coupled system.

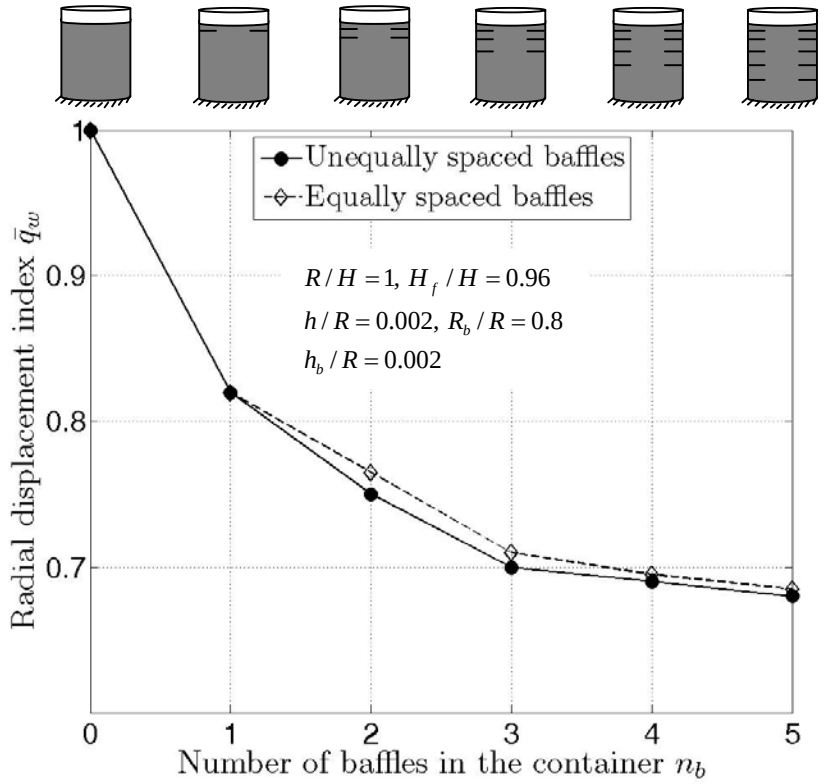

Figure 6.15 Effect of number of baffles on radial displacement index of container wall

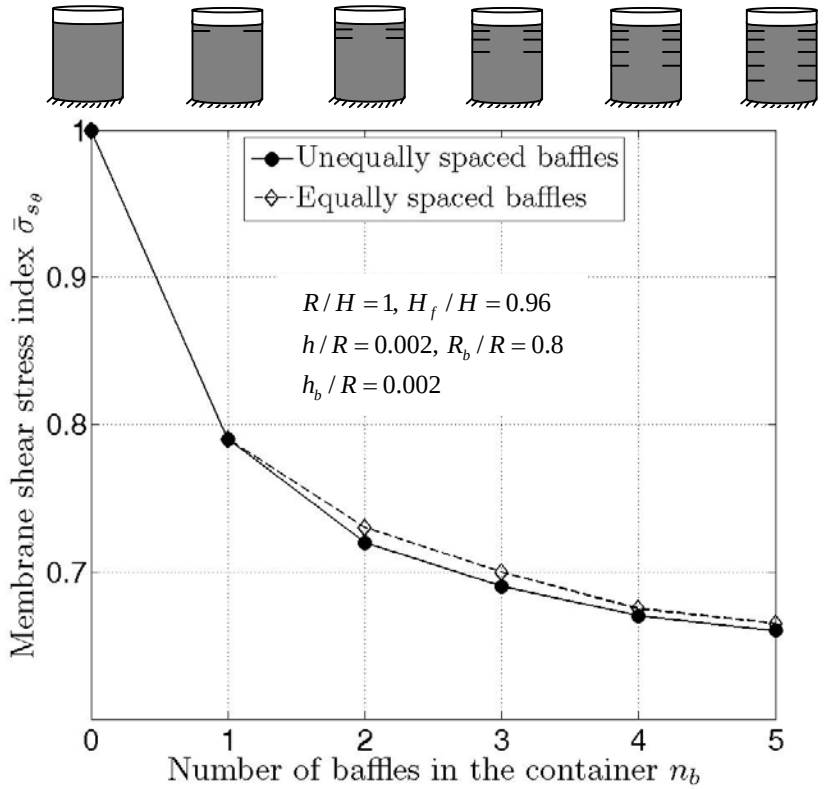

Figure 6.16 Effect of number of baffles on membrane shear stress of container wall

6.5 Concluding remarks

In this chapter, the study on the problem of liquid sloshing in tanks has been extended to allow for the presence of baffles which may be used for the effective mitigation of sloshing effect. By solving the fully interaction problem between liquid sloshing, containers with baffles and ship moving across the ocean, one can observe the effect of baffles on mitigating the sloshing effect and the structural response. Significant influence of the baffle parameters, such as the number, installation position and size of the baffle on the structural response of tank due to the coupled interaction was presented. Some interesting findings include:

- When considering a single baffle, greater mitigation influence is obtained when the baffle is placed close to the liquid free surface. Likewise, increasing the inner radius and thickness of the baffle will lead to more reduction in the deformation and stresses in the tank wall. On the other hand, placing the baffle near the bottom of the container results in negligible reduction in the structural response.
- For a more cost-effective use of the baffle in the mitigation of liquid sloshing, the recommendations are: (1) to use more thin baffles as practically possible instead of employing only one single thick baffle, (2) the inner radius of the baffle should be 0.6 times the container radius, and (3) the baffle thickness should not be thicker than the tank wall thickness.

In summary, the determination of a suitable combination of baffle parameters is critical towards an optimal design of the container for use in the transportation of liquid via ships.

CHAPTER 7 CONCLUSIONS AND FUTURE WORK

The main objective of this thesis is to investigate the dynamic analysis of fully coupled interaction problem between sloshing liquid, multi-containers and the ship used to transport the containers. The entire investigation is carried out using the proposed axisymmetric RD-shell and fluid elements where RD denotes that the finite element formulation is based on the relative displacement concept. This problem has not been studied extensively before. The closest study is by Lee et al. (2007b) who did not consider for the sum effects of environmental forces such as wind, wave and current. Their study adopted the linear ship motion and treated the environmental forces that were due to wave loading only. This thesis also explored how concentric baffles can be used effectively for the mitigation of liquid sloshing in the liquid-container-ship system.

To perform this aforementioned investigation, the proposed RD-shell and fluid elements were first formulated in Chapter 2. The free vibration analysis of single/multi-layer cylindrical containers filled with liquid was discussed in Chapter 3 to demonstrate the capability and generality of the present RD concept. Chapters 4 and 5 investigated the uncoupled and coupled dynamic analysis of liquid-filled containers on the ship, respectively. Chapter 6 considered the use of baffles for stiffening the tank wall and more importantly for the mitigation of sloshing effects on the coupled system motion.

In this chapter, a summary of the results and their implications are presented. The chapter ends with some recommendations for future work.

7.1 Conclusions

The significant contributions and important conclusions made in this thesis are:

1. An axisymmetric RD-shell element for the analysis of coupled natural frequencies of single/multi-layer cylindrical containers filled with an inviscid and incompressible liquid was developed. A coupling matrix to capture the interaction between the shell and neighbouring fluid elements was introduced. The results showed that the proposed RD method predicted the natural frequencies more accurately than the traditional thin shell theory. The reason is that the present study accounted for the effects of transverse shear and rotary inertia, which are neglected in the classical thin shell theory. Therefore, this proposed method can be applied to any kind of shell structures without distinguishing between thin and thick shells. It may be remarked that the present method using RD concept can easily be extended to study the influence of arbitrary support conditions, varying thickness and material of container wall on the natural frequencies of liquid and container.

2. The finite element method based on the relative displacement concept was developed to analyze the dynamic behaviour of liquid-filled containers that are transported on ships moving across the ocean. The study showed the effects of various influencing factors on the dynamic response of system due to ship motions. These factors include the levels of liquid filling, container parameters (e.g. thickness-to-radius and radius-to-container height ratios) and environmental settings such as the directions of wave and wind acting on the ship. The deformation of the tank wall due to the sloshing effect arising from the transportation of liquid via ships was found to increase when the thickness of

container decreases or the level of liquid increases. The sloshing effect becomes especially significant when the liquid-to-container height ratio is greater than 0.4 or the radius-to-container height ratio is less than 0.8. The most critical direction of wave or wind acting on the ship was found to be in the beam sea direction, i.e. its direction is perpendicular to the ship length.

3. The problem of complicated interaction between sloshing liquid, multi-containers and ship was conducted. The study showed that it is necessary to take into account the liquid-container-ship interaction. The investigation on the dynamic behaviour of the moving ship demonstrated that the volume of containers-to-volume of ship ratio and location of containers mounted on the moving ship are the most important factors affecting the ship response. Containers farther away from the centre of gravity (COG) of the ship affect the global ship motion more significantly than containers close to the COG of the ship. Therefore, in the event that a ship has to carry only partial load of its maximum capacity, it is best that containers near to the ship's COG be filled with fuel and the containers at the ends of the ship be left unfilled. Likewise, in the event that a ship has to unload part of the fuel at its destination, then it is best that the fuel in the tanks farthest away from the COG be unloaded first.

4. The shape of containers (circular cylindrical or spherical containers) has little effect on the ship as compared to their sizes. When the container's size increases, the effect of liquid sloshing on the ship motion is increased. In particular, the roll motion of the ship with fully-filled containers can decrease by 20% as compared to that of the ship with empty containers. Therefore, the liquid cargo can be used

to play the role of a vibration absorber for ship motion if the external forcing frequencies of the ship are away from the natural sloshing frequencies. To control the ship motion, thruster modeling is also recommended for use as it can provide better stability for the moving ship and therefore, the sloshing effects can be significantly reduced. The results showed that the ship motion in roll can be significantly decreased by 16% when using thrusters.

5. For the same amount of liquid, tank base radius, thickness and material properties of liquid and tank wall, the maximum deformation and stress resultants in the tank wall of cylindrical containers are noticeably smaller as compared with those of spherical containers. The difference can increase up to 25% between their two different shapes of containers. The cylindrical containers perform better than their spherical counterparts in withstanding static and dynamic pressures due to liquid sloshing. Therefore, it may be concluded that cylindrical containers are superior to spherical ones when used as containers in the transportation of liquid cargo via marine vessels.

6. Baffles are effective in mitigating the sloshing of liquid and the deformation as well as stress resultants induced in the tank wall. The dynamic response of the coupled container-ship system is significantly affected by various baffle parameters, such as the number of baffles, the installation position from the tank base and size of baffles. In the presence of a single baffle, it was found that the best position for the baffle to reduce liquid sloshing effect is near the liquid free surface. Conversely, placing the baffle at the bottom of the container is to be discouraged as this leads to negligible effect in the mitigation of liquid sloshing.

The reason is that liquid near the surface sloshes significantly whereas liquid near the bottom behaves like a rigid mass. Results also showed that flexible baffles are better suited in producing better slosh damping than rigid baffles. For a more cost-effective use of baffles in the mitigation of liquid sloshing, the recommendations are: (1) use as many thin baffles as practically possible instead of employing only one single thick baffle, (2) the size of baffle should be optimally chosen and this corresponds to the case when the inner radius of the baffle is 0.6 times the container radius, and (3) the baffle thickness should not be thicker than the tank wall thickness. In the case of container with three baffles, the effective locations of the first, second and third baffles are 0.9, 0.7 and 0.5 times of the container height. By using properly designed baffles, the maximum deformation and stress resultants in the tank wall can be significantly decreased by up to 30% as compared with corresponding cylindrical containers that do not employ any baffles. Therefore, the determination of a suitable combination of such baffle parameters is critical towards the design of baffled liquid-filled containers.

7.2 Recommendations for future work

Some important contributions of the present study were mentioned above. However, some unexplored problems still remain and need further studies. These problems include:

1. All liquid-filled containers were assumed to be fixed at the base throughout this thesis. However, most medium to large tanks in reality are not fully-fixed at the base because of economic and technical reasons. The tanks are just simply mounted or bolted at some points in the ground. Therefore, the partially-fixed container has much more complicated behaviour as compared to a fully-fixed container. This is due to the highly nonlinear phenomenon of the base uplift mechanism, which occurs as the resultant overturning moment generated from the liquid motion is large enough. Therefore, the uplift phenomenon due to loosely connection systems should be investigated to obtain the real behaviour of the coupled liquid-container problems.

2. The present study was based on an assumption that the amplitude of motion is small. In practice, design of liquid storage tanks would obviously need to consider worst case scenario such as rough/high sea states. Liquid motion on ship in a rough/high sea state can be of large amplitude. Therefore, this method is not applicable and it is recommended that the higher-order wave theory could be adopted for large amplitude motion and even for wave breaking where the discontinuity of motion may need to be considered.

3. The study may indeed be extended to three dimensions, both within the models of liquid-filled containers and the ship. The 3-D model will find more general applications because of its applicability to containers of any shape and configuration. The more realistic behaviour of the ship can be obtained with a 3-D model.

4. The focus of this thesis was on the development of the RD concept and their applications in various types of fluid-structure problems. Experimental studies are necessary in order to verify and validate the proposed numerical results based on the RD concept. The effects of the location from the tank base, inner radius and thickness of baffles should be also examined experimentally to demonstrate the effectiveness of the proposed sloshing damping devices.

5. The proposed method based on the RD concept for fluid-structure interaction problems should be further studied and applied to other promising aspects, such as (1) the liquid-filled containers with piecewise varying thickness along the cylindrical shell, and (2) the functionally graded cylindrical shells where the properties of material are varied and the temperature effects are included.

6. Bulk carrying ships make up 40% of the trading fleet and carry 66% of the world trade. Thus, a recent concerned problem is the increase in the size of a ship to improve transportation efficiency. Further studies should therefore be focused on the variation of the ship sizes as close to reality as possible. On the other hand, the effect of ship sizes on the sloshing flow inside containers should be investigated carefully.

REFERENCES

Abdel, G.A.F., Ragab, S.A., Nayfeh, A.H. and Mook, D.T. (2001). Roll stabilization by anti-roll passive tanks. *Ocean Engineering*, **28**, 457-469.

Akita, Y. (1967). Dynamic pressure of cargo oil due to pitching and effectiveness of swash bulkhead in long tanks. *Japan Shipbuilding & Marine Engineering*, **2**(5), 42-55.

Amabili, M. (2000). Eigenvalue problems for vibrating structures coupled with quiescent fluids with free surface. *Journal of Sound and Vibration*, **231**(1), 79-97.

Amabili, M., Païdoussis, M.P. and Lakis, A.A. (1998). Vibrations of partially filled cylindrical tanks with ring-stiffeners and flexible bottom. *Journal of Sound and Vibration*, **213**(2), 259-299.

Anderson, J.G., Turan, O.F. and Semercigil, S.E. (2001). Experiments to control sloshing in cylindrical containers. *Journal of Sound and Vibration*, **240**(2), 398-404.

Ang, K.K. (1980). Seismic analysis of liquid storage tanks using finite element technique. *Master Engineering Thesis*, Department of Civil Engineering, National University of Singapore, Singapore.

Arai, M. (1986). Experimental and numerical studies of sloshing in liquid cargo tanks with internal structures. *Ishikawajima-harima Heavy Industrial Engineering Review*, **19**(2), 51-56.

Aslam, M. (1981). Finite element analysis of earthquake-induced sloshing in axisymmetric tanks. *International Journal for Numerical Methods in Engineering*, **17**, 159-170.

Balchen, J.G., Jenssen, N.A., Mathisen, E. and Sælid, S. (1980). A dynamic positioning system based on Kalman filtering and optimal control. *Modeling, Identification and Control*, **1**(3), 135-163.

Balendra, T. and Nash, W.A. (1978). Earthquake analysis of a cylindrical liquid storage with a dome by finite element method. *Research Report*, Department of Civil Engineering, University of Massachusetts, USA.

Balendra, T. and Nash, W.A. (1980). Seismic analysis of a cylindrical liquid storage tank with a dome by finite element method. *Century 2, Pressure Vessels and Piping Conference*, San Francisco, USA.

Balendra, T., Ang, K.K., Paramasivam, P. and Lee, S.L. (1982a). Free vibration analysis of cylindrical liquid storage tanks. *International Journal of Mechanical Sciences*, **24**(1), 47-59.

Balendra, T., Ang, K.K., Paramasivam, P. and Lee, S.L. (1982b). Seismic design of flexible cylindrical liquid storage tanks. *Earthquake Engineering and Structural Dynamics*, **10**, 477-496.

Bass, D.W. (1998). Roll stabilization for small fishing vessels using paravanes and anti-roll tanks. *Marine Technology*, **35**(2), 74-84.

Bass, R.L. (1975). Dynamic slosh induced loads on liquid cargo tank bulkheads. *The Society of Naval Architects and Marine Engineers*, Report No. R-19.

Bathe, K.J. (1996). *Finite Element Procedures*. Prentice-Hall, New Jersey.

Bermudez, A., Rodriguez, R. and Santamarina, D. (2003). Finite element computation of sloshing modes in containers with elastic baffle plates. *International Journal for Numerical Methods in Engineering*, **56**, 447-467.

Biswal, K.C., Bhattacharyya, S.K. and Sinha, P.K. (2003). Free-vibration analysis of liquid-filled tank with baffles. *Journal of Sound and Vibration*, **259**(1), 177-192.

Biswal, K.C., Bhattacharyya, S.K. and Sinha, P.K. (2004). Dynamic response analysis of a liquid-filled cylindrical tank with annular baffle. *Journal of Sound and Vibration*, **274**, 13-37.

Biswal, K.C., Bhattacharyya, S.K. and Sinha, P.K. (2006). Non-linear sloshing in partially liquid filled containers with baffles. *International Journal for Numerical Methods in Engineering*, **68**, 317-337.

Brathu, M.C., Huther, M. and Planeix, J.M. (1972). Computer calculations of liquid motions in tanks. *Shipping World and Shipbuilder*, December.

Buzhinskii, V.A. (1990). The energy of vortex formation for oscillations in a fluid of a body with sharp edges. *Doklady Akademiia Nauk SSSR*, **313**(2), 1072-1074.

Buzhinskii, V.A. (1998). Vortex damping of sloshing in tanks with baffles. *Journal of Applied Mathematics and Mechanics*, **62**, 217-224.

Chang, J.S. and Chiou, W.J. (1995). Natural frequencies and critical velocities of fixed-fixed laminated circular cylindrical shells conveying fluids. *Computer & Structures*, **57**, 929-939.

Cho, J.R., Kim, K.W., Lee, J.K., Park, T.H. and Lee, W.Y. (2002a). Axisymmetric modal analysis of liquid-storage tanks considering compressibility effects. *International Journal for Numerical Methods in Engineering*, **55**, 733-752.

Cho, J.R., Lee, H.W. and Ha, S.Y. (2005). Finite element analysis of resonant sloshing response in 2-D baffled tank. *Journal of Sound and Vibration*, **288**, 829-845.

Cho, J.R., Lee, H.W. and Kim, K.W. (2002b). Free vibration analysis of baffled liquid-storage tanks by the structural-acoustic finite element formulation. *Journal of Sound and Vibration*, **258**(5), 847-866.

Chopra, A.K. (1995). *Dynamics of Structures*. Prentice Hall.

Clough, R.W. (1969). Analysis of structural vibration and dynamics response. *Recent Advances in Matrix Methods of Structural Analysis and Design*, 441-486.

Dalzell, J.F., Chu, W.H. and Modisette, J.E. (1964). Studies of ship roll stabilization tanks. *Technical Report*, No. 1AD607765.

Dean, R.G. and Dalrymple, R.A. (1991). *Water Wave Mechanics for Engineers and Scientists*. World Scientific, Singapore.

Epstein, H.I. (1976). Seismic design of liquid-storage tanks. *Journal of the Structural Division*, ASCE, **102**(9), 1659-1673.

Ernest, H., Johann, S. and Mustafa, O. (2003). *Analysis and Optimization of Prismatic and Axisymmetric Shell Structures*. Springer Verlag, London, UK.

Faltinsen, O.M, Rognebakke, O.F. and Timokha, A.N. (2005). Classification of three-dimensional nonlinear sloshing in a square-base tank with finite depth. *Journal of Fluids and Structures*, **20**, 81-103.

Faltinsen, O.M. (1978). A numerical nonlinear method of sloshing in tanks with two-dimensional flow. *Journal of Ship Research*, **18**(4), 224-241.

Faltinsen, O.M. (1990). *Sea Loads on Ships and Offshore Structures*. Cambridge University Press, UK.

Faltinsen, O.M. and Løken, A.E. (1979). Slow-drift oscillations of a ship in irregular wave. *Applied Ocean Research*, **1**(1), 21-31.

Fossen, T.I. (2002). *Marine Control Systems*. Tapir Trykkeri, Trondheinm, Norway, 2nd Edition.

Frandsen, J.B. (2004). Sloshing motions in excited tanks. *Journal of Computational Physics*, **196**, 53-87.

Froude, W. (1874). Considerations respecting the rolling of ships at sea. *Transactions of the Institute Naval Architecture*, **14**, 96-116.

Gavrilyuk, I., Lukovsky, I., Trotsenko, Y. and Timokha, A. (2006). Sloshing in a vertical circular cylindrical tank with an annular baffle. Part 1. Linear fundamental solutions. *Journal of Engineering Mathematics*, **54**, 71-88.

Gedikli, A. and Ergüven, M.E. (1999). Seismic analysis of a liquid storage tank with a baffle. *Journal of Sound and Vibration*, **223**(1), 141-155.

George, Z.V. and Pawel, W. (2004). A refined theory for thick spherical shells. *International Journal of Solids Structure*, **41**, 3747-3769.

Geradin, M. and Rixen, D. (1994). *Mechanical Vibrations and Structural Dynamics*. John Wiley.

Haroun, M.A. and Housner, G.W. (1981a). Seismic design of liquid storage tanks. *Journal of Technical Councils of ASCE*, **107**, 191-207.

Haroun, M.A. and Housner, G.W. (1981b). Earthquake response of deformable liquid storage tanks. *Journal of Applied Mechanics*, **48**, 411-418.

Haroun, M.A. and Housner, G.W. (1982). Dynamic characteristics of liquid storage tanks. *Journal of Engineering Mechanics*, ASCE, **108**, 783-800.

Hibbeler, R.C. (2006). *Engineering Mechanics-Principles of Dynamics*. Pearson Prentice Hall, Pearson Education, Inc. Upper Saddle River, New Jersey 07458.

Hoskins, L.M. and Jacobsen, L.S. (1934). Water pressure in a tank caused by a simulated earthquake. *Bulletin of the Seismological Society of America*, **24**(1), 1-32.

Housner, G.W. (1967). Dynamics pressures on accelerated fluid containers. *Bulletin of the Seismological Society of America*, **47**(1), 15-35.

Howell, E. and Ebler, F.G. (1956). Experimental investigation of the influence of mechanical baffles on fundamental sloshing mode of water in a cylindrical tank. *Space Technical Lab Report*, GM-TR-69.

Hsiung, H.C.H. and Weingarten, V.I. (1973). Dynamic analysis of hydro-elastic systems using the finite element method. *Report USCCE013*, Department of Civil Engineering, University of Southern California, USA.

Huang, K.H. and Dasgupta, A. (1995). A layer-wise analysis for free-vibration of thick composite cylindrical shells. *Journal of Sound and Vibration*, **186**, 207-222.

Ibrahim, R.A. (2005). *Liquid sloshing dynamics: Theory and applications*. Cambridge University Press, UK.

Jacobsen, L.S. (1949). Impulsive hydrodynamics of fluid inside a cylindrical tank and of fluid surrounding a cylindrical pier. *Bulletin of the Seismological Society of America*, **39**, 189-203.

Jing, H.S. and Tzeng, K.G. (1993). Refined shear deformation theory of laminated shells. *American Institute of Aeronautics and Astronautics AIAA Journal*, **31**, 765-773.

Joseph, W.T. (1999). *Structural Dynamics*. William G. McDougal, C. Allen Ross Addison-Wesley.

Journee, J.M.J. (1997). Liquid cargo and its effect on ship motions. *Six International Conference on Stability of Ships and Ocean Structures*, Varna, Bulgaria, 22-27.

Khai, S.L (1993). Seismic coupled modeling of axisymmetric tanks containing liquid. *Journal of Engineering Mechanics*, **119**(9), 1747-1761.

Kim, J.W., Kim, K., Kim, P.S. and Shin, Y.S. (2005). Sloshing-ship motion coupling effect for the sloshing impact load on the LNG containment system. *Proceedings of the Fifteenth International Offshore and Polar Engineering Conference*, Seoul, Korea, **3**, 282-291.

Kim, Y. (2002). A numerical study on sloshing flows coupled with ship motion – the anti-rolling tank problem. *Journal of Ship Research*, **46**(1), 52-62.

Kim, Y., Nam, B.W., Kim, D.W. and Kim, Y.S. (2007). Study on coupling effects of ship motion and sloshing. *Ocean Engineering*, **34**, 2176-2187.

Kim, Y., Nam, B.W., Kim, D.W., Lee, Y.B. and Lee, J.H. (2006). Study on couple effects of sloshing and ship motion. *Proceedings of the Sixteenth International Offshore and Polar Engineering Conference*, San Francisco, California, USA, **3**, 225-229.

Kim, Y.S. and Yun, C.B. (1997). A spurious free four-node displacement-based fluid element for fluid-structure interaction analysis. *Engineering Structures*, **19**(8), 665-678.

Kumar, R.R. and Rao, Y.V.K.S. (1988). Free vibration of multilayered thick composite shells. *Computer & Structures*, **28**(6), 717-722.

Kyeong, H.J. and Seong, C.L. (1995). Fourier series expansion method for free vibration analysis of either a partially liquid-filled or a partially liquid-surrounded circular cylindrical shell. *Computers & Structures*, **58**(5), 931-946.

Kyeong, H.J. and Seong, C.L. (1998). Hydroelastic vibration of a liquid-filled circular cylindrical shell. *Computers & Structures*, **66**(2-3), 173-185.

Lam, K.Y. and Wu, Q. (1999). Vibrations of thick rotating laminated composite cylindrical shells. *Journal of Sound and Vibration*, **225**(3), 483-501.

Lee, D.H., Kim, M.H., Kwon, S.H., Kim, J.W. and Lee, Y.B. (2007a). A parametric sensitivity study on LNG tank sloshing loads by numerical simulations. *Ocean Engineering*, **34**, 3-9.

Lee, D.Y. and Choi, H.S. (1999). Study on sloshing in cargo tanks including hydroelastic effects. *Journal of Marine Science and Technology*, **4**, 27-34.

Lee, S.J., Kim, M.H., Lee, D.H., Kim, J.W. and Kim, Y.H. (2007b). The effects of LNG-tank sloshing on the global motions of LNG carriers. *Ocean Engineering*, **34**, 10-20.

Love, A.E.H. (1944). *A Treatise on the Mathematical Theory of Elasticity*. Dover Publications, 4th Edition, New York.

Loy, C.T. and Lam, K.Y. (1999). Vibration of thick cylindrical shells on the basis of three dimensional theory of elasticity. *Journal of Sound and Vibration*, **226**(4), 719-737.

Ma, D.C., Gvildys, J., Chang, Y.W. and Liu, W.K. (1982). Seismic behavior of liquid-filled shells. *Nuclear Engineering and Design*, **70**, 437-455.

Ma, Y.Q. and Ang, K.K. (2006). Free vibration of Mindlin plates based on the relative displacement plate element. *Finite Element in Analysis and Design*, **42**, 1021-1028.

Ma, Y.Q., Ang, K.K. and McGuckin, D. (2005). A plate element based on relative displacement concept. *International Journal for Computational Methods in Engineering Science and Mechanics*, **6**(3), 153-159.

Maleki, A. and Ziyaeifar, M. (2007). Damping enhancement of seismic isolated cylindrical liquid storage tanks using baffles. *Engineering Structures*, **29**(12), 3227-3240.

Maleki, A. and Ziyaeifar, M. (2008). Sloshing damping in cylindrical liquid storage tanks with baffles. *Journal of Sound and Vibration*, **311**(1-2), 372-385.

Malenica, S., Zalar, M. and Chen, X.B. (2003). Dynamic coupling of seakeeping and sloshing. *Proceedings of the 13th International Offshore and Polar Engineering Conference*, Hawaii, USA, **3**, 484-490.

McCarty, J.L. and Stephens, D.G. (1960). Investigation of the natural frequencies of fluid in spherical and cylindrical tanks, *NASA TN D-252*.

Mikelis, N.E. and Journee, J.M.J. (1984). Experimental and numerical simulations of sloshing behaviour in liquid cargo tanks and its effect on ship motions. *National Conference on Numerical Methods for Transient and Coupled Problems*, Venice, Italy, 9-13.

Moan, T. (2003). Marine structures for the future. *CORE Report No. 2003-01,* Centre for Offshore Engineering & Research, National University of Singapore.

Molin, B., Remy, F., Rigaud, S. and De Jouette, Ch. (2002). LNG-FPSO's: frequency domain, coupled analysis of support and liquid cargo motion. *Proceedings of the IMAM Conference*, Rethymnon, Greece.

Naeem, M.N. and Sharma, C.B. (2000). Prediction of natural frequencies for thin circular cylindrical shells. *Proceedings of the Institution of Mechanical Engineers. Part C, Journal of Mechanical Engineering Science*, **214**(10), 1313-1328.

Nguyen, T.D. (2006). Design of hybrid marine control systems for dynamic positioning. *PhD Thesis*, Department of Civil Engineering, National University of Singapore, Singapore.

Nukulchai, W.K. and Tam, B.T. (1999). Structure-fluid interaction model of tuned liquid dampers. *International Journal for Numerical Methods in Engineering*, **46**, 1541-1558.

Park, J.J., Kim, M.S. and Ha, M.K. (2005). Three-dimensional sloshing analysis of LNG carriers in irregular waves. *Proceedings of the Fifteenth International Offshore and Polar Engineering Conference*, Seoul, Korea, **3**, 209-213.

Price, W.G. and Bishop, R.E.D. (1974). *Probabilistic Theory of Ship Dynamics*. Chapman and Hall, London.

Rammerstorfer, F.G., Scharf, K., Fischer, F.D. and Seeber, R. (1988). Collapse of earthquake excited tanks. *Journal of Mechanical Research*, **25**, 129-143.

Rao, S.S. (1990). *Mechanical Vibrations*. Addison-Wesley Publishing Company, USA.

Reddy, J.N. (1984). A simple higher-order theory for laminated composite plates. *Journal of Applied Mechanics*, **51**, 745-752.

Reed, F.E. (1961). Dynamic vibration absorbers and auxiliary mass dampers. *Shock and Vibration Handbook*, edited by Harris, C.M. and Crede, C.E., New York, McGraw-Hill.

Rognebakke, O.F. and Faltinsen, O.M. (2003). Coupling of sloshing and ship motions. *Journal of Ship Research*, **47**(3), 208-221.

Sewall, J.L. and Naumann, E.C. (1968). An experimental and analytical vibration study of thin cylindrical shells with and without longitudinal stiffeners. *NASA TN D-4705*.

Shin, J.R., Choi, K. and Kang, S.Y. (2006). An analytical solution to sloshing natural periods for a prismatic liquid cargo tank with baffles. *Proceedings of the*

Sixteenth International Offshore and Polar Engineering Conference, San Francisco, California, USA, **3**, 236-242.

Shrimali, M.K. and Jangid, R.S. (2002). Seismic response of liquid storage tanks isolated by sliding bearings. *Engineering Structures*, **24**, 909-921.

Silveira, M.A., Stephens, D.C. and Leonard, H.W. (1961). An experimental investigation of damping of liquid oscillations in cylindrical tanks with various baffles. *NASA TN D-715*.

SNAME (1950). Nomenclature for treating the motion of a submerged body through a fluid. *The Society of Naval Architects and Marine Engineers, Technical and Research Bulletin*, 1-5.

Sørensen, A.J. (2004). *Short Course on Marine Control Systems*. National University of Singapore, 3rd-5th May.

Sørensen, A.J., Sagatun, S.I. and Fossen, T.I. (1996). Design of a dynamic position system using model-based control. *Control Engineering Practice*, **4**(3), 359-368.

Stephens, D.G. and Scholl, H.F. (1967). Effectiveness of flexible and rigid ring baffles for damping liquid oscillations in large-scale cylindrical tanks. *NASA TND-3878*.

Stofan, A.J. and Pauli, A.J. (1962). Experimental damping of liquid oscillations in a spherical tank by positive expulsion bags and diaphragms, *NASA TND-1311*.

Subhash, B.S. and Bhattacharyya, S.K. (1996). Finite element analysis of fluid-structure interaction effect on liquid retaining structures due to sloshing. *Computers & Structures*, **59**(6), 1165-1171.

Tedesco, J.W., Landis, D.W. and Kostem, C.N. (1989). Seismic analysis of cylindrical liquid storage tanks. *Computer & Structures*, **32**(5), 1165-1174.

To, C.W.S. and Wang, B. (1991). An axisymmetric thin shell finite element for vibration analysis. *Computers & Structures*, **40**(3), 555-568.

Vamsi, K.B. and Ganesan, N. (2006). Polynomial approach for calculating added mass for fluid-filled cylindrical shells. *Journal of Sound and Vibration*, **291**, 1221-1228.

Vasta, J., Giddings, A.J., Taplin, A. and Stillwell, J.J. (1961). Roll stabilization by means of passive tanks. *Transactions of the Society of Naval Architects and Marine Engineers, SNAME*, **69**, 411-460.

Veletsos, A.S. (1974). Seismic effects in flexible liquid storage tanks. *Proceedings of the International Association for Earthquake Engineering Fifth World Conference*, Rome, Italy, **1**, 630-639.

Veletsos, A.S. and Tang, Y. (1987). Rocking response of liquid storage tanks. *Journal of Engineering Mechanics*, ASCE, **113**(11), 1774-1792.

Veletsos, A.S. and Yang, J.Y. (1976). Dynamics of fixed base liquid storage tanks. *Proceedings of U.S-Japan Seminar on Earthquake Engineering Research with Emphasis on Lifeline Systems*, Japan Society for Promotion of Earthquake Engineering, Tokyo, Japan, 317-341.

Veletsos, A.S. and Yang, J.Y. (1977). Earthquake response of liquid storage tanks. *Advances in Civil Engineering through Engineering Mechanics*, ASCE, 1-24.

Warnitchai, P. and Pinkaew, T. (1998). Modelling of liquid sloshing in rectangular tanks with flow-dampening devices. *Engineering Structures*, **20**(7), 593-600.

Watson, E.B.B. and Evans, D.V. (1991). Resonant frequencies of a fluid container with internal bodies. *Journal of Engineering Mathematics*, **25**, 115-135.

Watts, P. (1883). On a method of reducing the rolling of ship at sea. *Transactions of the Institute Naval Architecture*, **1**, 165.

Watts, P. (1885). The use of water chambers for reducing the rolling of ships at sea. *Transactions of the Institute Naval Architecture*, **2**, 30.

Weng, C. (1992). Roll motion stabilization for small fishing vessels. *Ph.D. thesis*, Memorial University of Newfoundland, Canada.

Westergaard, H.M. (1933). Water pressure on dams during earthquakes. *Transactions of the American Society of Civil Engineers*, **98**, 418-433.

Xi, Z.C., Yam, L.H. and Leung, T.P. (1997). Free vibration of a laminated composite circular cylindrical shell partially filled with fluid. *Computer Part B*, **28B**, 359-375.

Yang, J.Y. (1976). Dynamic behavior of fluid-tank systems. *Ph.D. Thesis*, Rice University, Houston, Texas, USA.

Youssef, K.S., Ragab, S.A., Nayfeh, A.H. and Mook, D.T. (2002). Design of passive anti-roll tanks for roll stabilization in the nonlinear range. *Ocean Engineering*, **29**, 177-192.

Yue, B., Wang, Z. and Li, J. (1996). Liquid sloshing in cylindrical tank with elastic spacer. *Communications in Nonlinear Science and Numerical Simulation*, **1**(2), 67-70.

Zhang, A. and Suzuki, K. (2007). A comparative study of numerical simulations for fluid–structure interaction of liquid-filled tank during ship collision. *Ocean Engineering*, **34**, 645-652.

Zienkiewicz, O.C. (1971). *The Finite Element Method in Engineering Science*. McGraw-Hill, New York.

APPENDIX A RD-SHELL AND FLUID ELEMENTS

A.1 Axisymmetric RD-shell element

The matrix of membrane rigidity $\mathbf{D}_m$ is given by

$$\mathbf{D}_m = \frac{Eh}{1-\nu^2}\begin{bmatrix} 1 & \nu & 0 \\ \nu & 1 & 0 \\ 0 & 0 & \dfrac{1-\nu}{2} \end{bmatrix}_{3\times 3} \tag{A.1}$$

The matrix of flexural rigidity $\mathbf{D}_b$ is written as

$$\mathbf{D}_b = \frac{Eh^3}{12\left(1-\nu^2\right)}\begin{bmatrix} 1 & \nu & 0 \\ \nu & 1 & 0 \\ 0 & 0 & \dfrac{1-\nu}{2} \end{bmatrix}_{3\times 3} \tag{A.2}$$

The matrix of shear rigidity $\mathbf{D}_s$ has the form

$$\mathbf{D}_s = \frac{\kappa Eh}{2\left(1+\nu\right)}\begin{bmatrix} 1 & 0 \\ 0 & 1 \end{bmatrix}_{2\times 2} \tag{A.3}$$

where κ is the shear modification factor and is taken to be 5/6 for an isotropic material.

A.2 Stiffness matrix of axisymmetric fluid element

The fluid element stiffness matrix $\mathbf{K}_f^e$ can be expressed in term of shape functions as

$$\begin{aligned}\mathbf{K}_f^e &= \frac{\pi}{\rho_f}\int_{-a}^{a}\int_{-b}^{b}\left(\left[\frac{\partial \mathbf{N}_f}{\partial x}\right]^T\frac{\partial \mathbf{N}_f}{\partial x}+\left[\frac{\partial \mathbf{N}_f}{\partial y}\right]^T\frac{\partial \mathbf{N}_f}{\partial y}+\frac{n^2}{\left(x_0+x\right)^2}\left[\mathbf{N}_f\right]^T\mathbf{N}_f\right)\left(x_0+x\right)dxdy \\ &= \mathbf{K}_1+\mathbf{K}_2+\mathbf{K}_3\end{aligned} \tag{A.4}$$

in which

$$\mathbf{K}_1 = \frac{\pi}{\rho_f}\int_{-a}^{a}\int_{-b}^{b}\left[\frac{\partial \mathbf{N}_f}{\partial x}\right]^T\frac{\partial \mathbf{N}_f}{\partial x}\left(x_0+x\right)dxdy \tag{A.5}$$

or

$$\mathbf{K}_1 = \frac{x_0 b}{90a}\begin{bmatrix}
4(4\bar{a}-7) & 16(\bar{a}-2) & 4 & 2 \\
16(\bar{a}-2) & 64 & -16(\bar{a}+2) & -8(\bar{a}+2) \\
4 & -16(\bar{a}+2) & 4(4\bar{a}+7) & 2(4\bar{a}+7) \\
2 & -8(\bar{a}+2) & 2(4\bar{a}+7) & 16(4\bar{a}+7) \\
-1 & 4(\bar{a}+2) & -(4\bar{a}+7) & 2(4\bar{a}+7) \\
4(2-\bar{a}) & -16 & 4(\bar{a}+2) & -8(\bar{a}+2) \\
(4\bar{a}-7) & 4(2-\bar{a}) & -1 & 2 \\
2(7-4\bar{a}) & 8(\bar{a}-2) & 2 & 16 \\
8(\bar{a}-2) & 32 & -8(\bar{a}+2) & -64(\bar{a}+2)
\end{bmatrix}$$

$$\begin{bmatrix}
-1 & 4(2-\bar{a}) & (4\bar{a}-7) & 2(7-4\bar{a}) & 8(\bar{a}-2) \\
4(\bar{a}+2) & -16 & 4(2-\bar{a}) & 8(\bar{a}-2) & 32 \\
-(4\bar{a}+7) & 4(\bar{a}+2) & -1 & 2 & -8(\bar{a}+2) \\
2(4\bar{a}+7) & -8(\bar{a}+2) & 2 & 16 & -64(\bar{a}+2) \\
4(4\bar{a}+7) & -16(\bar{a}+2) & 4 & 2 & -8(\bar{a}+2) \\
-16(\bar{a}+2) & 64 & 16(\bar{a}-2) & 8(\bar{a}-2) & 32 \\
4 & 16(\bar{a}-2) & 4(7-4\bar{a}) & 2(4\bar{a}-7) & 8(\bar{a}-2) \\
2 & 8(\bar{a}-2) & 2(4\bar{a}-7) & 16(4\bar{a}-7) & 64(\bar{a}-2) \\
-8(\bar{a}+2) & 32 & 8(\bar{a}-2) & 64(\bar{a}-2) & 256
\end{bmatrix}_{9x9}^{sym} \tag{A.6}$$

where x_0 is a distance from the geometric axis of the tank to the centre of the liquid element; a and b the dimensions of the liquid element; and $\bar{a} = a / x_0$.

$$\mathbf{K}_2 = \frac{\pi}{\rho_f} \int_{-a}^{a} \int_{-b}^{b} \left[\frac{\partial \mathbf{N}_f}{\partial y} \right]^T \frac{\partial \mathbf{N}_f}{\partial y} \left(x_0 + x \right) dxdy \tag{A.7}$$

or

$$\mathbf{K}_2 = \frac{x_0 b}{90a} \begin{bmatrix} 7(4-3\bar{a}) & 14(1-\bar{a}) & -7 & 8 \\ 14(1-\bar{a}) & 112 & 14(\bar{a}+1) & -16(\bar{a}+1) \\ -7 & 14(\bar{a}+1) & 7(3\bar{a}+4) & -8(3\bar{a}+4) \\ 8 & -16(\bar{a}+1) & -8(3\bar{a}+4) & 16(3\bar{a}+4) \\ -1 & 2(\bar{a}+1) & (3\bar{a}+4) & -8(3\bar{a}+4) \\ 2(1-\bar{a}) & 16 & 2(\bar{a}+1) & -16(\bar{a}+1) \\ (4-3\bar{a}) & 2(1-\bar{a}) & -1 & 8 \\ 8(3\bar{a}-4) & 16(\bar{a}-1) & 8 & -16 \\ 16(\bar{a}-1) & -128 & -16(\bar{a}+1) & 32(\bar{a}+1) \end{bmatrix}$$

$$\ldots \begin{bmatrix} -1 & 2(1-\bar{a}) & (4-3\bar{a}) & 8(3\bar{a}-4) & 16(\bar{a}-1) \\ 2(\bar{a}+1) & 16 & 2(1-\bar{a}) & 16(\bar{a}-1) & -128 \\ (3\bar{a}+4) & 2(\bar{a}+1) & -1 & 8 & -16(\bar{a}+1) \\ -8(3\bar{a}+4) & -16(\bar{a}+1) & 8 & -16 & 32(\bar{a}+1) \\ 7(3\bar{a}+4) & 14(\bar{a}+1) & -7 & 8 & -16(\bar{a}+1) \\ 14(\bar{a}+1) & 112 & 14(1-\bar{a}) & 16(\bar{a}-1) & -128 \\ -7 & 14(1-\bar{a}) & 7(4-3\bar{a}) & 8(3\bar{a}-4) & 16(\bar{a}-1) \\ 8 & 16(\bar{a}-1) & 8(3\bar{a}-4) & 16(4-3\bar{a}) & 32(1-\bar{a}) \\ -16(\bar{a}+1) & -128 & 16(\bar{a}-1) & 32(1-\bar{a}) & 256 \end{bmatrix}_{9x9}^{sym} \tag{A.8}$$

and

$$\mathbf{K}_3 = \frac{\pi}{\rho_f} \int_{-a}^{a} \int_{-b}^{b} \frac{n^2}{\left(x_0 + x \right)^2} \left[\mathbf{N}_f \right]^T \mathbf{N}_f \left(x_0 + x \right) dxdy \tag{A.9}$$

A.3 Mass matrix of axisymmetric fluid element

The fluid element mass matrix $\mathbf{M}_f^e$ can be written in term of shape functions as

$$\mathbf{M}_f^e = \frac{\pi}{\rho_f g}\int_{S_f}\left[\mathbf{N}_f\right]^T\mathbf{N}_f dS = \frac{\pi}{\rho_f g}\int_{-a}^{a}\left[\mathbf{N}_f^s\right]^T\mathbf{N}_f^s\left(x_0+x\right)dx \tag{A.10}$$

where $\mathbf{N}_f^s$ is the shape function of liquid element at the free surface ($\eta = 1$ or $y = b$).

After integrating Eq. (A.10), one obtains the fluid element mass matrix $\mathbf{M}_f^e$ as

$$\mathbf{M}_f^e = \frac{\pi a}{15\rho_f g}\begin{bmatrix} 0 & 0 & 0 & 0 & 0 & 0 & 0 & 0 & 0 \\ 0 & 0 & 0 & 0 & 0 & 0 & 0 & 0 & 0 \\ 0 & 0 & 0 & 0 & 0 & 0 & 0 & 0 & 0 \\ 0 & 0 & 0 & 0 & 0 & 0 & 0 & 0 & 0 \\ 0 & 0 & 0 & 0 & 4x_0+3a & 2\left(x_0+a\right) & -x_0 & 0 & 0 \\ 0 & 0 & 0 & 0 & 2\left(x_0+a\right) & 16x_0 & 2\left(a-x_0\right) & 0 & 0 \\ 0 & 0 & 0 & 0 & -x_0 & 2\left(a-x_0\right) & 4x_0-3a & 0 & 0 \\ 0 & 0 & 0 & 0 & 0 & 0 & 0 & 0 & 0 \\ 0 & 0 & 0 & 0 & 0 & 0 & 0 & 0 & 0 \end{bmatrix}_{9\times 9} \tag{A.11}$$

A.4 Shell-liquid coupling force matrix

The element shell-liquid coupling matrix $\mathbf{S}^e$ based on RD concept is given by

$$\mathbf{S}^e = \pi R\int_{-b}^{b}\left[\mathbf{N}_f^i\right]^T\mathbf{N}_s^w dy \tag{A.12}$$

where $\mathbf{N}_f^i$ is the shape function for the liquid dynamic pressure at the liquid-shell interface ($\xi = 1$ or $x = a$) and $\mathbf{N}_s^w$ is the shape function corresponding to radial displacement of the shell given by

$$\mathbf{N}_s^w = \begin{bmatrix} 0 & 0 & N_{1w} & N_{1\Delta u} & 0 & 0 & 0 & N_{2w} & N_{2\Delta u} & 0 & 0 & 0 & N_{3w} & N_{3\Delta u} & 0 \end{bmatrix}_{1\times 15}$$

(A.13)

where

$$N_{1w} = 1 - 23p^2 + 66p^3 - 68p^4 + 24p^5 \tag{A.14}$$

$$N_{1\Delta u} = \frac{Lp}{h}\left(1 - 6p + 13p^2 - 12p^3 + 4p^4\right) \tag{A.15}$$

$$N_{2w} = 16p^2 - 32p^3 + 16p^4 \tag{A.16}$$

$$N_{2\Delta u} = \frac{Lp^2}{h}\left(-8 + 32p - 40p^2 + 16p^3\right) \tag{A.17}$$

$$N_{3w} = p^2\left(7 - 34p + 52p^2 - 24p^3\right) \tag{A.18}$$

$$N_{3\Delta u} = \frac{Lp^2}{h}\left(-1 + 5p - 8p^2 + 4p^3\right) \tag{A.19}$$

in which $p = \dfrac{b+y}{L}$ and $L = 2b$.

APPENDIX B VESSEL

B.1 Wave load

The linear wave forces are purely oscillatory loads which oscillate at the wave frequency, while higher order wave forces have magnitudes which are proportional to the square (or higher order) of the wave amplitudes. The second-order wave effects include mean loads, slowly-varying loads due to frequency difference and rapidly-varying wave loads due to frequency summation.

The second-order wave force τ_{wave2} can be approximated as a summation of second-order 'transfer' functions of difference frequency wave components as (Faltinsen and Løken, 1979; and Nguyen, 2006)

$$\tau_{wave2}^{i} = \sum_{j=1}^{N}\sum_{i=1}^{N} A_j A_k \left[T_{jk}^{ic} \cos\left((\omega_k - \omega_j)t + (\varepsilon_k - \varepsilon_j)\right) + T_{jk}^{is} \sin\left((\omega_k - \omega_j)t + (\varepsilon_k - \varepsilon_j)\right)\right] \quad \text{(B.1)}$$

where ω_i is the wave frequency; ε_i the random phase angle; N the number of wave components considered; $A_i = \sqrt{2S(\omega_i)\Delta\omega}$ wave amplitudes determined from the wave spectrum $S(\omega)$; $\Delta\omega = (\omega_{\max} - \omega_{\min})/N$; and T_{jk}^{ic} and T_{jk}^{is} can be interpreted as second-order transfer functions for the difference frequency loads (Faltinsen, 1990). To avoid slow-drift wave force repetition after $2\pi N/(\omega_{\max} - \omega_{\min})$, ω_i is chosen to be random in the interval $\left[\omega_i - \Delta\omega/2,\ \omega_i + \Delta\omega/2\right]$.

B.2 Wind load

The effects of wind can be divided into mean, slowly-varying and rapidly-varying wind loads. Based on assumptions that the wind velocity is much larger than the vessel velocity (Fossen, 2002), the wind load is given by

$$\boldsymbol{\tau}_{wind} = 0.5\rho_a \begin{bmatrix} A_x C_{wx}(\gamma_w)|u_w|u_w \\ A_y C_{wy}(\gamma_w)|v_w|v_w \\ 0 \\ A_y L_{yz} C_{wx}(\gamma_w)|v_w|v_w \\ A_x L_{xz} C_{wx}(\gamma_w)|u_w|u_w \\ A_y L_{oa} C_{w\psi}(\gamma_w)|v_w|v_w \end{bmatrix} \tag{B.2}$$

where ρ_a is the density of air; A_x and A_y the lateral and longitudinal areas of the non-submerged part of the ship projected on the *xz*-plane and *yz*-plane; L_{oa} the overall length of vessel; L_{xz} and L_{yz} the vertical distances between transverse and longitudinal origin and the wind load point of attack; $C_{wx}(\gamma_w)$, $C_{wy}(\gamma_w)$, and $C_{w\psi}(\gamma_w)$ the non-dimensional wind coefficients in surge, sway and yaw, respectively. These coefficients are often found by model testing or by employing semi-empirical formulas. $\gamma_w = \beta_w - \psi$ is the relative wind angle; u_w and v_w are components of wind velocities defined as

$$u_w = V_w \cos(\beta_w - \psi) \tag{B.3}$$

$$v_w = V_w \sin(\beta_w - \psi) \tag{B.4}$$

where V_w is the wind velocity and β_w the wind direction.

PUBLICATIONS

1. International journal papers

[1] **Hai, L.V.**, Ang, K.K. and Wang, C.M. (2007). RD-Finite elements for free vibration analysis of liquid-filled cylindrical containers. *International Journal of Solids and Structures*. (Under review).

[2] **Hai, L.V.**, Ang, K.K. and Wang, C.M. (2007). Axisymmetric RD-shell and fluid elements for vibration analysis of liquid-filled containers due to moving ship. *Ocean Engineering*. (Under second review).

[3] **Hai, L.V.**, Ang, K.K. and Wang, C.M. (2008). Vibration analysis of axisymmetric multi-layer liquid-filled cylindrical containers using RD-finite element method. *The International Journal of Offshore and Polar Engineering IJOPE*, **18**(1), 43-49.

[4] **Hai, L.V.**, Ang, K.K. and Wang, C.M. (2008). Vibration analysis of coupled interaction problem between liquid sloshing, multi-containers and moving ship based on RD concept. *Engineering Structures*. (Under review).

2. International conference papers

[1] **Hai, L.V.**, Ang, K.K. and Wang, C.M. (2005). Axisymmetric RD shell and fluid elements for vibration analysis of liquid-filled cylindrical containers. *Proceedings of the Eighteenth KKCNN Symposium on Civil Engineering, Kaohsiung, Taiwan*, 509-514.

[2] Ang, K.K., **Hai, L.V.** and Wang, C.M. (2006). Vibration analysis of liquid-filled containers due to ship motion. *The First International Conference on Enhancement and Promotion of Computational Methods in Engineering Science and Mechanics CMESM, Changchun, China*, 782. (Invited paper).

[3] **Hai, L.V.**, Ang, K.K. and Wang, C.M. (2006). RD-Shell element coupled with fluid element for vibration analysis of axisymmetric multi-layer cylindrical containers with liquid. *Proceedings of the Nineteenth KKCNN Symposium on Civil Engineering, Kyoto, Japan*, 477-480.

[4] **Hai, L.V.**, Ang, K.K. and Wang, C.M. (2007). Interaction between sloshing liquid, container and moving ship. *Proceedings of the 2nd International Maritime-Port Technology and Development Conference MTEC, Singapore*, 306-312.

[5] **Hai, L.V.**, Ang, K.K. and Wang, C.M. (2007). Coupled interaction problem between liquid sloshing, multi-containers and ship motion. *Fifth International Conference on Advances in Steel Structures ICASS, Singapore*, **3**, 639-644.

[6] Ang, K.K., **Hai, L.V.** and Wang, C.M. (2008). Mitigation of liquid sloshing using baffles. *12th International Conferences on Computing in Civil and Building Engineering & 2008 International Conference on Information Technology in Construction ICCCBE-XII & INCITE, Beijing, China*, 302.

[7] Mitra, S., **Hai, L.V.** and Khoo, B.C. (2009). A study on complicated coupling effects of 3-D sloshing in rectangular tanks and ship motion. *The Nineteenth International Offshore and Polar Engineering Conference, Osaka, Japan*. (Accepted).